DEVELOPING A FUNDAMENTAL UNDERSTANDING OF BIOMASS STRUCTURAL FEATURES RESPONSIBLE FOR ENZYMATIC DIGESTIBILITY

A Dissertation

by

JONATHAN PATRICK O'DWYER

Submitted to the Office of Graduate Studies of
Texas A&M University
in partial fulfillment of the requirements for the degree of

DOCTOR OF PHILOSOPHY

August 2005

Major Subject: Chemical Engineering

DEVELOPING A FUNDAMENTAL UNDERSTANDING OF BIOMASS STRUCTURAL FEATURES RESPONSIBLE FOR ENZYMATIC DIGESTIBILITY

A Dissertation

by

JONATHAN PATRICK O'DWYER

Submitted to the Office of Graduate Studies of
Texas A&M University
in partial fulfillment of the requirements for the degree of

DOCTOR OF PHILOSOPHY

Approved by:

Chair of Committee, Mark Holtzapple
Committee Members, Dan Shantz
Richard Davison
Cady Engler
Head of Department, Kenneth Hall

August 2005

Major Subject: Chemical Engineering

ABSTRACT

Developing a Fundamental Understanding of Biomass Structural Features Responsible for Enzymatic Digestibility. (August 2005)

Jonathan Patrick O'Dwyer, B.S., University of Louisiana-Lafayette

Chair of Advisory Committee: Dr. Mark Holtzapple

Lignocellulosic biomass is one of the most valuable alternative energy sources because it is renewable, widely available, and environmentally friendly. Unfortunately, enzymatic hydrolysis of biomass has been shown to be a limiting factor in the conversion of biomass to chemicals and fuels. This limitation is due to inherent structural features (i.e., acetyl content, lignin content, crystallinity, surface area, particle size, and pore volume) of biomass. These structural features are barriers that prevent complete hydrolysis; therefore, pretreatment techniques are necessary to render biomass highly digestible.

The ability to predict the biomass reactivity based solely on its structural features would be of monumental importance. Unfortunately, no study to date can predict with certainty the digestibility of pretreated biomass. A concerted effort with Auburn University and Michigan State University has been undertaken to study hydrolysis mechanisms on a fundamental level. Predicting enzymatic hydrolysis based solely on structural features (lignin content, acetyl content, and crystallinity index) would be a major breakthrough in understanding enzymatic digestibility.

It was proposed to develop a fundamental understanding of the structural features that affect the enzymatic reactivity of biomass. The effects of acetyl content, crystallinity index (CrI), and lignin content on the digestibility of biomass (i.e., poplar wood, bagasse, corn stover, and rice straw) were explored.

In this fundamental study, 147 poplar wood model samples with a broad spectrum of acetyl content, CrI, and lignin were subjected to enzymatic hydrolysis to determine digestibility. Correlations between acetyl, lignin, and CrI and linear

hydrolysis profiles were developed with a neural network model in Matlab®. The average difference between experimentally measured and network-predicted data were ±12%, ±18%, and ±27% for 1-, 6-, and 72-h total sugar conversions, respectively. The neural network models that included cellulose crystallinity as an independent variable performed better compared to networks with biomass crystallinity, thereby indicating that cellulose crystallinity is more effective at predicting enzymatic hydrolysis than biomass crystallinity. Additionally, including glucan slope in the 6-h and 72-h xylan slope networks and glucan intercept in the 6-h and 72-h xylan intercept networks improved their predictive ability, thereby suggesting glucan removal affects later-stage xylan digestibility.

ACKNOWLEDGEMENTS

This work was a difficult and challenging experience and may not have been possible without the support of my family and friends, those in College Station and back home in Plaquemine, LA. They helped me through the difficult times and always believed in me.

I would like to thank Dr. Holtzapple for serving as my advisor. He has been extremely helpful in helping fine-tune my written and oral presentation skills. He has always been a source of knowledge and encouragement.

I would like to thank my committee members – Dr. Richard Davison, Dr. Dan Shantz, and Dr. Cady Engler – for their helpful comments and suggestions. I would also like to thank the following members of my lab group who helped in so many ways: Cesar Granda, Guillermo Coward-Kelly, Sehoon Kim, Frank Agbogbo, Zhihong Fu. I would like to specifically thank Li Zhu (Julie) for performing hydrolysis on half of the 1,323 experiments. It has been my pleasure to learn and grow as a student along side her.

Lastly, I would like to especially thank my parents for their love and support throughout graduate school. Without them, this would have not been possible.

TABLE OF CONTENTS

Page

LIST OF TABLES

TABLE Page

LIST OF FIGURES

FIGURE Page

FIGURE Page

FIGURE Page

FIGURE Page

INTRODUCTION

Improving energy efficiency is a possible means to reduce dependence on imported oil; however, even with better energy efficiency, consumption is likely to grow with increasing population. The world currently consumes 30 billion barrels per year; Colin (2003) estimates that oil reserves will become scarce by the 2050s. Because petroleum is a nonrenewable resource, there is an urgent need to seek alternative energy sources that are inexhaustible.

BIOMASS CONVERSION PROCESSES

Lignocellulosic biomass is one of the most valuable alternative energy sources because it is renewable, widely available, and environmentally friendly. Available biomass reserves in the U.S. are approximately 200 million dry tons per year (U.S. Department of Energy, 1998). Biomass can be converted to liquid fuels such as ethanol (Szczodrak and Fiedurek, 1996) and chemicals such as carboxylic acids (Blasig et al., 1992). Demand for ethanol is expected to rise because of concerns related to national security, economic stability, environmental impact, and global warming (Bothast et al., 1999). Figure 1 shows two biological processes that convert biomass into economically viable products.

The more conventional approach to biomass conversion uses two individual steps: (1) saccharification, whereby the biomass is converted to sugars using enzymes and (2) fermentation, whereby the sugars are converted to alcohol using yeast. An alternative to the aforementioned approach combines the saccharification and fermentation steps and is called simultaneous saccharification and fermentation (SSF). The advantage of SSF is that it minimizes product inhibition by maintaining low sugar concentrations. This discovery is important because it improves overall efficiency and reduces operating expenses of biomass conversion processes (Sun and Cheng, 2002).

This dissertation follows the style and format of Biotechnology and Bioengineering.

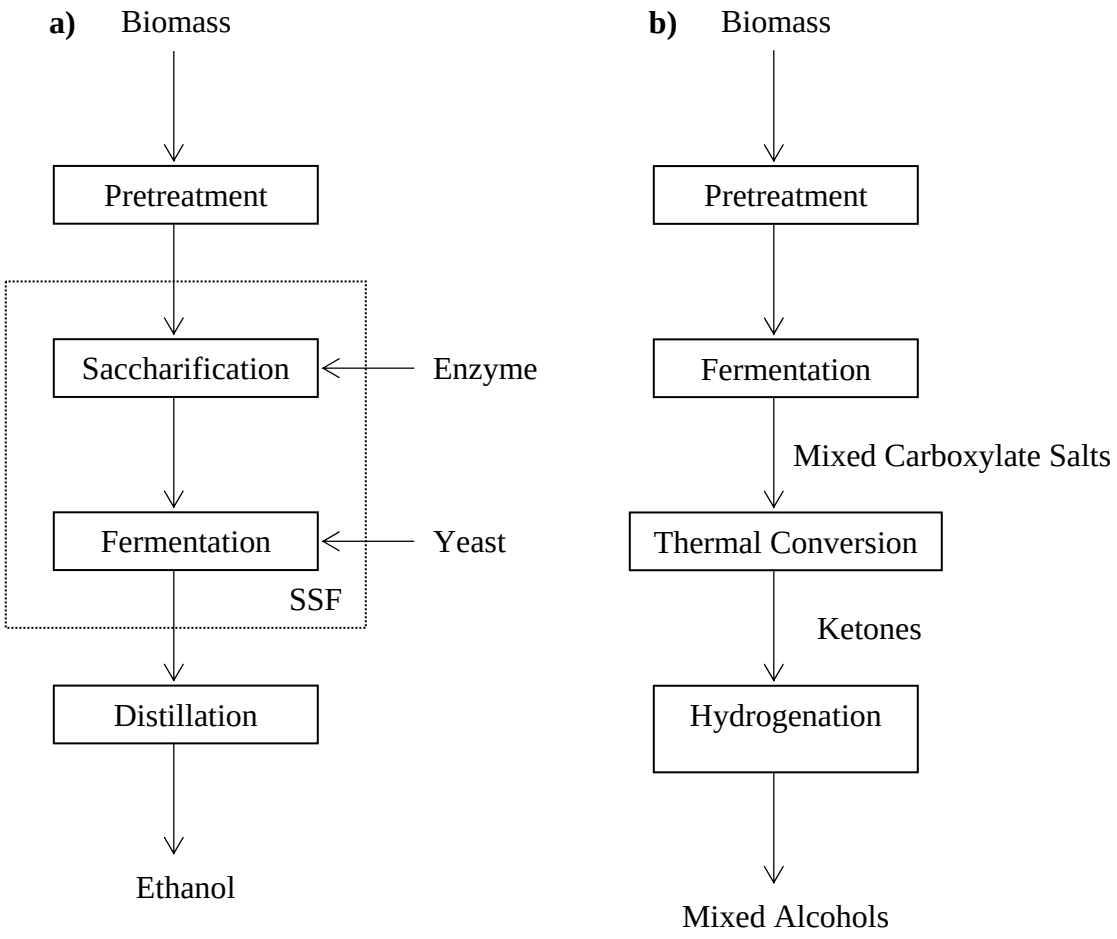

Figure 1. Overview of current process schemes used to convert lignocellulose into fuels and chemicals: (a) Traditional biomass conversion process (b) MixAlco Process.

An alternative to the aforementioned enzyme-based processes is the MixAlco process developed by Holtzapple et al. (1997). The MixAlco Process uses a mixed culture of marine microorganisms to convert lignocellulosic biomass into carboxylate salts (e.g., calcium acetate, propionate, and butyrate), which are thermally converted to ketones and subsequently hydrogenated to alcohols. The MixAlco Process has advantages over traditional biomass conversion processes due to its robustness, ability to handle a variety of feedstocks, and lower operating costs.

STRUCTURE OF LIGNOCELLULOSIC BIOMASS

On a dry weight basis, lignocelluloses contain 35–50% cellulose, 20–35% hemicellulose, and 10–15% lignin (Wyman, 1994). Together, these components represent approximately 90% of the dry weight of most plant material (Ingram, 1999). Plant cell walls can be described as a macromolecule, which is composed of cellulose fibers embedded in a covalently joined matrix of lignin and hemicellulose (Brett and Waldron, 1996). The interactions between cell wall components render cellulose and hemicellulose unavailable for enzymatic hydrolysis.

Cellulose is a linear, unbranched polymer of anhydroglucose connected by β-1,4 linkages with high molecular weights of 600,000–1,500,000 (Holtzapple, 1993a). Native cellulose occurs as densely packed, hydrogen-bonded elementary fibrils of pure cellulose embedded in a matrix of hemicellulose. Native cellulose is water insoluble and contains both crystalline and amorphous regions. This complexity makes cellulose resist enzymatic hydrolysis without prior pretreatment.

Hemicellulose consists of short, branched chains of many sugars and modified sugars. It consists of three hexoses (D-glucose, D-galactose, and D-mannose) and two pentoses (D-xylose and L-arabinose). Native xylan is highly modified with acetyl groups at the C2 and C3 positions and is amorphous because of its highly branched nature (Holtzapple, 1993b). Because of their amorphous morphology, hemicelluloses are partially soluble or swellable in water. Highly acetylated xylans resist enzymatic

degradation; therefore, deacetylation of xylan increases enzymatic hydrolysis (Kong et al., 1992).

Lignin is an important component of plants serving as a glue that holds plant cell walls together. Lignin is a highly cross-linked phenylpropylene polymer that resists enzymatic degradation from invading insects and microbes (Holtzapple, 1993c). Pure lignin does not exist in nature; instead, lignin always occurs in complex with polysaccharides as a composite material called lignocellulose as shown in Figure 2. The primary building blocks of lignin are guaiacyl, syringyl, and coumaryl. The guaiacyl and syringyl units are dominant in softwoods and hardwoods respectively, whereas the coumaryl unit is primarily found in grasses (Holtzapple, 1993c).

CELLULASE ENZYME COMPLEX

All cellulolytic enzymes share the same chemical specificity for β-1,4-glycosidic bonds (Teeri, 1997). The major enzyme components of the cellulase enzyme complex are cellobiohydrolase (E.C. 3.2.1.91), endoglucanase (E.C. 3.2.1.4), and β-glucosidase (E.C. 3.2.1.21). The filamentous fungus *Trichoderma reesei*, which is known to have one of the most efficient cellulase systems, produces two cellobiohydrolases (CBHs) and four endoglucanases (EGs); however, sufficient amounts of β-glucosidase (cellobiase) are not produced in wild-type *Trichoderma reesei* to convert all cellobiose to glucose (Medve et al., 1998). The cooperative action of the three enzymes is required to achieve efficient enzymatic hydrolysis of lignocellulosic biomass. The cellobiohydrolase and endoglucanase act synergistically (Figure 3) to achieve sugar yields that are greater than the sum of the action of the individual enzymes (Srishdsuk et al., 1998).

As shown in Figure 4, most cellulolytic enzymes have two functionally distinct domains, the cellulose-binding domain and the catalytic domain. Adsorption of the cellulose-binding domain consists largely of entropically driven interactions between aromatic amino acids (tryptophan and tyrosine) and cellulose (Creagh et al., 1996). There are two fundamental mechanisms in which glycosidases cleave β 1-4 glycosidic

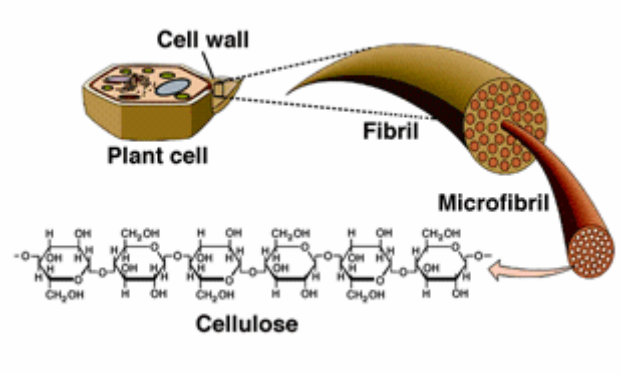

Figure 2. General overview of the structure of a plant cell wall. The brown-colored material encasing the cellulose in the microfibril is a matrix of hemicellulose and lignin (Moore and Dennis, 1999).

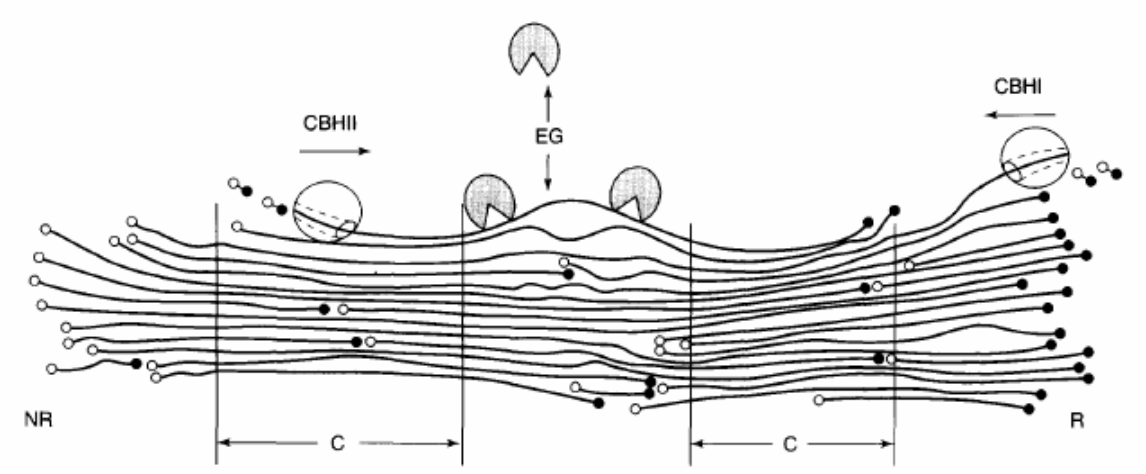

Figure 3. Schematic representation of the mode of action of cellobiohydrolases (CBH) and endoglucanases (EG) acting in a synergistic manner. The filled circles (R) represent the reducing ends and the open circles (NR) represent the nonreducing ends, and C defines the highly ordered crystalline regions (Teeri, 1997).

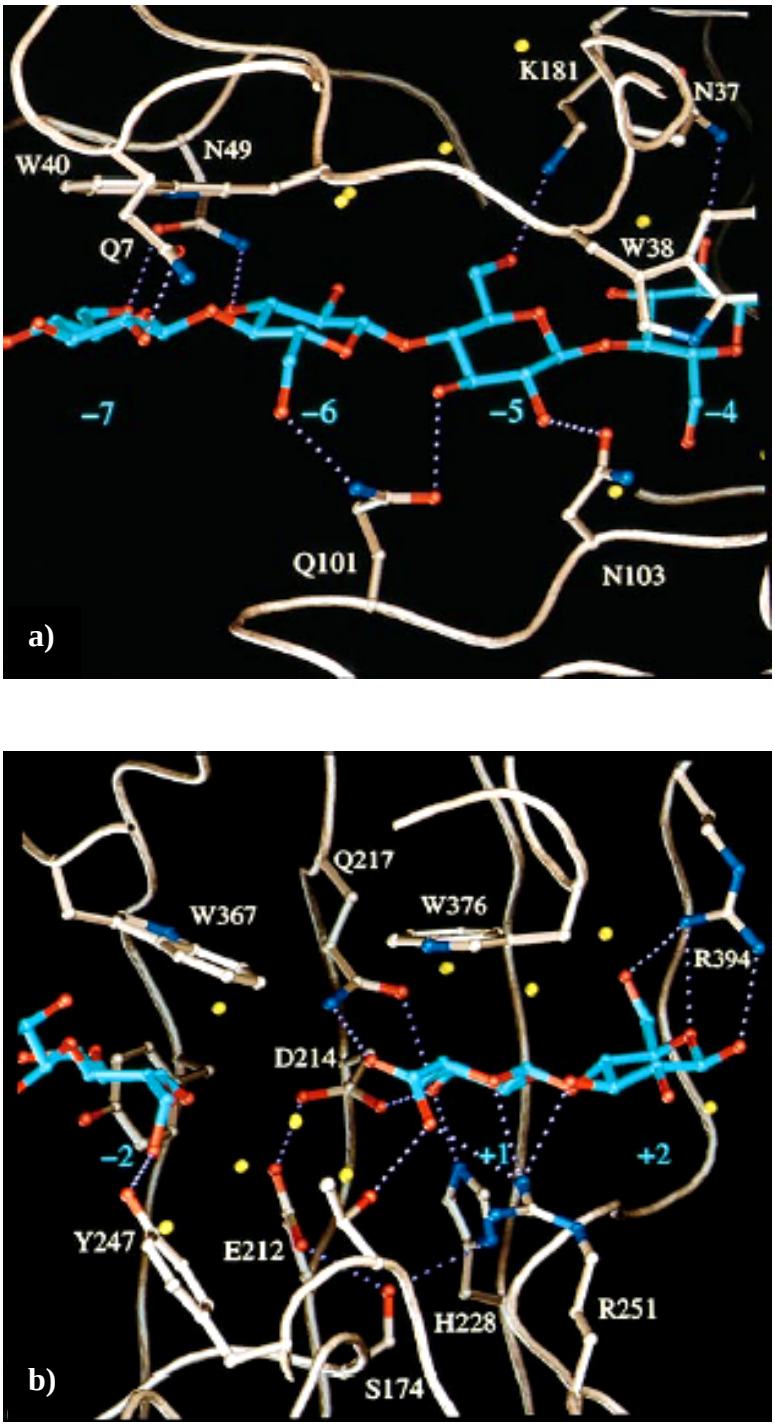

Figure 4. Enzyme-carbohydrate interaction inside CBHI tunnel: (a) binding domain and (b) catalytic domain (Divne et al., 1998).

bonds. The stereochemical outcome of the reaction characterizes the reaction mechanisms. If the stereochemistry at the anomeric carbon is retained in the product (β-glucose), then the enzyme is termed retaining; however, if the enzyme inverts the stereochemistry of the product (α-glucose), then it is classified as an inverting enzyme (Withers et al., 1986). The inverting enzyme uses a single-displacement mechanism whereby water attacks the anomeric carbon, displacing the leaving group in a general acid/base-catalyzed process (Withers et al., 1986; Liu et al., 1991). In contrast, retaining enzymes use a double-displacement mechanism involving a covalent glycosyl-enzyme intermediate. The first step involves attack of an enzymatic nucleophile at the anomeric center with general acid-catalyzed displacement of the leaving group followed by a molecule of water attacking the anomeric center of this intermediate in a general base-catalyzed process to yield the product (Liu et al., 1991; Sinnott, 1990; Withers et al., 1993).

Cellobiohydrolases (1,4-β-D-glucan cellobiohydrolase, exoglucanase) act as exoglucanases (Medve et al., 1998), which must adsorb onto the insoluble substrate before releasing cellobiose as the main product by attacking both reducing and nonreducing ends of the cellulose chain. In addition to the catalytic site, which is located in the core of the enzyme, these enzymes have a short extra binding domain connected to the core via a flexible arm (Ong et al., 1989). This organization improves binding to and therefore hydrolysis of crystalline cellulose (Stahlberg et al., 1988). CBHs have been shown to efficiently degrade crystalline cellulose but are almost inactive on soluble cellulose derivatives (Vrsanska and Biely, 1992). In *Trichoderma reesei*, CBHs account for roughly 80% of the total cellulolytic protein, accounting for most of its cellulolytic activity (Teeri, 1997).

Endoglucanases (*endo*-1,4-β-D-glucan 4-glucanohydrolase) cleave glycosidic bonds randomly along the cellulose chains leading to a rapid decrease in the degree of polymerization of the substrate. This action produces new binding sites for cellobiohydrolases giving rise to *endo-exo synergism* (Goyal et al., 1991). The individual isocomponents (enzymes that catalyze the same reaction but are encoded by

different genes) of the CBH and EG enzymes have been shown to elicit exo-exo (Nidetzky et al., 1993) and endo-endo (Mansfield et al., 1998a; Mansfield et al., 1998b) synergism among cellulases. EGs are known to bind very poorly to crystalline regions of cellulose; therefore, they exhibit higher activity towards the more disordered regions of cellulose. In many practical applications, endoglucanase activity has been found to be detrimental to the strength of cellulose fibers (Pere et al., 1995).

Cellobiase hydrolyzes cellobiose to glucose and removes glucosyl residues from the nonreducing end of the soluble cellooligosaccharides (Mansfield et al., 1999). Hoh et al. (1992) discovered that cellobiase plays a vital role in cellulose hydrolysis because it removes the inhibitory effect that cellobiose has on other cellulase enzymes (Hoh et al., 1992). Holtzapple et al. (1990) have shown that converting cellobiose to glucose reduces the effective inhibitor binding constant by a factor of six. Reducing end-product inhibition is an important step in developing an economically viable process for converting lignocellulose to alcohols and fuels.

OBJECTIVES

The main objective of this research was to determine if crystallinity, acetyl content, and lignin content can fully explain the inherent reactivity of biomass, or are there other structural features that play a vital role in the enzymatic hydrolysis of biomass. If the empirical model developed can accurately predict biomass digestibility for numerous biomasses that have been subjected to different pretreatment techniques, then we can say that we have identified the fundamental factors responsible for enzymatic hydrolysis. This work has the potential to lead to the design of selective pretreatment techniques that can alter one or more of the structural features to render the biomass digestible, which will lead to more efficient and economical pretreatments. Because pretreatment is expensive, this work could help develop a more economically viable biomass conversion technology, thereby improving its potential as an alternative to fossil fuels. The following is a list of the steps performed to meet the main objective:

1. Determine the effect of experimental conditions (substrate concentration, enzyme loading) on substrate and/or product inhibition. This is important because measured reactivity should reflect biomass chemical and physical features and not be influenced by inhibition.
2. Perform enzymatic hydrolysis of 147 poplar wood model samples at various times (1, 6, 72 h) and strategically selected enzyme loadings.
3. Determine if crystallinity, lignin content, and acetyl content are the major influencers of biomass digestibility by approximating a function of the three structural features utilizing the neural network toolbox in MATLAB®.
4. Test the predictive ability of mathematical models with different substrates (bagasse, corn stover, rice straw) that were pretreated with various techniques (dilute acid, aqueous ammonia, ammonia fiber explosion, oxidative and nonoxidative lime).

OPTIMIZATION OF REACTION CONDITIONS

INTRODUCTION

Lignocellulosic biomass can be converted to ethanol, which is a renewable liquid fuel that offers simultaneous environmental benefits. One major step in the conversion of biomass to ethanol is sugar production. Converting biomass with either free enzymes or microorganisms facilitates sugar production. The sugars are then fermented into alcohol or a mixture of organic acids. Cellulose enzymatic hydrolysis offers major advantages over other chemical routes (i.e., acid hydrolysis) such as higher yields, minimal byproduct formation, low energy requirements, mild operating conditions, and low chemical disposal costs (Van Wyk, 2001; Kadam et al., 1999; Ghose and Ghosh, 1978). Even though current costs of the enzymatic route are higher than other routes, what drives research is its long-term potential for cost reduction through genetic and/or metabolic engineering and economic viability over more established routes (Lynd et al., 1991).

A major hindrance of current processing schemes is the high cost associated with enzymes and pretreatments. Despite the high costs, pretreatment is an essential prerequisite to alter biomass structural features, thereby improving the susceptibility of biomass to enzymatic hydrolysis (Chang, 1999; Chang and Holtzapple, 2000). Most pretreatments can be classified as either chemical (e.g., acid and alkaline) or physical (e.g., milling and irradiation). Economic evaluations of processes that convert biomass to bioethanol indicate that pretreatment is the single most expensive process step, accounting for roughly one-third of the overall processing cost (Lynd et al., 1996). The pretreated biomass is subsequently hydrolyzed through the synergistic action of a complex mixture of enzymes to produce soluble monosaccharides (glucose, xylose, arabinose, and mannose). The sugars are an intermediate in the chemical route before being fermented. Enzyme production alone can account for as much as 30% of the total process cost (Lynd et al., 1996). A thorough understanding of what structural features

hinder enzymatic hydrolysis has the potential to aid in the design of more effective and economically feasible conditions of the two major contributors to the high cost of current biomass technologies: pretreatment techniques and enzyme loading.

Various theoretical, empirical, and hybrid models have been developed by researchers to predict the enzymatic hydrolysis of biomass (Holtzapple et al., 1984; Medve et al., 1998; Movagarnejad et al., 2000; Tarantili et al., 1996). Because cellulose is a highly complex substrate, its hydrolysis involves two distinct stages: enzyme-substrate complex formation and cellulose hydrolysis. Enzyme-substrate complex formation consists of two major steps including mass transfer of enzyme from the bulk aqueous phase to the cellulose surface and formation of the enzyme-substrate complex following enzyme adsorption. Cellulose hydrolysis consists of three major steps including transfer of reactant molecules to the active site of the enzyme-substrate complex, reaction promoted by the enzyme, and transfer of soluble products to the bulk aqueous phase. The complex-heterogeneous reaction mechanism involved in cellulose hydrolysis and the intricate morphology of biomass make it difficult to model enzymatic hydrolysis (Movagarnejad et al., 2000; Zhang et al., 1999).

The classic Michaelis-Menton parametric model is inadequate to explain the action of cellulases on insoluble cellulose. In contrast, the kinetic behavior of cellulases, in particular β-glucosidase, fits the Michaelis-Menton model on well-defined soluble oligosaccharides (Schou et al., 1993). This is due to the homogeneous nature of the reaction mechanism involved in cellobiose hydrolysis to glucose. The nonlinearity observed when plotting sugar conversion versus hydrolysis time at a given enzyme loading indicates that the rate of cellulose hydrolysis decreases and often stops before all of the substrate is consumed (Zhang et al., 1999). There are several factors that lead to a decrease in hydrolysis rates as the reaction progresses including end-product inhibition, lower substrate reactivity (higher crystallinity, higher lignin content, substrate accessibility, etc.), enzyme inactivation, and enzyme loss due to irreversible lignin adsorption. Without the complication of product inhibition or cellulase inactivation, Desai and Converse (1997) concluded that the loss of substrate reactivity is not the

principal cause for the long residence time required for complete biomass conversion. Likewise, Eriksson et al. (2002) concluded that thermal instability of the enzymes and product inhibition were not the main cause of reduced hydrolysis rates, instead enzymes become inactivated while adsorbed to the substrate and that unproductive binding is the main cause of hydrolysis rate reduction.

In studies with pure celluloses, amorphous regions were shown to degrade 5–10 times faster than highly crystalline celluloses by fungal enzymes (Klyosov, 1990; Gama et al., 1994; Lynd et al., 2002). This suggests that the high initial rates are due to preferential hydrolysis of the more easily degraded amorphous regions and the rate decreases as the enzymes encounter the more recalcitrant crystalline regions. Therefore, models have been developed that account for the bicomposition (amorphous and crystalline) of cellulose (Huang, 1975). However, validation of such models is extremely difficult if not impossible. Accurately determining the quantity of cellulose that is crystalline and amorphous as the reaction progresses is extremely tricky. In contrast, several researchers have observed no substantial change in crystallinity as enzymatic hydrolysis progresses beyond the initial stage (Puls and Wood, 1991; Lenz et al., 1990; Ohmine et al., 1983). The inconsistencies in the rate of hydrolysis of crystalline cellulose may be due to the crude/impure nature of the cellulase enzyme complex. The quantities of EGs relative to CBHs can be inconsistent from batch to batch. Because CBHs have been shown to degrade crystalline cellulose whereas EGs are very ineffective, the differences in enzyme batches may lead to conflicting results when investigating the increase or decrease of crystallinity as the reaction progresses.

Product inhibition of cellulases is a central limitation to the practical use of cellulases in biomass conversion processes. This explains the interest in SSF technology as an alternative to the two-step technique that allows for the accumulation of low-molecular-weight sugars. Even though product inhibition is accepted as a limitation to thoroughly hydrolyzing biomass, the type of inhibition is a subject of much debate. The discrepancies result from the difficulty in conducting experiments that show the type of inhibition because of the high inhibitor concentrations required to elicit an inhibitory

effect. Researchers have reported conflicting results; while some measure competitive inhibition (Dwivedi and Ghose, 1979; Beltrame et al., 1984; Gonzalez et al., 1989) and noncompetitive inhibition (Holtzapple et al., 1984; Wald et al., 1984; Scheiding et al., 1984) others measure uncompetitive inhibition (Beltrame et al., 1984). This discrepancy could be a result of the substrate to enzyme ratio employed, source of cellulase enzyme complex, and/or the hydrolysis time over which the experiments were conducted.

It is possible to predict the enzymatic digestibility of lignocellulose if the function of chemical and physical features that determine digestibility can be modeled (Chang and Holtzapple, 2000). Previously, Holtzapple et al. (1984) developed a generalized theoretical model of cellulose hydrolysis, termed the HCH-1 Model. It was shown that the HCH-1 Model could be simplified in such a way that a plot of conversion versus the logarithm of enzyme loading is linear (Holtzapple et al., 1994). The linearity of this plot has been observed over a tenfold range in enzyme loading and a threefold range in initial cellulose concentration (Mandels et al., 1981).

MATHEMATICAL BACKGROUND

It was shown previously that the HCH-1 Model, which uses noncompetitive inhibition and does not predict linear reaction rates in enzyme concentration as does the classic Michaelis-Menton model, could consistently correlate cellulose hydrolysis (Holtzapple et al., 1984); therefore, it was chosen to aid in the development of an empirical model that predicts carbohydrate conversion based on biomass structural features. The HCH-1 Model may be written as

$$V = -\frac{dG_x}{dt} = \frac{\kappa G_x Ei}{\alpha + \phi G_x + \varepsilon E} \tag{1}$$

where G_x is the cellulose concentration, E is the enzyme concentration, ϕ is the fraction of the cellulose surface that is free to be hydrolyzed, and κ, α, and ε are parameters that describe the degree of substrate reactivity and hence are related to biomass structural features. To determine the inhibition pattern exhibited by the reaction system at constant

substrate concentration, Equation 1 may be linearized into a double-reciprocal form by inverting both sides to give

$$\frac{1}{V} = \frac{\alpha + \phi[G_x]}{\kappa[G_x]i}\frac{1}{[E]} + \frac{\varepsilon}{\kappa[G_x]i} \tag{2}$$

Both the intercept and slope will be increased by the factor 1/*i*. This is indicative of the classic noncompetitive inhibition pattern where both free enzyme and enzyme-substrate complex bind the inhibitor. A noncompetitive inhibitor binds to enzyme sites that participate in both substrate binding and catalysis and is illustrated with reaction network in Figure 5. For multiple inhibitors, the inhibition parameter *i*, which is the fraction of total enzyme not inhibited by product, is given as

$$i = \frac{1}{1 + \beta_1 G_1 + \beta_2 G_2} \tag{3}$$

where β_1 and β_2 are glucose and cellobiose binding constants, respectively. When cellobiase is added in excess, all cellobiose is converted to glucose and Equation 3 can simplified to give

$$i = \frac{1}{1 + \beta_1 G_1} \tag{4}$$

where G_1 is the glucose concentration and β_1 the glucose binding constant (Holtzapple et al., 1990). If one assumes that fraction of binding sites that are free (ϕ) is close unity and the conversion (x) is greater than 0.1 and less than 0.9, Equation 1 can be integrated and simplified to become

$$x = B\ln(E_0) + A \tag{5}$$

where x and E_o are sugar conversion/yield and enzyme loading, respectively (Holtzapple et al., 1994). The linearity of Equation 5 has been observed over a tenfold range in enzyme loading, E_o, and a threefold range in initial cellulose concentration, G_x (Mandels et al., 1981). Holtzapple et al. (1994) determined that parameters *A* and *B* are affected by the inhibition parameter *i*. Therefore, it is important to eliminate product inhibition to ensure parameter estimation reproducibility when using the linear form of the HCH-1 Model to predict enzymatic hydrolysis of biomass.

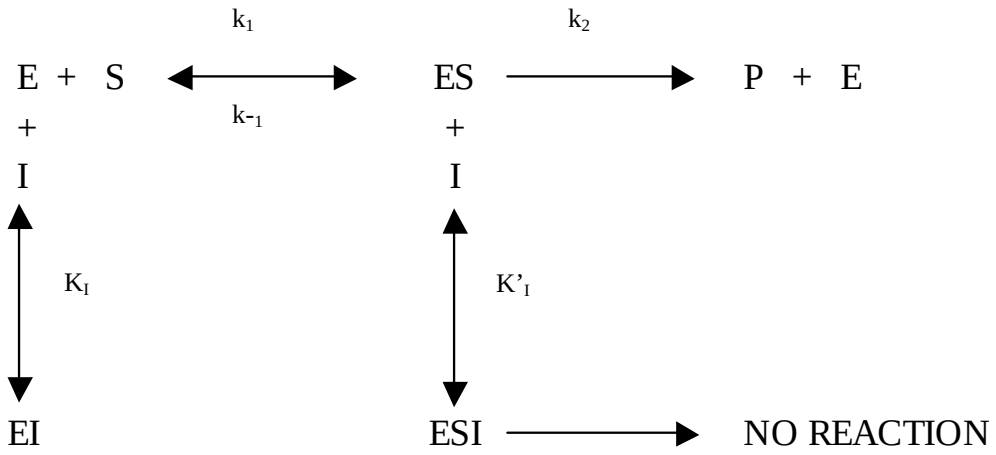

Figure 5. A reaction network illustrating noncompetitive inhibition where the inhibitor binds to free enzyme as well as the enzyme-substrate complex.

OBJECTIVES

The purpose of this research was to discover the type of inhibition pattern demonstrated by the enzyme-substrate system employed. Additionally, the degree of inhibition was investigated to determine the reaction conditions that would result in minimal product inhibition, thereby reflecting the inherent reactivity of the biomass. Lastly, the range of substrate concentrations and enzyme loadings over which the simplified HCH-1 Model (Equation 5) is valid was investigated. Corn stover was employed as the substrate throughout all experiments. It was prepared by lime pretreatment as described in Appendix C. The specific objectives were:

1. Determine the inhibition pattern exhibited by enzymatically hydrolyzed lime pretreated corn stover with a *Trichoderma reesei* cellulase complex. This is important because the kinetic model used to describe digestibility, the HCH-1 Model, was developed with a noncompetitive inhibition term.
2. Calculate inhibition parameters (*i*) to determine optimal reaction conditions (i.e., minimal inhibition).
3. Explore the range of conditions (i.e., enzyme loading and substrate concentration) over which the simplified HCH-1 Model is valid.

INHIBITION STUDY

Purpose

The HCH-1 Model was proposed as a means of predicting enzymatic hydrolysis of biomass. The model assumes that the inhibition pattern is noncompetitive (Holtzapple et al., 1990). The purpose of this study is to determine if the assumption of noncompetitive inhibition of cellulase in the HCH-1 Model is valid with the reaction system employed. Additionally, the degree of inhibition was measured to determine the combination of enzyme loading and substrate concentration that leads to minimal

product inhibition. The hydrolysis experiments described in subsequent sections will be conducted to predict enzymatic hydrolysis based solely on biomass structural features; therefore, measured reactivity should reflect biomass chemical and physical features and not be influenced by product inhibition.

Materials and Methods

Substrate Preparation

Corn stover was prepared by grinding 100 g in a coffee grinder and sieved with a 40-mesh screen. The ground and sieved biomass was pretreated with 0.1 g lime ($Ca(OH)_2$)/g dry biomass and 10 g water/g dry biomass for 2 hours while the temperature was maintained at 100^{o}C. After pretreating, the pH was 11.5, which is incompatible with cellulase; therefore, an appropriate amount of acetic acid (CH_3COOH) was added to neutralize (pH = 5.5) any residual lime. After pH adjustment, the corn stover was repeatedly washed with distilled water and centrifuged to separate the wash water from the biomass until the supernatant was clear. The pretreated and washed corn stover was air dried at 45^{o}C for 3 days. The dried corn stover was again ground in a coffee grinder and sieved with a 40-mesh screen. The moisture content of the air-dried corn stover was determined as described in NREL standard procedure No. 001.

Enzyme Measurements

To verify the activity of the *Trichoderma reesei* cellulase preparation received from NREL, a filter paper assay was performed according to NREL standard procedure No. 006. The filter paper activity of the cellulase was 65 FPU/mL enzyme. A comparison of the standard filter paper assay and an improved standard filter paper assay developed by Coward-Kelly et al. (2003) is described in Appendix D. Cellobiase activity (Novozym 188, Novo Nordisk Biochem) determined by Novo Nordisk was 321 CBU/mL based on the company's assay.

Enzymatic Hydrolysis

The experiments were conducted in screw-cap glass vials with 0.2 g dry weight of lime treated corn stover in a solution of citrate buffer (0.05 *M*, pH 4.8) and sodium azide (0.01 g/L) to maintain constant pH and inhibit microbial contamination, respectively. The reaction vessels were agitated in a 100-rpm air-bath shaker. When the solution reached 50^{o}C, the hydrolysis was initiated by adding 0.2 mL of appropriately diluted cellulase (Table I) and an excess cellobiase loading of 30 μL. The excess cellobiase ensures all cellobiose, which has significant inhibitory effects, is converted to glucose. A series of experiments was conducted with varying enzyme loadings (0.25–50 FPU/g biomass) at four substrate concentrations (10, 20, 50, and 100 g biomass/L). After 1 or 72 h, depending on the experiment being conducted, the vials were removed from the air-bath shaker, boiled for 15 minutes to denature the enzymes, cooled, centrifuged, and the filtrate was frozen until sugar analysis was performed. (Note: Upon thawing, the samples were well mixed to ensure uniform sugar concentration). Reducing sugars were measured using the DNS assay (Miller, 1959) against a glucose standard and reported as "mg equivalent glucose/g dry biomass." Cellulase and cellobiase were incubated independently in the absence of biomass for 3 days at 50^{o}C as explained in Appendix A "Enzymatic Hydrolysis." The experiments were performed in triplicate. Background sugar contributed by cellulase and cellobiase were measured by the DNS assay. No sugars were detected for the cellulase enzyme mixture. The cellobiase enzyme had a mean sugar contribution of 0.56 mg glucose/mL solution and standard error of ±0.017. This background sugar contribution was subtracted from experimental sugar yields.

Table I. Cellulase enzyme dilution calculations used for all experiments.

Desired Loading (FPU/g biomass)	Total Volume (mL)	Stock Enzyme (mL)	Dilution Water (mL)
0.1	16.250	0.025	16.225
0.25	13.00	0.05	12.95
0.5	13.0	0.1	12.9
0.75	8.67	0.1	8.57
1	6.5	0.1	6.4
1.5	4.33	0.1	4.23
2	3.25	0.1	3.15
3	3.25	0.15	3.10
5	3.25	0.25	3.00
10	3.25	0.50	2.75
20	3.25	1.00	2.25
30	2.17	1.00	1.17
50	1.95	0.45	1.50

Results and Discussion

A total of 136 experiments were conducted at four different substrate concentrations and ten different enzyme loadings. The experiments exhibited the classic nonlinear kinetic profile of a heterogeneous reaction system as shown by Figure 6. This type of profile was expected due to the heterogeneous nature of lignocellulose hydrolysis, which requires an adsorption step prior to cleavage of the glycosidic bond.

To determine the inhibition pattern exhibited by the reaction system, a total of 28 experiments were conducted at various substrate concentrations and enzyme loadings. The experiments were terminated after 1 h by boiling for 15 minutes to denature the enzymes. The experiments were conducted in duplicate. The average velocity was measured over a period of one hour as

$$V_{AVG} = \frac{G_S\big|_2 - G_S\big|_1}{t_2 - t_1} \tag{6}$$

where G_S is the soluble product concentration and t is time. To verify that the soluble products act as noncompetitive inhibitors, Equation 2 was used to construct a Lineweaver-Burke plot of $1/V_{AVG}$ versus $1/[E]$. Because the lines intersect after the ordinate, Figure 7 provides evidence that the inhibition pattern is indeed noncompetitive for soluble substrates. Because excess cellobiase was added to the reaction mixture, the predominant soluble product was glucose. Thus, glucose binds to enzyme sites that participate in both substrate binding and catalysis. The lines intersect on the $1/[E]$ axis indicating that glucose has an equal binding affinity for the free enzyme and the enzyme-substrate complex (i.e., the binding constants in Figure 5 K_I and K'_I are equivalent). Another explanation for the noncompetitive inhibition pattern may be due to inactivation of the enzyme due to non-preferential and irreversible binding to lignin, hence reducing the effective level of $[E]$ at all values of $[S]$. Therefore, double reciprocal plots for irreversible enzyme inactivation resembles those for noncompetitive inhibition.

Contrary to expectations, Figure 8 demonstrates that sugar yields for the 100-g/L substrate concentration were lower than for the 50-g/L substrate concentration. This phenomenon may be due to increased product inhibition as shown in Table II at higher

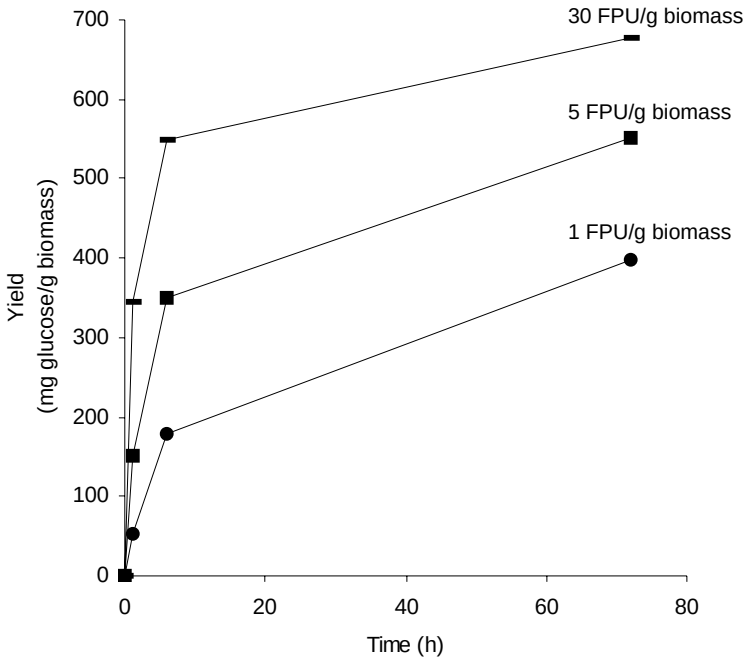

Figure 6. Nonlinear hydrolysis profile of a heterogeneous reaction system with lime-pretreated corn stover. Hydrolysis conditions: 20 g/L and 48 CBU/g biomass.

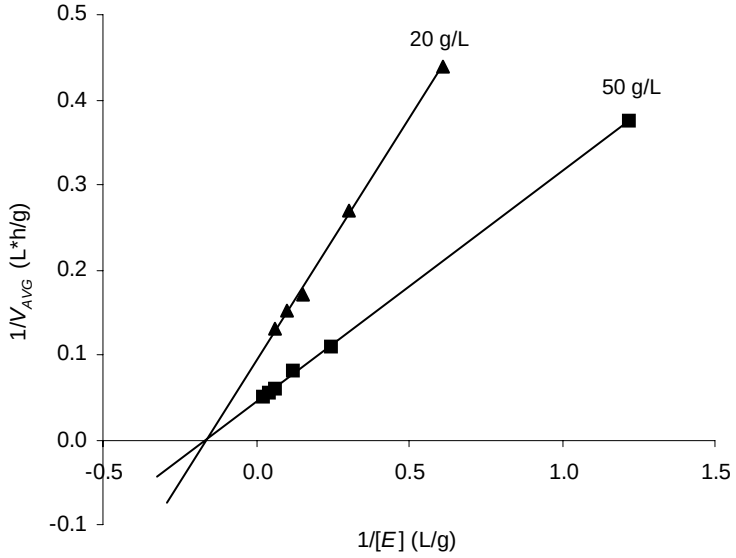

Figure 7. Lineweaver-Burke plot illustrating the noncompetitive inhibition pattern. Hydrolysis conditions: 1 h, 48 CBU/g dry biomass, 1–30 FPU/g dry biomass.

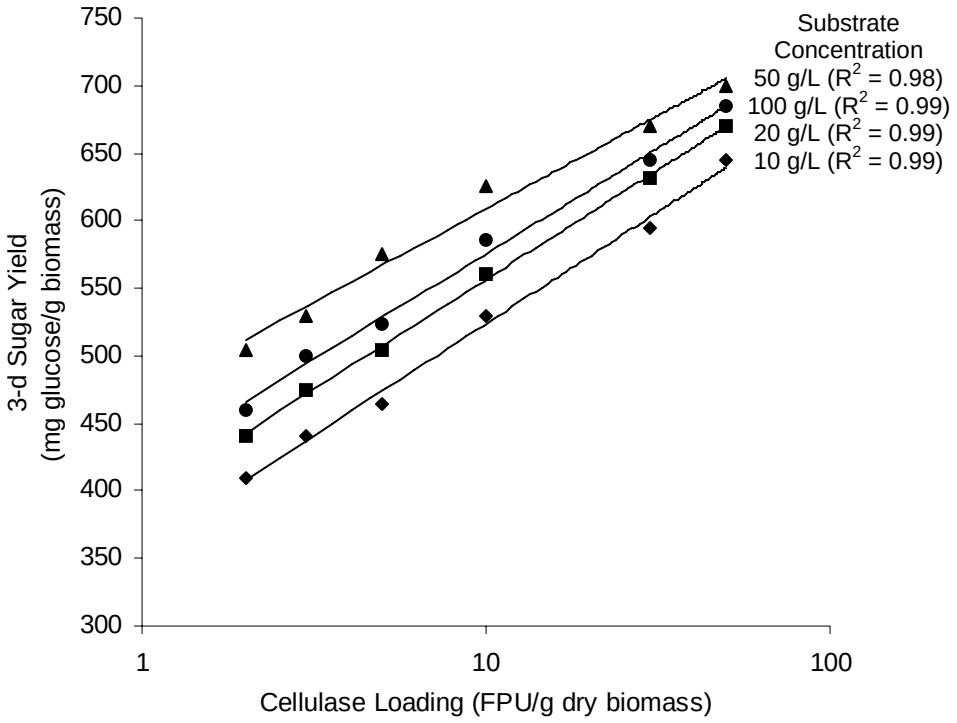

Figure 8. Hydrolysis profile of 3-d reducing sugar yields of lime-pretreated corn stover for the substrate concentration study. Hydrolysis conditions: 48 CBU/g biomass, 72 h, 2–50 FPU/g dry biomass.

Table II. Inhibition parameters (*i*) calculated using Equation 4 with a glucose-binding constant (β_1) of 0.00313 L/g for the *Trichoderma reesei* cellulase complex.

Enzyme Loading (FPU/g biomass)	Substrate Concentration			
	10 g/L	20 g/L	50 g/L	100 g/L
0.25	0.992 (±0.00030)	-	-	-
0.5	0.991 (±0.00037)	-	-	-
0.75	0.989 (±0.00006)	-	-	-
1	0.988 (±0.00010)	-	-	-
2	0.986 (±0.00007)	0.970 (±0.00034)	0.925 (±0.00034)	0.867 (±0.00115)
3	0.986 (±0.00055)	0.970 (±0.00050)	0.919 (±0.00032)	0.858 (±0.00058)
5	0.985 (±0.00096)	0.965 (±0.00058)	0.914 (±0.00077)	0.853 (±0.00048)
10	0.983 (±0.00057)	0.964 (±0.00000)	0.906 (±0.00097)	0.839 (±0.00181)
30	0.981 (±0.00206)	0.959 (±0.00223)	0.901 (±0.00342)	0.828 (±0.00028)
50	0.979 (±0.00244)	0.956 (±0.00342)	0.898 (±0.00460)	0.824 (±0.00033)

Note: Numbers in parentheses are standard errors.

substrate concentrations resulting in reduced total enzyme activity; hence a decreased rate of reaction and ultimately lower sugar yields. It was proposed that substrate inhibition might explain this phenomenon. Huang and Penner (1991) found that substrate inhibition occurred above 5 g cellulose/FPU of enzyme. The highest substrate to enzyme ratio employed throughout the experiments was 2 g cellulose/FPU of enzyme leading one to believe that substrate inhibition had no effect on the reaction rate. The hydrodynamics of the hydrolysis system may help explain the observed decrease in sugar yield at higher substrate concentrations. It was observed that the reaction mixtures of the 100-g/L experiments were a thick slurry (i.e., less free water). Cellulose is known to contain numerous microscopic and macroscopic capillary pores that tend to retain a large volume of water (i.e., measure of biomass swellability) (Mansfield et al., 1999). This can entrap a large portion of the water from the cellulose suspension, making it thicker and less mobile. Enhanced biomass swellability has been shown to enhance biomass digestibility with the caveat of sufficient aqueous mobile phase remaining in the reaction system to ensure adequate enzyme mobility. The lack of a mobile aqueous phase in the higher substrate concentration experiments may have led to diffusion limitations for the enzyme leading to reduced reaction rates at all enzyme loadings. More than likely, it was a combination of increased product inhibition and a reduced aqueous phase that led to lower sugar yields at the higher substrate concentration (100 g/L versus 50 g/L).

As stated previously, excess cellobiase (48 CBU/g dry biomass) was added to the reaction mixture to minimize cellobiose accumulation allowing the exclusive use of Equation 4. When cellobiase activity is high, inhibitory cellobiose is converted to glucose, which allows *i* to be close to unity. This is important because Holtzapple et al. (1990) have shown that cellobiose is 6 times more inhibitory than glucose for *Trichoderma reesei* cellulase. Table II shows inhibition parameters calculated using Equation 4 with a 0.00313 L/g glucose binding constant (β_1) for a *Trichoderma reesei* cellulase enzyme system (Holtzapple et al., 1990). As shown in Table II, the inhibition

parameter values decreased with increasing substrate concentration. This was expected because the higher substrate concentrations resulted in higher quantities of glucose, the only soluble product in a significant amount to elicit an inhibitory effect. Because the inhibition parameter is a measure of the fraction of enzyme that is active, it is desirable to have values that are closest to unity to ensure that the enzymes are being effectively utilized. Inhibition parameters calculated at a substrate concentration of 10 g/L were closest to unity, suggesting the measured reactivity reflects biomass chemical and physical features and is not influenced by product inhibition. Therefore, all experiments in "Enzymatic Hydrolysis of Model Samples" and "Predictive Ability of Neural Networks Study" will be conducted with a substrate concentration of 10 g/L as shown in Table III.

It has been shown that the slope (*B*) and intercept (*A*) are affected by the inhibition parameter *i*. When *i* increases, the intercept decreases and the slope increases. This causes an upward shift in the linear plot. Therefore, it is important to eliminate product inhibition to ensure slope and intercept parameter estimation reproducibility when using the linear form of the HCH-1 Model to predict enzymatic hydrolysis of biomass.

Table III. Recommended enzymatic hydrolysis conditions to ensure minimal product inhibition for subsequent experiments of model samples.

Variables	Recommended Values
Enzyme Loading	≤ 30 FPU/g dry biomass
Substrate Concentration	10 g/L
Cellobiase Loading	≥ 48 CBU/g dry biomass
Hydrolysis Time	1, 6, and 72 h

REACTION CONDITIONS STUDY

Purpose

The purpose of this study was to determine the range of substrate concentrations and enzyme loadings in which Equation 5 is valid. This will determine the reaction conditions employed for experiments conducted in "Enzymatic Hydrolysis of Model Samples" and "Predictive Ability of Neural Networks Study."

Materials and Methods

Substrate preparation, enzyme activity measurements, and enzymatic hydrolysis procedures were followed as described in "Inhibition Study."

Results and Discussion

The range of enzyme loadings and substrate concentrations over which Equation 5 could predict enzymatic hydrolysis was investigated by conducting experiments at 34 different combinations of enzyme loading and substrate concentration. The experiments were performed in triplicate. A plot of glucose yield versus the natural logarithm of enzyme loading is linear, as predicted by Equation 5. The ability to interpolate reducing sugar yield is illustrated in Figure 8 for cellulase loadings between 2 and 50 FPU/g dry biomass at substrate concentrations of 10, 20, 50, and 100 g/L and Figure 9 for cellulase loadings between 0.25 and 50 FPU/g dry biomass at a substrate concentration of 10 g/L. The linearity of Equation 5 has been observed over a 10-fold range in enzyme loading and a 3-fold range in substrate concentration (Mandels et al., 1981). Figures 8 and 9 demonstrate this linearity holds over a 10-fold range in substrate concentration and a 200-fold range in enzyme loading at a 10-g/L substrate concentration, respectively. This is significant because the ability to linearly interpolate sugar yields will substantially reduce the complexity of developing a nonparametric empirical model to predict enzymatic digestibility as described in "Neural Network Modeling of Structural Features Responsible for Enzymatic Digestibility."

It was discovered that the range over which Equation 5 could accurately predict enzymatic hydrolysis highly depends on the biomass inherent reactivity, which is defined by its chemical and physical features. This is best illustrated in Figures 10a and 10b in which the hydrolysis profiles are clearly a function of the inherent reactivity of the biomass (i.e., biomass structural features). Figure 10a shows that there are three distinct regions in a complete hydrolysis profile. The two nonlinear regions occur at extreme high (>90%) and low (<10%) conversions, which is expected due to the assumptions made in simplifying the HCH-1 Model into a linear form represented by Equation 5. At high and low conversions, the assumptions made to simplify the HCH-1 Model are no longer valid.

Figure 10b illustrates that the same biomass subjected to different degrees of pretreatment (i.e., not ball milled versus ball milled for 3 days) alters the slope (*B*) and intercept (*A*) of the linear region. Assuming that the change in slope and intercept is based solely on different structural features, this will be exploited to develop a model to predict *B* and *A* based solely on a sample's biomass structural features. It should be noted that once *B* and *A* are known, one can predict sugar conversion/yield by reconstructing a plot of sugar conversion/yield versus the natural logarithm of enzyme loading. The ability to predict conversion based exclusively on biomass structural features is a major step in improving the efficiency and economic viability of current biomass conversion technologies.

CONCLUSIONS

The studies indicate the inhibition pattern was noncompetitive, which agrees with the inhibition pattern used to develop the HCH-1 Model. Also, the degree of inhibition was lowest at a substrate concentration of 10 g/L. Reduced inhibition was experienced at lower substrate concentrations because of the reduced quantity of glucose in the reaction vessel. The range of enzyme loadings and substrate concentrations over which the simplified HCH-1 Model was valid for lime pretreated corn stover are 0.25–50 FPU/g dry biomass and 10–100 g/L, respectively.

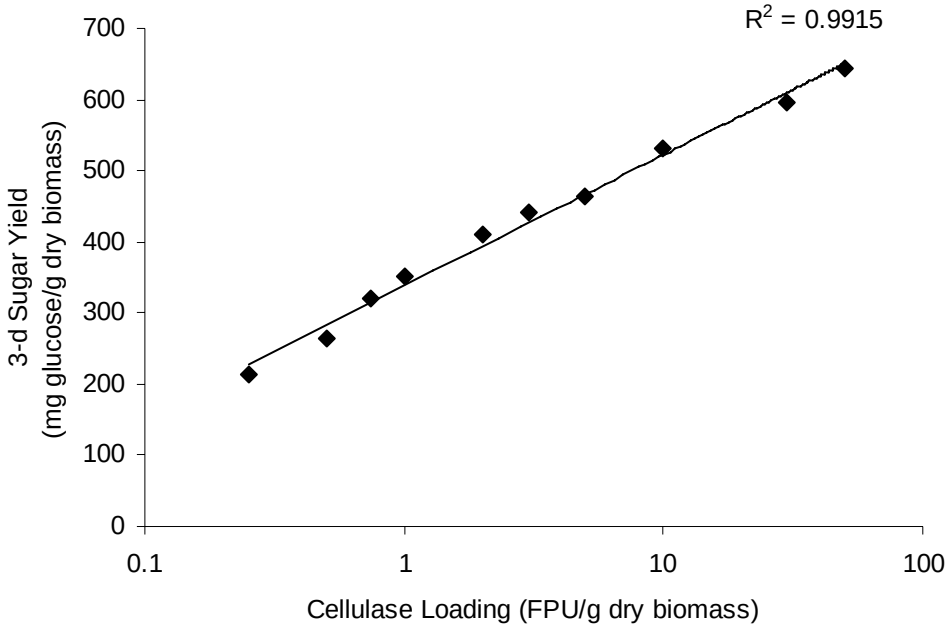

Figure 9. Hydrolysis profile of 3-d reducing sugar yields of lime-pretreated corn stover for the enzyme loading study. Hydrolysis conditions: 48 CBU/g biomass, 72 h, 0.25–50 FPU/g dry biomass.

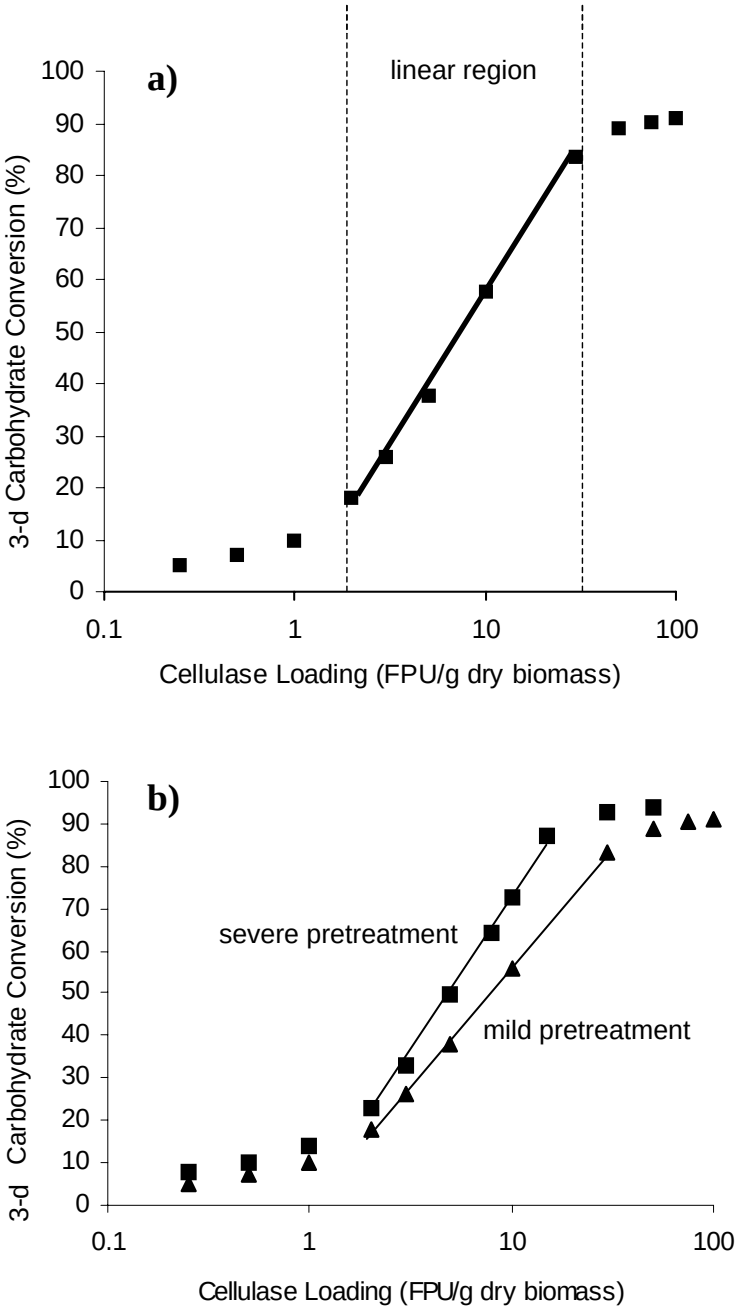

Figure 10. Complete hydrolysis profile illustrating (a) three distinct regions of hydrolysis and (b) two samples subjected to different degrees of pretreatment. Hydrolysis conditions: 10 g poplar wood/L, 0.25–100 FPU/g dry biomass, 48 CBU/g dry biomass, 72 h.

ENZYMATIC HYDROLYSIS OF MODEL SAMPLES

INTRODUCTION

Economically converting biomass to ethanol and/or organic acids would fulfill many goals such as providing a clean-burning fuel substitute to gasoline that does not add net carbon dioxide to the atmosphere, providing additional employment opportunities, and reducing the United States' dependence on unstable oil supplies (Holtzapple et al., 1994). To be economical, biomass conversion processes require either low pretreatment costs and/or low saccharification costs. Extensive pretreatment, which is costly, renders biomass highly digestible thereby lowering saccharification costs. Likewise, an abundance of enzymes, which are expensive, will thoroughly digest biomass thereby lowering the costs associated with necessary pretreatments. An optimum between the two costs exists, as shown in Figure 11. Finding the optimum point would allow for the design of more effective and less expensive pretreatment techniques, which currently accounts for roughly one-third of total production costs (Lynd et al., 1996).

Factors that affect the enzymatic hydrolysis of cellulose and hemicellulose include substrate characteristics, enzyme activity, and reaction conditions. Overcoming limitations to thoroughly hydrolyze biomass by enzymes has been the main focus of a massive amount of research since the early 1970s (Kadam et al., 2004; Mosier et al., 2004; Chang, 1999; Claeyssens et al., 1990; Lee and Fan, 1982; Holtzapple et al., 1990; Pere et al., 1995; Medve et al., 1998; Davies and Henrissat, 1995; Chang and Holtzapple, 2000; Ghose and Ghosh, 1978). Due to the heterogeneous nature of the biomass reaction system, direct physical contact between enzyme and substrate (i.e., cellulose and hemicellulose) is required. This means enzyme adsorption is a prerequisite to hydrolysis. The efficiency of enzyme adsorption has been shown to be a function of biomass structural features such as lignin (Sewalt et al., 1997a). Consequently, the efficiency of enzymes to hydrolyze complex lignocellulosic biomass is closely linked to

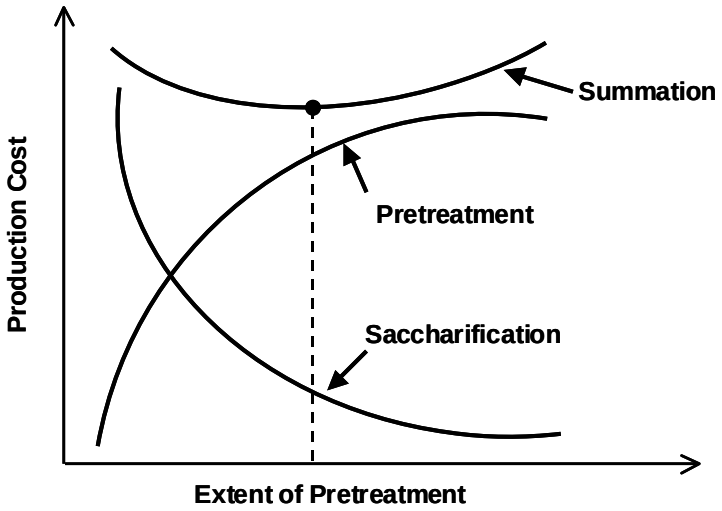

Figure 11. Diagram representing the balance between the two major costs associated with current biomass conversion processes.

the inherent structural characteristics of the substrate (Lee and Fan, 1982). Lee and Fan (1982) found that the various mass-transfer steps do not control the overall hydrolysis rate. Instead, it is mainly controlled by the surface reaction step promoted by the adsorbed enzyme. According to Cowling (1975), any structural feature that limits the accessibility of enzyme to substrate will diminish its susceptibility to hydrolysis. Several features deemed important in affecting enzymatic digestibility include lignin content, the presence of acetyl groups, cellulose crystallinity, degree of polymerization, surface area/pore volume of cellulose fiber, and particle size (Converse et al., 1990; Sewalt et al., 1997b; Wong et al., 1988; Chang, 1999). However, elucidating the relative importance of these structural features is complicated because of the complex nature of lignocellulosic biomass and the difficulty of studying the effect of individual structural features while holding all others constant.

Literature Review

The effect of structural features on enzymatic digestibility has been investigated since the 1950s (Walseth, 1952; Sullivan, 1959; Mansfield et al., 1999; Chang and Holtzapple, 2000; Kong et al., 1992; Lee and Fan, 1982). Conventionally, structural features have been divided into two groups and classified as physical or chemical. The chemical structural features consist of hemicellulose, lignin, cellulose, and acetyl groups bound to hemicellulose. The physical structural features consist of crystallinity, pore size, surface area, degree of polymerization, and the biomass particle size. Much work has been conducted to elucidate the effect of structural features on biomass digestibility as is summarized in Table IV. It appears that the most attention has been devoted to lignin and cellulose crystallinity with a lesser degree towards acetyl groups, particle size, degree of polymerization, and surface area.

Researchers have reported conflicting results regarding the relationship between biomass digestibility and crystallinity. Crystallinity has been shown to both improve and impede the enzymatic hydrolysis of biomass. Native biomass contains cellulose with crystalline regions interspersed with amorphous regions. Some groups have found that

crystallinity has a major inverse affect on enzymatic hydrolysis (Chang and Holtzapple 2000; Fan et al., 1980; Mansfield el al., 1999; Bertran and Dale, 1985; Sinitsyn et al., 1991; Koullas et al., 1992; Thompson et al., 1992; Gharpuray et al., 1983; Weimer and Weston, 1985; Rivers and Emert, 1988). However, others have reported that additional structural features may play a more prominent role in affecting biomass digestibility, such as surface area (Puri, 1984; Caulfield and Moore, 1974; Grethlein, 1985; Lee and Fan, 1982; Nazhad et al., 1995), degree of polymerization (Puri, 1984; Nazhad et al., 1995), and particle size (Caulfield and Moore, 1974; Puri, 1984; Rivers and Emert, 1988; Sangseethong et al., 1998).

Numerous researchers have reported improved digestibility with increasing lignin removal. The extent to which increasing a substrate's surface area increases its digestibility appears to be influenced by its lignin content (Wong et al., 1988). The lignin studies have all demonstrated the inhibitory effect lignin has on enzyme adsorption and subsequent enzymatic hydrolysis (Saddler et al., 1998; Gharpuray et al., 1983; Kong et al., 1992; Koullas et al., 1992; Vinzant et al., 1997; Thompson et al., 1992; Sewalt et al., 1997a; Sewalt et al., 1997b; Fan et al., 1981b). However, others have concluded that lignin removal is not necessary to achieve effective biomass hydrolysis (Grohmann et al., 1989). One thing to note is that most lignin removal techniques alter other biomass structural features making it difficult to isolate the role of lignin removal in cellulose hydrolysis.

The enzymatic hydrolysis of wood holocelluloses (delignified biomass) has been shown to depend on acetyl removal (Sinner et al., 1979). Native hemicellulose is extensively acetylated (CH_3COO-), with about 70% of xylan residues containing acetyl groups (Browning, 1967). The removal of acetyl groups from hemicellulose has been shown to improve enzymatic digestibility of biomass through increased swellability (Kong et al., 1992; Grohmann et al., 1989; Weimer and Weston, 1985). The hypothesis is that acetyl groups sterically hinder enzyme activity. Specifically, removal of acetyl groups with minimal alteration of lignin resulted in a 5–7 fold and 2–3 fold increase in xylan digestion and cellulose digestion, respectively (Grohmann et al., 1989).

Table IV. Overview of correlation between structural features and digestibility.

Study (Biomass)	Structural Features[a]							Correlation[b]
	CrI	DP	SSA	Lignin	OAc	HC	PS	
Fan et al., 1981a (solka floc)	×		×					$X_8=0.38(SSA)^{0.195}(100\text{-}CrI)^{1.04}$
Lee and Fan, 1982 (solka floc)	×		×					CrI=inverse; SSA=linear
Gharpuray et al., 1983 (wheat straw)	×		×	×				$D=2.04SSA^{0.99}(100\text{-}CrI)^{0.26}L^{-0.39}$
Puri, 1984 (bagasse, wheat straw, wood, cotton)	×	×	×				×	PS, DP=inverse; SSA=linear CrI=n/c
Bertran and Dale, 1985 (celluloses)	×							CrI=inverse
Sinitsyn et al., 1991 (cellulose, bagasse)	×	×	×				×	SSA=linear; CrI=linear (cellulose) PS, DP=n/c
Kong et al., 1992 (aspen wood)				×	×	×		L, OAc=inverse; HC=n/c
Nazhad et al., 1995 (pulped spruce)	×	×	×					DP,CrI=inverse; SSA=linear
Gregg and Saddler, 1996 (woods)				×				L=inverse
Tarantili et al., 1996 (celluloses)	×			×				CrI, L=inverse
Sewalt et al., 1997a (grasses)				×				L=inverse
Saddler et al., 1998 (douglass fir)				×				L=inverse
Chang, 1999 (poplar wood)	×			×	×			CrI, L, OAc=inverse

[a] CrI=crystallinity, DP=degree of polymerization, SSA=specific surface area, OAc=acetyl, HC=hemicellulose, PS=particle size.

[b] D=digestibility, X=conversion, n/c=no correlation.

Previous studies had limitations that bring into question the validity of the effect the structural features were reported to have on biomass enzymatic hydrolysis. Most studies were not extensive enough in the number of samples employed. Additionally, the narrow range of structural features, biomass types, and pretreatment types that were used in the studies may have led to reduced model predictions. Another major limitation is that types of biomass other than those from which the models were derived were not used to test the model's predictive ability. Therefore, the versatility and range of predictive ability of previous models are unknown. Maybe the most significant limitation to prior studies is they do not address cross effects between structural features that may have occurred during pretreatment. This may lead to a masking of the true underlying feature that may affect biomass digestibility. It was observed that lime (Kim, 2004) and aqueous ammonia (Kim et al., 2003) pretreatments alter both lignin content as well as acetyl content. Wong et al. (1988) reported increased fiber swelling due to lignin removal resulting in a larger surface area upon wetting. Therefore, when investigating a particular structural feature, pretreatments that alter only one feature while leaving all others unchanged should be employed. Studies that have not considered the possible change of other structural features while altering the target feature may result in misleading information. This may be one of the reasons why researchers have arrived at conflicting conclusions regarding the affect of crystallinity, lignin, particle size, and surface area on biomass digestibility. Kong et al. (1992), Chang (1999), and Sangseethong et al. (1998) are a few of the researchers that have attempted to account for the interaction of structural features when pretreating biomass. As a result, a comprehensive study of the structural features that elicit a major effect on enzymatic hydrolysis of biomass is needed to conclusively determine a dependable relationship between the structural features and digestibility. Theoretically, it is possible to predict the enzymatic digestibility of lignocellulosic biomass if the function of chemical and physical features that determine digestibility can be modeled (Chang and Holtzapple, 2000). This would allow for the design of more effective and less expensive pretreatment techniques.

OBJECTIVES

The objective of this study was to perform enzymatic hydrolysis of the 147 poplar wood model samples to determine their degree of digestibility. The resulting sugars were analyzed via HPLC and slopes (*B*) and intercepts (*A*) were determined according to Equation 5. It should be noted that the slopes and intercepts were determined by plotting conversion versus the natural logarithm of enzyme loading.

ENZYMATIC HYDROLYSIS STUDY

Purpose

The purpose of this study was to investigate the effects biomass structural features (lignin content, acetyl content, and crystallinity) have on digestibility (i.e., slopes and intercepts).

Materials and Methods

Substrate Preparation

Chang (1999) prepared 147 poplar wood model samples with a variety of lignin contents (0.7–26.3%), acetyl contents (0.1–3.1%), and crystallinities (5.4–68.8%) as illustrated in Figure 12 and Table V. The structural features of the samples were directly manipulated via selective delignification with peracetic acid, selective deacetylation with KOH, and selective decrystallization with ball milling. The pretreatment techniques were selected to minimize cross effects. The effect of lignin removal on acetyl content and the effect of acetyl removal on lignin content are summarized in Figure 13. Ball-milling was an extremely effective method for reducing biomass crystallinity due to the crushing and shearing action of the zirconia grinding medium (Fan et al., 1981b). Although crystallinity has been reported to be less important than the removal of lignin on sugar yield (Fan et al., 1981a; Millet and Baker, 1975), ball milling decreases particle size and increases the surface area of cellulose fiber (Gharpuray et al., 1983).

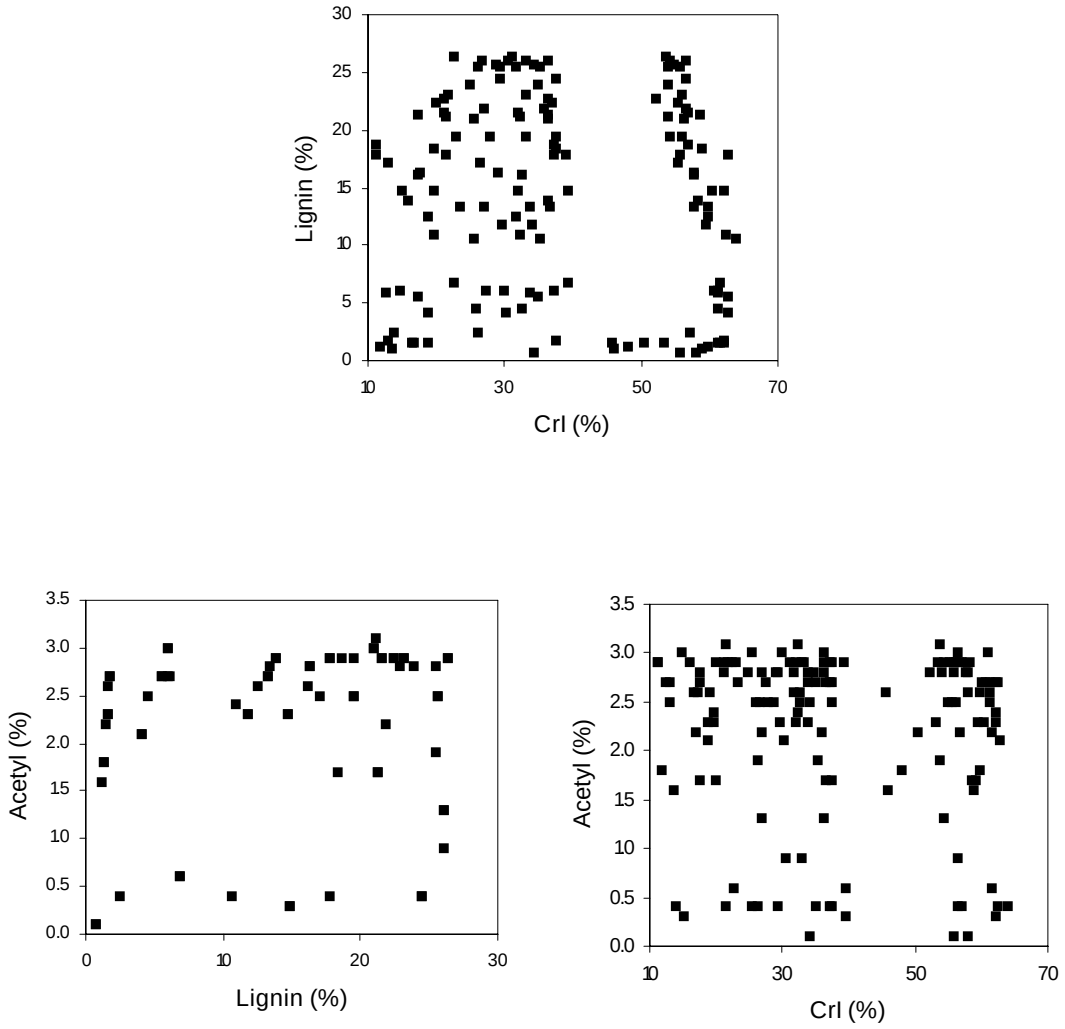

Figure 12. Structural features distribution of poplar wood model samples. Data are taken from Table V.

Table V. Summary of structural features and carbohydrate contents of the 147 poplar wood model samples.

Sample No.	Sample Description	Structural Features (%)				Carbohydrate Content[a,b] (%)		
		Lignin[a,b]	Acetyl[a,b]	Biomass CrI[c]	Cellulose CrI[d]	Glucan	Xylan	Total[e]
1	DL00-DA000-DC0	26.3	2.9	55.4	62.4	44.4	13.9	58.3
2	DL00-DA000-DC3	26.3	2.9	29.4	33.9	44.4	13.9	58.3
3	DL00-DA000-DC6	26.3	2.9	14.9	18.0	44.4	13.9	58.3
4	DL00-DA007-DC0	25.5	2.8	57.3	65.1	46.6	14.5	61.1
5	DL00-DA007-DC3	25.5	2.8	32.1	37.4	46.6	14.5	61.1
6	DL00-DA007-DC6	25.5	2.8	20.3	24.5	46.6	14.5	61.1
7	DL00-DA015-DC0	25.6	2.5	57.8	65.3	46.0	14.2	60.2
8	DL00-DA015-DC3	25.6	2.5	27.5	32.1	46.0	14.2	60.2
9	DL00-DA015-DC6	25.6	2.5	18.9	22.6	46.0	14.2	60.2
10	DL00-DA035-DC0	25.5	1.9	56.3	64.1	47.0	14.7	61.7
11	DL00-DA035-DC3	25.5	1.9	25.2	30.0	47.0	14.7	61.7
12	DL00-DA035-DC6	25.5	1.9	20.4	24.8	47.0	14.7	61.7
13	DL00-DA055-DC0	26.0	1.3	56.0	63.5	46.4	14.4	60.8
14	DL00-DA055-DC3	26.0	1.3	32.8	38.1	46.4	14.4	60.8
15	DL00-DA055-DC6	26.0	1.3	12.5	15.8	46.4	14.4	60.8
16	DL00-DA075-DC0	26.0	0.9	60.0	68.3	47.5	14.8	62.3
17	DL00-DA075-DC3	26.0	0.9	21.6	26.2	47.5	14.8	62.3
18	DL00-DA075-DC6	26.0	0.9	9.9	13.3	47.5	14.8	62.3
19	DL00-DA150-DC0	24.5	0.4	66.2	74.3	49.2	13.9	63.1
20	DL00-DA150-DC3	24.5	0.4	31.2	35.9	49.2	13.9	63.1
21	DL00-DA150-DC6	24.5	0.4	27.3	31.6	49.2	13.9	63.1
22	DL01-DA000-DC0	23.9	2.8	60.2	68.5	47.3	14.8	62.1
23	DL01-DA000-DC3	23.9	2.8	25.9	30.9	47.3	14.8	62.1
24	DL01-DA000-DC6	23.9	2.8	8.2	11.5	47.3	14.8	62.1
25	DL01-DA007-DC0	23.1	2.9	60.4	68.6	46.4	14.6	61.0
26	DL01-DA007-DC3	23.1	2.9	16.4	20.3	46.4	14.6	61.0
27	DL01-DA007-DC6	23.1	2.9	13.9	17.5	46.4	14.6	61.0
28	DL01-DA015-DC0	22.8	2.8	59.8	68.3	47.3	15.0	62.3

Table V. Continued

Sample No.	Sample Description	Structural Features (%)				Carbohydrate Content[a,b] (%)		
		Lignin[a,b]	Acetyl[a,b]	Biomass CrI[c]	Cellulose CrI[d]	Glucan	Xylan	Total[e]
29	DL01-DA015-DC3	22.8	2.8	22.7	27.6	47.3	15.0	62.3
30	DL01-DA015-DC6	22.8	2.8	14.0	18.0	47.3	15.0	62.3
31	DL01-DA035-DC0	22.4	2.9	60.0	68.3	47.8	14.8	62.6
32	DL01-DA035-DC3	22.4	2.9	27.0	32.1	47.8	14.8	62.6
33	DL01-DA035-DC6	22.4	2.9	22.0	26.6	47.8	14.8	62.6
34	DL01-DA055-DC0	21.8	2.2	55.7	64.0	48.6	15.2	63.8
35	DL01-DA055-DC3	21.8	2.2	24.8	30.1	48.6	15.2	63.8
36	DL01-DA055-DC6	21.8	2.2	14.8	19.1	48.6	15.2	63.8
37	DL01-DA075-DC0	21.3	1.7	60.8	69.4	48.9	15.0	63.9
38	DL01-DA075-DC3	21.3	1.7	21.1	25.8	48.9	15.0	63.9
39	DL01-DA075-DC6	21.3	1.7	17.3	21.6	48.9	15.0	63.9
40	DL01-DA150-DC0	17.8	0.4	68.8	78.4	54.9	15.3	70.2
41	DL01-DA150-DC3	17.8	0.4	28.3	34.0	54.9	15.3	70.2
42	DL01-DA150-DC6	17.8	0.4	18.8	23.6	54.9	15.3	70.2
43	DL02-DA000-DC0	21.5	2.9	59.3	67.5	47.5	14.8	62.3
44	DL02-DA000-DC3	21.5	2.9	19.0	23.3	47.5	14.8	62.3
45	DL02-DA000-DC6	21.5	2.9	16.0	20.0	47.5	14.8	62.3
46	DL02-DA007-DC0	21.1	3.1	58.9	67.5	48.4	15.2	63.6
47	DL02-DA007-DC3	21.1	3.1	23.3	28.4	48.4	15.2	63.6
48	DL02-DA007-DC6	21.1	3.1	12.8	16.9	48.4	15.2	63.6
49	DL02-DA015-DC0	20.9	3.0	59.0	67.6	47.9	15.2	63.1
50	DL02-DA015-DC3	20.9	3.0	27.4	32.9	47.9	15.2	63.1
51	DL02-DA015-DC6	20.9	3.0	27.4	32.9	47.9	15.2	63.1
52	DL02-DA035-DC0	19.5	2.9	59.4	68.1	48.7	15.3	64.0
53	DL02-DA035-DC3	19.5	2.9	26.5	32.0	48.7	15.3	64.0
54	DL02-DA035-DC6	19.5	2.9	22.0	27.1	48.7	15.3	64.0
55	DL02-DA055-DC0	19.5	2.5	61.8	70.8	49.2	15.4	64.6
56	DL02-DA055-DC3	19.5	2.5	25.2	30.7	49.2	15.4	64.6
57	DL02-DA055-DC6	19.5	2.5	23.0	28.3	49.2	15.4	64.6
58	DL02-DA075-DC0	18.4	1.7	61.4	70.6	50.0	15.6	65.6

Table V. Continued

Sample No.	Sample Description	Structural Features (%)				Carbohydrate Content[a,b] (%)		
		Lignin[a,b]	Acetyl[a,b]	Biomass CrI[c]	Cellulose CrI[d]	Glucan	Xylan	Total[e]
59	DL02-DA075-DC3	18.4	1.7	28.5	34.5	50.0	15.6	65.6
60	DL02-DA075-DC6	18.4	1.7	9.2	13.3	50.0	15.6	65.6
61	DL02-DA150-DC0	14.8	0.3	66.4	76.0	55.8	15.5	71.3
62	DL02-DA150-DC3	14.8	0.3	30.1	36.1	55.8	15.5	71.3
63	DL02-DA150-DC6	14.8	0.3	9.6	13.7	55.8	15.5	71.3
64	DL03-DA000-DC0	18.7	2.9	61.2	70.3	49.3	15.5	64.8
65	DL03-DA000-DC3	18.7	2.9	23.5	28.9	49.3	15.5	64.8
66	DL03-DA000-DC6	18.7	2.9	9.8	13.9	49.3	15.5	64.8
67	DL03-DA007-DC0	17.8	2.9	62.5	72.0	50.1	15.8	65.9
68	DL03-DA007-DC3	17.8	2.9	30.8	37.2	50.1	15.8	65.9
69	DL03-DA007-DC6	17.8	2.9	10.5	14.9	50.1	15.8	65.9
70	DL03-DA015-DC0	17.1	2.5	61.9	71.4	50.0	15.9	65.9
71	DL03-DA015-DC3	17.1	2.5	23.5	29.3	50.0	15.9	65.9
72	DL03-DA015-DC6	17.1	2.5	10.4	14.9	50.0	15.9	65.9
73	DL03-DA035-DC0	16.3	2.8	61.9	71.5	50.5	16.0	66.5
74	DL03-DA035-DC3	16.3	2.8	24.6	30.6	50.5	16.0	66.5
75	DL03-DA035-DC6	16.3	2.8	14.2	19.2	50.5	16.0	66.5
76	DL03-DA055-DC0	16.2	2.6	62.9	72.6	51.2	16.0	67.2
77	DL03-DA055-DC3	16.2	2.6	22.6	28.4	51.2	16.0	67.2
78	DL03-DA055-DC6	16.2	2.6	12.0	16.8	51.2	16.0	67.2
79	DL03-DA075-DC0	14.7	2.3	63.0	73.2	53.1	16.5	69.6
80	DL03-DA075-DC3	14.7	2.3	23.7	30.1	53.1	16.5	69.6
81	DL03-DA075-DC6	14.7	2.3	20.4	26.4	53.1	16.5	69.6
82	DL03-DA150-DC0	10.6	0.4	67.2	77.3	59.6	16.0	75.6
83	DL03-DA150-DC3	10.6	0.4	34.2	41.1	59.6	16.0	75.6
84	DL03-DA150-DC6	10.6	0.4	26.0	32.1	59.6	16.0	75.6
85	DL05-DA000-DC0	13.9	2.9	57.4	66.9	51.9	16.4	68.3
86	DL05-DA000-DC3	13.9	2.9	19.0	24.8	51.9	16.4	68.3
87	DL05-DA000-DC6	13.9	2.9	9.5	14.4	51.9	16.4	68.3
88	DL05-DA007-DC0	13.4	2.8	60.5	70.5	53.5	16.6	70.1

Table V. Continued

Sample No.	Sample Description	Structural Features (%)				Carbohydrate Content[a,b] (%)		
		Lignin[a,b]	Acetyl[a,b]	Biomass CrI[c]	Cellulose CrI[d]	Glucan	Xylan	Total[e]
89	DL05-DA007-DC3	13.4	2.8	25.3	31.9	53.5	16.6	70.1
90	DL05-DA007-DC6	13.4	2.8	24.0	30.5	53.5	16.6	70.1
91	DL05-DA015-DC0	13.3	2.7	62.1	72.2	52.7	16.5	69.2
92	DL05-DA015-DC3	13.3	2.7	24.1	30.5	52.7	16.5	69.2
93	DL05-DA015-DC6	13.3	2.7	11.9	17.1	52.7	16.5	69.2
94	DL05-DA035-DC0	12.5	2.6	61.7	72.0	53.7	16.8	70.5
95	DL05-DA035-DC3	12.5	2.6	25.9	32.8	53.7	16.8	70.5
96	DL05-DA035-DC6	12.5	2.6	12.7	18.3	53.7	16.8	70.5
97	DL05-DA055-DC0	11.8	2.3	65.6	76.2	54.2	16.7	70.9
98	DL05-DA055-DC3	11.8	2.3	25.6	32.3	54.2	16.7	70.9
99	DL05-DA055-DC6	11.8	2.3	25.6	32.3	54.2	16.7	70.9
100	DL05-DA075-DC0	10.9	2.4	65.9	76.7	56.0	16.9	72.9
101	DL05-DA075-DC3	10.9	2.4	23.9	30.7	56.0	16.9	72.9
102	DL05-DA075-DC6	10.9	2.4	21.0	27.5	56.0	16.9	72.9
103	DL05-DA150-DC0	6.8	0.6	67.7	78.2	63.6	16.3	79.9
104	DL05-DA150-DC3	6.8	0.6	39.0	46.7	63.6	16.3	79.9
105	DL05-DA150-DC6	6.8	0.6	24.6	30.9	63.6	16.3	79.9
106	DL10-DA000-DC0	6.1	2.7	66.1	77.5	57.0	17.5	74.5
107	DL10-DA000-DC3	6.1	2.7	21.1	28.1	57.0	17.5	74.5
108	DL10-DA000-DC6	6.1	2.7	17.5	24.2	57.0	17.5	74.5
109	DL10-DA007-DC0	6.0	3.0	65.3	76.5	58.7	17.3	76.0
110	DL10-DA007-DC3	6.0	3.0	28.9	36.5	58.7	17.3	76.0
111	DL10-DA007-DC6	6.0	3.0	14.7	20.9	58.7	17.3	76.0
112	DL10-DA015-DC0	5.9	2.7	66.0	77.1	59.1	17.2	76.3
113	DL10-DA015-DC3	5.9	2.7	32.0	39.8	59.1	17.2	76.3
114	DL10-DA015-DC6	5.9	2.7	17.0	23.4	59.1	17.2	76.3
115	DL10-DA035-DC0	5.6	2.7	66.3	76.9	58.7	16.6	75.3
116	DL10-DA035-DC3	5.6	2.7	32.1	39.4	58.7	16.6	75.3
117	DL10-DA035-DC6	5.6	2.7	15.1	20.7	58.7	16.6	75.3
118	DL10-DA055-DC0	4.5	2.5	68.3	79.2	60.9	16.7	77.6

Table V. Continued

Sample No.	Sample Description	Structural Features (%)				Carbohydrate Content[a,b] (%)		
		Lignin[a,b]	Acetyl[a,b]	Biomass CrI[c]	Cellulose CrI[d]	Glucan	Xylan	Total[e]
119	DL10-DA055-DC3	4.5	2.5	32.1	39.5	60.9	16.7	77.6
120	DL10-DA055-DC6	4.5	2.5	27.9	34.9	60.9	16.7	77.6
121	DL10-DA075-DC0	4.1	2.1	67.5	78.2	61.0	16.6	77.6
122	DL10-DA075-DC3	4.1	2.1	26.0	32.7	61.0	16.6	77.6
123	DL10-DA075-DC6	4.1	2.1	21.2	27.4	61.0	16.6	77.6
124	DL10-DA150-DC0	2.5	0.4	62.7	72.5	70.4	16.1	86.5
125	DL10-DA150-DC3	2.5	0.4	22.4	28.3	70.4	16.1	86.5
126	DL10-DA150-DC6	2.5	0.4	19.5	25.1	70.4	16.1	86.5
127	DL50-DA000-DC0	1.8	2.7	68.8	79.8	67.0	16.8	83.8
128	DL50-DA000-DC3	1.8	2.7	37.0	44.9	67.0	16.8	83.8
129	DL50-DA000-DC6	1.8	2.7	5.4	10.3	67.0	16.8	83.8
130	DL50-DA007-DC0	1.6	2.6	68.2	77.9	70.2	15.4	85.6
131	DL50-DA007-DC3	1.6	2.6	46.9	54.5	70.2	15.4	85.6
132	DL50-DA007-DC6	1.6	2.6	21.5	26.6	70.2	15.4	85.6
133	DL50-DA015-DC0	1.6	2.3	65.7	74.7	70.9	15.0	85.9
134	DL50-DA015-DC3	1.6	2.3	50.6	58.2	70.9	15.0	85.9
135	DL50-DA015-DC6	1.6	2.3	19.2	23.7	70.9	15.0	85.9
136	DL50-DA035-DC0	1.5	2.2	64.6	72.9	71.7	14.3	86.0
137	DL50-DA035-DC3	1.5	2.2	48.0	54.7	71.7	14.3	86.0
138	DL50-DA035-DC6	1.5	2.2	14.9	18.3	71.7	14.3	86.0
139	DL50-DA055-DC0	1.3	1.8	65.4	73.6	72.7	14.1	86.8
140	DL50-DA055-DC3	1.3	1.8	47.1	53.5	72.7	14.1	86.8
141	DL50-DA055-DC6	1.3	1.8	11.7	14.6	72.7	14.1	86.8
142	DL50-DA075-DC0	1.1	1.6	62.3	70.4	73.1	14.4	87.5
143	DL50-DA075-DC3	1.1	1.6	44.8	51.2	73.1	14.4	87.5
144	DL50-DA075-DC6	1.1	1.6	10.8	13.9	73.1	14.4	87.5
145	DL50-DA150-DC0	0.7	0.1	66.0	75.2	76.5	15.1	91.6
146	DL50-DA150-DC3	0.7	0.1	50.9	58.6	76.5	15.1	91.6
147	DL50-DA150-DC6	0.7	0.1	33.0	39.0	76.5	15.1	91.6

Table V. Continued

a The chemical composition of the ball-milled samples was assumed to be the same as the delignified and deacetylated samples.

b Based on dry weight at 105^{o}C.

c Biomass crystallinity measured by X-ray powder diffraction at the XRD Laboratory, Department of Chemistry, Texas A&M University.

d As explained in "Predicting Cellulose Crystallinity," cellulose crystallinity was predicted based on a empirical relationship developed in SAS as given by the following expression:

CrIc = 1.09734 (CrIb) + 0.93874 (Xylan content) – 11.43285

e Total carbohydrate is equal to the summation of the glucan and xylan components.

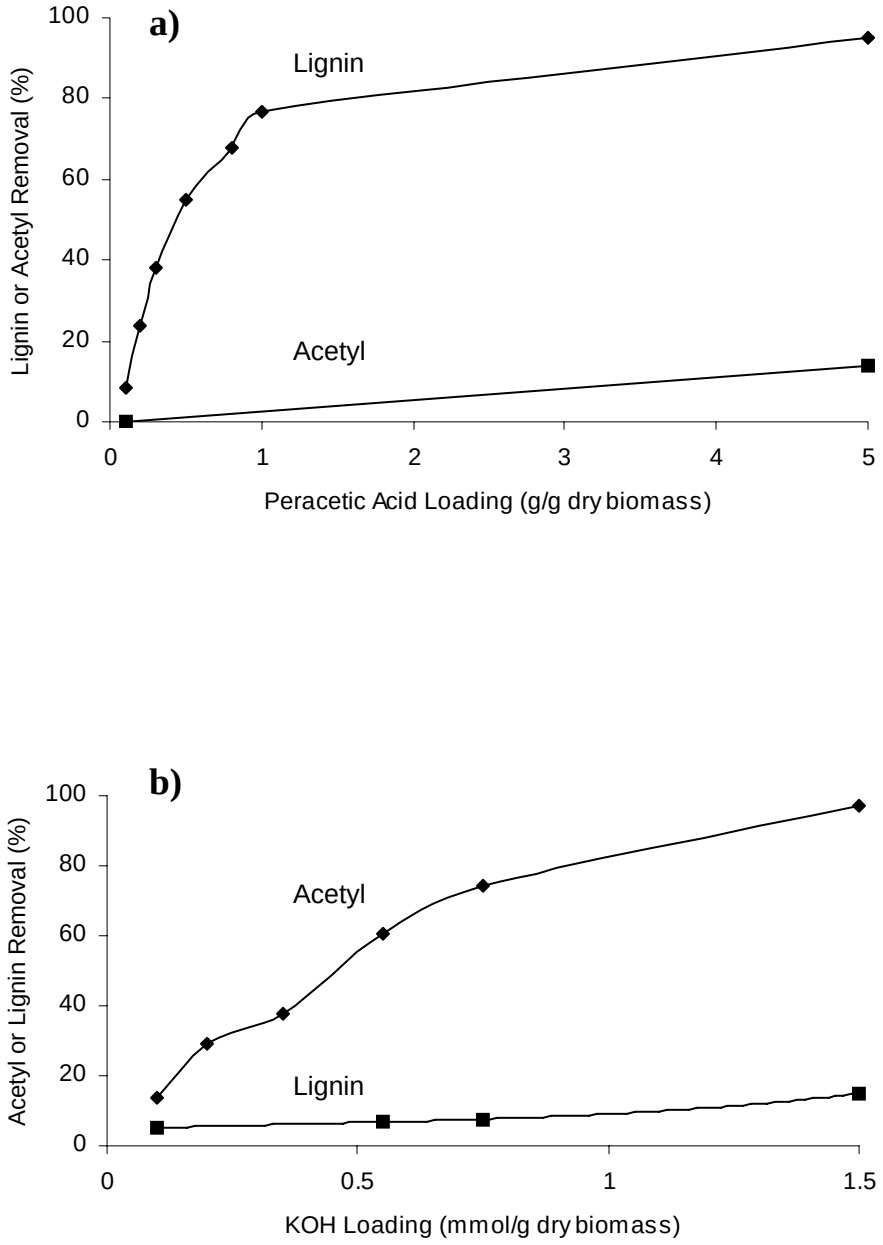

Figure 13. Effects of peracetic acid and KOH loading on (a) delignification and (b) deacetylation, respectively (Chang, 1999).

It was discovered that 58 of the 147 model samples that were subjected to ball milling had been exhausted in a prior study. Therefore, 58 non-milled samples were subjected to either 3- or 6-d ball milling. The rotary ball mill was built with two 1/6-hp 156-rpm AC gearmotors (Dayton Electric Mfg. Co., Niles, IL). The ball mill consists of four 1-in diameter × 25-in long steel blower shafts enclosed with 1.5-in O.D. Buna-N rubber tubing (McMaster-Carr, Atlanta, GA). A 300-mL porcelain jar was charged with 0.375-in zirconia grinding medium (U.S. Stoneware, East Palestine, OH) to ~50% of the jar volume (~258 g of zirconia). Biomass was placed in the jar to fill the void volume between the balls. The ratio of grinding medium to biomass was 43 g zirconia/g dry biomass. Then, the jars were placed between the rollers and rotated at 68 rpm for either 3 or 6 d.

Crystallinity Measurements

Biomass crystallinity was measured by the X-ray Diffraction Laboratory, Department of Chemistry, Texas A&M University using a Bruker-AXS Powder High Resolution X-Ray Diffractometer. The biomass was packed in the depression of an aluminum sample holder flush to the top. The sample was scanned at 2°/min from 2θ = 10° to 26° with a step size of 0.05°. The biomass crystallinity index (CrIb) was determined as the percentage of crystalline material in the biomass (Segal et al., 1959).

$$CrIb = \frac{I_{002} - I_{am}}{I_{002}} \times 100 \quad (7)$$

In this equation, CrIb expresses the relative degree of crystallinity, I_{002} is the maximum intensity of the 002 peak at 2θ = 22.5°and I_{am} is the intensity at 2θ = 18.7°. Figure 14 illustrates a typical diffraction pattern of poplar wood that was not ball milled.

Enzyme Preparation

To verify the activity of the *Trichoderma reesei* cellulase preparation received from NREL, a filter paper assay was performed according to NREL standard procedure No. 006. The filter paper activity of the cellulase was 65 FPU/mL enzyme. Cellobiase

activity (Novozym 188, Novo Nordisk Biochem) determined by Novo Nordisk was 321 CBU/mL based on the company's assay.

Enzymatic Hydrolysis

The experiments were performed in 50-mL Erlenmeyer flasks with 0.2 g dry weight of pretreated poplar wood, 18 mL of distilled water, 1.0 mL of 1 *M* citrate buffer and 0.6 mL of 0.01 g/L sodium azide (NaN_3) solution, and placed inside a 100-rpm air-bath shaker at 50^{o}C. Citrate buffer and sodium azide were added to keep the pH constant (pH = 4.8) and prevent the growth of microorganisms, respectively. When the reaction slurry temperature reached 50^{o}C (~ 1 h), the hydrolysis was initiated by adding 0.2 mL of appropriately diluted cellulase (activity = 65 FPU/mL) and 0.05 mL of cellobiase (activity = 321 CBU/g). It was discovered that the same range of enzyme loadings could not be used for all samples. The inherent reactivity of the biomass samples affected the range over which Equation 5 was valid. Therefore, the 147 samples were divided into three classes (low, medium, and high) based on their inherent reactivity. Table VI summarizes the range of enzyme loadings in which the three classes of biomass exhibit a linear profile as predicted by Equation 5. The detailed procedure for enzymatic hydrolysis is given in Appendix A.

Samples were removed after the desired incubation time of 1, 6, or 72 h. These times were chosen because 1-h samples are indicative of the initial rates of digestion, 72-h samples indicate the extent of reaction, and it was discovered that 6 h is when approximately 50% of the carbohydrates had been digested. The incubation times were selected to determine the role the structural features play in digestibility with changes in hydrolysis time. After removal, the Erlenmeyer flasks were boiled for 15 minutes to denature the enzymes thereby quenching the reaction. The reaction slurry was transferred to 15-mL conical centrifuge tubes, centrifuged, and the supernatant was frozen until sugar analysis was performed. (Note: When thawed, the samples were well mixed to ensure uniform concentration).

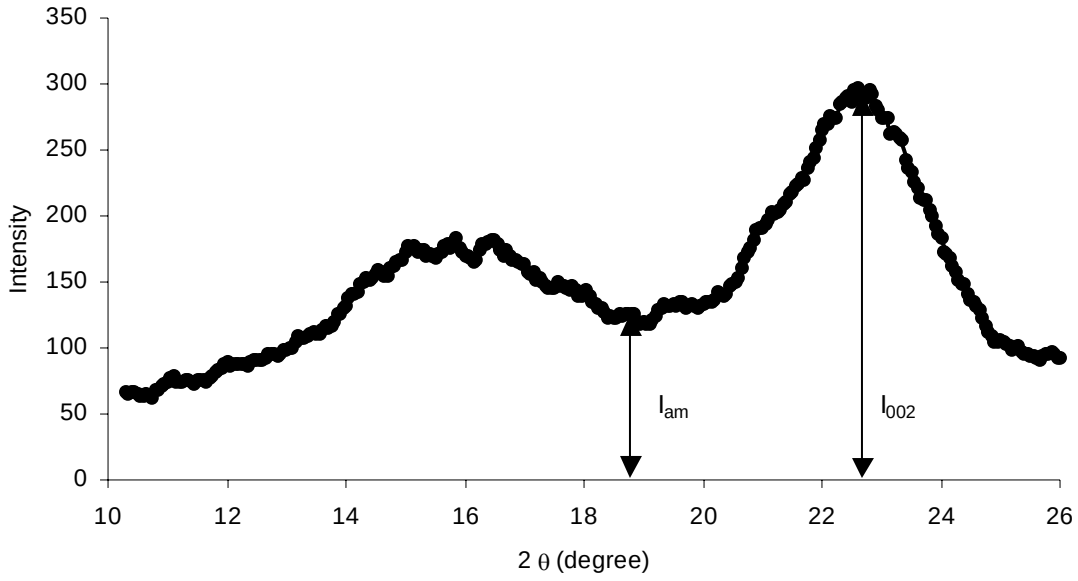

Figure 14. Typical X-ray diffraction pattern of chemically treated, but not ball milled, poplar wood. CrIb = 58.8%.

Table VI. Enzyme loadings employed for the 147 poplar wood model samples in "Enzymatic Hydrolysis of Model Samples" and the 22 prediction samples in "Predictive Ability of Neural Network Model."

Biomass Classification	Enzyme Loading (FPU/g dry biomass)		
	1 h	6 h	72 h
Low[a]	1, 5, 30	1, 5, 30	1, 5, 30
Medium[b]	1, 3, 10	1, 3, 10	0.5, 1.5, 5
High[c]	1, 3, 10	1, 3, 10	0.25, 0.75, 2

[a] Conversion < 60%; yield < 400 mg/g biomass

[b] Conversion > 60%; 400 ≤ yield ≤ 800

[c] Conversion > 60%; yield > 800

Analyses

The hydrolysis products, glucose, xylose and cellobiose, were determined by high performance liquid chromatography (HPLC) with a Biorad Aminex HPX-87P column with 0.2-μm filtered reverse osmosis deionized water as the mobile phase. The column temperature was 85°C and flow rate was 0.6 mL/min. The equipment used for HPLC analysis was as follows:

Pump: LDC Analytical Pump, constaMetric 3200

Autosampler: Spectra-Physics, AS 100

Column Heater: Jones Chromatography

RI Detector: Lab Alliance RI 2000

Software: PeakSimple 3.21, SRI Instruments

The detailed procedure for HPLC sugar analysis is given in Appendix B. Knowing the carbohydrate contents in each of the poplar wood model samples and the sugar yields of the samples, the glucan, xylan, and total sugar conversions were calculated as follows:

$$X_G = \frac{([G]-[G_0])\times V \times 0.9}{W \times \text{glucan content} \times 1000\ \text{mg/g}} \times 100 \tag{8}$$

$$X_X = \frac{([X]-[X_0])\times V \times 0.9}{W \times \text{xylan content} \times 1000\ \text{mg/g}} \times 100 \tag{9}$$

$$X_T = \frac{X_G \times \frac{\text{glucan content}}{0.9} + X_X \times \frac{\text{xylan content}}{0.88}}{\frac{\text{glucan content}}{0.9} + \frac{\text{xylan content}}{0.88}} \times 100 \tag{10}$$

where

X_G = 1-, 6-, or 72-h glucan conversion (%)

X_X = 1-, 6-, or 72-h xylan conversion (%)

X_T = 1-, 6-, or 72-h total sugar conversion (%)

$[G]$ = 1-, 6-, or 72-h glucose concentration (mg/mL)

$[G]_0$ = initial glucose concentration (mg/mL)

$[X]$ = 1-, 6-, or 72-h xylose concentration (mg/mL)

$[X]_0$ = initial xylose concentration (mg/mL)

V = initial volume of biomass slurry (mL)

W = initial dry weight of biomass (g)

0.9 = glucose conversion factor to equivalent glucan

0.88 = xylose conversion factor to equivalent xylan

Results and Discussion

Carbohydrate conversions of glucan, xylan, and total sugar were calculated at the various enzyme loadings (Table VI) and incubation times (1, 6, 72 h) using Equations 8, 9, and 10, respectively. Using Equation 5, carbohydrate conversion versus enzyme loading was plotted for all the 147 poplar wood model samples at 1, 6, and 72 h. Figure 15 (Sample 43) illustrates this plot for one of the 33 low-reactivity samples. Likewise, Figures 16 (Sample 133) and 17 (Sample 77) are examples of one of the 58 medium-reactivity and one of the 56 high-reactivity samples, respectively. From these plots, the slopes (B) and intercepts (A) were determined in Microsoft Excel® using the linear regression trendline option. As Figures 15, 16, and 17 indicate, Equation 5 was successful in modeling carbohydrate conversion (glucan, xylan, and total sugar) as a function of enzyme loading. It was important that the enzyme loadings were chosen to ensure the conversions were never too high (>95%). Conversions in excess of 95% resulted in nonlinear profiles. From our data, low conversion (<10%) does not appear to significantly affect the linearity of the figures. However, ideally one would want conversions to lie between 10% and 90%. These are the boundary conditions of the linear form of the HCH-1 Model that accurately predicts carbohydrate conversion.

The slopes (B) and intercepts (A) calculated for the 147 poplar wood model samples are summarized in Tables VII, VIII, and IX for glucan, xylan, and total sugar, respectively. In general, the tables show an inverse relationship between both B and A and crystallinity, lignin, and acetyl content. Discerning the relative importance of the structural features will aid in understanding if they play a major or minor role in affecting digestibility or if there are other structural features that may be more important. If our study is successful, we should be able to answer the following questions: Do all

structural features need to be altered to render biomass digestible or is it sufficient to alter only one or two of them? Are the effects the structural features have on the slope and intercept a function of time? Are the initial hydrolysis rates (1 h), rates at 50% of maximum (6 h), and ultimate conversions (72 h) correlated? Are glucan, xylan, and total sugar digestibility affected by different combinations of structural features? Because of the amount of data and size of the tables, the answers to the previously proposed questions are better illustrated graphically.

Due to the scatter of the data in Figure 18, it is evident that there is no correlation between slopes or intercepts. As discussed in "Neural Network Modeling Study," the neural network model developed to predict the slope did not improve when the intercept was included as an input to the network and vice versa. This indicates that there are differences in the 1-h, 6-h, and 72-h hydrolysis rates. Therefore, a sample with a large 1-h or 6-h (initial rate) slope or intercept will not necessarily have a high 72-h slope or intercept (ultimate digestion). This may be due to one or two structural features having a major affect on the 1-h rate while eliciting only a minor affect on the 72-h rate. Therefore, all possible combinations of structural features will be investigated at 1, 6, and 72 h.

Figures 19, 20, and 21 were created to understand how the structural features affect the slope and intercept independent of one another. The figures were constructed by plotting the structural feature of interest over a wide range while holding the other structural features constant. Figure 19 indicates that a six-fold decrease in crystallinity results in a 10.5, 8.2, and 2.3 fold increase in the 1-, 6-, and 72-h total sugar slope, respectively. Likewise, a six-fold decrease in crystallinity results in a 4.5, 7.3, and 8.2 fold increase in the 1-, 6-, and 72-h total sugar intercept, respectively. A similar inverse relationship is illustrated between the slope and intercept and the acetyl and lignin contents in Figures 20 and 21, respectively. It appears that either low lignin or low crystallinity results in high total sugar slopes and intercepts, whereas low acetyl results in only moderate slopes and intercepts. In this research, the slope and intercept are intimately coupled to sugar conversion. Therefore, it was no surprise that Chang (1999)

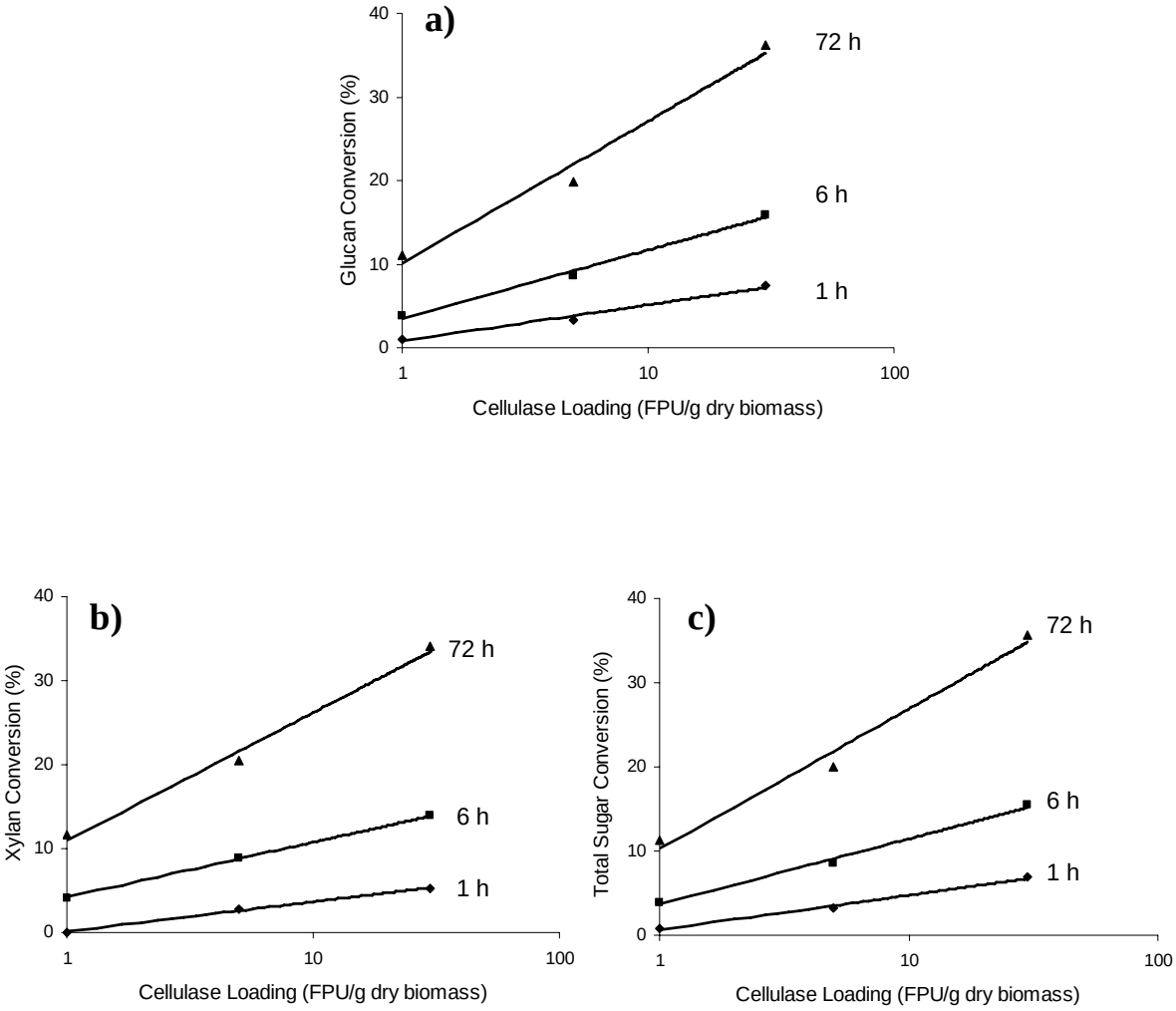

Figure 15. Low reactivity biomass. Plot of Equation 5 for Sample 43: (a) glucan conversion, (b) xylan conversion, (c) total sugar conversion. Hydrolysis conditions: 1 g/L and 48 CBU/g dry biomass.

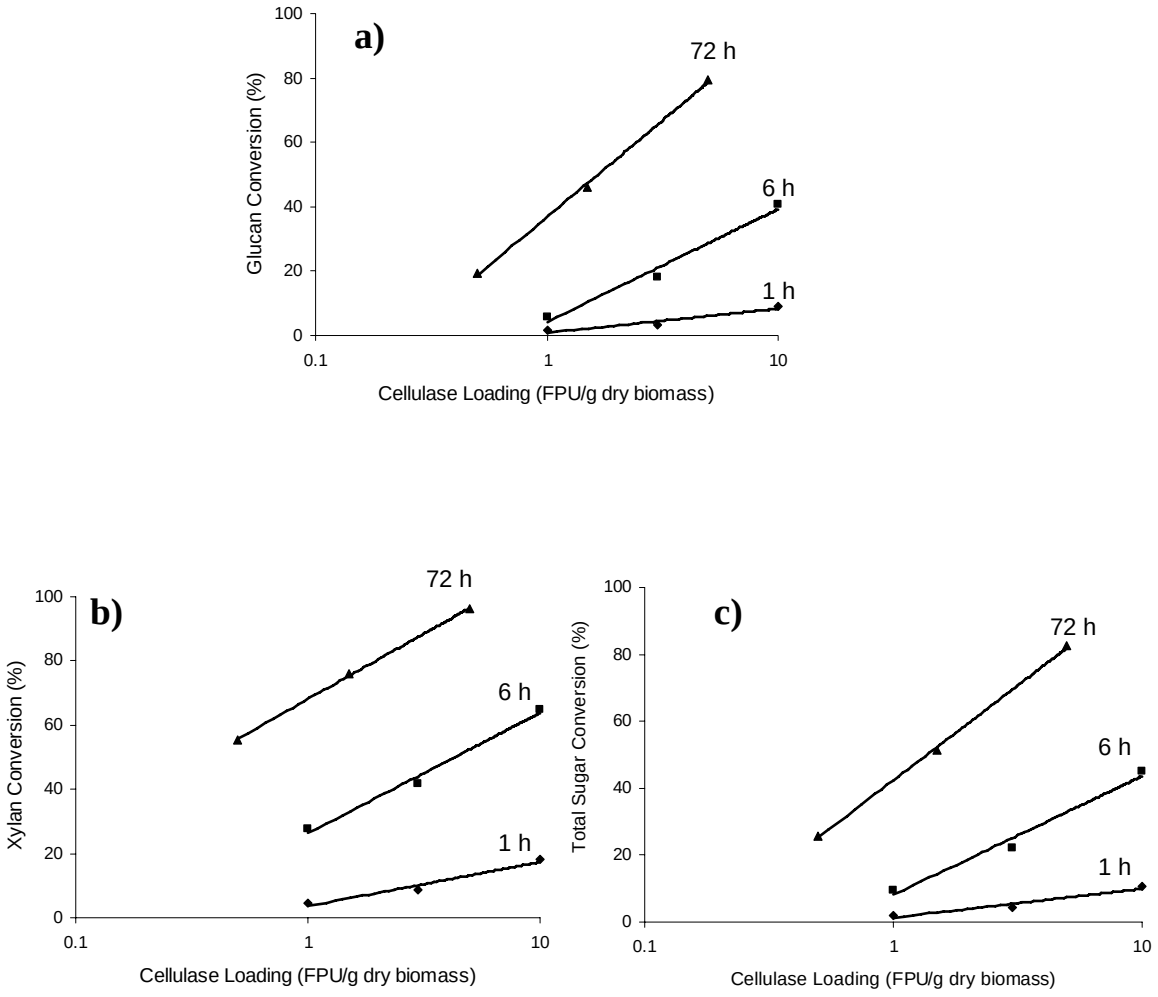

Figure 16. Medium reactivity biomass. Plot of Equation 5 for Sample 133: (a) glucan conversion, (b) xylan conversion, (c) total sugar conversion. Hydrolysis conditions: 1 g/L and 48 CBU/g dry biomass.

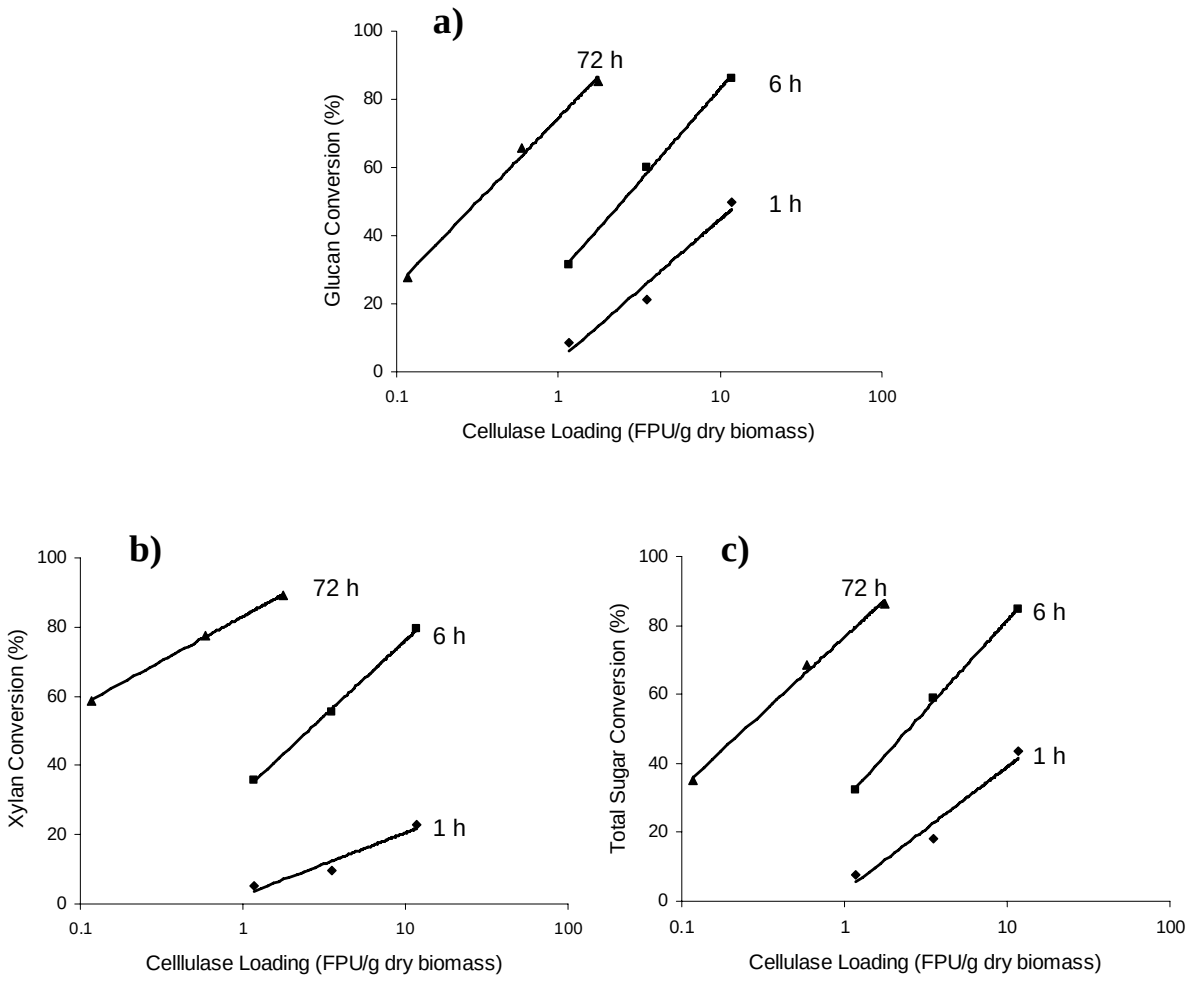

Figure 17. High reactivity biomass. Plot of Equation 5 for Sample 77: (a) glucan conversion, (b) xylan conversion, (c) total sugar conversion. Hydrolysis conditions: 1 g/L and 48 CBU/g dry biomass.

Table VII. Summary of the glucan slopes (*B*) and intercepts (*A*) determined from Equation 5 for the 147 poplar wood model samples.

Sample No.	CrIb	Lignin	Acetyl	1-h Glucan			6-h Glucan			72-h Glucan		
				B	*A*	R^2	*B*	*A*	R^2	*B*	*A*	R^2
1	55	26.3	2.9	1.06	0.00	0.99	1.88	1.82	1.00	2.19	5.85	0.98
2	29	26.3	2.9	8.85	3.25	0.99	9.41	15.47	0.99	6.45	35.74	0.99
3	15	26.3	2.9	12.02	2.88	0.97	14.25	19.62	0.99	7.01	53.50	0.96
4	57	25.5	2.8	0.93	0.44	1.00	1.77	1.46	0.99	2.75	5.21	0.99
5	32	25.5	2.8	7.95	2.51	0.97	10.30	12.71	0.99	7.29	35.04	0.96
6	20	25.5	2.8	11.00	2.67	0.98	12.53	16.50	0.99	6.20	45.50	0.98
7	58	25.6	2.5	0.98	0.00	0.99	1.90	0.81	0.99	2.25	5.79	1.00
8	28	25.6	2.5	8.88	2.76	0.98	9.79	14.90	0.99	5.70	36.74	0.99
9	19	25.6	2.5	7.81	4.97	0.96	15.66	16.06	1.00	10.35	45.42	0.99
10	56	25.5	1.9	1.06	0.57	0.96	1.74	2.44	0.99	2.78	6.29	0.99
11	25	25.5	1.9	8.28	2.67	0.98	9.47	14.10	0.99	6.88	33.64	0.99
12	20	25.5	1.9	10.06	3.56	0.97	13.30	16.02	0.99	10.65	40.97	0.99
13	56	26	1.3	1.24	0.07	0.98	1.75	2.94	1.00	2.98	6.79	0.99
14	33	26	1.3	13.45	3.21	0.98	13.37	21.08	0.97	6.43	52.03	0.98
15	13	26	1.3	12.92	4.29	0.98	17.36	21.26	1.00	12.28	54.18	0.94
16	60	26	0.9	1.43	0.76	0.99	2.68	2.52	0.99	4.43	7.19	0.99
17	22	26	0.9	15.29	3.47	0.98	15.37	23.39	0.98	7.32	58.11	0.95
18	9.9	26	0.9	14.30	5.11	0.98	17.91	23.21	0.99	8.72	59.26	0.99
19	66	24.5	0.4	2.74	0.00	0.97	6.08	0.99	0.96	12.82	6.19	0.97
20	31	24.5	0.4	12.41	5.64	0.98	15.75	18.63	1.00	13.87	42.59	0.99
21	27	24.5	0.4	12.34	7.25	0.97	14.66	23.12	1.00	14.09	51.49	1.00
22	60	23.9	2.8	1.31	0.06	0.97	2.30	1.90	0.99	4.21	6.70	0.99
23	26	23.9	2.8	9.87	3.39	0.95	14.73	18.46	1.00	12.03	46.24	0.99
24	8.2	23.9	2.8	13.97	2.87	0.96	20.44	21.17	0.99	16.40	61.13	0.98
25	60.4	23.1	2.9	1.26	0.37	1.00	2.60	2.21	0.99	4.90	6.84	0.99
26	16.4	23.1	2.9	13.24	2.61	0.99	14.57	20.24	0.99	11.20	51.88	0.99
27	13.9	23.1	2.9	11.40	2.46	0.94	18.81	18.26	1.00	13.17	54.70	0.99
28	59.8	22.8	2.8	1.24	1.06	0.96	2.51	2.89	0.99	4.99	7.94	0.99
29	22.7	22.8	2.8	11.19	2.58	0.97	13.40	17.74	1.00	8.68	48.02	0.97
30	14	22.8	2.8	14.18	3.47	0.97	18.78	21.83	0.99	10.70	60.20	0.97

Table VII. Continued

Sample No.	CrIb	Lignin	Acetyl	1-h Glucan			6-h Glucan			72-h Glucan		
				B	*A*	R^2	*B*	*A*	R^2	*B*	*A*	R^2
31	60	22.4	2.9	1.60	0.35	0.99	2.71	2.63	1.00	5.22	8.16	0.99
32	27	22.4	2.9	11.43	3.50	0.98	15.45	18.81	0.99	11.37	48.44	0.99
33	22	22.4	2.9	14.38	3.71	0.97	19.06	24.88	1.00	17.14	63.68	0.99
34	55.7	21.8	2.2	2.16	0.78	0.96	4.03	3.55	0.99	7.19	10.72	0.99
35	24.8	21.8	2.2	12.93	3.88	0.96	17.51	22.14	1.00	11.79	55.74	0.98
36	14.8	21.8	2.2	15.05	2.54	0.95	19.90	22.64	0.99	19.33	64.75	0.99
37	60.8	21.3	1.7	2.55	1.31	1.00	5.51	5.03	0.98	8.36	15.72	0.99
38	21.1	21.3	1.7	13.62	6.09	0.98	18.95	23.43	1.00	13.93	58.08	0.99
39	17.3	21.3	1.7	17.02	4.56	0.97	21.28	28.11	1.00	13.81	65.82	0.94
40	68.8	17.8	0.4	4.89	0.83	0.96	14.97	4.72	0.97	19.11	32.60	0.99
41	28.3	17.8	0.4	17.30	5.61	0.96	20.96	32.08	1.00	20.18	68.89	0.98
42	18.8	17.8	0.4	20.80	7.08	0.98	24.26	34.36	0.99	19.95	79.83	0.99
43	59.3	21.5	2.9	1.87	0.81	0.98	3.55	3.50	0.99	7.40	10.05	0.98
44	19	21.5	2.9	13.16	5.65	0.94	20.57	22.29	0.99	13.00	59.72	0.96
45	16	21.5	2.9	15.64	2.01	0.97	20.83	23.61	1.00	7.80	45.47	0.99
46	58.9	21.1	3.1	1.95	0.62	0.96	3.96	3.45	0.98	8.10	7.46	0.99
47	23.3	21.1	3.1	7.53	6.27	0.99	19.18	20.05	1.00	12.71	57.01	0.98
48	12.8	21.1	3.1	16.88	2.58	0.96	22.94	25.25	0.99	24.53	75.66	0.99
49	59	20.9	3	2.04	1.65	0.97	4.57	4.11	0.97	8.89	11.92	0.99
50	27.4	20.9	3	11.46	4.80	0.96	16.83	20.53	0.99	10.82	55.73	0.99
51	27.4	20.9	3	13.25	3.31	0.96	20.60	19.33	1.00	7.64	67.44	0.98
52	59.4	19.5	2.9	2.64	0.61	0.96	5.79	3.00	0.99	9.06	15.15	0.98
53	26.5	19.5	2.9	14.39	3.00	0.96	20.14	20.96	1.00	16.25	56.49	0.95
54	22	19.5	2.9	14.28	4.04	0.98	21.68	20.85	0.99	18.99	64.98	0.99
55	61.8	19.5	2.5	3.55	1.29	0.96	7.47	6.04	0.99	10.85	20.65	1.00
56	25.2	19.5	2.5	12.59	5.53	0.96	19.72	21.74	0.99	12.28	61.57	0.99
57	23	19.5	2.5	15.63	3.13	0.97	20.99	24.66	1.00	12.54	65.31	0.95
58	61.4	18.4	1.7	4.40	0.49	0.95	9.68	4.92	0.98	12.04	24.23	0.99
59	28.5	18.4	1.7	17.14	3.49	0.97	21.49	28.36	1.00	13.15	68.37	0.97
60	9.2	18.4	1.7	21.15	3.95	0.96	23.92	31.62	0.98	21.97	83.57	0.99
61	66.4	14.8	0.3	6.76	2.14	0.95	20.08	8.92	0.97	23.94	46.62	1.00

Table VII. Continued

Sample No.	CrIb	Lignin	Acetyl	1-h Glucan			6-h Glucan			72-h Glucan		
				B	*A*	R^2	*B*	*A*	R^2	*B*	*A*	R^2
62	30.1	14.8	0.3	18.66	7.96	0.97	24.06	31.34	0.99	19.68	73.75	0.99
63	9.6	14.8	0.3	23.25	8.01	0.98	20.44	47.71	0.94	26.46	84.47	0.72
64	61.2	18.7	2.9	3.38	0.04	0.93	7.56	3.51	0.97	13.20	16.27	0.99
65	23.5	18.7	2.9	18.09	3.41	0.96	23.16	29.77	1.00	21.49	74.48	0.98
66	9.8	18.7	2.9	20.16	2.60	0.95	23.22	33.42	0.98	22.62	85.53	0.99
67	62.5	17.8	2.9	3.68	1.09	0.95	8.28	4.97	0.98	11.75	26.80	0.98
68	30.8	17.8	2.9	13.17	3.43	0.98	22.14	20.34	1.00	14.22	59.90	0.98
69	10.5	17.8	2.9	15.45	3.93	0.97	23.31	32.35	0.99	8.68	77.48	0.90
70	61.9	17.1	2.5	3.81	0.30	0.93	8.74	4.16	0.98	13.32	21.30	0.99
71	23.5	17.1	2.5	16.66	2.44	0.96	22.89	25.18	1.00	14.77	67.30	0.93
72	10.4	17.1	2.5	19.43	2.18	0.96	24.13	29.88	0.99	23.12	83.81	0.94
73	61.9	16.3	2.8	4.69	0.84	0.96	11.36	5.55	0.99	13.09	30.92	0.99
74	24.6	16.3	2.8	13.99	5.82	0.97	24.77	24.06	0.99	18.70	69.96	0.98
75	14.2	16.3	2.8	20.66	2.08	0.95	23.63	32.79	0.99	21.26	79.05	0.98
76	62.9	16.2	2.6	4.20	1.11	0.99	12.71	5.13	0.99	14.29	32.54	0.99
77	22.6	16.2	2.6	18.05	3.26	0.96	23.78	28.43	1.00	21.37	74.51	1.00
78	12	16.2	2.6	21.80	2.97	0.96	21.80	37.40	0.97	24.37	90.70	0.99
79	63	14.7	2.3	4.72	1.30	0.94	16.32	6.28	0.97	18.91	40.34	0.99
80	23.7	14.7	2.3	15.62	6.24	0.97	25.02	29.64	0.99	21.78	76.95	0.99
81	20.4	14.7	2.3	20.28	3.69	0.95	23.31	31.78	0.98	20.71	77.12	1.00
82	67.2	10.6	0.4	7.66	1.46	0.94	22.84	8.16	0.97	21.56	50.12	0.99
83	34.2	10.6	0.4	20.05	5.80	0.96	22.93	34.92	0.99	21.61	76.96	0.94
84	26	10.6	0.4	22.01	6.04	0.97	28.35	33.58	0.99	24.33	87.84	0.96
85	57.4	13.9	2.9	3.71	1.08	0.95	14.32	4.97	0.97	20.80	36.62	1.00
86	19	13.9	2.9	18.47	4.05	0.96	26.06	26.01	0.99	16.12	73.23	1.00
87	9.5	13.9	2.9	22.14	3.70	0.96	22.67	37.41	0.94	20.80	82.85	0.96
88	60.5	13.4	2.8	3.04	1.29	0.96	11.27	5.16	0.96	17.05	32.98	0.99
89	25.3	13.4	2.8	17.57	2.56	0.96	24.29	26.89	1.00	23.08	76.31	0.99
90	24	13.4	2.8	19.62	2.28	0.96	24.95	26.94	0.99	26.37	83.31	0.95
91	62.1	13.3	2.7	1.79	1.94	0.98	7.26	7.58	0.96	23.19	37.65	1.00
92	24.1	13.3	2.7	15.22	5.07	0.98	22.14	24.51	0.99	21.12	68.26	0.99

Table VII. Continued

Sample No.	CrIb	Lignin	Acetyl	1-h Glucan			6-h Glucan			72-h Glucan		
				B	*A*	R^2	*B*	*A*	R^2	*B*	*A*	R^2
93	11.9	13.3	2.7	21.96	1.57	0.98	23.47	35.25	0.97	19.32	80.16	0.91
94	61.7	12.5	2.6	4.43	0.69	0.96	18.21	5.10	0.92	19.88	40.25	0.99
95	25.9	12.5	2.6	17.96	3.07	0.95	24.31	27.46	1.00	21.82	74.40	1.00
96	12.7	12.5	2.6	22.50	3.28	0.96	24.94	33.63	0.97	25.62	88.96	0.99
97	65.6	11.8	2.3	4.74	1.13	0.96	18.20	5.78	0.95	22.27	43.26	0.99
98	25.6	11.8	2.3	17.78	5.62	0.94	25.06	25.77	0.99	25.79	80.32	0.99
99	25.6	11.8	2.3	18.33	5.85	0.94	25.29	27.25	0.98	26.14	77.69	0.74
100	65.9	10.9	2.4	5.38	2.05	0.98	19.68	5.04	0.95	24.22	43.38	0.99
101	23.9	10.9	2.4	19.02	3.85	0.97	24.11	29.15	0.99	25.95	77.60	0.77
102	21	10.9	2.4	23.00	4.23	0.97	23.60	34.82	0.95	25.39	90.70	0.99
103	67.7	6.8	0.6	7.69	1.69	0.95	23.93	8.82	0.97	21.80	53.59	0.95
104	39	6.8	0.6	17.78	7.69	0.98	26.58	28.82	0.99	27.04	87.86	0.99
105	24.6	6.8	0.6	21.26	5.22	0.96	23.54	35.99	0.97	26.31	85.80	0.96
106	66.1	6.1	2.7	4.86	0.32	0.97	19.23	2.90	0.92	26.01	43.64	0.99
107	21.1	6.1	2.7	19.66	4.32	0.97	23.71	32.46	0.98	27.02	83.69	0.94
108	17.5	6.1	2.7	20.60	4.73	0.96	24.43	31.38	0.98	26.20	87.56	0.99
109	65.3	6	3	4.45	0.99	0.94	21.18	3.75	0.94	24.67	46.43	0.98
110	28.9	6	3	17.34	4.52	0.95	27.21	22.87	0.99	25.71	76.38	0.98
111	14.7	6	3	21.11	3.05	0.97	23.71	35.62	0.97	28.83	93.08	1.00
112	66	5.9	2.7	4.99	1.67	0.99	19.51	6.05	0.96	27.55	45.95	0.99
113	32	5.9	2.7	17.44	3.01	0.96	24.96	26.01	1.00	22.86	74.35	0.97
114	17	5.9	2.7	21.93	2.57	0.95	24.20	32.22	0.98	26.68	88.57	0.99
115	66.3	5.6	2.7	4.56	1.18	0.93	20.05	5.05	0.94	24.61	47.39	0.99
116	32.1	5.6	2.7	16.81	5.81	0.96	26.94	25.59	0.99	23.03	78.56	0.99
117	15.1	5.6	2.7	21.04	3.24	0.97	23.74	34.62	0.98	20.62	79.83	0.93
118	68.3	4.5	2.5	5.82	0.78	0.92	22.43	5.08	0.93	25.73	49.04	0.99
119	32.1	4.5	2.5	17.54	3.69	0.97	24.21	26.26	1.00	33.41	69.30	0.91
120	27.9	4.5	2.5	19.32	3.49	0.97	25.30	26.63	0.99	25.75	81.48	0.95
121	67.5	4.1	2.1	5.09	1.00	0.94	21.22	5.06	0.94	23.30	47.47	0.98
122	26	4.1	2.1	18.20	6.20	0.95	26.54	28.45	0.99	24.07	77.75	0.98
123	21.2	4.1	2.1	19.42	4.20	0.97	25.30	29.71	0.99	19.74	80.39	0.94

Table VII. Continued

Sample No.	CrIb	Lignin	Acetyl	1-h Glucan			6-h Glucan			72-h Glucan		
				B	*A*	R^2	*B*	*A*	R^2	*B*	*A*	R^2
124	62.7	2.5	0.4	8.46	3.44	0.97	26.54	10.20	0.95	29.18	65.62	0.99
125	22.4	2.5	0.4	18.42	4.13	0.96	25.27	28.30	0.99	28.78	87.46	0.99
126	19.5	2.5	0.4	20.81	4.77	0.97	29.95	30.15	0.99	30.32	89.26	0.99
127	68.8	1.8	2.7	3.18	0.43	0.92	7.09	6.21	0.99	24.56	38.18	1.00
128	37	1.8	2.7	14.25	4.55	0.97	26.27	18.66	0.99	21.35	72.71	0.99
129	5.4	1.8	2.7	17.31	3.39	0.97	25.76	27.01	0.98	30.24	73.74	0.83
130	68.2	1.6	2.6	4.09	0.79	0.92	18.08	2.54	0.93	27.26	40.74	0.99
131	46.9	1.6	2.6	12.44	1.47	0.96	25.97	13.18	0.99	33.68	61.39	0.96
132	21.5	1.6	2.6	16.34	2.05	0.95	29.39	19.29	0.99	22.28	67.70	0.99
133	65.7	1.6	2.3	3.26	0.85	0.93	15.25	4.17	0.98	26.10	36.76	1.00
134	50.6	1.6	2.3	10.67	2.57	0.93	22.81	14.72	0.99	23.20	58.77	0.99
135	19.2	1.6	2.3	15.47	1.24	0.95	26.21	19.15	1.00	21.36	73.83	0.97
136	64.6	1.5	2.2	4.86	2.01	0.95	18.94	5.25	0.94	28.14	40.08	0.99
137	48	1.5	2.2	12.03	1.11	0.95	24.94	11.69	0.99	25.71	60.89	1.00
138	14.9	1.5	2.2	17.94	1.91	0.95	24.94	24.80	0.99	29.61	83.83	0.99
139	65.4	1.3	1.8	4.62	1.00	0.91	17.62	4.71	0.95	23.83	42.60	1.00
140	47.1	1.3	1.8	12.57	2.49	0.97	25.70	12.86	0.99	24.83	64.77	0.99
141	11.7	1.3	1.8	17.36	1.23	0.95	26.36	24.03	0.99	28.59	83.62	0.95
142	62.3	1.1	1.6	6.33	2.44	0.95	21.83	5.69	0.95	26.13	48.20	0.99
143	44.8	1.1	1.6	12.70	2.34	0.97	26.59	13.62	1.00	27.68	67.79	0.98
144	10.8	1.1	1.6	16.35	2.59	0.95	26.13	22.75	0.99	28.96	83.64	0.99
145	66	0.7	0.1	8.97	1.95	0.94	25.57	10.82	0.97	27.65	60.39	0.99
146	50.9	0.7	0.1	15.75	2.34	0.97	30.13	12.78	0.98	24.36	71.77	0.99
147	33	0.7	0.1	16.45	2.66	0.96	26.24	22.38	1.00	32.01	71.02	0.93

Table VIII. Summary of the xylan slopes (*B*) and intercepts (*A*) determined from Equation 5 for the 147 poplar wood model samples.

Sample No.	CrIb	Lignin	Acetyl	1-h Xylan			6-h Xylan			72-h Xylan		
				B	*A*	R^2	*B*	*A*	R^2	*B*	*A*	R^2
1	55	26.3	2.9	-	-	-	-	-	-	1.49	3.26	0.95
2	29	26.3	2.9	5.82	0.00	0.95	7.78	10.47	0.99	6.91	28.43	0.99
3	15	26.3	2.9	8.26	0.00	0.93	11.04	18.46	1.00	8.28	48.92	1.00
4	57	25.5	2.8	-	-	-	-	-	-	1.34	2.90	0.95
5	32	25.5	2.8	4.91	0.89	0.95	7.79	10.51	1.00	7.22	31.23	0.96
6	20	25.5	2.8	7.18	0.00	0.94	10.26	11.89	0.99	7.52	36.50	1.00
7	58	25.6	2.5	-	-	-	-	-	-	-	-	-
8	28	25.6	2.5	6.07	0.00	0.94	8.22	11.10	0.99	6.48	29.48	0.99
9	19	25.6	2.5	6.25	2.67	0.99	9.19	24.71	0.98	8.12	45.16	1.00
10	56	25.5	1.9	-	-	-	-	-	-	1.26	4.94	0.94
11	25	25.5	1.9	5.69	0.88	0.92	8.48	11.11	1.00	6.73	28.59	1.00
12	20	25.5	1.9	5.80	1.28	0.94	10.67	13.62	0.99	11.54	34.94	0.99
13	56	26	1.3	-	-	-	2.04	2.65	1.00	2.63	4.97	1.00
14	33	26	1.3	10.31	0.00	0.93	11.80	19.71	0.99	7.71	49.22	0.99
15	13	26	1.3	8.36	4.14	0.94	10.52	33.17	0.99	13.40	52.15	0.98
16	60	26	0.9	1.95	0.29	0.98	2.21	4.67	0.99	3.11	8.40	0.99
17	22	26	0.9	11.96	1.10	0.92	12.82	28.25	1.00	8.45	59.68	0.98
18	9.9	26	0.9	8.18	3.28	0.95	15.02	25.38	0.99	9.35	61.39	0.99
19	66	24.5	0.4	8.86	0.00	0.94	11.71	9.36	0.98	14.31	21.73	0.98
20	31	24.5	0.4	9.53	6.00	0.93	15.93	34.67	0.99	12.15	66.17	0.99
21	27	24.5	0.4	9.24	6.74	0.94	8.64	50.19	0.85	8.70	75.10	0.87
22	60	23.9	2.8	-	-	-	1.53	2.81	0.99	3.36	6.41	0.99
23	26	23.9	2.8	6.48	2.51	0.84	9.04	27.07	0.80	13.31	45.43	1.00
24	8.2	23.9	2.8	7.58	1.43	0.94	17.49	20.24	0.99	13.75	62.62	1.00
25	60.4	23.1	2.9	-	-	-	2.62	0.26	0.99	3.57	5.82	0.99
26	16.4	23.1	2.9	10.18	0.00	0.92	13.83	17.50	0.99	10.36	53.26	0.99
27	13.9	23.1	2.9	6.97	2.28	0.86	6.97	27.21	0.87	11.63	58.74	0.95
28	59.8	22.8	2.8	-	-	-	1.75	3.02	0.99	3.94	5.93	0.99
29	22.7	22.8	2.8	8.36	0.27	0.90	12.09	17.11	0.99	9.75	46.47	0.98
30	14	22.8	2.8	7.69	1.31	0.96	16.37	19.77	0.99	11.69	59.65	0.99

Table VIII. Continued

Sample No.	CrIb	Lignin	Acetyl	1-h Xylan			6-h Xylan			72-h Xylan		
				B	*A*	R^2	*B*	*A*	R^2	*B*	*A*	R^2
31	60	22.4	2.9	-	-	-	1.20	2.91	0.98	3.48	7.46	1.00
32	27	22.4	2.9	6.89	1.01	0.94	14.74	17.18	0.99	11.84	48.27	0.99
33	22	22.4	2.9	8.68	3.36	0.93	15.19	32.57	0.96	11.19	68.32	0.95
34	55.7	21.8	2.2	2.41	0.00	0.99	3.87	3.74	0.99	6.38	9.48	0.99
35	24.8	21.8	2.2	7.52	2.55	0.92	14.92	24.42	1.00	12.82	57.58	1.00
36	14.8	21.8	2.2	7.20	1.00	0.93	17.62	20.91	0.99	12.79	62.65	0.99
37	60.8	21.3	1.7	2.77	0.13	1.00	5.16	7.10	0.99	7.08	17.53	1.00
38	21.1	21.3	1.7	7.51	3.96	0.97	15.34	28.78	0.99	10.74	65.00	0.99
39	17.3	21.3	1.7	9.82	3.46	0.94	16.36	39.24	0.95	11.62	76.81	0.99
40	68.8	17.8	0.4	6.99	2.38	0.98	17.87	19.00	0.99	15.53	59.41	0.99
41	28.3	17.8	0.4	10.20	4.98	0.82	15.43	48.48	0.95	13.32	85.06	1.00
42	18.8	17.8	0.4	8.22	5.21	0.94	17.97	40.37	0.99	11.91	86.87	0.99
43	59.3	21.5	2.9	1.53	0.13	0.99	2.85	4.19	1.00	6.62	10.96	0.99
44	19	21.5	2.9	7.73	2.81	0.91	16.51	25.81	0.99	15.48	61.66	0.99
45	16	21.5	2.9	7.72	3.38	0.97	14.02	33.66	0.95	0.99	52.93	0.90
46	58.9	21.1	3.1	1.76	0.00	0.99	3.42	3.52	0.97	7.84	7.46	0.99
47	23.3	21.1	3.1	5.54	1.66	0.99	17.74	21.53	0.99	10.79	64.44	0.96
48	12.8	21.1	3.1	8.25	1.04	0.94	19.70	26.53	0.99	14.66	74.78	0.99
49	59	20.9	3	2.02	0.00	1.00	3.49	4.98	0.92	8.52	10.02	1.00
50	27.4	20.9	3	6.50	1.94	0.92	14.46	21.24	0.99	9.52	60.70	0.99
51	27.4	20.9	3	7.47	2.26	0.89	15.17	28.02	0.95	12.13	66.27	0.98
52	59.4	19.5	2.9	-	-	-	6.50	2.97	0.95	8.84	15.96	0.99
53	26.5	19.5	2.9	7.58	2.44	0.87	14.48	29.35	0.93	12.36	67.19	0.99
54	22	19.5	2.9	8.65	0.83	0.96	18.56	24.35	0.99	11.62	66.96	0.99
55	61.8	19.5	2.5	3.97	0.00	0.99	6.54	9.88	0.97	9.93	23.98	0.99
56	25.2	19.5	2.5	7.15	3.80	0.96	16.92	28.09	0.99	16.27	66.35	0.99
57	23	19.5	2.5	8.18	3.16	0.88	15.61	34.37	0.97	10.11	75.32	0.99
58	61.4	18.4	1.7	5.72	0.00	0.97	9.47	9.30	0.98	11.62	29.05	0.99
59	28.5	18.4	1.7	7.90	2.69	0.95	18.45	30.39	1.00	13.54	74.00	0.99
60	9.2	18.4	1.7	8.89	3.41	0.92	20.78	33.88	0.99	12.49	84.56	0.99
61	66.4	14.8	0.3	6.48	4.32	0.96	18.35	27.83	0.99	17.99	71.73	0.99

Table VIII. Continued

Sample No.	CrIb	Lignin	Acetyl	1-h Xylan			6-h Xylan			72-h Xylan		
				B	*A*	R^2	*B*	*A*	R^2	*B*	*A*	R^2
62	30.1	14.8	0.3	8.64	6.69	0.93	15.58	43.70	0.99	13.84	87.25	0.97
63	9.6	14.8	0.3	7.72	5.64	0.96	16.57	43.93	1.00	12.43	89.03	0.75
64	61.2	18.7	2.9	4.48	0.00	0.95	7.80	6.73	0.98	14.07	21.22	0.99
65	23.5	18.7	2.9	8.37	2.70	0.93	19.69	31.84	1.00	11.62	79.84	1.00
66	9.8	18.7	2.9	9.12	2.92	0.92	20.50	35.49	0.99	11.61	85.25	0.99
67	62.5	17.8	2.9	3.98	0.00	0.98	8.31	5.99	0.98	11.94	28.85	0.98
68	30.8	17.8	2.9	6.47	3.08	0.96	15.40	26.99	0.98	14.93	64.31	0.99
69	10.5	17.8	2.9	6.26	2.37	0.95	19.81	29.80	1.00	10.39	81.54	0.99
70	61.9	17.1	2.5	4.35	0.00	0.95	8.78	5.65	0.98	14.42	24.82	0.99
71	23.5	17.1	2.5	7.71	1.37	0.94	19.43	26.20	1.00	13.81	74.27	0.98
72	10.4	17.1	2.5	8.39	1.88	0.95	20.13	30.87	1.00	11.12	83.44	0.99
73	61.9	16.3	2.8	4.82	0.00	0.99	10.49	8.45	0.99	12.95	34.30	1.00
74	24.6	16.3	2.8	6.83	2.94	0.93	16.78	30.00	0.99	11.77	75.13	0.99
75	14.2	16.3	2.8	7.99	1.88	0.94	19.77	31.40	1.00	11.29	84.00	1.00
76	62.9	16.2	2.6	5.29	0.19	0.99	12.39	10.59	0.99	13.25	40.07	0.99
77	22.6	16.2	2.6	7.85	2.50	0.94	18.99	32.43	1.00	11.21	83.09	1.00
78	12	16.2	2.6	8.68	2.56	0.91	18.25	37.98	0.99	10.57	89.35	0.99
79	63	14.7	2.3	4.85	1.76	0.97	14.22	15.85	1.00	16.10	51.01	0.99
80	23.7	14.7	2.3	6.44	5.24	0.92	19.20	37.19	0.99	12.46	83.62	0.99
81	20.4	14.7	2.3	7.96	3.62	0.91	18.48	35.33	1.00	9.86	84.99	0.99
82	67.2	10.6	0.4	7.86	2.60	0.95	20.61	28.07	0.99	16.93	77.95	0.99
83	34.2	10.6	0.4	7.37	5.25	0.91	17.64	41.23	0.98	12.31	86.44	0.98
84	26	10.6	0.4	8.38	5.23	0.93	16.97	42.06	0.99	10.65	90.12	0.99
85	57.4	13.9	2.9	4.13	3.05	0.97	13.45	15.36	1.00	18.45	49.96	1.00
86	19	13.9	2.9	7.43	5.26	0.96	18.89	32.51	0.99	11.38	77.51	0.99
87	9.5	13.9	2.9	8.03	3.61	0.94	17.88	37.73	1.00	9.20	87.45	1.00
88	60.5	13.4	2.8	5.10	0.00	1.00	13.08	9.89	0.99	15.80	44.87	0.99
89	25.3	13.4	2.8	7.41	2.70	0.93	18.32	33.86	1.00	12.06	85.90	1.00
90	24	13.4	2.8	8.76	2.54	0.94	18.98	35.16	0.99	11.84	86.67	0.99
91	62.1	13.3	2.7	3.91	0.16	1.00	9.93	12.71	0.99	21.96	47.15	1.00
92	24.1	13.3	2.7	5.88	3.36	0.97	13.20	33.40	0.98	15.20	83.18	0.99

Table VIII. Continued

Sample No.	CrIb	Lignin	Acetyl	1-h Xylan			6-h Xylan			72-h Xylan		
				B	*A*	R^2	*B*	*A*	R^2	*B*	*A*	R^2
93	11.9	13.3	2.7	8.01	2.16	0.96	19.22	34.74	1.00	11.04	87.89	1.00
94	61.7	12.5	2.6	6.05	0.00	0.99	13.92	18.40	0.99	16.09	57.19	0.99
95	25.9	12.5	2.6	7.88	2.15	0.93	18.96	32.98	1.00	10.83	83.84	1.00
96	12.7	12.5	2.6	8.53	2.61	0.93	18.81	37.53	1.00	10.01	88.06	0.99
97	65.6	11.8	2.3	4.54	2.41	0.98	12.66	24.28	0.95	17.44	59.22	0.99
98	25.6	11.8	2.3	8.40	4.09	0.94	16.88	38.46	0.99	9.84	85.73	0.99
99	25.6	11.8	2.3	7.40	3.38	0.91	19.54	32.31	1.00	10.89	84.85	0.73
100	65.9	10.9	2.4	6.02	2.80	0.98	16.60	22.61	0.99	16.36	64.89	0.99
101	23.9	10.9	2.4	7.85	2.97	0.94	18.16	35.66	1.00	13.85	84.59	0.92
102	21	10.9	2.4	8.70	4.17	0.94	16.82	41.96	0.99	8.87	89.89	0.99
103	67.7	6.8	0.6	5.69	4.40	0.97	19.37	24.96	1.00	15.96	72.33	0.93
104	39	6.8	0.6	6.73	7.69	0.96	17.53	41.46	0.97	13.32	89.01	0.99
105	24.6	6.8	0.6	7.76	4.87	0.92	16.47	41.63	1.00	11.18	87.45	0.98
106	66.1	6.1	2.7	6.76	3.68	0.91	16.01	29.71	0.98	12.62	77.33	0.99
107	21.1	6.1	2.7	7.76	4.97	0.93	15.75	43.10	1.00	10.14	88.26	1.00
108	17.5	6.1	2.7	8.26	5.11	0.92	15.77	43.26	0.99	9.26	86.79	0.99
109	65.3	6	3	5.41	3.33	0.96	18.38	24.16	1.00	15.19	73.23	0.96
110	28.9	6	3	7.91	4.71	0.94	17.18	39.47	0.98	16.09	85.88	0.97
111	14.7	6	3	7.85	3.28	0.94	17.98	37.82	1.00	10.96	90.77	1.00
112	66	5.9	2.7	6.64	1.65	0.95	17.26	26.21	0.99	17.81	75.08	0.98
113	32	5.9	2.7	7.84	2.96	0.93	18.19	36.86	1.00	12.53	87.32	1.00
114	17	5.9	2.7	8.51	3.50	0.92	16.49	41.06	0.99	8.15	86.05	0.99
115	66.3	5.6	2.7	5.50	3.30	0.96	17.16	26.23	0.99	15.73	73.90	0.97
116	32.1	5.6	2.7	8.30	5.40	0.94	17.73	42.78	0.99	11.00	91.40	0.99
117	15.1	5.6	2.7	8.09	3.10	0.93	18.06	37.92	1.00	15.25	87.24	0.98
118	68.3	4.5	2.5	6.90	2.95	0.93	18.06	29.65	0.98	16.46	77.95	0.99
119	32.1	4.5	2.5	7.94	3.58	0.95	16.97	38.24	1.00	15.53	85.97	0.96
120	27.9	4.5	2.5	8.18	3.85	0.94	16.85	39.66	0.99	11.54	86.98	0.99
121	67.5	4.1	2.1	5.85	3.08	0.96	17.53	25.91	0.98	14.48	71.42	0.98
122	26	4.1	2.1	7.70	6.14	0.93	14.78	45.93	0.99	14.40	87.75	0.99
123	21.2	4.1	2.1	7.90	3.82	0.94	16.90	39.46	1.00	9.71	88.24	1.00

Table VIII. Continued

Sample No.	CrIb	Lignin	Acetyl	1-h Xylan			6-h Xylan			72-h Xylan		
				B	*A*	R^2	*B*	*A*	R^2	*B*	*A*	R^2
124	62.7	2.5	0.4	5.85	6.01	0.98	19.48	30.29	0.96	20.17	84.22	0.99
125	22.4	2.5	0.4	7.18	5.26	0.93	16.44	38.87	1.00	13.30	87.39	1.00
126	19.5	2.5	0.4	7.82	6.45	0.94	14.45	43.11	0.99	11.48	85.34	0.99
127	68.8	1.8	2.7	5.92	4.06	0.94	10.90	30.05	1.00	14.73	69.00	1.00
128	37	1.8	2.7	7.67	7.73	0.92	14.58	42.32	0.99	11.96	89.32	0.99
129	5.4	1.8	2.7	8.62	4.80	0.95	15.58	44.32	1.00	13.95	82.12	0.98
130	68.2	1.6	2.6	7.15	3.60	0.94	17.13	28.65	0.98	17.36	74.81	0.99
131	46.9	1.6	2.6	9.20	3.59	0.95	17.82	38.99	1.00	15.78	81.23	0.98
132	21.5	1.6	2.6	8.72	4.56	0.94	17.02	39.18	0.99	11.42	82.55	0.99
133	65.7	1.6	2.3	5.97	3.61	0.96	16.30	26.28	0.99	17.70	68.11	1.00
134	50.6	1.6	2.3	8.26	5.38	0.92	16.87	41.24	0.97	11.09	80.45	0.99
135	19.2	1.6	2.3	9.27	3.32	0.95	18.49	37.23	1.00	14.16	87.22	1.00
136	64.6	1.5	2.2	8.31	3.80	0.99	18.15	31.84	0.99	19.20	72.92	0.99
137	48	1.5	2.2	11.35	3.20	0.89	16.14	42.49	1.00	10.14	81.89	0.96
138	14.9	1.5	2.2	9.28	5.56	0.94	16.16	42.76	0.99	10.16	86.84	0.99
139	65.4	1.3	1.8	6.35	4.37	0.92	17.78	26.79	0.99	16.06	72.67	0.96
140	47.1	1.3	1.8	9.30	5.74	0.94	17.25	40.77	0.99	12.82	84.56	0.99
141	11.7	1.3	1.8	9.53	4.93	0.95	16.18	44.69	1.00	15.08	88.94	0.99
142	62.3	1.1	1.6	8.46	3.23	0.97	20.18	27.31	0.99	18.42	75.44	0.99
143	44.8	1.1	1.6	10.26	4.27	0.92	17.00	41.08	0.99	15.25	84.27	1.00
144	10.8	1.1	1.6	8.42	6.44	0.92	16.35	42.68	0.99	11.36	85.81	0.98
145	66	0.7	0.1	6.56	4.53	0.95	20.40	26.97	0.98	21.81	76.14	0.99
146	50.9	0.7	0.1	8.07	4.96	0.93	20.93	28.88	0.99	15.25	80.04	0.99
147	33	0.7	0.1	8.04	4.78	0.93	17.37	35.07	0.99	20.17	81.51	1.00

Table IX. Summary of the total sugar slopes (*B*) and intercepts (*A*) determined from Equation 5 for the 147 poplar wood model samples.

Sample No.	CrIb	Lignin	Acetyl	1-h Total Sugar			6-h Total Sugar			72-h Total Sugar		
				B	*A*	R^2	*B*	*A*	R^2	*B*	*A*	R^2
1	55	26.3	2.9	0.80	0.00	0.99	1.78	1.18	1.00	2.02	5.22	0.97
2	29	26.3	2.9	8.12	2.42	0.98	9.02	14.26	0.99	6.56	33.96	0.99
3	15	26.3	2.9	11.11	2.10	0.97	13.47	19.34	0.99	7.32	52.39	0.98
4	57	25.5	2.8	0.71	0.33	1.00	1.68	0.92	0.98	2.41	4.66	0.99
5	32	25.5	2.8	7.22	2.12	0.97	9.69	12.18	1.00	7.27	34.12	0.96
6	20	25.5	2.8	10.08	1.93	0.98	11.98	15.39	0.99	6.52	43.33	0.99
7	58	25.6	2.5	0.74	0.00	0.99	1.75	0.71	1.00	1.94	5.28	1.00
8	28	25.6	2.5	8.20	2.08	0.98	9.41	13.99	0.99	5.88	35.00	0.99
9	19	25.6	2.5	7.44	4.42	0.97	14.11	18.13	0.99	9.81	45.36	0.99
10	56	25.5	1.9	1.00	0.32	0.93	1.73	2.04	0.98	2.41	5.96	0.99
11	25	25.5	1.9	7.65	2.24	0.97	9.23	13.37	1.00	6.84	32.42	0.99
12	20	25.5	1.9	9.03	3.01	0.97	12.66	15.44	0.99	10.86	39.51	0.99
13	56	26	1.3	1.27	0.00	0.94	1.82	2.87	1.00	2.89	6.35	1.00
14	33	26	1.3	12.69	2.34	0.97	12.99	20.75	0.98	6.74	51.35	0.98
15	13	26	1.3	11.82	4.25	0.97	15.71	24.13	1.00	12.55	53.69	0.95
16	60	26	0.9	1.56	0.64	0.99	2.57	3.04	1.00	4.11	7.48	0.99
17	22	26	0.9	14.48	2.90	0.97	14.75	24.56	0.98	7.59	58.49	0.96
18	9.9	26	0.9	12.82	4.67	0.97	17.21	23.73	0.99	8.88	59.78	0.99
19	66	24.5	0.4	4.11	0.00	0.96	7.34	2.86	0.97	13.15	9.67	0.97
20	31	24.5	0.4	11.77	5.72	0.97	15.79	22.23	0.99	13.48	47.87	0.99
21	27	24.5	0.4	11.65	7.13	0.96	13.31	29.19	1.00	12.88	56.78	1.00
22	60	23.9	2.8	1.25	0.10	0.94	2.12	2.17	1.00	4.00	6.63	0.99
23	26	23.9	2.8	9.05	3.18	0.93	13.35	20.55	0.99	12.34	46.04	0.99
24	8.2	23.9	2.8	12.42	2.52	0.96	19.72	20.94	0.99	15.76	61.49	0.99
25	60.4	23.1	2.9	1.21	0.14	0.98	2.60	1.73	1.00	4.57	6.59	0.99
26	16.4	23.1	2.9	12.50	1.59	0.97	14.39	19.57	0.99	11.00	52.22	0.99
27	13.9	23.1	2.9	10.32	2.42	0.93	17.22	20.44	0.99	12.80	55.68	1.00
28	59.8	22.8	2.8	1.22	0.64	0.93	2.32	2.92	0.99	4.73	7.45	0.99
29	22.7	22.8	2.8	10.49	2.02	0.96	13.08	17.58	1.00	8.94	47.64	0.97
30	14	22.8	2.8	12.59	2.94	0.97	18.19	21.32	0.99	10.94	60.06	0.98

Table IX. Continued

Sample No.	CrIb	Lignin	Acetyl	1-h Total Sugar			6-h Total Sugar			72-h Total Sugar		
				B	*A*	R^2	*B*	*A*	R^2	*B*	*A*	R^2
31	60	22.4	2.9	1.53	0.09	0.97	2.35	2.70	1.00	4.81	7.99	0.99
32	27	22.4	2.9	10.34	2.90	0.98	15.28	18.42	0.99	11.48	48.40	0.99
33	22	22.4	2.9	13.01	3.63	0.96	18.13	26.73	1.00	15.71	64.80	0.99
34	55.7	21.8	2.2	2.22	0.55	0.97	3.99	3.60	0.99	7.00	10.42	0.99
35	24.8	21.8	2.2	11.62	3.56	0.95	16.89	22.69	1.00	12.04	56.18	0.99
36	14.8	21.8	2.2	13.15	2.16	0.95	19.34	22.23	0.99	17.74	64.24	0.99
37	60.8	21.3	1.7	2.60	1.03	1.00	5.43	5.53	0.98	8.06	16.15	1.00
38	21.1	21.3	1.7	12.16	5.58	0.98	18.09	24.71	0.99	13.17	59.74	0.99
39	17.3	21.3	1.7	15.30	4.30	0.96	20.11	30.76	1.00	13.29	68.44	0.97
40	68.8	17.8	0.4	5.36	1.17	0.97	15.61	7.89	0.99	18.32	38.55	0.99
41	28.3	17.8	0.4	17.28	5.47	0.95	19.74	35.72	1.00	18.65	72.70	0.99
42	18.8	17.8	0.4	18.01	6.67	0.98	22.78	35.75	0.99	18.16	81.39	0.99
43	59.3	21.5	2.9	1.79	0.64	0.99	3.38	3.67	0.99	7.21	10.27	0.98
44	19	21.5	2.9	11.85	4.96	0.94	19.59	23.14	0.99	13.60	60.19	0.98
45	16	21.5	2.9	13.72	2.34	0.97	19.19	26.04	1.00	6.15	47.27	0.99
46	58.9	21.1	3.1	1.90	0.43	0.97	3.83	3.46	0.97	8.03	7.46	0.99
47	23.3	21.1	3.1	7.05	5.15	1.00	18.83	20.41	1.00	12.24	58.81	0.99
48	12.8	21.1	3.1	14.78	2.20	0.96	22.16	25.56	0.99	22.13	75.44	0.99
49	59	20.9	3	2.04	1.25	0.98	4.31	4.32	0.97	8.80	11.45	0.99
50	27.4	20.9	3	10.24	4.10	0.96	16.25	20.71	0.99	10.50	56.94	0.99
51	27.4	20.9	3	11.83	3.05	0.95	19.27	21.46	1.00	8.74	67.15	0.98
52	59.4	19.5	2.9	2.74	0.30	0.96	5.96	3.00	0.98	9.00	15.35	0.98
53	26.5	19.5	2.9	12.73	2.86	0.95	18.76	23.00	1.00	15.31	59.09	0.98
54	22	19.5	2.9	12.91	3.26	0.97	20.92	21.70	0.99	17.19	65.46	0.99
55	61.8	19.5	2.5	3.65	0.90	0.97	7.25	6.97	0.99	10.63	21.46	1.00
56	25.2	19.5	2.5	11.27	5.11	0.96	19.04	23.28	0.99	13.24	62.73	0.99
57	23	19.5	2.5	13.82	3.13	0.96	19.68	27.02	1.00	11.95	67.74	0.98
58	61.4	18.4	1.7	4.72	0.10	0.96	9.63	5.98	0.98	11.94	25.39	0.99
59	28.5	18.4	1.7	14.90	3.30	0.97	20.75	28.85	1.00	13.25	69.73	0.97
60	9.2	18.4	1.7	18.19	3.82	0.95	23.16	32.17	0.99	19.66	83.80	0.99
61	66.4	14.8	0.3	6.70	2.62	0.95	19.70	13.10	0.97	22.62	52.18	1.00

Table IX. Continued

Sample No.	CrIb	Lignin	Acetyl	1-h Total Sugar			6-h Total Sugar			72-h Total Sugar		
				B	*A*	R^2	*B*	*A*	R^2	*B*	*A*	R^2
62	30.1	14.8	0.3	16.44	7.68	0.97	22.19	34.07	0.99	18.38	76.73	0.99
63	9.6	14.8	0.3	19.81	7.49	0.98	19.58	46.87	0.96	23.35	85.48	0.72
64	61.2	18.7	2.9	3.65	0.23	0.93	7.62	4.30	0.98	13.41	17.48	0.99
65	23.5	18.7	2.9	15.72	3.24	0.95	22.32	30.27	1.00	19.09	75.78	0.98
66	9.8	18.7	2.9	17.48	2.68	0.95	22.56	33.92	0.99	19.94	85.46	0.99
67	62.5	17.8	2.9	3.75	0.69	0.96	8.29	5.22	0.98	11.79	27.30	0.98
68	30.8	17.8	2.9	11.54	3.35	0.98	20.49	21.96	1.00	14.39	60.98	0.99
69	10.5	17.8	2.9	13.21	3.55	0.97	22.45	31.73	1.00	9.10	78.47	0.93
70	61.9	17.1	2.5	3.94	0.04	0.94	8.75	4.53	0.98	13.59	22.17	0.99
71	23.5	17.1	2.5	14.46	2.18	0.95	22.04	25.43	1.00	14.53	69.01	0.94
72	10.4	17.1	2.5	16.72	2.11	0.96	23.15	30.12	0.99	20.18	83.72	0.99
73	61.9	16.3	2.8	4.72	0.51	0.97	11.15	6.26	0.99	13.06	31.75	0.99
74	24.6	16.3	2.8	12.24	5.12	0.96	22.82	25.50	1.00	17.15	71.22	0.99
75	14.2	16.3	2.8	17.56	2.03	0.95	22.68	32.45	0.99	18.82	80.26	0.99
76	62.9	16.2	2.6	4.46	0.88	0.99	12.63	6.45	0.99	14.04	34.36	0.99
77	22.6	16.2	2.6	15.58	3.07	0.96	22.62	29.40	1.00	18.91	76.59	1.00
78	12	16.2	2.6	18.62	2.87	0.95	20.94	37.54	0.98	21.62	90.83	0.99
79	63	14.7	2.3	4.75	1.41	0.95	15.81	8.59	0.98	18.23	42.91	0.99
80	23.7	14.7	2.3	13.40	6.00	0.97	23.26	31.46	0.99	19.54	78.56	0.99
81	20.4	14.7	2.3	17.31	3.67	0.95	22.14	32.63	0.99	18.10	79.02	1.00
82	67.2	10.6	0.4	7.70	1.71	0.94	22.36	12.45	0.98	20.56	56.12	0.99
83	34.2	10.6	0.4	17.32	5.68	0.96	21.79	36.28	0.99	19.60	79.00	0.95
84	26	10.6	0.4	19.08	5.87	0.97	25.72	35.52	0.99	21.45	88.43	0.99
85	57.4	13.9	2.9	3.81	1.56	0.95	14.11	7.51	0.98	20.23	39.88	1.00
86	19	13.9	2.9	15.78	4.34	0.96	24.30	27.60	1.00	14.96	74.27	1.00
87	9.5	13.9	2.9	18.69	3.68	0.96	21.50	37.49	0.96	17.70	83.98	0.97
88	60.5	13.4	2.8	3.54	0.98	0.98	11.70	6.30	0.97	16.75	35.85	0.99
89	25.3	13.4	2.8	15.12	2.59	0.96	22.85	28.57	1.00	20.45	78.62	1.00
90	24	13.4	2.8	17.00	2.34	0.96	23.51	28.92	0.99	22.87	84.11	0.99
91	62.1	13.3	2.7	2.31	1.51	0.99	7.91	8.82	0.97	22.89	39.96	1.00
92	24.1	13.3	2.7	12.96	4.66	0.98	19.97	26.67	0.99	19.69	71.88	0.99

Table IX. Continued

Sample No.	CrIb	Lignin	Acetyl	1-h Total Sugar			6-h Total Sugar			72-h Total Sugar		
				B	*A*	R^2	*B*	*A*	R^2	*B*	*A*	R^2
93	11.9	13.3	2.7	18.58	1.71	0.97	22.44	35.13	0.98	17.31	82.03	0.94
94	61.7	12.5	2.6	4.83	0.43	0.97	17.17	8.32	0.95	18.96	44.36	0.99
95	25.9	12.5	2.6	15.52	2.84	0.95	23.01	28.80	1.00	19.15	76.69	1.00
96	12.7	12.5	2.6	19.11	3.11	0.96	23.46	34.58	0.98	21.83	88.74	0.99
97	65.6	11.8	2.3	4.69	1.44	0.96	16.87	10.21	0.95	21.11	47.08	0.99
98	25.6	11.8	2.3	15.55	5.25	0.94	23.10	28.81	0.99	22.24	81.63	0.99
99	25.6	11.8	2.3	15.71	5.25	0.94	23.91	28.46	0.98	22.49	79.41	0.74
100	65.9	10.9	2.4	5.53	2.23	0.98	18.95	9.18	0.96	22.36	48.45	0.99
101	23.9	10.9	2.4	16.39	3.64	0.97	22.71	30.68	0.99	22.48	79.58	0.77
102	21	10.9	2.4	19.63	4.22	0.97	22.00	36.51	0.97	21.50	90.51	0.99
103	67.7	6.8	0.6	7.27	2.26	0.95	22.98	12.17	0.97	20.58	57.48	0.95
104	39	6.8	0.6	15.49	7.69	0.98	24.70	31.44	0.99	23.81	87.94	0.99
105	24.6	6.8	0.6	18.45	5.15	0.96	22.07	37.16	0.98	23.16	86.14	0.96
106	66.1	6.1	2.7	5.31	1.12	0.96	18.46	9.31	0.94	22.81	51.69	0.99
107	21.1	6.1	2.7	16.81	4.47	0.96	21.81	35.00	0.99	22.54	84.67	0.94
108	17.5	6.1	2.7	17.66	4.82	0.96	22.36	34.07	0.99	21.52	86.89	0.99
109	65.3	6	3	4.67	1.53	0.95	20.53	8.47	0.96	22.48	52.64	0.98
110	28.9	6	3	15.16	4.56	0.95	24.89	26.71	0.99	23.48	78.58	0.98
111	14.7	6	3	18.04	3.10	0.96	22.39	36.13	0.98	24.69	92.52	1.00
112	66	5.9	2.7	5.49	0.98	0.92	19.78	8.71	0.94	25.32	52.62	0.99
113	32	5.9	2.7	15.24	3.00	0.96	23.41	28.50	1.00	20.49	77.33	0.98
114	17	5.9	2.7	18.86	2.79	0.95	22.44	34.29	0.99	22.44	88.00	0.99
115	66.3	5.6	2.7	4.77	1.66	0.94	19.40	9.80	0.96	22.62	53.34	0.99
116	32.1	5.6	2.7	14.90	5.72	0.96	24.87	29.45	0.99	20.33	81.44	0.99
117	15.1	5.6	2.7	18.14	3.21	0.97	22.46	35.36	0.99	19.41	81.49	0.94
118	68.3	4.5	2.5	6.06	1.26	0.92	21.48	10.46	0.94	23.70	55.37	0.99
119	32.1	4.5	2.5	15.44	3.66	0.97	22.62	28.88	1.00	29.49	72.95	0.92
120	27.9	4.5	2.5	16.88	3.57	0.96	23.45	29.48	0.99	18.68	76.12	0.99
121	67.5	4.1	2.1	5.26	1.45	0.95	20.42	9.60	0.95	21.38	52.68	0.98
122	26	4.1	2.1	15.91	6.18	0.95	23.98	32.26	1.00	21.96	79.93	0.99
123	21.2	4.1	2.1	16.91	4.11	0.96	23.47	31.83	0.99	17.56	82.10	0.95

Table IX. Continued

Sample No.	CrIb	Lignin	Acetyl	1-h Total Sugar			6-h Total Sugar			72-h Total Sugar		
				B	*A*	R^2	*B*	*A*	R^2	*B*	*A*	R^2
124	62.7	2.5	0.4	7.96	3.93	0.97	25.19	14.03	0.95	27.46	69.17	0.99
125	22.4	2.5	0.4	16.29	4.35	0.96	23.59	30.31	0.99	25.84	87.45	0.99
126	19.5	2.5	0.4	18.34	5.09	0.97	26.98	32.64	0.99	26.73	88.52	0.99
127	68.8	1.8	2.7	3.74	1.17	0.93	7.87	11.07	0.99	22.55	44.47	1.00
128	37	1.8	2.7	12.91	5.20	0.96	23.88	23.49	0.99	19.44	76.10	0.99
129	5.4	1.8	2.7	15.54	3.68	0.97	23.68	30.54	0.99	26.92	75.45	0.85
130	68.2	1.6	2.6	4.65	1.31	0.92	17.90	7.32	0.94	25.44	46.98	0.99
131	46.9	1.6	2.6	11.85	1.86	0.96	24.48	17.91	0.99	30.40	65.02	0.96
132	21.5	1.6	2.6	14.95	2.51	0.95	27.12	22.93	0.99	20.18	69.83	0.99
133	65.7	1.6	2.3	3.74	1.34	0.94	15.44	8.10	0.98	24.61	42.33	1.00
134	50.6	1.6	2.3	10.24	3.07	0.93	21.75	19.43	0.99	21.05	62.63	0.99
135	19.2	1.6	2.3	14.37	1.61	0.95	24.83	22.36	1.00	20.08	76.22	0.98
136	64.6	1.5	2.2	5.45	2.31	0.98	18.81	9.78	0.95	26.62	45.68	0.99
137	48	1.5	2.2	11.91	1.46	0.95	23.45	16.91	0.99	23.07	64.45	1.00
138	14.9	1.5	2.2	16.47	2.56	0.95	23.45	27.86	0.99	26.86	84.50	0.99
139	65.4	1.3	1.8	4.91	1.56	0.92	17.65	8.36	0.96	22.54	47.58	0.99
140	47.1	1.3	1.8	12.03	3.03	0.96	24.30	17.48	0.99	22.85	68.04	0.99
141	11.7	1.3	1.8	16.06	1.84	0.95	24.67	27.45	0.99	25.85	84.46	0.95
142	62.3	1.1	1.6	6.69	2.57	0.96	21.55	9.31	0.96	24.84	52.76	0.99
143	44.8	1.1	1.6	12.29	2.66	0.96	24.98	18.23	0.99	25.59	70.55	0.98
144	10.8	1.1	1.6	15.02	3.23	0.95	24.49	26.09	0.99	26.24	84.35	0.99
145	66	0.7	0.1	8.57	2.38	0.94	24.70	13.54	0.97	26.67	63.04	0.99
146	50.9	0.7	0.1	14.46	2.78	0.96	28.59	15.48	0.99	22.83	73.16	0.99
147	33	0.7	0.1	15.03	3.02	0.96	24.75	24.51	1.00	30.02	72.78	0.94

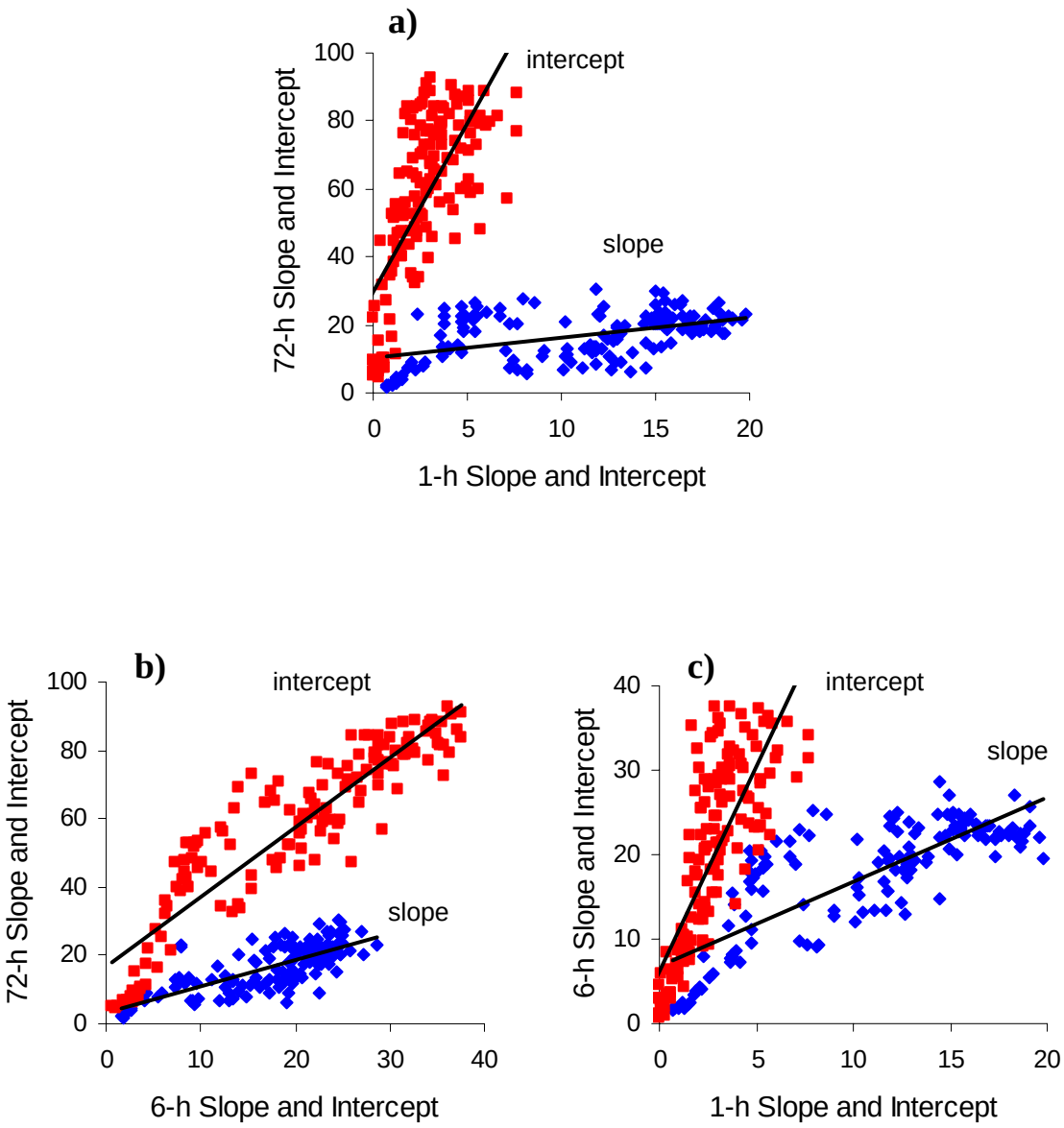

Figure 18. Correlation between total sugar slope and intercept: (a) 1-h slope versus 72-h slope and 1-h intercept versus 72-h intercept, (b) 72-h slope versus 6-h slope and 72-h intercept and 6-h intercept, (c) 1-h slope and 6-h slope and 1-h intercept versus 6-h intercept. Data from Table IX.

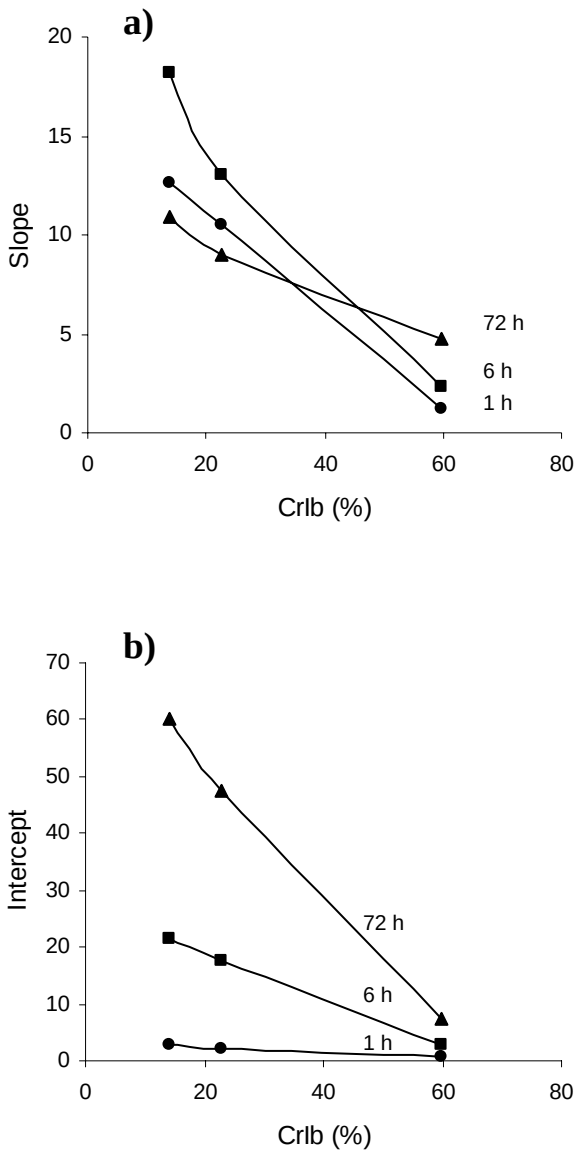

Figure 19. Effect of CrIb on total sugar (a) slope and (b) intercept while holding acetyl (2.8%) and lignin (22.8%) constant. Data taken from Table IX.

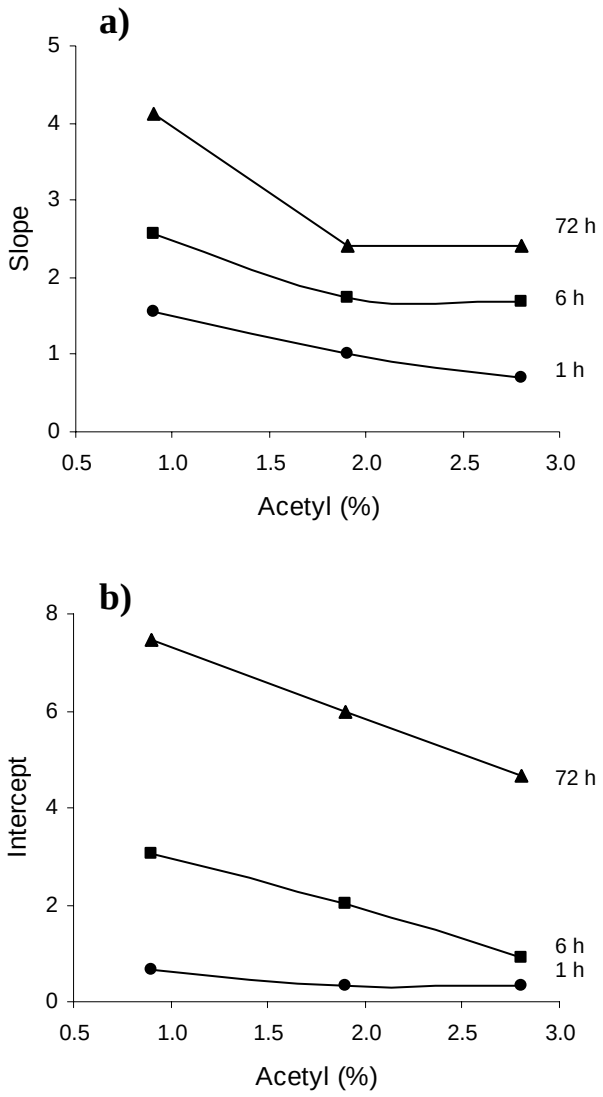

Figure 20. Effect of acetyl on total sugar (a) slope and (b) intercept while holding CrIb (56.3–60%) and lignin (25.5–26%) constant. Data taken from Table IX.

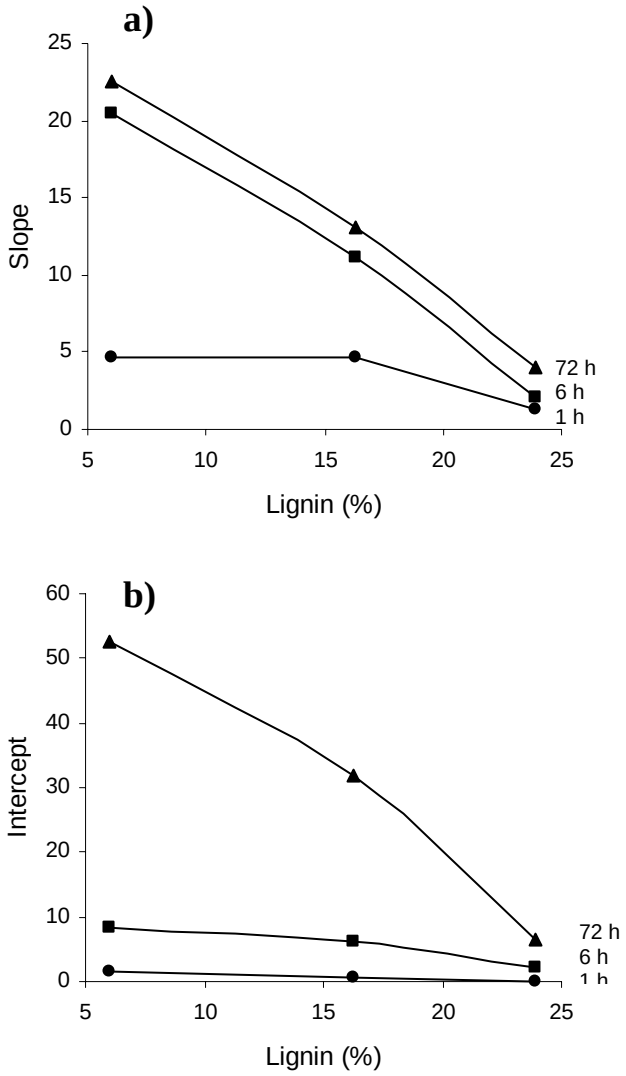

Figure 21. Effect of lignin on total sugar (a) slope and (b) intercept while holding CrIb (60.2–65.3%) and acetyl (2.8–3.0%) constant. Data taken from Table IX.

arrived at a similar conclusion when studying the effect of lignin, crystallinity, and acetyl content on sugar conversion. When investigated independently, crystallinity and lignin have a major affect on the slope and intercept whereas acetyl elicits only a minor affect on the slope and intercept at 1, 6, and 72 h. This suggests that the major barriers limiting initial rates and ultimate conversions are biomass crystallinity and lignin content. In agreement with our work, Fan et al. (1981a) discovered that initial hydrolysis rates strongly depend on the effectiveness of the adsorbed protein to promote hydrolysis, which was shown to be a function of the crystallinity index.

Figures 22 and 23 illustrate the effects of crystallinity and acetyl content on total sugar slopes and intercepts at 1, 6, and 72 h for high-lignin (24.5–26.3%) and low-lignin (0.7–1.8%) samples, respectively. Figures 24 and 25 illustrate the effects of crystallinity and lignin content on total sugar slopes and intercepts at 1, 6, and 72 h for high-acetyl (2.7–2.9%) and low-acetyl (0.3–0.6%) samples, respectively. Figures 26 and 27 illustrate the effects of acetyl and lignin content on total sugar slopes and intercepts at 1, 6, and 72 h for high-crystallinity (55.4–66.2%) and low-crystallinity (9.4–20.6%) samples, respectively. Table X summarizes the effects of lignin, acetyl, and crystallinity on the slopes (*B*) and intercepts (*A*) of the 147 poplar wood model samples. It appears that low crystallinity results in moderate increases in 1-h slopes regardless of lignin content or acetyl content. Low lignin and low crystallinity led to high 1-h slopes regardless of acetyl content. Interestingly, none of the structural features investigated had a significant effect on 1-h intercepts, which ranged from 1–6. Either low lignin or low crystallinity led to moderate increases in 6-h slopes. It was shown that low lignin and low crystallinity resulted in large 6-h slopes regardless of acetyl content. High 6-h intercepts were observed with either low crystallinity and acetyl or low crystallinity and lignin. Only a moderate increase in 6-h intercepts occurred with low lignin and low acetyl. This supports the findings from Figure 19 that suggest crystallinity elicits a major influence on early biomass digestibility. Low lignin, low lignin and low acetyl, or low lignin and low crystallinity resulted in high 72-h slopes. Low lignin resulted in a moderate increase in 72-h intercepts regardless of crystallinity or acetyl content. Low

lignin and low crystallinity gave rise to high 72-h intercepts regardless of acetyl content. In summary, crystallinity appears to be the rate-limiting factor in 1-h and 6-h biomass digestibility whereas lignin content appears to be the rate-limiting factor in 72-h biomass digestibility. Consequently, acetyl content appears to have minimal affect on 1-h, 6-h, and 72-h rates. However, when low acetyl is combined with low crystallinity, 1-h and 6-h intercepts increase from moderate to high. This suggests that acetyl content alone does not greatly affect reactivity, but when combined with another structural feature such as low crystallinity, it can alter the extent of digestibility.

Biomass hydrolysis is complicated due to its complex physical structure and the intricate nature of its internal associations. The resulting heterogeneous reaction system requires enzyme diffusion to the substrate and subsequent adsorption prior to hydrolysis. Once adsorbed, the enzymes can begin to elicit their catalytic effects on hemicellulose and cellulose.

As discovered in prior experiments and proposed by Mansfield et al. (1999), enzyme diffusion only becomes a limiting factor in enzymatic hydrolysis at high substrate concentrations because of the limited mobility of the enzymes. When enzyme diffusion obstacles are eliminated, enzymatic hydrolysis solely depends on enzyme accessibility and efficiency, which depends on biomass structural features such as lignin content, acetyl content, and crystallinity. Mansfield et al. (1999) also proposed that the initial hydrolysis rate is strongly affected by the degree of cellulose crystallinity and the amount of adsorbed enzyme, which has been shown to be a function of specific surface area or particle size (Lee and Fan, 1982) and pore volume or accessible surface area (Mooney et al., 1998). Likewise, Lee and Fan (1982) suggested that the initial hydrolysis rate strongly depends on the initial extent of enzyme adsorption and the effectiveness of the adsorbed enzyme to hydrolyze the substrate. Additionally, Kong et al. (1992) have shown that as the degree of acetyl content decreases the biomass swellability increases (i.e., water retained by biomass). This increased swellability resulted in an increase in glucose and xylose conversion. Lignin is thought to affect biomass digestibility by acting as a barrier to prevent successful binding of the enzyme

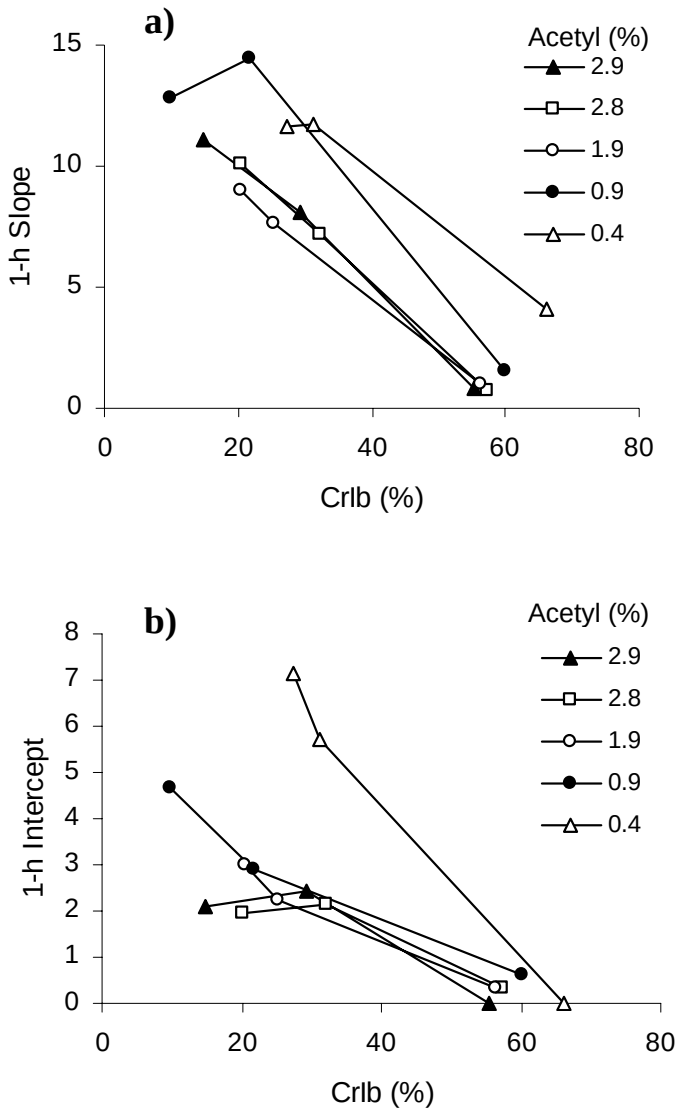

Figure 22. Effects of CrIb and acetyl on 1-h total sugar (a) slope and (b) intercept, 6-h total sugar (c) slope and (d) intercept, and 72-h total sugar (e) slope and (f) intercept. All samples had a high lignin content (24.5–26.3%). Data from Table IX.

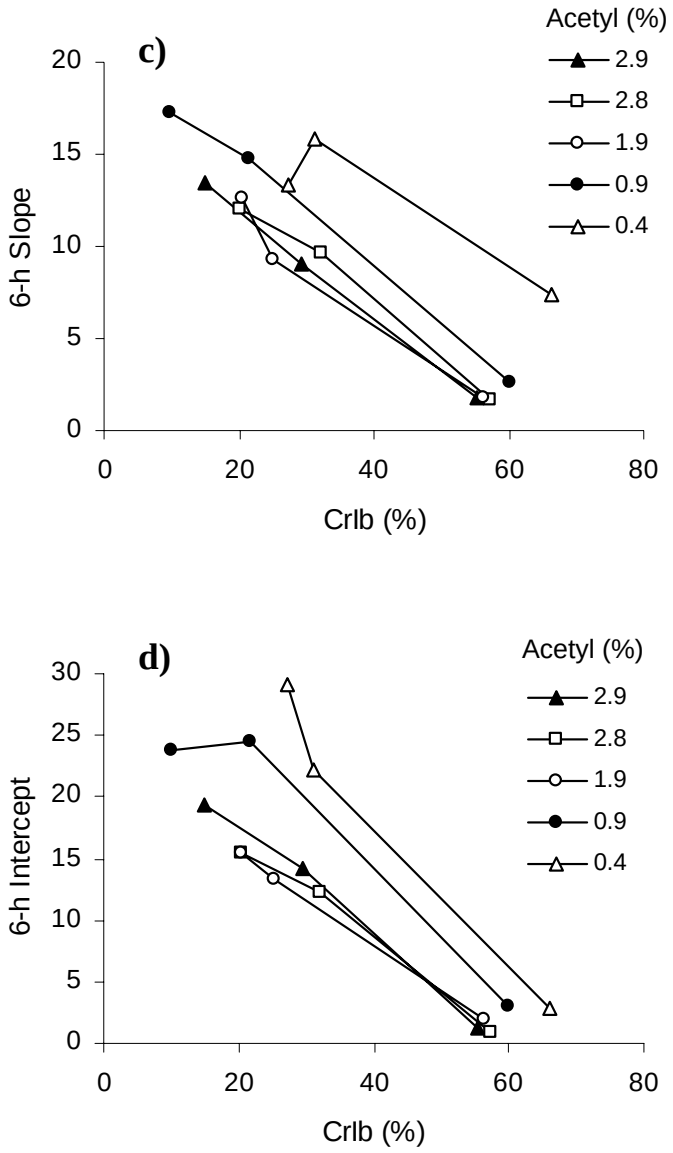

Figure 22. Continued

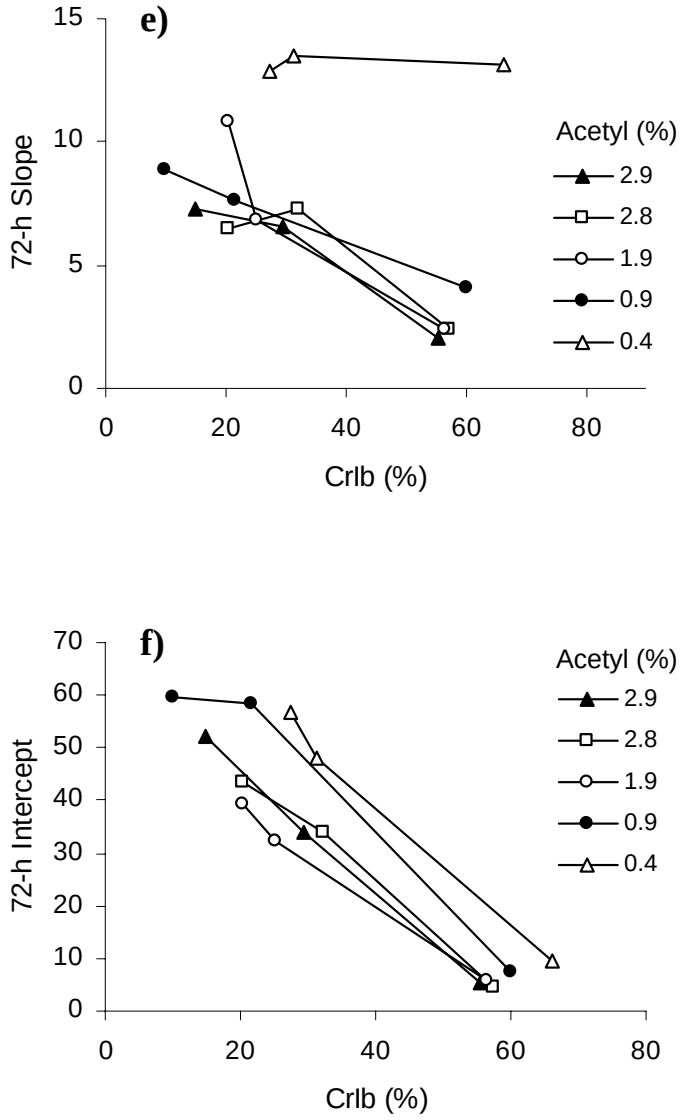

Figure 22. Continued

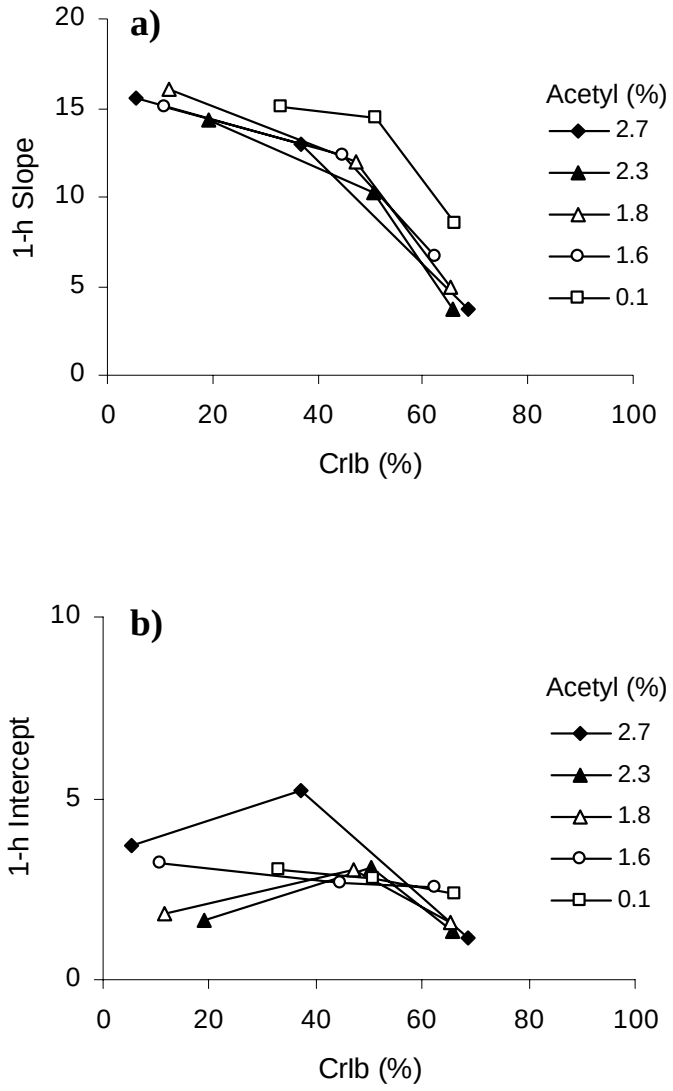

Figure 23. Effects of CrIb and acetyl on 1-h total sugar (a) slope and (b) intercept, 6-h total sugar (c) slope and (d) intercept, and 72-h total sugar (e) slope and (f) intercept. All samples had a low lignin content (0.7–1.8%). Data from Table IX.

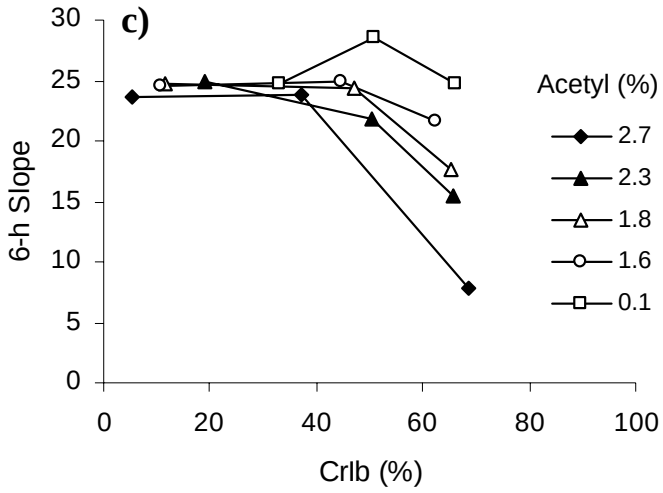

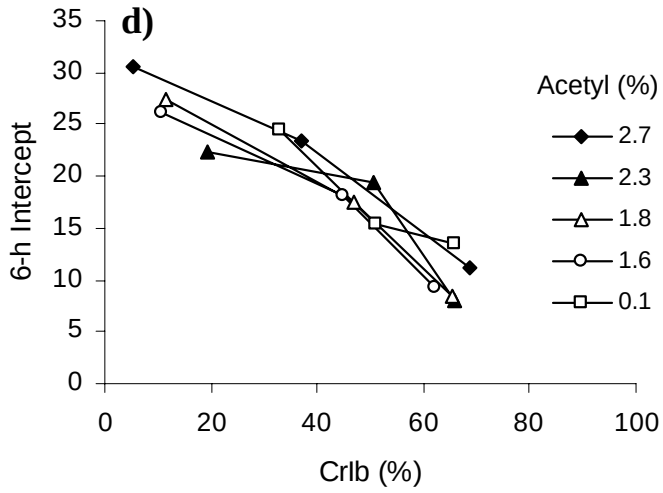

Figure 23. Continued

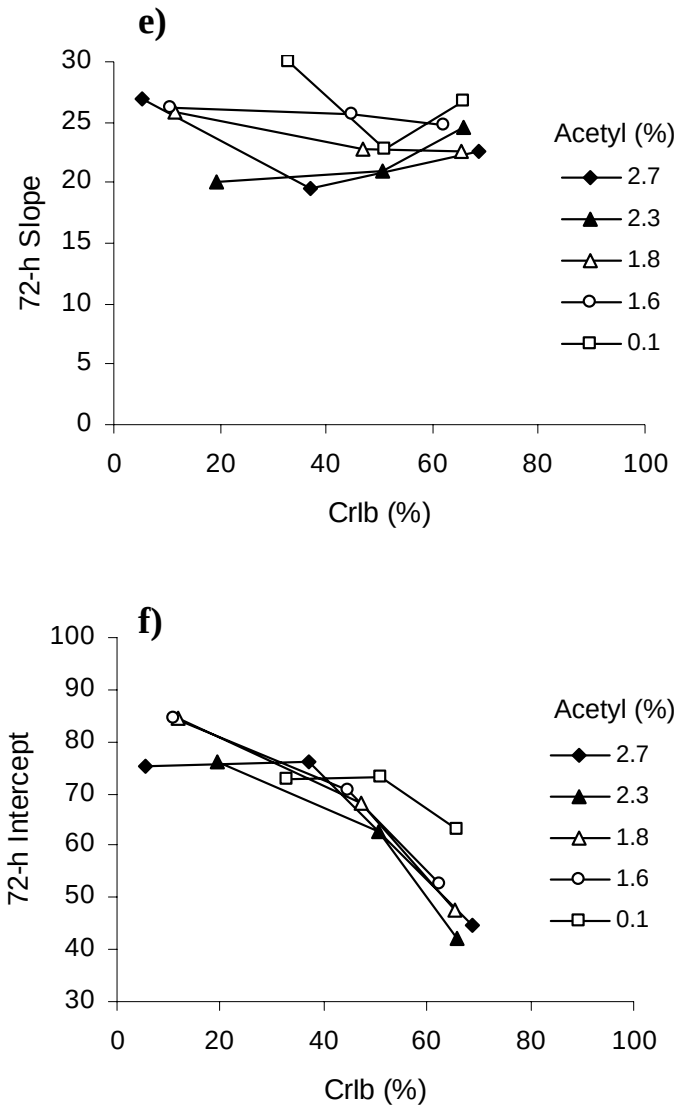

Figure 23. Continued

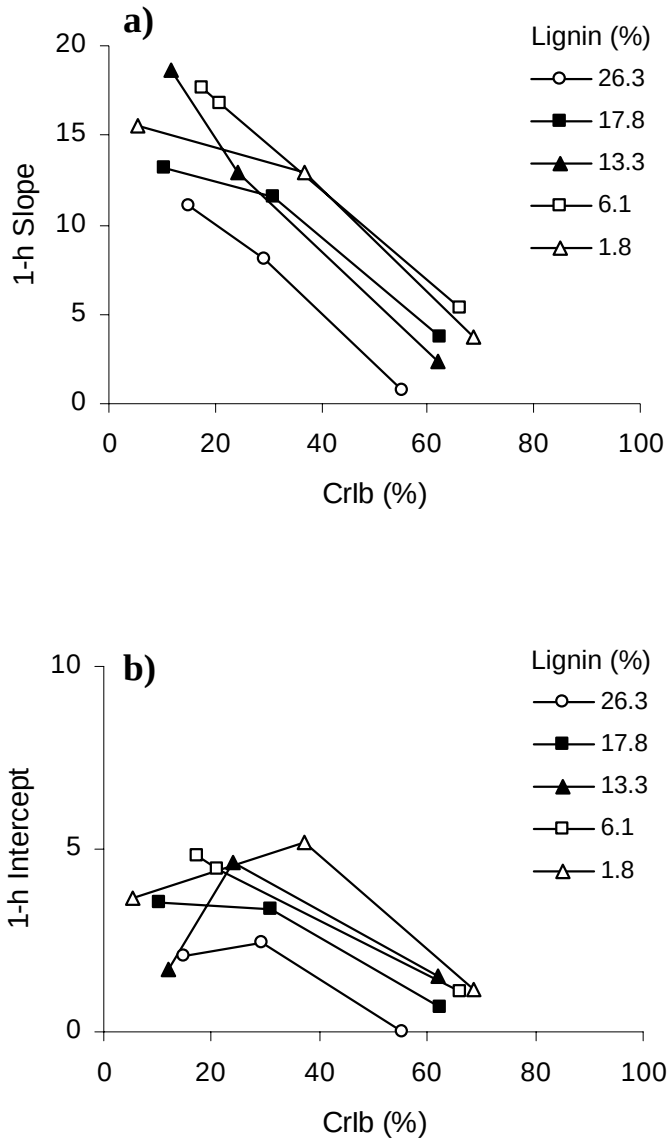

Figure 24. Effects of CrIb and lignin on 1-h total sugar (a) slope and (b) intercept, 6-h total sugar (c) slope and (d) intercept, and 72-h total sugar (e) slope and (f) intercept. All samples had a high acetyl content (2.7–2.9%). Data from Table IX.

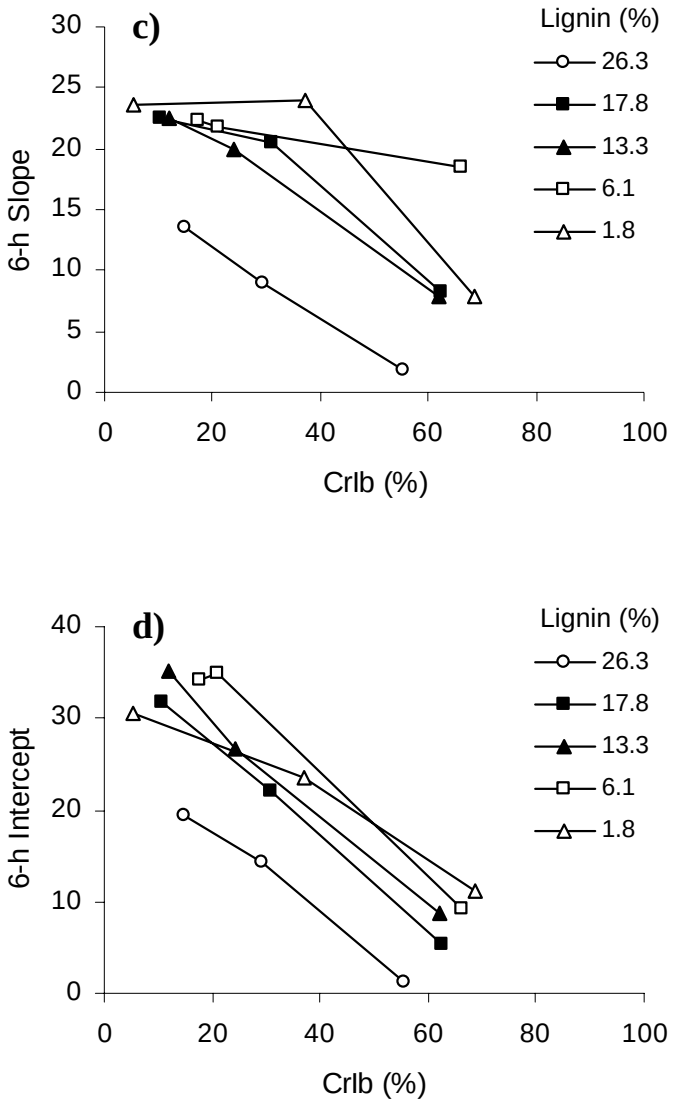

Figure 24. Continued

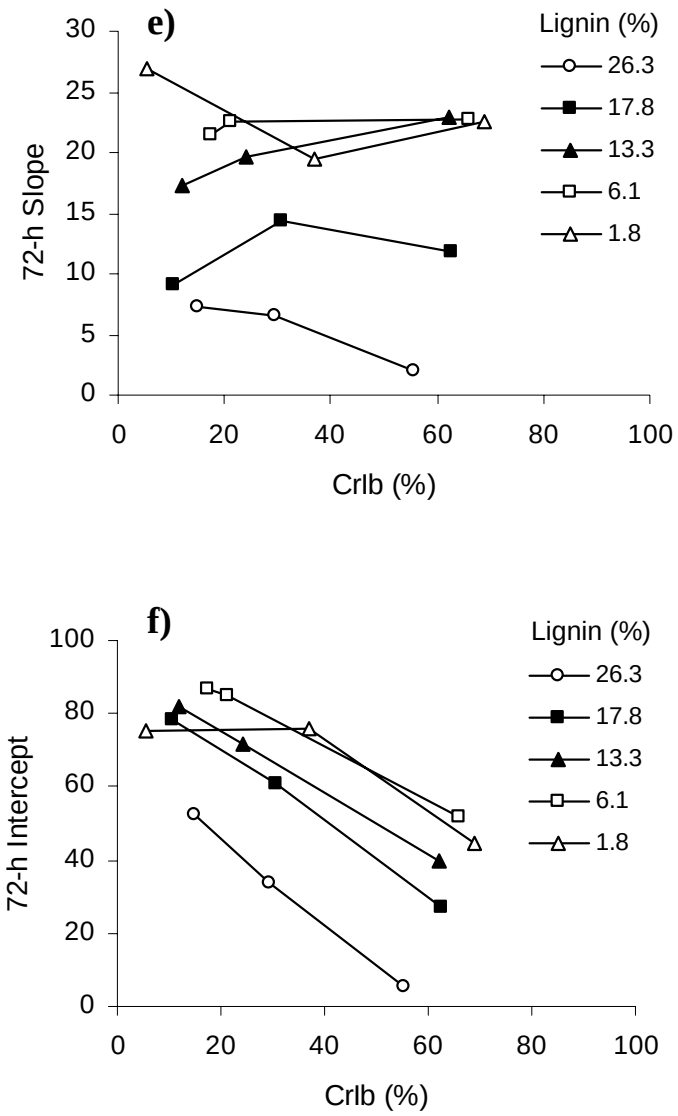

Figure 24. Continued

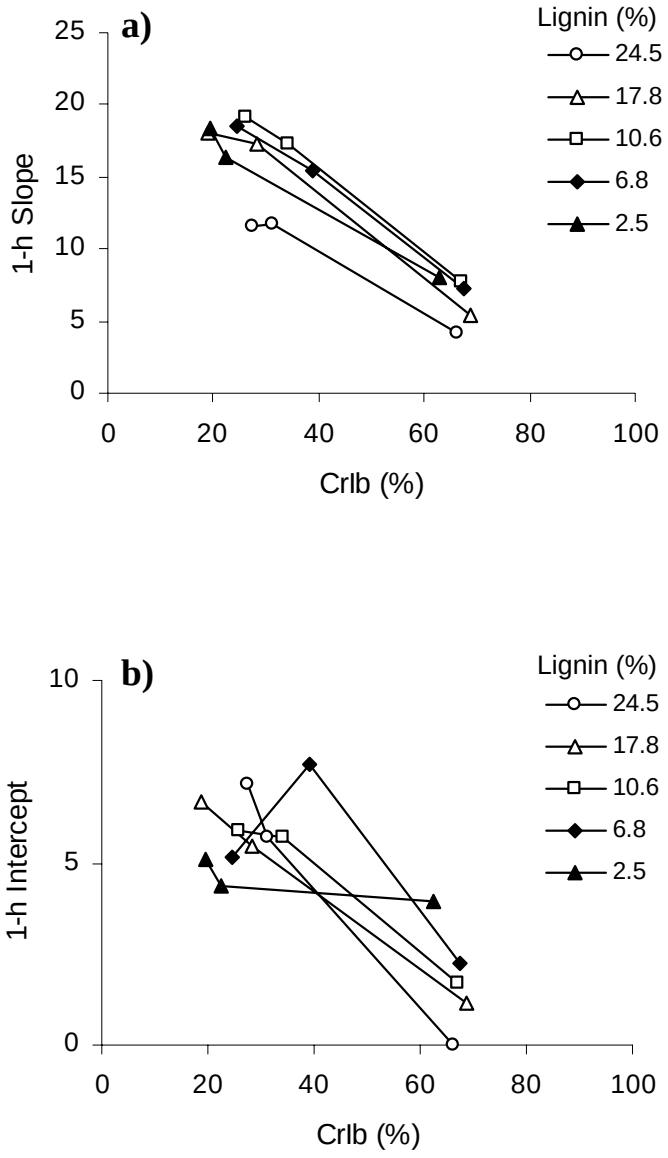

Figure 25. Effects of CrIb and lignin on 1-h total sugar (a) slope and (b) intercept, 6-h total sugar (c) slope and (d) intercept, and 72-h total sugar (e) slope and (f) intercept. All samples had a low acetyl content (0.3–0.6%). Data from Table IX.

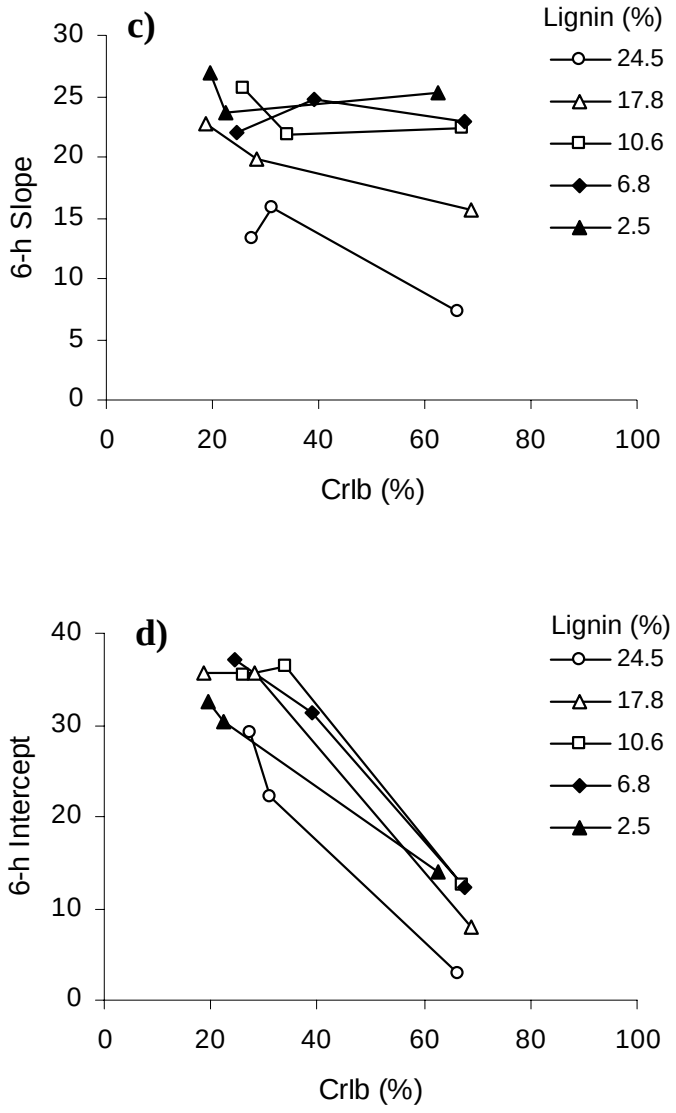

Figure 25. Continued

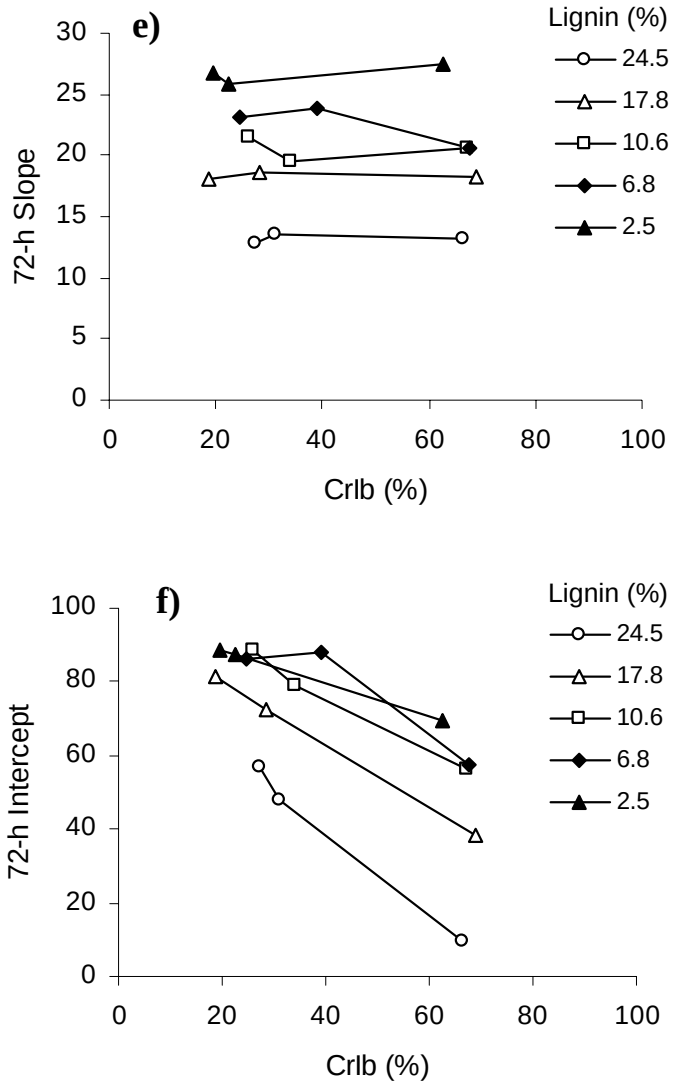

Figure 25. Continued

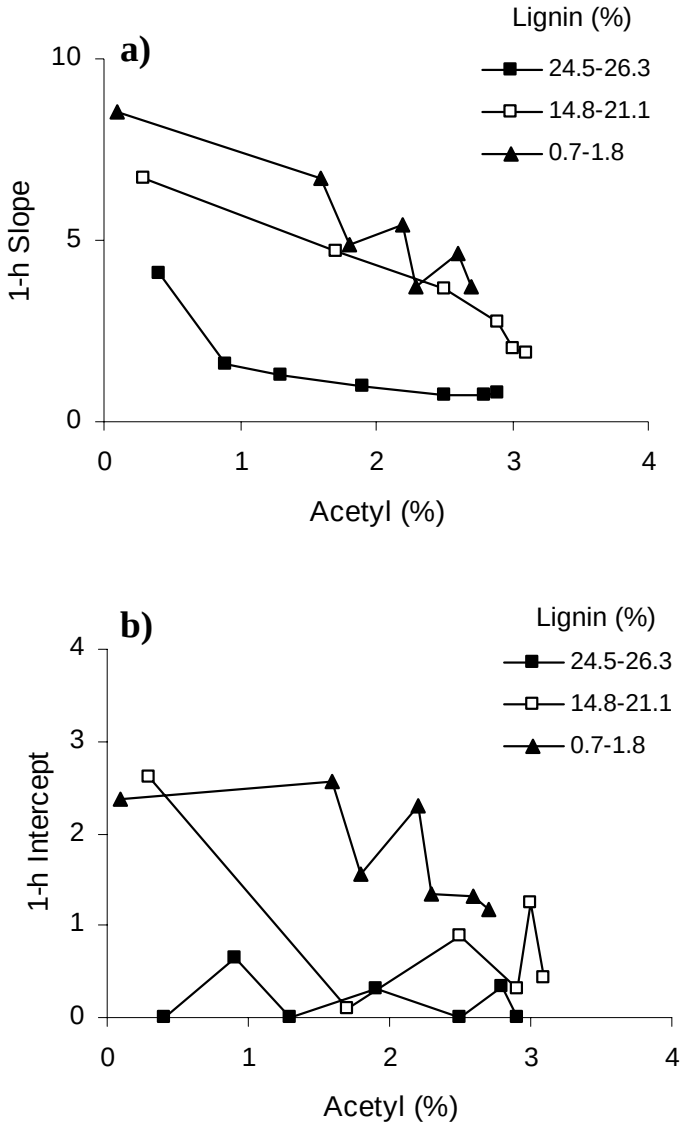

Figure 26. Effects of acetyl and lignin on 1-h total sugar (a) slope and (b) intercept, 6-h total sugar (c) slope and (d) intercept, and 72-h total sugar (e) slope and (f) intercept. All samples had a high crystallinity index (55.4–66.2%). Data from Table IX.

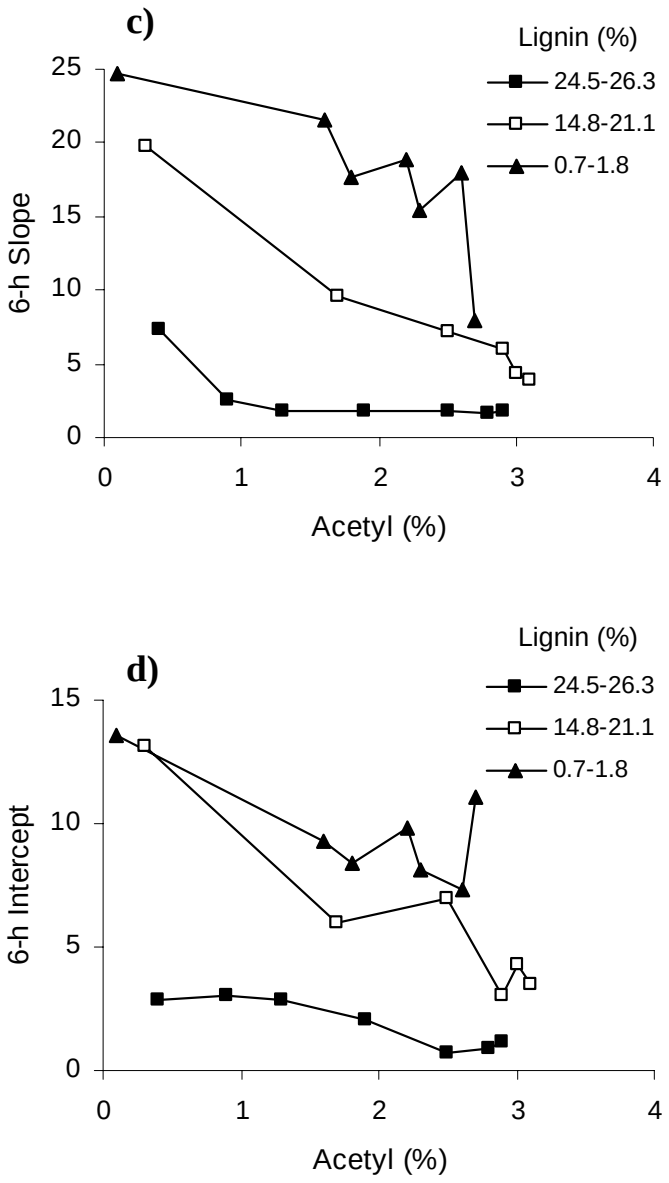

Figure 26. Continued

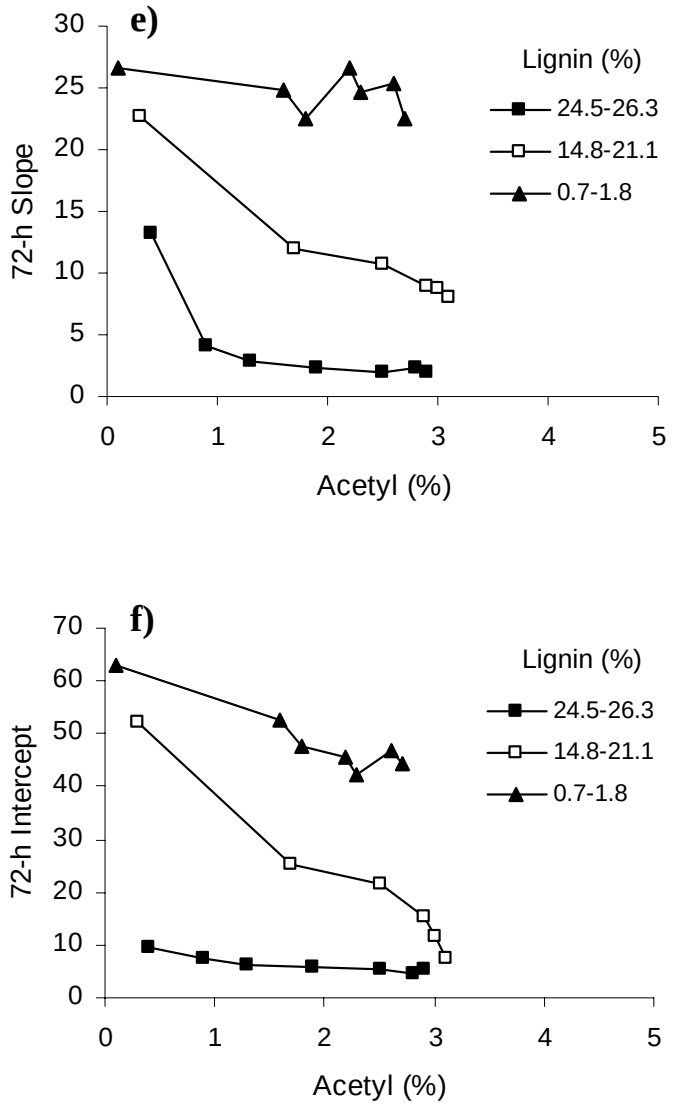

Figure 26. Continued

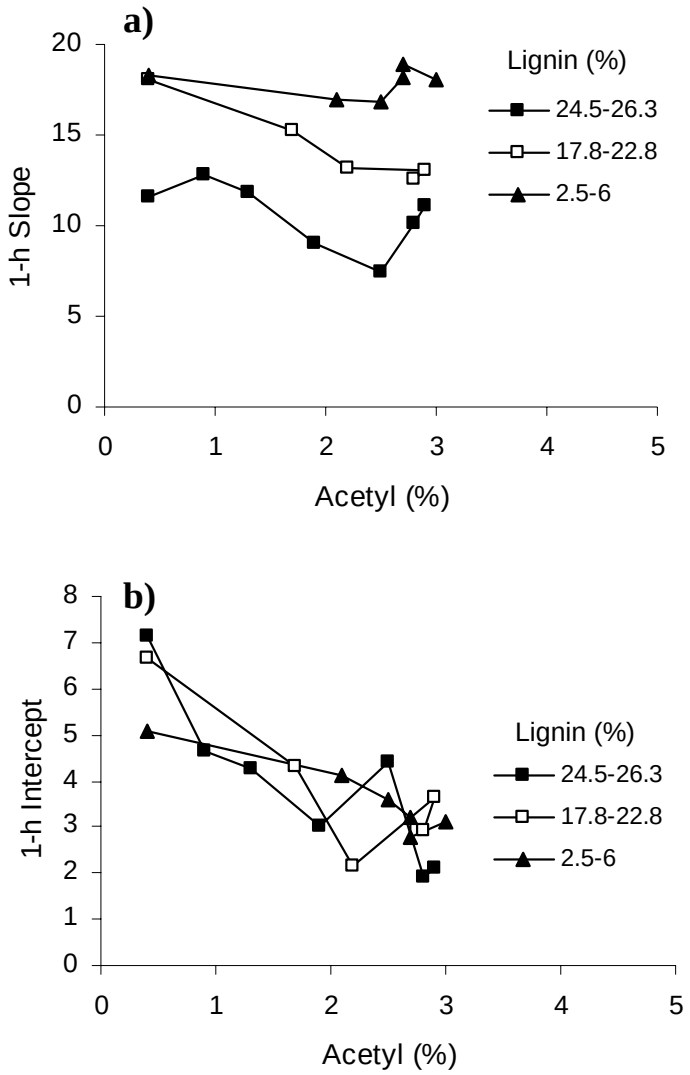

Figure 27. Effects of acetyl and lignin on 1-h total sugar (a) slope and (b) intercept, 6-h total sugar (c) slope and (d) intercept, and 72-h total sugar (e) slope and (f) intercept. All samples had a low crystallinity index (9.4–20.6%). Data from Table IX.

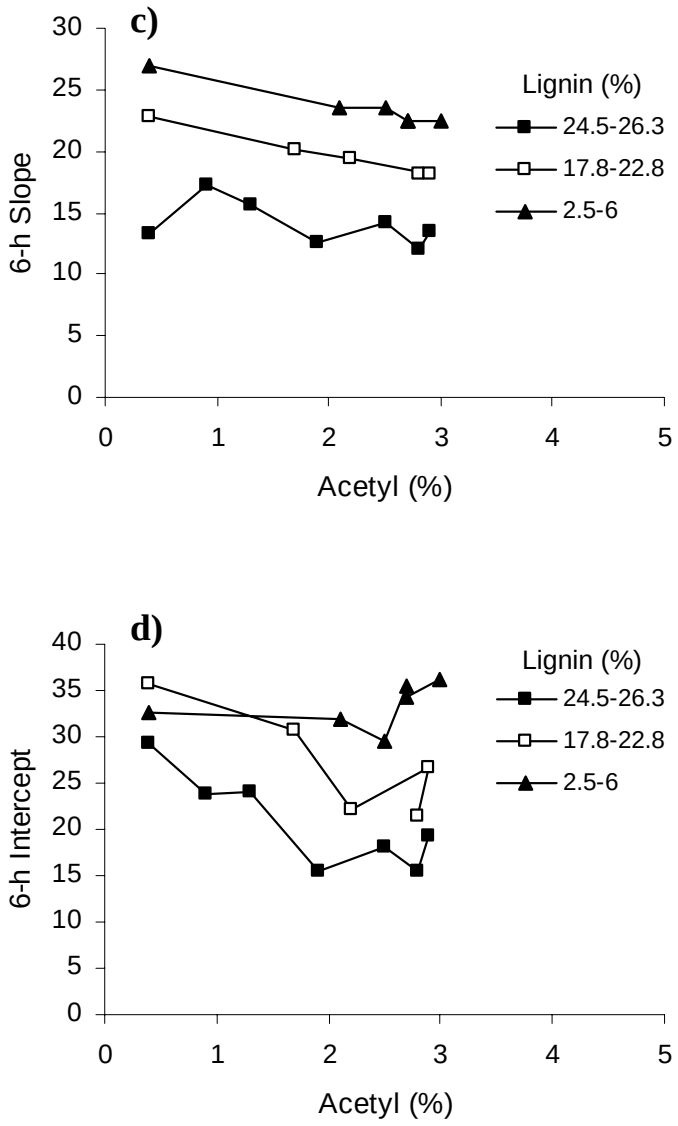

Figure 27. Continued

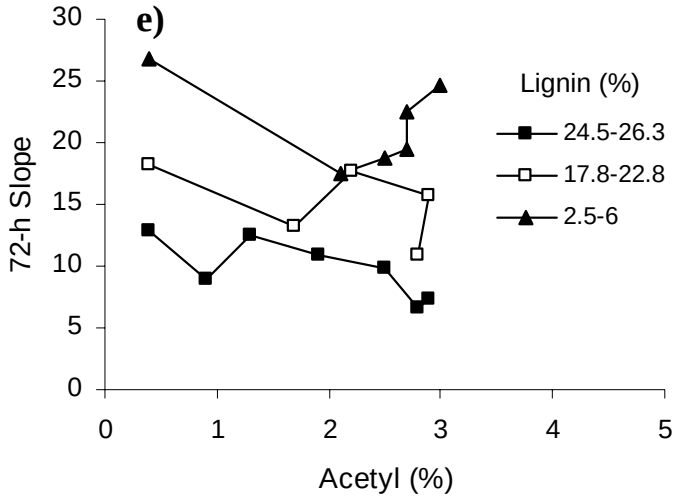

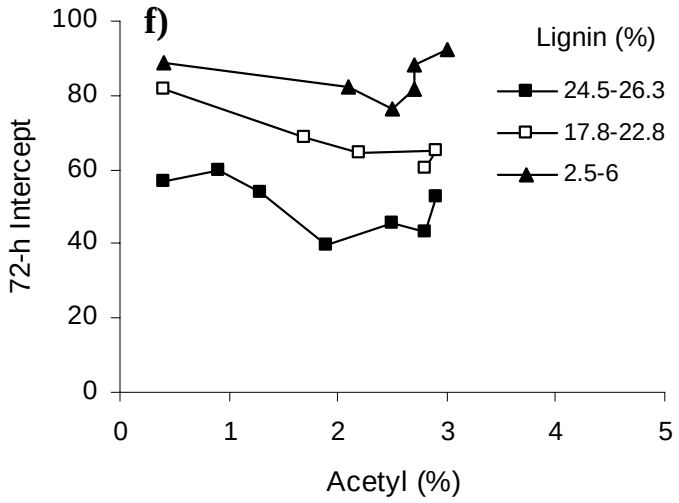

Figure 27. Continued

Table X. Summary of the effects of lignin, acetyl, and crystallinity on 1-, 6-, and 72-h total sugar slopes (*B*) and intercepts (*A*)[a].

Lignin		Acetyl		Crystallinity		Total Sugar					
						1 h		6 h		72 h	
High	Low	High	Low	High	Low	*B*	*A*	*B*	*A*	*B*	*A*
×		×		×		L[b]	L	L	L	L	L
×		×			×	M	M	M	M	M	M
×			×	×		L	L	L	L	M	L
×			×		×	M	H	M	H	M	M
	×	×		×		L	L	M	M	H	M
	×	×			×	H	H	H	H	H	H
	×		×	×		M	M	H	M	H	M
	×		×		×	H	H	H	H	H	H

[a] Summarized from Figures 22–27.

[b] L = low, M = moderate, and H = high. These are relative to the actual tabulated values.

to the substrate and by irreversibly binding free enzyme. Additionally, Grethlein (1984) and Saddler et al. (1998) have shown that lignin removal increased porosity, which led to increased biomass swellability. This increase in swellability is related to enzyme accessibility due to larger pore volumes and increased internal surface area, which increased biomass hydrolysis.

The structural features (acetyl content, lignin content, and crystallinity) chosen to be investigated can be divided into two categories. The first category is classified as those features (crystallinity) that affect the rate of reaction (i.e., the effectiveness of the enzymes). Structural features (lignin and acetyl) that not only limit enzyme access to the substrate but also in the case of lignin bind and inactivate otherwise active enzymes define the second category.

The results of our work agree with Mansfield et al. (1999), Lee and Fan (1982), and Saddler et al. (1998). A summary of the structural features effect on slopes (*B*) and intercepts (*A*) of the 147 model samples can be found in Table X. Figures 22a and 22b show that low crystallinity had a significant effect on 1-h slopes and intercepts, respectively. We discovered that low lignin had a slightly less influential effect on 1-h slopes (Figure 24a) and intercepts (Figure 24b) when compared to low crystallinity. As illustrated in Figure 24, 6-h slopes and intercepts increased significantly with either decreasing lignin content or crystallinity. The slopes and intercepts increased from baseline levels to 50% of the maximum values observed at 1 h and 6 h when investigating either low lignin or low crystallinity. By comparing Figure 24 (high acetyl samples) to Figure 25 (low acetyl samples), it was discovered that acetyl content had little affect on 1-h slopes and intercepts and 6-h slopes and intercepts compared to samples with either low crystallinity or low lignin. When samples with both low lignin and low crystallinity were investigated, the combined effect resulted in a two-fold increase in the 1-h slopes and intercepts and 6-h slopes and intercepts (Figure 24) versus the case when either low lignin or low crystallinity was investigated alone. Thus, either low lignin or low crystallinity is enough to elicit a marked effect on digestibility whereas a combination of the two results in maximal 1-h slopes and intercepts and 6-h slopes and

intercepts regardless of acetyl content. Therefore, our results support the theory that the initial rate of hydrolysis depends on both the extent of enzyme adsorption and the effectiveness of the adsorbed enzyme. This is best explained by thinking of lignin as a bottleneck that prevents enzyme access to the substrate, but once there, enzyme effectiveness is controlled by the degree of cellulose crystallinity. This is logical because crystalline cellulose has been shown to be more recalcitrant than the amorphous portions due to the slow action of the CBHs required to degrade crystalline cellulose (Mansfield et al., 1999; Lee and Fan, 1982; Liu et al., 1991; Srishdsuk et al., 1998). Therefore, biomass samples with similar lignin contents but different crystallinity indices will illustrate noticeably different initial digestibilities with the higher crystalline biomass being more recalcitrant. Others (Sinitsyn et al., 1991; Nieves et al., 1991) have shown that cellulases primarily attack the more disordered portions of the cellulose fiber during initial hydrolysis. Our work suggests that lignin content and crystallinity are obstacles linked in series that hinder the initial rate of hydrolysis. Removing either one will enhance digestibility while removing both significantly increases digestibility.

Saddler et al. (1998) found that even though initial hydrolysis conversions of a Douglas-fir refiner mechanical pulp (high lignin content) and kraft pulp (low lignin content) were similar (5% and 12% respectively), their ultimate conversions (72-h or longer incubation times) were markedly different with the kraft pulp having an 85% conversion versus a 20% conversion for the Douglas-fir pulp. Our results agree with Saddler et al. (1998). We discovered that low lignin alone resulted in the highest observed 72-h slopes (ca. 27) regardless of acetyl or crystallinity. This is illustrated in Figure 23e where the slope is constant even when acetyl content and crystallinity were decreased. Figure 23f illustrates that low lignin in combination with low crystallinity resulted in the highest 72-h intercepts (ca. 90). Figure 23f also shows that reducing acetyl content from 2.7–0.1% moderately increased the 72-h intercept from 45 to 62. Therefore, it was concluded that lignin was the major hurdle in limiting complete hydrolysis of the biomass carbohydrate components. Even though 1 h hydrolysis rates are influenced by both lignin (enzyme accessibility) and crystallinity (enzyme

efficiency), the ultimate digestibility is predominantly controlled by lignin. As compared to 1-h and 6-h digestibility, 72-h digestibility appears to be limited by the distribution and amount of lignin. It is hypothesized that after 72 h the undigested biomass has a very high lignin content and the cellulose and hemicellulose are closely associated if not completely surrounded by the lignin, thereby preventing enzyme access to the carbohydrates. This makes sense because one could envision a biomass sample having low lignin and high crystallinity, which would give rise to low initial hydrolysis rates. However, the enzymes will completely degrade the biomass sample given sufficient time because the enzymes have complete access to the substrate. This assumes there are sufficient amounts of the CBH enzymes, which have been shown to degrade crystalline cellulose.

It has been shown by several authors that hardwood substrates are inherently less resistant to lignin removal and redistribution than softwoods (Grethlein et al., 1984; Ramos et al., 1992). The lignin in softwoods is primarily guaiacyl whereas hardwoods have a mix of guaiacyl and syringyl lignin. Ramos et al. (1992) suggest that guaiacyl lignin restricts fiber swelling and thus enzyme accessibility more so than syringyl lignin. The fiber swelling can result in a larger specific surface area upon wetting. The fact that our substrate was hardwood (poplar wood) should be considered when comparing results to other types of biomass.

Puri (1984) found that mechanically pretreating (ball milling) biomass not only decreased crystallinity but also resulted in decreased particle size and increased available surface area. This was due to the crushing and shearing action of the ball mill. Our samples that were subjected to ball milling had a smaller average particle size and an increased swellability versus the samples not subjected to ball milling. Gharpuray et al. (1983) proposed that the increased digestibility from ball-milled samples is a result of decreased particle size and increased available specific surface area, rather than a result of reduced crystallinity. However, some studies have reported conflicting results in regard to the effect of SSA on biomass digestibility. Fan et al. (1980) concluded that surface area had no effect on the digestibility of biomass. In contrast, Gharpuray et al.

(1983), Sinitsyn et al. (1991), and Nazhad et al. (1995) determined that specific surface area plays a major role in limiting biomass enzymatic hydrolysis. The conflicting results may be due to different methods (N_2 adsorption versus solute exclusion method) used to determine specific surface area. We have shown that crystallinity exhibits an inverse relationship with slopes and intercepts, but whether or not this is the underlying structural feature responsible for the observed increase in digestibility will be discovered when developing the neural network models. If the models do not accurately predict slopes and intercepts, this would suggest that there are other structural features that may play a more prominent role in affecting biomass digestibility.

Figures 28 and 29 were created with data from Tables VII and VIII. Figures 28 and 29 illustrate the effect of lignin, crystallinity, and acetyl on glucan and xylan intercepts. Figure 28 displays flat profiles for 1-h and 72-h glucan intercepts. Therefore, glucan intercepts are not influenced by biomass acetyl content. However, xylan intercepts in Figure 28 display a strong correlation with biomass acetyl content. Figure 29b shows that both 72-h glucan and 72-h xylan intercepts are a function of biomass lignin content. However, 1-h xylan intercepts demonstrate a more significant correlation with lignin content than 1-h glucan intercepts. Our results show that acetyl content has a major affect on 1-h and 72-h xylan digestibility. This concurs with the findings of Grohmann et al. (1989). The same cannot be said when investigating glucan digestibility. Because the acetyl content, lignin content, and crystallinity affect glucan and xylan digestibility differently, separate neural network models will be developed for glucan, xylan, and total sugar at 1, 6, and 72 h.

Method of Reproducibility

The reproducibility of biomass enzymatic hydrolysis experiments was determined by conducting internal and external tests. The experimental conditions were the same as described in “Material and Methods.” Samples 7 and 145 were chosen as representative samples of the extremes exhibited of our poplar wood model samples’ inherent digestibility. Sample 7 is highly recalcitrant (small slopes and intercepts)

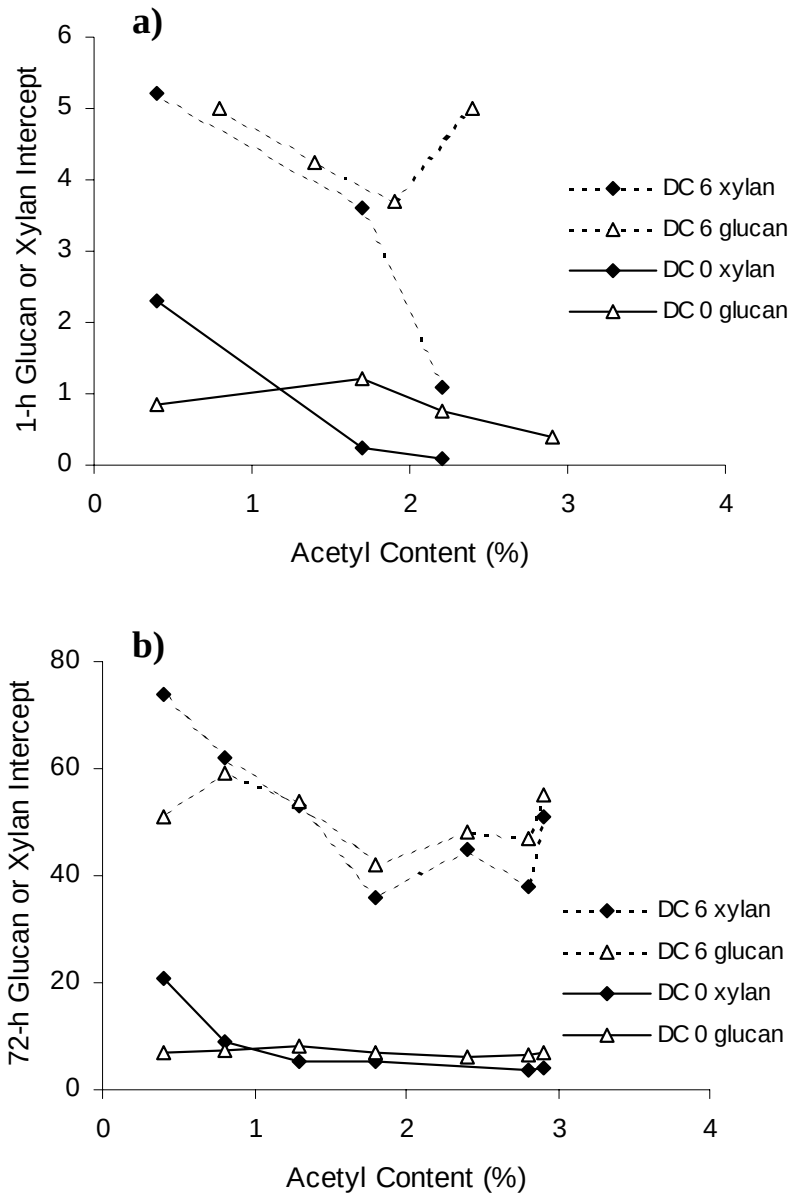

Figure 28. Effect of acetyl content on (a) 1-h glucan and xylan intercepts with a moderate lignin content (17.8–21.8%) and (b) 72-h glucan and xylan intercepts with a high lignin content (24.5–26.3%). DC 0, DC6 = ball milled 0 days or 6 days. Data from Tables VII and VIII.

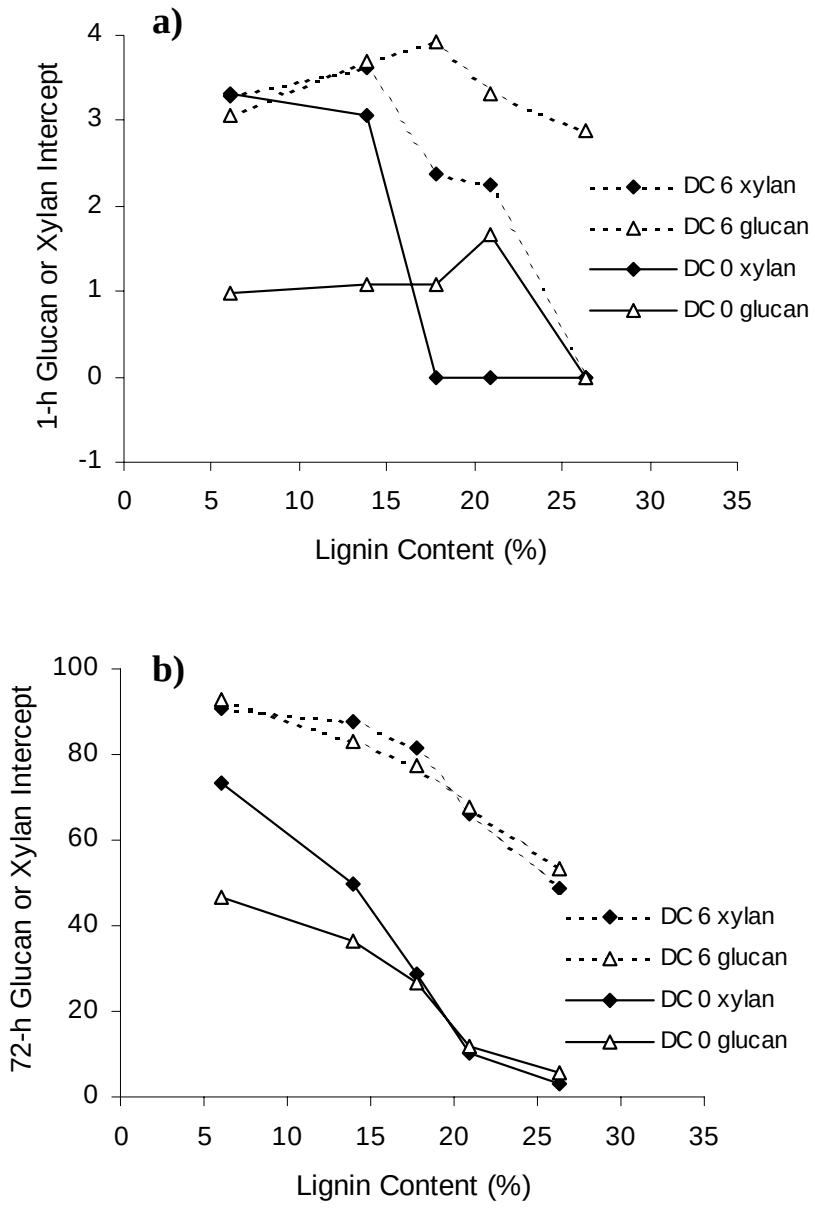

Figure 29. Effect of lignin content on (a) 1-h glucan and xylan intercepts with a high acetyl content (2.9–3.0%) and (b) 72-h glucan and xylan intercepts with a high acetyl content (2.9–3.0%). DC 0, DC 6 = ball milled 0 days or 6 days. Data from Tables VII and VIII.

whereas Sample 145 is highly digestible (large slopes and intercepts). Table XI summarizes the experiments that were performed to determine the internal degree of variability. Internal tests for Sample 7 were performed at an enzyme loading of 30 FPU/g dry biomass at 1 h and 72 h. Internal tests for Sample 145 were performed with an enzyme loading of 10 FPU/g dry biomass at 1 h and an enzyme loading of 2 FPU/g dry biomass at 72 h. The internal tests were conducted in parallel by loading 0.2 g dry biomass into 25-mL Erlenmeyer flasks and performing simultaneous saccharification. Enzyme aliquots were taken from the same dilution for each enzyme loading employed. There were five experiments performed for each of the four conditions as outlined in Table XI.

The external degree of variability was determined by comparing the internal tests conducted on Samples 7 and 145 on August 17, 2004 to hydrolysis experiments conducted on September 30, 2003 (Sample 7) and October 25, 2003 (Sample 145). Table XII summarizes the experiments conducted to determine the degree of external variability.

From the data summarized in Tables XI and XII, our enzymatic hydrolysis experiments are reproducible. The same batch of cellulase enzyme from the National Renewable Energy Laboratory (NREL) was used for all experiments. It should be noted that it might be difficult to reproduce results if experiments are conducted with a different batch of cellulase enzyme due to the unpurified nature of the cellulase mixture. For example, even when adding the same 5 FPU/g dry biomass enzyme loading, our lab has experienced different biomass conversions with different cellulase mixtures.

CONCLUSIONS

The 147 poplar wood model samples had a broad spectrum of lignin contents (0.7–26.3%), acetyl contents (0.1–3.1%), and crystallinity indices (5.4–68.8%). The slopes (*B*) and intercepts (*A*) calculated from Equation 5 for the model samples were determined at 1, 6, and 72 h. The results show that lignin and crystallinity have a major effect on 1-h total sugar slopes and intercepts and 6-h total sugar slopes and intercepts

Table XI. Internal degree of reproducibility for enzymatic hydrolysis experiments.

Sample[a]	Sample Size	Mean[b]	Standard Deviation
7-30-1	5	3.39	0.07
7-30-72	5	13.37	0.10
145-10-1	5	24.06	0.07
145-2-72	5	80.87	0.17

[a] 7-30-1 is Sample 7, 30 FPU/g dry biomass enzyme loading, 1-h incubation time.

[b] Units are (% glucan conversion).

Table XII. External degree of reproducibility for enzymatic hydrolysis experiments.

Sample	Date of Experiment	Glucan Conversion (%)
7-30-1	August 17, 2004	3.07
7-30-1	September 30, 2003	3.39
7-30-72	August 17, 2004	12.96
7-30-72	September 30, 2003	13.37
145-10-1	August 17, 2004	23.24
145-10-1	October 25, 2003	24.06
145-2-72	August 17, 2004	79.76
145-2-72	October 25, 2003	80.87

whereas acetyl exhibits a minor effect. Therefore, a low crystallinity index is sufficient to achieve a moderate increase in total sugar slopes and intercepts regardless of the acetyl or lignin content. Also, low lignin in conjunction with low crystallinity is sufficient to achieve high total sugar slopes and intercepts regardless of the acetyl content. Low acetyl content with a moderate lignin content contributed to a moderate increase in 1-h and 6-h slopes and intercepts. This suggests that even though acetyl alone is not a major player in affecting biomass digestibility, when combined with the reduction of other structural features it does enhance biomass digestibility.

The 72-h total sugar slopes and intercepts (ultimate digestion) appear to be controlled by a slightly different mechanism. Low lignin is sufficient to achieve high slopes and moderate intercepts regardless of crystallinity or acetyl content. When low crystallinity and low lignin are considered together, nearly complete conversion of the poplar wood model samples was observed (i.e., > 95%). Figure 27 shows that with minimal acetyl content (0.1%) and moderate lignin content (17.8–22.8%) biomass can be significantly digested. Chang (1999) discovered that lime pretreatment is an effective technique to deacetylate and moderately delignify biomass. Consequently, samples that have been subjected to lime pretreatment have been shown to be readily digestible. This suggests that regardless of the pretreatment technique employed, biomass digestibility is a function of its structural features. Therefore, a pretreatment designed to alter at least two of the three biomass structural features investigated (acetyl content, lignin content, and crystallinity) would be sufficient to render biomass highly digestible. This would allow for the design of more effective and less expensive pretreatment techniques.

Lignin, crystallinity, and acetyl can described as inherent inhibitors of biomass digestibility. There are other factors such as enzyme activity, enzyme deactivation, enzyme and substrate concentration, and product inhibition that can limit or control the degree of biomass digestibility. However, our work has shown that by removing lignin, acetyl groups, and crystallinity biomass can be rendered highly digestible.

Our work suggests there are two main paths in which the enzymes can travel. On one path, they encounter lignin that acts to retard biomass digestion through limiting

biomass swellability and irreversibly binding enzymes. The other path is hindered by the presence of acetyl groups covalently bound to hemicellulose that sterically interfere with the enzymes in their quest to reach the cellulose and hemicellulose. These two paths are aligned in parallel until the enzymes reach the cellulose, where they merge into one path. Once arriving at the cellulose, the enzymes encounter crystalline cellulose that acts to retard the effectiveness of the enzymes resulting in reduced rates of digestibility.

Our results show that the structural features investigated affect glucan and xylan digestibilities differently. It was noticed that lignin content and crystallinity elicit a major effect on glucan digestibility whereas lignin content and acetyl content appear to be more influential on xylan digestibility. Crystallinity has a major influence on initial digestibility whereas lignin exhibits a minor influence. Lignin appears to have the greatest influence on ultimate digestibility. Additionally, 1-h, 6-h, and 72-h digestibilities appear to be controlled by different mechanisms. Therefore, separate models will be developed for glucan, xylan, and total sugar at each of the three incubation times (1, 6, and 72 h).

NEURAL NETWORK MODELING OF STRUCTURAL FEATURES RESPONSIBLE FOR ENZYMATIC DIGESTIBILITY

INTRODUCTION

Many tasks such as speech understanding and visual recognition are still beyond the reach of digital computers. However, neural networks have proven to be effective tools in approximating nonlinear functions, pattern recognition, and classification problems (Giustolisi, 2004). They act as model-free estimators. Compared to common analytical approaches, neural networks require no explicit model and no limiting assumptions of normality or linearity (Annema, 1995; Hagan et al., 1996), which gives neural networks a key advantage over traditional approaches to function estimation. One of the greatest neural network advantages is estimating a function without requiring a mathematical description of how the output depends on the input. Instead, neural networks learn from examples of input-output data sets supplied to them.

In the 1940s, McCulloch and Pitts showed that artificial neural networks (ANNs) could compute any arithmetic or logical function. It was not until the late 1950s that Rosenblatt solved a problem with a neural network for the first time (Rosenblatt, 1961). He solved a recognition pattern problem. In the 1980s, multi-layer perceptron (MLP) networks became the most widely used artificial neural networks for function approximation (Zupan and Gasteiger, 1999).

Artificial neural networks consist of numerous processing units or neurons that can be modified to estimate a desired function. ANN models represent a new extremely robust approach to modeling complex processes. A neural network is an array of nodes (neurons) linked by connections (synapses) that can be strengthened or weakened. Neural network behavior is defined by the way its elements are connected and by the strength of those connections, termed weights. The weights are automatically adjusted by training the network according to a specified learning rule until it properly performs the desired task (Annema, 1995). The idea was derived from the interconnected neurons

of the brain (Hagan et al., 1996). The human brain consists of ~10^{11} neurons with approximately 10,000 connections per neuron (Rao and Srinivas, 2003). Neural networks possess only a small fraction of the computing power of the human brain; however, they have proven successful in solving many complex problems in telecommunications, medicine, robotics, biotechnology, and engineering.

Neural networks are trained from a series of inputs and associated outputs. The network outputs are then compared to the actual target values after each iteration. If the performance function (e.g., mean square error) is not satisfied, the connections between neurons are strengthened or weakened according to the level of success in reproducing the correct outputs. This iterative approach is continued until the performance function is satisfied or the number of desired iterations is reached. An overview of a typical neural network scheme is shown in Figure 30. In contrast to function approximation techniques that use polynomials or general orthogonal functions, there are no guidelines on choosing the number of terms in a neural network (i.e., the number of layers and number of nodes in each layer of the network); these are determined through trial and error.

Neural networks consist of neurons that are interconnected to one another as well as other layers in the network. The high degree of interconnectivity makes artificial neural networks extremely powerful and robust tools (Annema, 1995). A typical neuron is shown in Figure 31. The input p is transmitted through a connection that multiplies its strength by the weight w, to form the product wp. A bias term b is added to the product wp by the summing junction. This sum is supplied as the input to the transfer function f, which keeps the final output signal n of the neuron non-negative, continuous, and confined to a specified interval. For nonlinear function approximation, the transfer function is typically a sigmoid function (Wang et al., 2004). The tangent-sigmoid transfer function takes the input, which may be any value between + and – infinity, and squashes the output into the range of –1 to 1 (see Figure 32). This operation can be distributed across several layers, where the output of one layer forms the input to another, and the magnitude and orientation of the weight vectors determine how

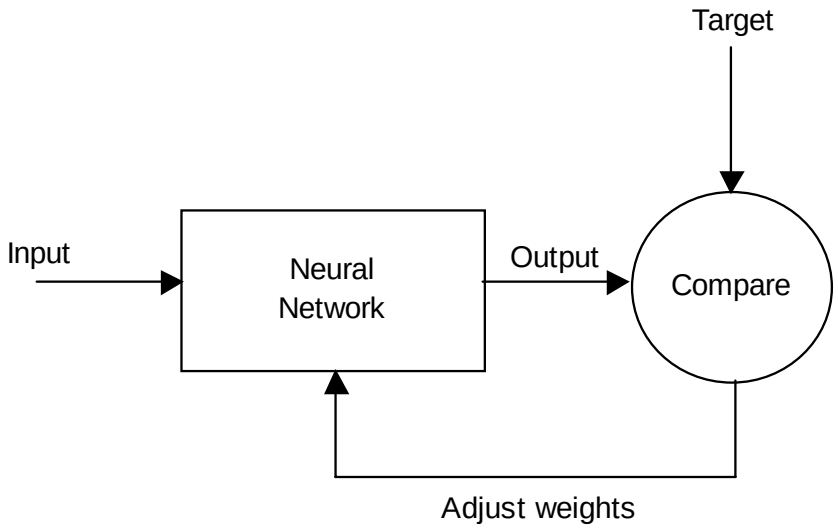

Figure 30. Black-box model of a general neural network scheme.

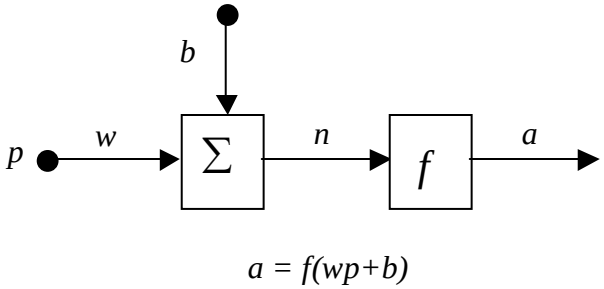

Figure 31. Simple neuron with single input and bias term.

knowledge is distributed in the overall network. Two or more neurons can be combined in a layer with a network possessing one or more such layers. The layers of a multi-layer network play different roles. The *output layer* produces the network output whereas all other layers in the network are called *hidden layers*. Multi-layer networks are extremely powerful. For instance, a network of two layers, where the first layer is sigmoid and the second layer is linear, can be trained to approximate any function arbitrarily well (Annema, 1995; Hagan et al., 1996). An overview of a typical multi-layer neural network is shown in Figure 33.

A single neuron, even with many inputs, is not sufficient for most applications. Likewise, single-layer networks are not adequate to approximate complex nonlinear functions, as is our case. Therefore, our work will use multi-layered networks with more than one neuron in the hidden layer. After building the network, it must be trained to perform the desired task. A *training algorithm* (also called *learning rule*) modifies the weights and biases of a network. The objective of training a network is to minimize the error between the actual outputs and the network outputs. Learning rules are classified as either supervised or unsupervised. In *supervised learning*, the network is provided with a set of examples of proper behavior (i.e., inputs and their corresponding targets). As the inputs are applied to the network, the network outputs are compared to the targets. If the outputs do not reflect the targets within a defined margin of error, the training algorithm is used to adjust the network weights and biases to move the network outputs closer to their target values. In *unsupervised learning*, the weights and biases are modified in response to the network inputs only. There are no target values for the network outputs to be compared against. The networks developed in our work will be trained using a supervised learning rule.

Backpropagation is a commonly used training algorithm in multi-layer networks that have a nonlinear differential transfer function such as `tan-sigmoid` (Wang et al., 2004; Zupan and Gasteiger, 1999). The backpropagation algorithm was developed for multi-layer networks by generalizing the Least Mean Squares learning rule (Demuth and Beale, 2004). The error for these algorithms (backpropagation and LMS)

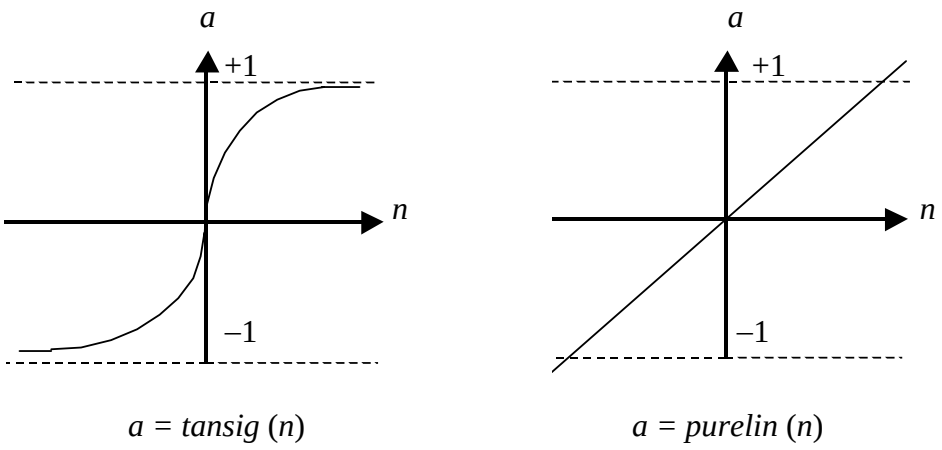

Figure 32. Tangent-sigmoid and pure-linear transfer functions (Demuth and Beale, 2004).

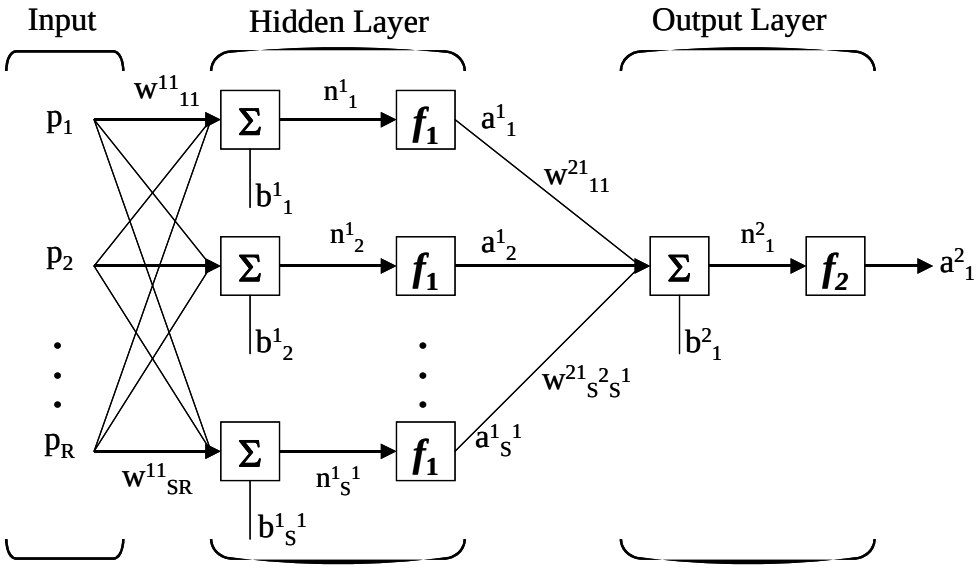

Figure 33. Three-layer neural network illustrating the high interconnectivity of multi-layer neural networks (Demuth and Beale, 2004).

is calculated as the difference between the target output and the network-simulated output. The goal is to minimize the average of the sum of these errors as shown in Equation 11

$$\text{MSE} = \frac{1}{N}\sum_{i=1}^{N}\left[t_i - a_i\right]^2 \tag{11}$$

where MSE is the mean square error, *t* is the target value, *a* is the network output, *N* is the number of examples of input-output data, and *i* is the number of iterations. The learning algorithm (i.e., backpropagation) adjusts the weights and biases to minimize the mean square error.

Standard backpropagation is a gradient descent algorithm, as is the Least Mean Squares algorithm (Demuth and Beale, 2004). Backpropagation refers to the manner in which the gradient is computed for nonlinear multiplayer networks, which involves performing computations backwards through the network. The backpropagation is derived using the chain rule of calculus (Hagan et al., 1996). The most basic implementation of backpropagation updates the network weights and biases in the direction in which the performance function (i.e., mean square error) decreases most rapidly – the negative of the gradient. The algorithm can be written as

$$\mathbf{x}_{k+1} = \mathbf{x}_k - \alpha_k \mathbf{g}_k \tag{12}$$

where $\mathbf{x}_k$ is a matrix of current weights and biases, $\mathbf{g}_k$ is the current gradient, and α_k is the learning rate. There are two different ways the gradient descent algorithm can be implemented: incremental mode or batch mode. This study employs the batch mode in which all of the inputs are applied to the network before the weights and biases are updated.

Backpropagation networks with biases, a hidden sigmoid layer, and a linear output layer can approximate any function with a finite number of discontinuities (Demuth and Beale, 2004). In batch training, the weights and biases are updated only once in each *epoch*, which is defined as a complete pass from the input vectors/matrix to the output.

Properly trained backpropagation networks give reasonable answers when presented with new inputs. Typically, new inputs lead to reasonably accurate outputs when the new inputs are similar to the inputs used to train the network. This generalization makes it possible to train a network on a representative set of input-output pairs without training the network on all possible pairs. However, one of the problems encountered when training neural networks is overfitting, which occurs when the error is driven to a very small value during training, but when new data are presented to the network, the error is large. In this situation, the network memorized the training examples, but did not learn to generalize to new situations. Matlab® has two techniques that are designed to improve network generalization – regularization and early stopping.

Regularization modifies the network performance function (Equation 11) by adding a term that consists of the mean of the sum of squares of the network weights as given by Equation 13

$$\mathrm{MSE}_{\mathrm{regularization}} = \gamma \frac{1}{N} \sum_{i=1} \left(t_i - a_i\right)^2 + \left(1-\gamma\right) \frac{1}{n} \sum_{j=1}^{n} w_j^2 \tag{13}$$

where γ is the performance ratio, which is a measure of how many parameters in the network are effectively used to reduce the error. Using the modified performance function causes the network to have smaller weights and biases, which gives a smoother network response. The performance ratio can be determined in an automated fashion by calling the `trainbr` function in Matlab®. `Trainbr` uses the Bayesian framework developed by MacKay (1992), in which the weights and biases are assumed to be random variables with specified distributions and the regularization parameters are related to the unknown variances associated with these distributions. The regularization parameters can then be estimated using statistical techniques. A detailed discussion of Bayesian regularization can be found in Foresee and Hagan (1997). Regularization produces a network that not only performs well with the training data, but also produces smoother behavior when presented with new data. The `trainbr` algorithm was used in this work to improve the network's generalization ability.

OBJECTIVES

The purpose of this research was to develop a neural network model that can predict slopes (*B*) and intercepts (*A*) based solely on biomass acetyl content, lignin content, and crystallinity. Matlab® was used to develop the neural network models by taking advantage of its built-in algorithms and programs. The specific objectives of this work were:

1. Develop neural network models to predict glucan, xylan, and total sugar slopes and intercepts at 1, 6, and, 72 h.
2. Test the neural network's predictive ability on lime- and AFEX-treated corn stover; lime- and dilute-acid-treated rice straw; and lime-, dilute-acid-, and aqueous-ammonia-treated bagasse.

NEURAL NETWORK MODELING STUDY

Purpose

The purpose of this study was to correlate slopes and intercepts (data from Tables VII, VIII, and IX) with biomass structural features (data from Table V) in Matlab® using neural networks, a nonparametric modeling technique. This was accomplished by supplying the networks with both inputs (i.e., biomass structural features) and outputs (i.e., experimentally measured slopes and intercepts from the 147 model samples).

Materials and Methods

Substrate Preparation

The 147 poplar wood model samples used in this study were selectively deacetylated with KOH, delignified with peracetic acid, and decrystallized by ball milling in a prior study (Chang, 1999).

Correlations for Poplar Wood Model Samples

A total of 18 networks were developed to correlate digestibility with acetyl, lignin, and crystallinity. Figure 34 summarizes the nine networks developed to predict slopes and the nine networks developed to predict intercepts. Because of the different responses of glucan and xylan digestibility to changes in structural features, correlations were developed separately for glucan, xylan, and total sugar. Due to the complexity of the biomass-cellulase reaction, a neural network model to determine the correlation between slopes and intercepts (Equation 14 and 15, respectively) and structural features was proposed.

$$\text{slope} = f(\text{acetyl}, \text{lignin}, \text{CrIc}) \tag{14}$$

$$\text{intercept} = f(\text{acetyl}, \text{lignin}, \text{CrIc}) \tag{15}$$

It was hypothesized that the predictive ability of glucan slope/intercept networks could be improved by including the glucan content and xylan slope/intercept, and the predictive ability of xylan slope/intercept networks could be improved by including the xylan content and glucan slope/intercept. For example, when developing the 1-h glucan slope neural network, the independent variables (i.e., acetyl content, lignin content, glucan content, biomass crystallinity (CrIb), and cellulose crystallinity (CrIc)) were systematically investigated as shown is Table XIII. After determining the best combination of independent variables (Run No. 6 in Table XIII), the 1-h xylan slope was added as an independent variable to see if the predictive ability of the networks could be improved. This procedure was followed when developing all glucan and xylan networks. The hypothesis being tested was if the digestibility of one component depended on the other, i.e., does removing xylan enhance glucan digestibility and/or does removing glucan enhance xylan digestibility. The criteria used to determine the best combination of independent variables was the MSE and R^2 (coefficient of determination) of the 147 poplar wood model samples and the MSE and R^2 of the 22 samples used to test the trained networks predictive ability. Only the 147 model samples from Tables VII, VIII, and IX with a $R^2 > 0.92$ were used to build the 18 networks. As a result, all networks did not have the same dimensionality.

The training algorithm (`trainbr`) of the 18 neural networks does not attempt to achieve a desired training goal such as the MSE. Instead, `trainbr` is a measure of how many network parameters (weights and biases) are being effectively used by the network. The effective number of parameters should remain approximately constant regardless of the network size (i.e., number of neurons in hidden layer). This indicates the network was trained for a sufficient number of iterations to ensure convergence.

The `trainbr` algorithm works best when the network inputs and targets are scaled so they fall in the range (-1,1) (Foresee and Hagan, 1997; Demuth and Beale, 2004). Because our inputs and targets did not fall in this range, the following functions were used in Matlab®: `premnmx` - to normalize the inputs and targets, `postmnmx` - to covert the network outputs back into the same units as the original targets, and `tramnmx` - to preprocess new inputs to be fed to the trained network with the means and standard deviations computed for the training set. The aforementioned Matlab® functions normalize the inputs and targets so that they have zero mean and unity standard deviations.

Building a Neural Network in Matlab®

Matlab® version 6.5.0.18013a Release 13 was used throughout the study. There are numerous neural networks to select in Matlab®, such as radial basis, backpropagation, and learning vector quantization. A multi-layer feedforward backpropagation neural network was the framework chosen for all 18 networks. All networks had one hidden layer with 15 neurons (`tan-sig` transfer functions) and an output layer with a single neuron (`purelin` transfer function). This type of network is commonly used for nonlinear function approximation because it can estimate almost any function as long as there are enough neurons in the hidden layer (Zupan and Gasteiger, 1999).

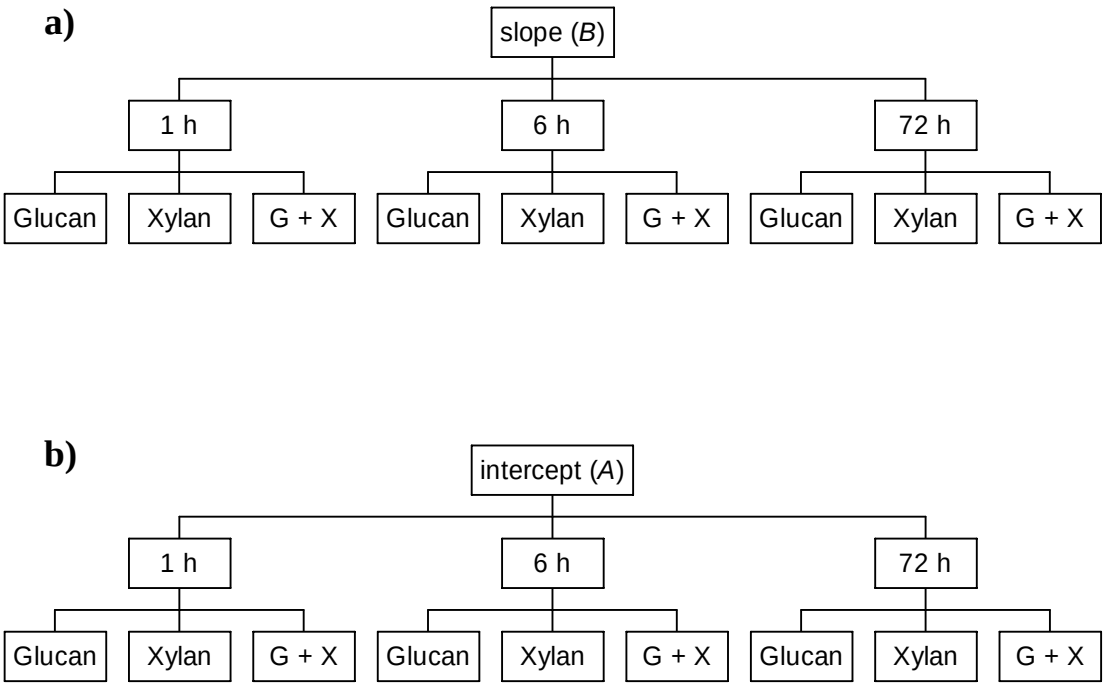

Figure 34. Organizational chart of nine neural network models used to correlate (a) slope and (b) intercept with lignin, acetyl, and crystallinity. G + X is defined as total sugar.

Table XIII. Summary of 1-h glucan slope network runs to identify best combination of independent variables[a].

Run No.	Input	Input	Input	Input	Input	Model Samples[b]		Prediction Samples[c]	
						R^2	MSE	R^2	MSE
1	L/G	A/G	CrIb/G	G		0.97	1.4	0.33	28.3
2	L	A/G	CrIb/G	G		0.97	1.3	0.32	30.0
3	L/G	A	CrIb/G	G		0.97	1.5	0.43	24.9
4	L/G	A/X	CrIb/G	G		0.97	1.5	0.44	24.6
5	L/G	A/X	CrIb	G		0.97	1.4	0.49	18.5
6	**L/G**	**A/X**	**CrIc**	**G**		**0.97**	**1.4**	**0.53**	**17.6**
7	L/G	A/X	CrIc/G	G		0.97	1.5	0.39	26.9
8	L/G	A/X	CrIc			0.96	2.0	0.16	43.0
9	L/G	A/X		G		0.15	38.0	0.05	45.0
10	L/G		CrIc	G		0.96	1.8	0.00	120.0
11		A/X	CrIc	G		0.95	2.0	0.03	123.0
12	L/G	A/X	CrIc	G	X1slope	0.99	0.45	0.00	49.0
13	L/G	A/X	CrIc	G	X1intercept	0.96	1.6	0.00	75.0
14	L/G	A/X	CrIc		X1slope	0.98	0.6	0.10	43.0
15	L/G	A/X	CrIc		X1intercept	0.96	1.7	0.21	35.0

[a] L=lignin; A=acetyl; CrIb=biomass crystallinity; CrIc=cellulose crystallinity; G=glucan; X=xylan; X1slope=1-h xylan slope; X1intercept=1-h xylan intercept.

[b] Simulated values for 147 poplar wood model samples.

[c] Predicted values for the 22 samples used to determine the models predictive ability.

As an example, the commands used to develop the 1-h glucan slope network are shown below. First, the input matrix had to be created from the data arranged in column vectors. The input vectors L_G, A_X, CrIc, and G were normalized and converted into a single input matrix of order 147×4 with the following Matlab® code.

```
load L_G.m
load A_X.m
load CrIc.m
load G.m
[L_Gn,minL_G,maxL_G]=premnmx(L_G);
[A_Xn,minA_X,maxA_X]=premnmx(A_X);
[CrIcn,minCrIc,maxCrIc]=premnmx(CrIc);
[Gn,minG,maxG]=premnmx(G);
[slope_G_1n,minslope_G_1,maxslope_G_1]=premnmx(slope_G
     _1);
for I=1:147,
    network_input_GS (I,1)=L_Gn(I)'
end
for I=1:147,
    network_input_GS (I,2)=A_Xn(I)'
end
for I=1:147,
    network_input_GS (I,3)=CrIcn(I)'
end
for I=1:147,
    network_input_GS (I,4)=Gn(I)'
end
```

The input matrix was named `network_input_GS`. For all networks, a multi-layer feedforward backpropagation network was used for training purposes with the Bayesian regularization modification `trainbr` to the MSE performance function. The network consisted of one hidden layer with 15 `tan-sig` neurons followed by an output layer

with one `purelin` neuron. The linear transfer function is commonly used in function approximation networks because it allows the output to be any value between -∞ and ∞ (Figure 32). The function `newff` was used to build the 1-h glucan slope network as well as the other 17 networks. The following code was written in a Matlab® to create the network.

```
net=newff([min(A_Xn)max(A_Xn);min(CrIcn)max(CrIcn)
     min(L_G) max(L_G); min(Gn) max(Gn)], [15 1],
     {'tansig','purelin'},'trainbr');
net.trainParam.show=10;
net.trainParam.epoch=100;
randn('seed',192836547);
net=init(net);
net=train(net,network_input_GS',slope_G_1n');
```

`Trainlm` (Levenberg-Marquardt) is the default training algorithm for feedforward backpropagation networks; therefore, we had to instruct the network to use the `trainbr` algorithm instead. The `train` function initiates network training with the 147×4 input matrix `network_input_GS` and the 147×1 target vector `slope_G_1n`. Next, the outputs were simulated for the given set of inputs using the trained network. Before comparing the simulated outputs (`yn`) to the actual outputs (`slope_G_1n`), the simulated outputs had to be converted back into the same units as the original targets with the function `postmnmx`. The difference between simulated and actual outputs was designated as `E`. The MSE of the difference between the two outputs was calculated. The network's ability the correlate 1-h glucan slopes with biomass structural features was evaluated by looking at the MSE and R^2, which were generated with the functions `perf` and `postreg`, respectively. The following code was written in Matlab® to accomplish this purpose:

```
yn=sim(net, network_input_GS');
y=postmnmx(yn,minslope_G_1,maxslope_G_1);
E=slope_G_1'-y;
```

```
min(E)
max(abs(E))
perf=mse(E)
[m,b,r]=postreg(y,slope_G_1')
Rsqr=r^2
```

For the 1-h glucan slope network, 15 `tan-sig` neurons in the hidden layer were sufficient to ensure convergence. By monitoring the number of effective parameters, 15 neurons proved adequate to achieve convergence for the other 17 networks as well.

The codes used in Matlab® to build the networks and simulate the outputs for the 147 poplar wood model samples are given in Appendix E. Also, the final weights and biases of the networks can be found in Appendix E.

All network simulated slopes and intercepts for the 147 poplar wood model samples are listed in Appendix F.

Results and Discussion

Neural Networks Validity

Because the neural networks were developed for the 147 poplar wood model samples, they are only valid in the region covered by the data sets used to simulate biomass digestibility. Results may vary when attempting to use the networks to predict slopes and intercepts of biomass samples with structural features that lie outside of the regions of the 147 model samples. The distribution of the independent variables of the 147 poplar wood model samples cover the region of

$$44.4 < G < 76.5 \quad (16)$$

$$13.9 < X < 17.5 \quad (17)$$

$$58.3 < TS < 91.6 \quad (18)$$

$$0.1 < A < 3.1 \quad (19)$$

$$0.7 < L < 26.3 \quad (20)$$

$$5.4 < CrIb < 68.8 \quad (21)$$

$$10.3 < CrIc < 79.8 \quad (22)$$

where *G*=glucan, *X*=xylan, *TS*=total sugar, *A*=acetyl content, *L*=lignin content, *CrIb*=biomass crystallinity, and *CrIc*=cellulose crystallinity. The 18 neural networks are only valid in the above region.

1-h Slope and Intercept

The functionalities (i.e., the independent variables that gave the lowest MSE and R^2 values) of the 1-h slope and intercept networks are summarized in Table XIV. Net-simulated outputs from 1-h glucan, xylan, and total sugar neural networks (Appendix F) were compared with measured slopes and intercepts from Tables VII, VIII, and IX as shown in Figures 35 and 36.

After training, the MSEs of the 1-h glucan networks were 5.3 and 0.7 for slopes and intercepts, respectively. Therefore, average differences between the experimentally measured and network-simulated glucan data were ±2.3% and ±0.8% for slopes and intercepts, respectively. In Figure 35a, the coefficient of determination (R^2) was 0.92 for measured versus simulated 1-h glucan slopes. The R^2 value of 1-h glucan intercepts was 0.81 (Figure 36a). Thus, the trained networks simulated the 1-h glucan slopes and intercepts of the 147 poplar wood model samples fairly satisfactorily. Another 1-h glucan slope network with a different functionality was run attempting to improve the network's ability to simulate the actual target values. Outputs (i.e., slopes) from the 1-h xylan slope network, which did not have 1-h glucan slope as an input, were fed to the 1-h glucan slope network as an additional independent variable. Similarly, another 1-h glucan intercept network with a different functionality was run attempting to improve the network's ability to simulate the actual target values. Outputs (i.e., intercepts) from the 1-h xylan intercept network, which did not have 1-h glucan intercepts as an input, were fed to the 1-h glucan intercept network as an additional input. There was no improvement in the MSE or R^2 for the 1-h glucan slope and intercept networks that included xylan functionality. Our data suggest that xylan digestibility had no affect on glucan digestibility during initial hydrolysis (1 h).

After training, the MSEs were 0.7 and 0.9 for 1-h xylan slopes and intercepts, respectively. Therefore, the average differences between the experimentally measured and network-simulated data were ±0.84% and ±0.95% for slopes and intercepts, respectively. The coefficients of determination (R^2) were 0.81 and 0.78 for the 1-h xylan slope (Figure 35b) and intercept (Figure 36b) regressions, respectively. As a result, the trained networks describe the 1-h xylan slopes and intercepts of the 147 model samples fairly satisfactorily. Another 1-h xylan slope network that included glucan slope functionality was run attempting to improve the networks ability to simulate the actual target values. Outputs (i.e., slopes) from the 1-h glucan slope network, which did not have 1-h xylan slopes as an input, were fed to the 1-h xylan slope network as an additional input. Similarly, another 1-h xylan intercept network with glucan intercept functionality was run attempting to improve the network's ability to simulate the actual target values. Outputs (i.e., intercepts) from the 1-h glucan intercept network, which did not have 1-h xylan intercepts as an input, were fed to the 1-h xylan intercept network as an additional independent variable. Similar to 1-h glucan networks, no improvement in the MSE or R^2 for 1-h xylan slope and intercept networks that included glucan functionality was observed. Our data suggest 1-h xylan digestibility is independent of initial glucan digestibility.

After training, the MSEs for the 1-h total sugar networks were 1.1 and 0.6 for slopes and intercepts, respectively. Therefore, the average differences between the experimentally measured and network-simulated data were ±1.05% and ±0.77% for slopes and intercepts, respectively. In Figure 35c, the coefficient of determination (R^2) was 0.96 for experimentally measured versus simulated 1-h total sugar slopes. The R^2 value of 1-h total sugar intercepts was 0.81 (Figure 36c). As a result, the total sugar networks describe the 1-h slopes and intercepts of the 147 poplar wood model samples fairly satisfactorily.

Table XIV. Summary of the functionality and goodness of fit for the 1-h slope and intercept neural networks.

		Functionality[a]	R^2	MSE
Glucan	Slope (*B)*	*B* = *f* (L/G, A/X, CrIc, G)	0.92	5.3
	Intercept (*A*)	*A* = *f* (L, A/X, CrIc, G)	0.81	0.7
Xylan	Slope (*B)*	*B* = *f* (L, A, CrIc, X)	0.81	0.7
	Intercept (*A*)	*A* = *f* (L, A, CrIc, X)	0.78	0.9
Total Sugar	Slope (*B)*	*B* = *f* (L/TS, A/TS, CrIc/TS, TS)	0.96	1.1
	Intercept (*A*)	*A* = *f* (L, A/X, CrIc, TS)	0.81	0.6

[a] L=lignin; A=acetyl; CrIc=cellulose crystallinity; G=glucan; X=xylan; TS=total sugar.

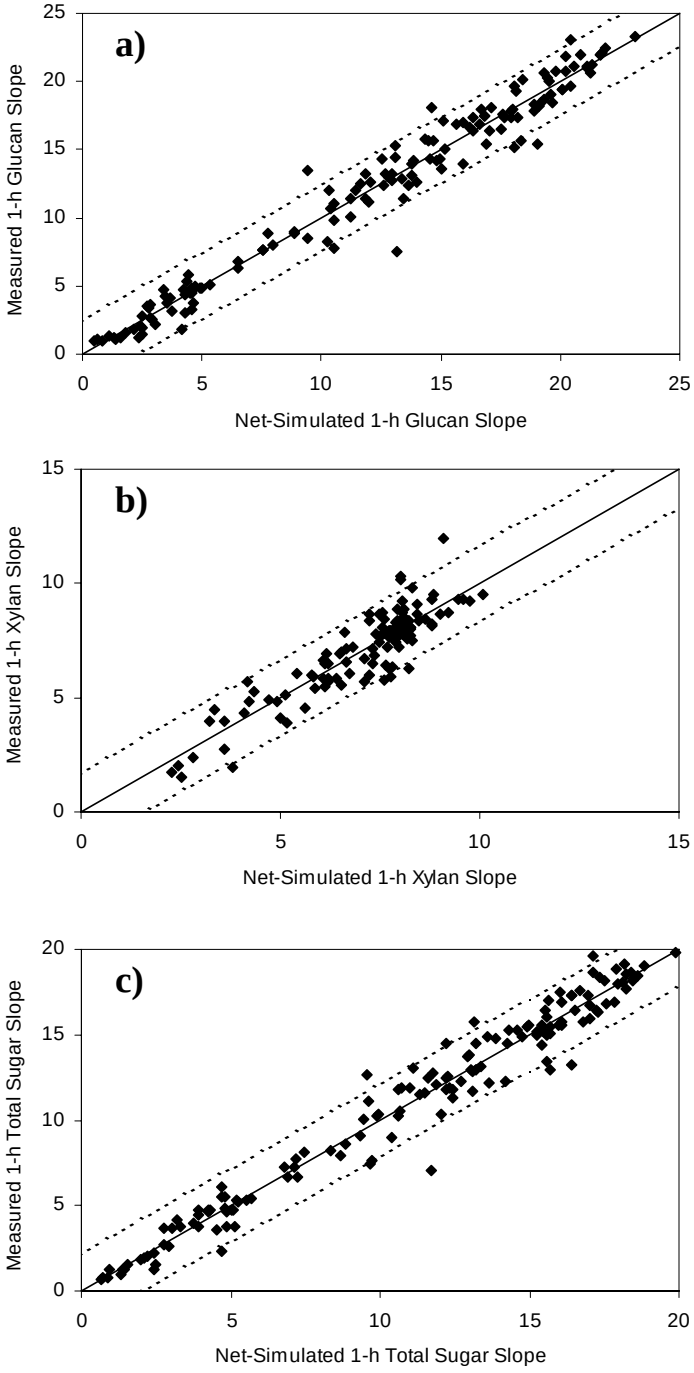

Figure 35. Correlation between experimentally measured and network-simulated slopes for (a) 1-h glucan, (b) 1-h xylan, and (c) 1-h total sugar. Dotted lines describe 95% prediction interval.

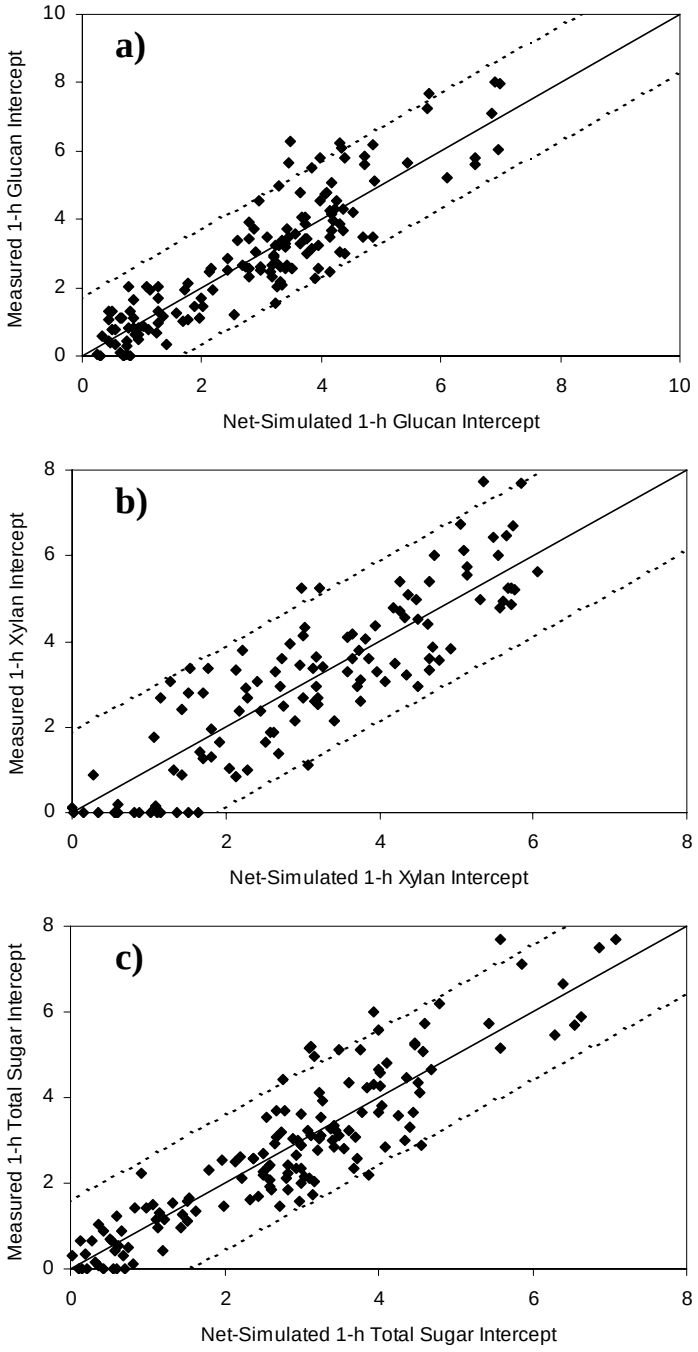

Figure 36. Correlation between experimentally measured and network-simulated intercepts for (a) 1-h glucan, (b) 1-h xylan, and (c) 1-h total sugar. Dotted lines describe 95% prediction interval.

Rather than biomass crystallinity (CrIb), it was hypothesized that cellulose crystallinity (CrIc) better measures the impediment to enzymatic cellulose degradation. X-ray diffraction measures the gross crystallinity of biomass (i.e., amount of crystalline material/total material). Hemicellulose (Holtzapple, 1993b) and lignin (Holtzapple, 1993c) are highly amorphous due to their branched and cross-linked structure; therefore, the crystallinity of biomass measured by X-ray diffraction predominantly results from the highly ordered regions of cellulose, but is expressed as gross crystallinity Lee and Fan (1982) have shown that cellulose crystallinity is a major limiting factor in pure cellulose digestibility; therefore, it would be advantageous to separate the crystallinity of cellulose from the gross crystallinity measured by X-ray diffraction to obtain a mass fraction of crystalline cellulose (i.e., mass of crystalline cellulose/mass of cellulose). We have shown that for the samples in our study, Equation 24 in "Predicting Cellulose Crystallinity" has the potential to predict cellulose crystallinity. By replacing biomass crystallinity with cellulose crystallinity as an independent variable, our results show that all 1-h networks better simulated the actual target values (i.e., networks with CrIc had a lower MSE). This suggests that CrIc calculated with Equation 24 is a better predictor of biomass reactivity than CrIb.

6-h Slope and Intercept

The functionalities (i.e., the independent variables that resulted in the lowest MSE and R^2 values) of the 6-h slope and intercept networks are summarized in Table XV. Net-simulated outputs from 6-h glucan, xylan, and total sugar slope and intercept neural networks (Appendix F) were compared with measured slopes and intercepts from Tables VII, VIII, and IX as shown in Figures 37 and 38.

After training, the MSEs of the glucan networks were 2.3 and 3.0 for 6-h slopes and intercepts, respectively. Therefore, average differences between the experimentally measured and network-simulated glucan data were ±1.5% and ±1.7% for slopes and intercepts, respectively. In Figure 37a, the coefficient of determination (R^2) was 0.96 for measured versus simulated 6-h glucan slopes. The R^2 value for 6-h glucan intercepts

was 0.97 (Figure 38a). Thus, the trained networks describe the 6-h glucan slopes and intercepts for the 147 model samples fairly satisfactorily. In attempting to improve the capability of the 6-h glucan slope network to simulate actual target values, outputs (i.e., slopes) from a 6-h xylan slope network, which did not have 6-h glucan slopes as an input, were fed to another 6-h glucan slope network as an additional independent variable. Similarly, another 6-h glucan intercept network with a different functionality was run attempting to improve the network's ability to simulate actual target values. Outputs (i.e., intercepts) from the 6-h xylan intercept network, which did not have 6-h glucan intercepts as an input, were fed to the 6-h glucan intercept network as an additional input. No improvement in the MSE or R^2 was observed for the 6-h glucan slope and intercept networks with xylan functionality. Our data conclude that xylan digestibility had no affect on glucan digestibility after 6 h.

After training, the MSEs of the 6-h xylan networks were 1.3 and 8.0 for slopes and intercepts, respectively. Therefore, average differences between the experimentally measured and network-simulated data for slopes and intercepts were ±1.1% and ±2.8%, respectively. The coefficients of determination were 0.94 and 0.95 for 6-h xylan slope (Figure 37b) and intercept (Figure 38b) regressions, respectively. As a result, the trained networks describe the 6-h xylan slopes and intercepts of the 147 poplar wood model samples fairly satisfactorily. Another 6-h xylan slope network that included glucan slope functionality was run attempting to improve the network's ability to simulate the actual target values. Outputs (i.e., slopes) from a 6-h glucan slope network, which did not have 6-h xylan slopes as an input, were fed to the 6-h xylan slope network as an additional input. Similarly, another 6-h xylan intercept network with glucan intercept functionality was run attempting to improve the networks ability to simulate the actual target values. Outputs (i.e., intercepts) from a 6-h glucan intercept network, which did not have 6-h xylan intercepts as an input, were fed to the 6-h xylan intercept network as an additional independent variable. Contrary to 1-h xylan networks, the 6-h xylan slope and intercept networks that included glucan functionality showed a minor

Table XV. Summary of the functionality and goodness of fit for the 6-h slope and intercept neural networks.

		Functionality[a]	R^2	MSE
Glucan	Slope (*B)*	*B* = *f* (L, A/G, CrIc/G, G)	0.96	2.3
	Intercept (*A*)	*A* = *f* (L/G, A/X, CrIc/G, G)	0.97	3.0
Xylan	Slope (*B)*	*B* = *f* (L, A/X, CrIc, G6slope)	0.94	1.3
	Intercept (*A*)	*A* = *f* (L, A, CrIc/G, G6intercept)	0.95	8.0
Total Sugar	Slope (*B)*	*B* = *f* (L, A, CrIc)	0.97	1.6
	Intercept (*A*)	*A* = *f* (L, A, CrIc, TS)	0.98	2.9

[a] L=lignin; A=acetyl; CrIc=cellulose crystallinity; G=glucan; X=xylan; TS=total sugar; G6slope=6-h glucan slope; G6intercept=6-h glucan intercept.

Table XVI. Comparison between 6-h xylan slope and intercept networks with and without glucan slope and intercept functionality.

		Functionality	R^2	MSE
Xylan	Slope (*B)*[a]	*B* = *f* (L, A/X, CrIc, X)	0.93	1.5
	Slope (*B)*[b]	*B* = *f* (L, A/X, CrIc, G6slope)	0.94	1.3
Xylan	Intercept (*A*)[a]	*A* = *f* (L, A, CrIc/G, X)	0.94	8.6
	Intercept (*A*)[b]	*A* = *f* (L, A, CrIc/G, G6intercept)	0.95	8.0

[a] Networks without glucan functionality.

[b] Networks with glucan functionality.

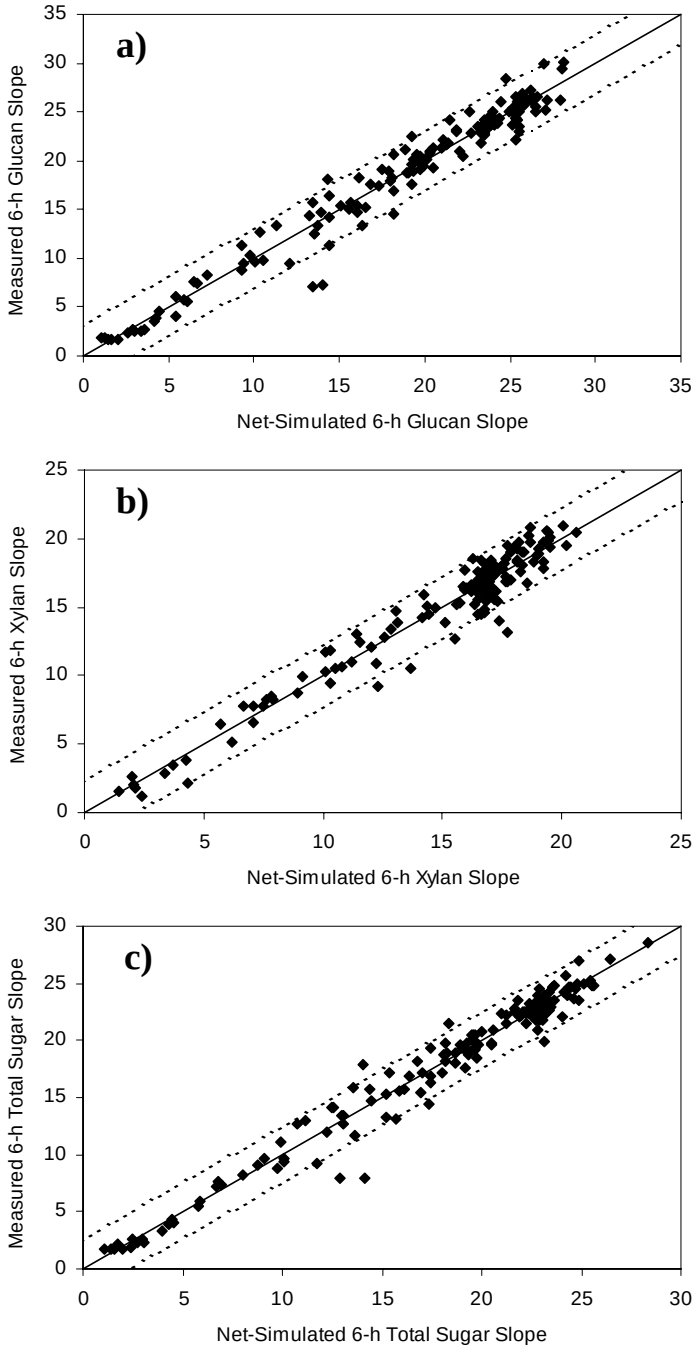

Figure 37. Correlation between experimentally measured and network-simulated slopes for (a) 6-h glucan, (b) 6-h xylan, and (c) 6-h total sugar. Dotted lines describe 95% prediction interval.

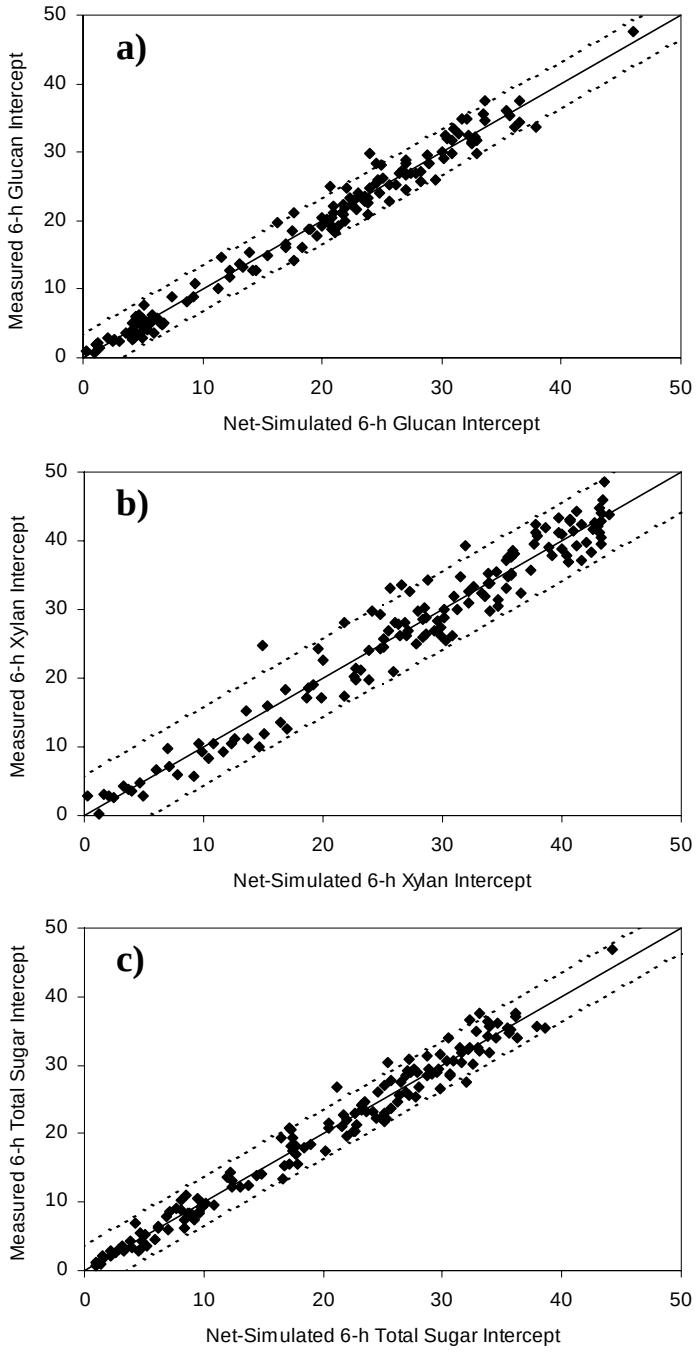

Figure 38. Correlation between experimentally measured and network-simulated intercepts for (a) 6-h glucan, (b) 6-h xylan, and (c) 6-h total sugar. Dotted lines describe 95% prediction interval.

improvement in the MSE and R^2 as shown in Table XVI. The data imply that glucan digestibility exhibits some effect on 6-h xylan digestibility.

After training, the MSE of the 6-h total sugar neural networks were 1.6 and 2.9 for slopes and intercepts, respectively. Therefore, the average differences between the experimentally measured and network-simulated data were ±1.3% and ±1.7% for slopes and intercepts, respectively. In Figure 37c, the coefficient of determination (R^2) was 0.97 for measured versus simulated 6-h total sugar slopes. The R^2 value of 6-h total sugar intercepts was 0.98 (Figure 38c). As a result, the total sugar networks describe 6-h slopes and intercepts of the 147 poplar wood model samples fairly satisfactorily.

Similar to the results observed in the 1-h networks, replacing biomass crystallinity with cellulose crystallinity as an independent variable improved all of the 6-h networks ability to simulate the actual target values of the 147 poplar wood model samples (i.e., the networks with CrIc had a lower MSE).

72-h Slope and Intercept

The functionalities (i.e., the independent variables that resulted in the lowest MSE and R^2 values) of the 72-h slope and intercept networks are summarized in Table XVII. Net-simulated outputs from 72-h glucan, xylan, and total sugar slope and intercept neural networks (Appendix F) were compared with the measured slopes and intercepts from Tables VII, VIII, and IX as shown in Figures 39 and 40.

After training, the MSEs of the glucan networks were 5.3 and 8.6 for 72-h slopes and intercepts, respectively. Therefore, average differences between the experimentally measured and network-simulated glucan data were ±2.3% and ±2.9% for slopes and intercepts, respectively. The coefficients of determination for 72-h glucan measured versus simulated slopes (Figure 39a) and intercepts (Figure 40a) were 0.92 and 0.99, respectively. Thus, the trained networks simulated the 72-h glucan slopes and intercepts for the 147 model samples fairly satisfactorily. In attempting to improve the predictive ability of the 72-h glucan slope network to simulate the actual target values, outputs (i.e., slopes) from the 72-h xylan slope network, which did not have 72-h glucan slopes as an

input, were fed to the 72-h glucan slope network as an additional independent variable. The same procedure was followed when testing xylan intercept functionality on a 72-h glucan intercept network. There was no improvement in the MSE or R^2 for the 72-h glucan slope and intercept networks that included xylan functionality. As a result, our data indicate that ultimate glucan digestibility (72 h) does not depend on xylan digestibility.

After training, the MSEs of the 72-h xylan networks were 2.0 and 3.4 for slopes and intercepts, respectively. Therefore, average differences between the experimentally measured and network-simulated data for slopes and intercepts were ±1.4% and ±1.8%, respectively. The coefficients of determination (R^2) were 0.87 and 0.99 for 72-h xylan slope (Figure 39b) and intercept (Figure 40b) regressions, respectively. As a result, the networks trained on the 147 poplar wood model samples describe the 72-h xylan slopes and intercepts fairly satisfactorily. Another 72-h xylan slope network that included glucan slope functionality was run in an attempt to improve the networks ability to simulate the actual target values. Outputs (i.e., slopes) from a 72-h glucan slope network, which did not have 72-h xylan slopes as an input, were fed to the 72-h xylan slope network as an additional input. The same procedure was followed when testing glucan intercept functionality on a 72-h xylan intercept network. Similar to 6-h xylan networks, the 72-h xylan slope and intercept networks that included glucan functionality showed an improvement in the MSE and R^2 as shown in Table XVIII. The data imply that glucan digestibility exhibits some effect on ultimate xylan digestibility.

After training, the MSEs of the 72-h total sugar neural networks were 3.6 and 8.8 for slopes and intercepts, respectively. Therefore, the average differences between the experimentally measured and network-simulated data were ±1.9% and ±3.0% for slopes and intercepts, respectively. In Figure 39c, the coefficient of determination (R^2) was 0.92 for measured versus simulated 72-h total sugar slopes. The R^2 value of 72-h total sugar intercepts was 0.99 (Figure 40c). As a result, the networks trained on the 147 model samples describe 72-h total sugar slopes and intercepts fairly satisfactorily.

Table XVII. Summary of the functionality and goodness of fit for the 72-h slope and intercept neural networks.

		Functionality[a]	R^2	MSE
Glucan	Slope (*B)*	*B* = *f* (L, A/X, CrIc)	0.92	5.3
	Intercept (*A*)	*A* = *f* (L, A/G, CrIc)	0.99	8.6
Xylan	Slope (*B)*	*B* = *f* (L/X, A/X, CrIc/X, G72slope)	0.87	2.0
	Intercept (*A*)	*A* = *f* (L/X, A, CrIc, X, G72intercept)	0.99	3.4
Total Sugar	Slope (*B)*	*B* = *f* (L, A/X, CrIc/G, TS)	0.92	3.6
	Intercept (*A*)	*A* = *f* (L, A, CrIc, TS)	0.99	8.8

[a] L=lignin; A=acetyl; CrIc=cellulose crystallinity; G=glucan; X=xylan; TS=total sugar; G6slope=72-h glucan slope; G6intercept=72-h glucan intercept.

Table XVIII. Comparison between 72-h xylan slope and intercept networks with and without glucan slope and intercept functionality.

		Functionality	R^2	MSE
Xylan	Slope (*B)*[a]	*B* = *f* (L/X, A/X, CrIc/X)	0.85	2.4
	Slope (*B)*[b]	*B* = *f* (L/X, A/X, CrIc/X, G72slope)	0.87	2.0
Xylan	Intercept (*A*)[a]	*A* = *f* (L/X, A, CrIc, X)	0.98	10.9
	Intercept (*A*)[b]	*A* = *f* (L/X, A, CrIc, X, G72intercept)	0.99	3.4

[a] Networks without glucan functionality.

[b] Networks with glucan functionality.

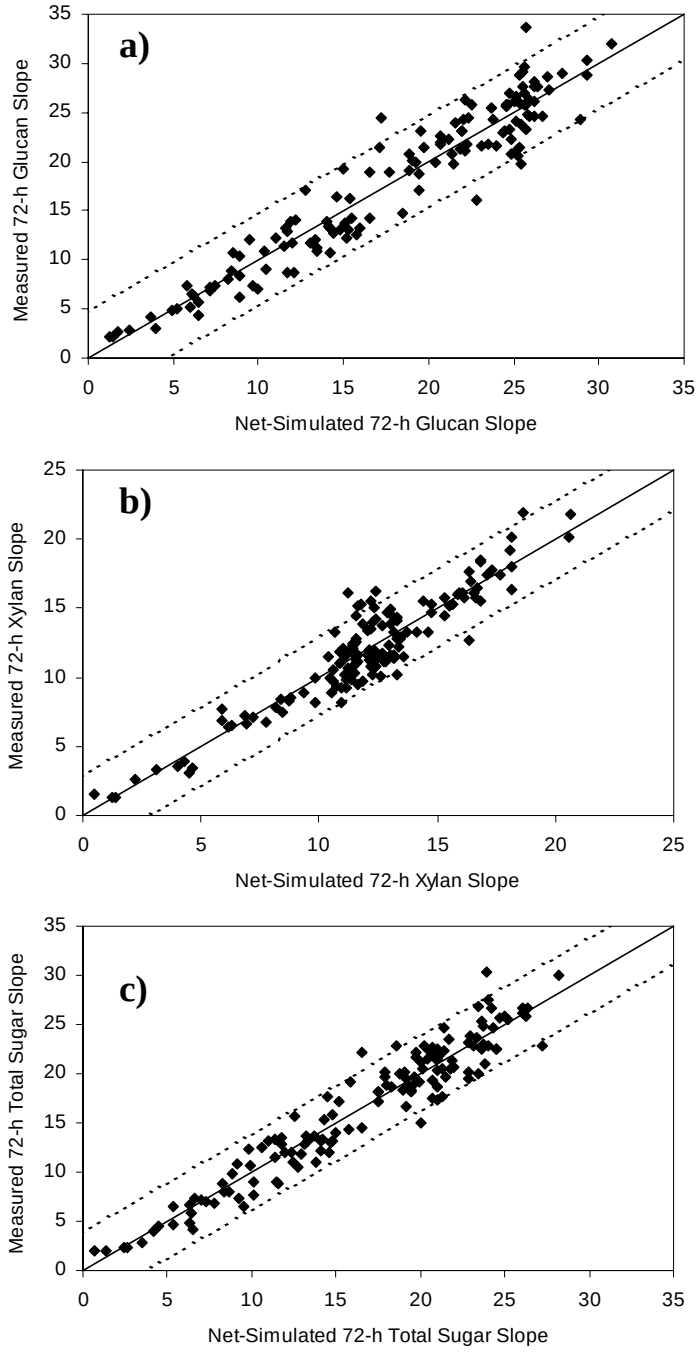

Figure 39. Correlation between experimentally measured and network-simulated slopes for (a) 72-h glucan, (b) 72-h xylan, and (c) 72-h total sugar. Dotted lines describe 95% prediction interval.

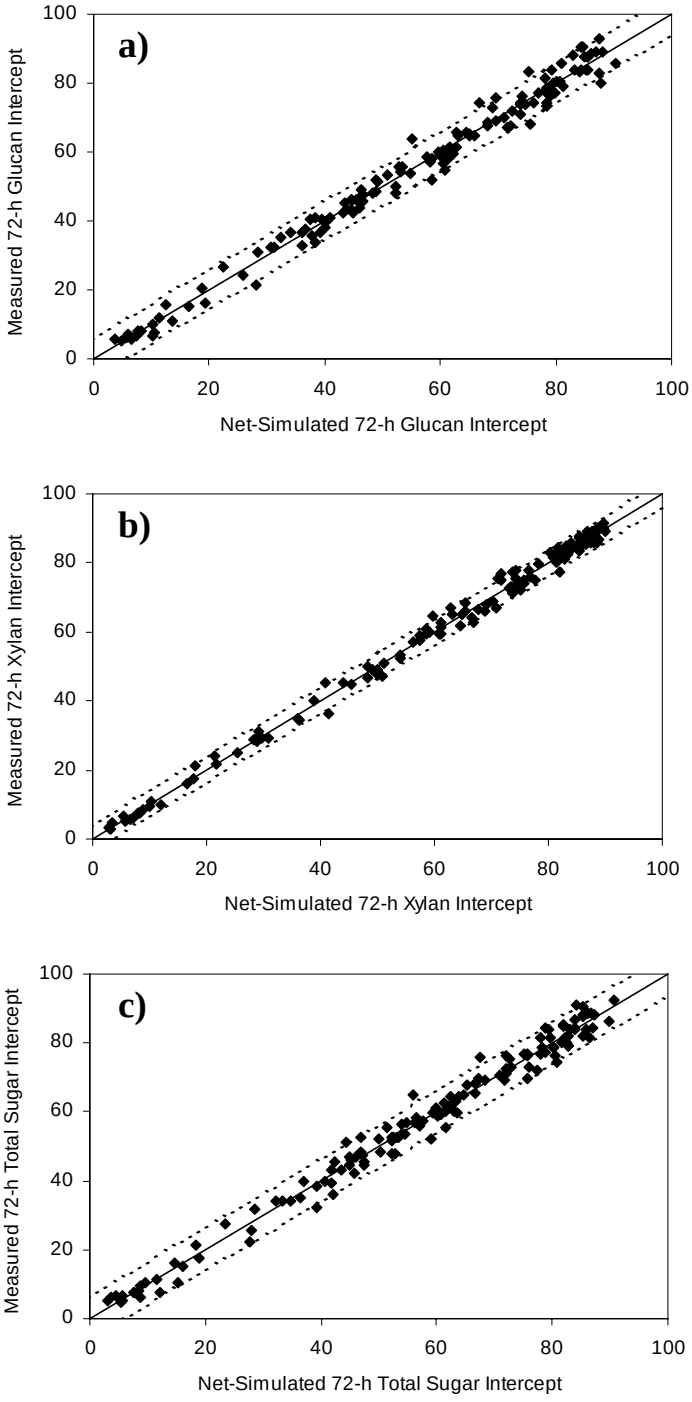

Figure 40. Correlation between experimentally measured and network-simulated intercepts for (a) 72-h glucan, (b) 72-h xylan, and (c) 72-h total sugar. Dotted lines describe 95% prediction interval.

Similar to the results observed in the 1-h and 6-h networks, the 72-h networks performed better with cellulose crystallinity as an independent variable instead of biomass crystallinity (i.e., the networks with CrIc had a lower MSE).

PREDICTIVE ABILITY OF NEURAL NETWORKS STUDY

Purpose

As previously explained, 18 neural networks were developed and trained with the 147 poplar wood model samples by supplying both the inputs (i.e., biomass structural features) and the target values (i.e., the experimentally measured slopes and intercepts) to the network. The purpose of this study was to test the 18 neural networks' abilities to predict slopes and intercepts of various biomass samples pretreated with different techniques (i.e., only the inputs were supplied to the networks). This would provide a measure of each network's ability to generalize to new inputs.

Materials and Methods

Substrate Preparation

For use in this study, a total of 22 samples were created from 11 chemically pretreated stock samples. There were six different pretreatment techniques performed on the 11 biomass stock samples: (1) long-term lime with air, (2) long-term lime without air, (3) short-term lime, (4) Ammonia Fiber Explosion (AFEX), (5) aqueous ammonia, and (6) dilute acid. The following feedstocks were employed: corn stover, bagasse, and rice straw. A more thorough description of long-term lime pretreatment with and without air and AFEX pretreatment can be found in Kim (2004) and Teymouri et al. (2004), respectively. These pretreatments were performed by others and donated for use in our study.

Carbohydrate (glucan and xylan) content, acetyl content, and lignin content of the 22 biomass samples were determined using a two-stage acid hydrolysis procedure as described in NREL standard procedure "Determination of Structural Carbohydrates and Lignin in Biomass" (NREL, 2004). First, the biomass was contacted with 72% sulfuric acid for 1 h at 30^{o}C, followed by a second 4% sulfuric acid hydrolysis for 1 h at 121^{o}C. The resulting sugar monomers were analyzed using high performance liquid chromatography (HPLC) with a Biorad HPX-87P column. The acetyl groups were analyzed as acetic acid using HPLC with a Biorad HPX-87H column. Klason lignin was determined as the difference between the residue remaining after acid hydrolysis and the residue after ashing at 575^{o}C overnight. After acid hydrolysis, the liquid fraction was analyzed for soluble lignin using a spectrophotometer. The total lignin content is the summation of the Klason lignin and acid-soluble lignin. Table XIX summarizes the structural features of the 22 pretreated biomass samples used in this study.

Short-term lime, dilute acid, and aqueous ammonia pretreatments were conducted according to protocols outlined in Appendix C. After pretreating, washing, and grinding the biomass, roughly 10 g of each of the 11 stock samples were subjected to 2-d, 3-d, 4-d, or 6-d ball milling to modify the crystallinity of the biomass. The procedures for ball milling and crystallinity measurements by X-ray diffraction are described in "Materials and Methods – Enzymatic Hydrolysis of Model Samples." Ball milling resulted in a total of 22 samples that were used to test the predictive ability of the 18 neural networks developed in "Neural Network Modeling Study." The chemical and mechanical pretreatments were performed to obtain a wide range of structural features, which include acetyl content (0.03–1.95%), lignin content (9.94–31.68%), and biomass crystallinity indices (11.0–61.6%) (see Table XIX). These samples were investigated to test the trained neural networks' abilities to predict slopes and intercepts.

Enzyme Preparation

To verify the activity of the *Trichoderma reesei* cellulase preparation received from NREL, a filter paper assay was performed according to NREL standard procedure

Table XIX. Summary of structural features for the 22 samples used to measure neural network's predictive ability.

Sample No.	Biomass	Treatment[a]	Ball Mill (d)	Glucan (%)	Xylan (%)	ASL[b] (%)	AIL[c] (%)	Total Lignin (%)	Acetyl (%)	CrIc (%)
1	corn stover	LT lime	0	44.3	14.4	1.1	8.9	9.9	0.03	69.7
2	corn stover	LT lime	0	48.1	21.8	0.8	13.5	14.4	0.11	73.6
3	corn stover	ST lime	3	45.8	20.8	0.9	17.2	18.1	0.03	29.1
4	corn stover	ST lime	6	47.4	21.5	1.0	17.1	18.1	0.03	21.7
5	bagasse	ST lime	0	33.5	13.5	6.5	20.6	27.2	0.50	67.1
6	bagasse	ST lime	4	33.5	13.5	6.5	20.6	27.2	0.50	21.5
7	rice straw	ST lime	0	30.1	14.1	7.2	24.0	31.2	0.80	58.2
8	rice straw	ST lime	2	29.8	14.0	7.1	23.7	30.8	0.80	21.6
9	bagasse	dilute acid	0	61.7	6.3	3.0	28.7	31.7	0.25	56.6
10	bagasse	dilute acid	3	61.7	6.3	3.0	28.7	31.7	0.25	38.9
11	rice straw	dilute acid	0	55.1	5.1	3.3	26.3	29.6	0.23	54.6
12	rice straw	dilute acid	2	55.1	5.1	3.3	26.3	29.6	0.23	39.0
13	corn stover	AFEX	0	37.9	21.3	2.5	15.6	18.1	1.88	64.2
14	corn stover	AFEX	0	36.3	20.9	2.5	15.6	18.1	1.82	56.6
15	corn stover	AFEX	0	37.3	21.2	2.5	16.1	18.6	1.95	57.5
16	corn stover	AFEX	2	37.9	21.3	2.5	15.6	18.1	1.88	39.9
17	corn stover	AFEX	4	36.3	20.9	2.5	15.6	18.1	1.82	26.1
18	corn stover	AFEX	6	37.3	21.2	2.5	16.1	18.6	1.95	20.5
19	bagasse	aqueous ammonia	0	49.2	18.7	5.5	17.5	22.9	0.04	68.6
20	bagasse	aqueous ammonia	0	48.7	18.7	5.4	17.6	23.0	0.05	67.5
21	bagasse	aqueous ammonia	2	49.2	18.7	5.5	17.5	22.9	0.04	27.5
22	bagasse	aqueous ammonia	2	48.7	18.7	5.4	17.6	23.0	0.05	33.7

[a] LT=long-term treatment; ST=short-term treatment; AFEX=Ammonia Fiber Explosion.

[b] ASL=acid-soluble lignin.

[c] AIL=acid-insoluble lignin.

No. 006. The filter paper activity of cellulase was 65 FPU/mL enzyme according to NREL standard procedure and 101 FPU/mL enzyme according to Coward-Kelly et al. (2003). (Note: NREL's standard filter paper activity was used in the models.) Cellobiase activity (Novozym 188, Novo Nordisk Biochem) determined by Novo Nordisk was 321 CBU/mL based on the company's assay.

Enzymatic Hydrolysis

The experiments were performed in 50-mL Erlenmeyer flasks with 0.2 g biomass, 18 mL of distilled water, 1.0 mL of 1-*M* citrate buffer and 0.6 mL of 0.01 g/L sodium azide solution, and placed inside a 100-rpm air-bath shaker at 50^{o}C. Citrate buffer and sodium azide were added to keep the pH constant (pH = 4.8) and prevent the growth of microorganisms, respectively. When the reaction slurry temperature reached 50^{o}C, hydrolysis was initiated by adding 0.2 mL of appropriately diluted cellulase (activity = 65 FPU/mL) and 0.05 mL of cellobiase (activity = 321 CBU/g). It was discovered that the same range of enzyme loadings could not be used for all samples. The biomass samples' inherent reactivities affected the range over which Equation 5 was valid. Therefore, the 22 samples were divided into three classes (low, medium, and high) based on their inherent reactivities. Table VI summarizes the range of enzyme loadings in which the three classes of biomass exhibit the linear profile predicted by Equation 5. The detailed procedure for enzymatic hydrolysis is given in Appendix A.

Samples were removed after an incubation time of 1, 6, or 72 h. After removal, the Erlenmeyer flasks were boiled for 15 minutes to denature the enzymes thereby quenching the reaction. The reaction slurry was transferred to 15-mL conical centrifuge tubes, centrifuged, and the supernatant was frozen until sugar analysis was performed.

Testing the Trained Networks Predictive Ability in Matlab®

Matlab® version 6.5.0.18013a Release 13 was used throughout the study. The 18 previously trained neural networks developed to simulate the 147 poplar wood model

samples were tested for their predictive ability on the 22 samples listed in Table XIX.

As an example, the commands used to predict 1-h glucan slopes of the 22 biomass samples are shown below. First, the input matrix had to be created from the data arranged in column vectors. Because `premnmx` was used to preprocess the training data (i.e., 147 model samples) for all 18 networks, new inputs (structural features from the 22 samples) to the previously trained networks should be preprocessed with the command `tramnmx`, which normalizes the new inputs using the minima and maxima that were computed for the training set. For this example, the input vectors `L_G_pred, A_X_pred, G_pred,` and `CrIc_pred` were normalized using the minimum and maximum values of the inputs from the 147 model samples with the command `tramnmx` and converted into a single-input matrix of order 22×4 with the following Matlab® code.

```
load L_G_pred.m
load A_X_pred.m
load G_pred.m
load CrIc_pred.m
load slope_G_1_pred.m
[slope_G_1_predn,minslope_G_1,maxslope_G_1]=premnmx(sl
     ope_G_1_pred);
CrIc_predn=tramnmx(CrIc_pred,minCrIc,maxCrIc);
A_X_predn=tramnmx(A_X_pred,minA_X,maxA_X);
L_G_predn=tramnmx(L_G_pred,minL_G,maxL_G);
G_predn=tramnmx(G_pred,minG,maxG);
for I=1:22,
    finS(I,1)=A_X_predn(I)';
end
for I=1:22,
    finS(I,2)=CrIc_predn(I)';
end
```

```
for I=1:22,
    finS(I,3)=L_G_predn(I)';
end
for I=1:22,
    finS(I,4)=G_predn(I)';
end
```

The 22×4 input matrix was named `finS`. The previously trained 1-h glucan slope network was renamed `netSG1`. It should be noted that the experimentally measured slopes and intercepts for the 22 samples (Tables XX, XXI, and XXII) were not fed to the network when testing its predictive ability. The command `sim` was used to call `netSG1` to predict the outputs (i.e., slopes) of the 22 samples. The output `ypredn` corresponds to the normalized inputs `finS`. The command `postmnmx` was used to un-normalize the outputs. The difference between predicted and actual outputs was designated as `E_pred`.

Then, the MSE was calculated as the difference between the two outputs. The predictive ability of the 1-h glucan slope network for the 22 samples was evaluated by looking at the MSE and R^2, which were generated with the functions `perf_pred` and `postreg`, respectively. To predict the 22 samples' 1-h glucan slopes, the following code was written in Matlab®.

```
ypredn=sim(netSG1,finS');
ypred=postmnmx(ypredn,minslope_G_1,maxslope_G_1);
E_pred=slope_G_1_pred'-ypred;
perf_pred=mse(E_pred)
[mpred,bpred,rpred]=postreg(ypred,slope_G_1_pred')
Rsqrpred=rpred^2
```

The codes used in Matlab® to test the networks' abilities to predict slopes and intercepts for the 22 samples are given in Appendix G. All network predicted slopes and intercepts for the 22 samples are listed in Appendix H.

Table XX. Summary of the glucan slopes (*B*) and intercepts (*A*) determined from Equation 5 for the 22 samples used to test the network's predictive ability.

Sample No.	Biomass	Treatment[a]	1-h Glucan			6-h Glucan			72-h Glucan		
			B	*A*	R^2	*B*	*A*	R^2	*B*	*A*	R^2
1	corn stover	LT lime w/Air	14.47	4.67	0.97	25.13	22.39	0.99	27.10	73.34	0.99
2	corn stover	LT lime w/N_2	11.63	3.64	0.98	18.62	17.19	0.99	15.55	50.00	0.99
3	corn stover	ST lime	19.29	6.00	0.94	25.09	26.38	0.99	22.38	69.82	0.99
4	corn stover	ST lime	20.82	8.08	0.96	23.32	32.41	0.99	20.25	75.52	0.98
5	bagasse	ST lime	6.12	0.74	0.98	8.68	9.76	1.00	7.98	27.72	0.94
6	bagasse	ST lime	19.94	9.51	0.96	21.76	37.30	0.98	19.83	77.25	0.97
7	rice straw	ST lime	10.74	3.00	0.96	11.81	20.50	0.98	8.49	45.41	1.00
8	rice straw	ST lime	23.24	8.70	0.96	20.86	41.38	0.95	9.59	77.95	0.96
9	bagasse	dilute acid	2.63	1.17	0.99	4.88	4.86	0.99	8.93	10.32	1.00
10	bagasse	dilute acid	4.40	1.60	0.97	11.44	5.33	0.97	10.07	20.88	0.99
11	rice straw	dilute acid	8.90	4.43	1.00	8.94	21.84	0.95	6.23	42.06	0.98
12	rice straw	dilute acid	8.50	2.74	0.99	20.42	13.34	1.00	18.00	46.52	0.96
13	corn stover	AFEX	6.44	3.77	0.99	12.45	13.16	0.99	12.62	39.10	0.99
14	corn stover	AFEX	6.37	5.20	0.99	13.19	13.64	0.99	13.58	42.07	0.99
15	corn stover	AFEX	6.20	3.88	0.94	13.50	15.81	1.00	11.70	42.85	0.99
16	corn stover	AFEX	14.80	11.41	0.98	16.60	28.72	0.99	12.43	59.16	0.99
17	corn stover	AFEX	18.24	13.22	0.97	19.40	34.70	0.99	13.95	68.69	0.98
18	corn stover	AFEX	19.24	13.96	0.98	17.40	39.48	0.99	13.29	72.48	0.99
19	bagasse	aq. ammonia	6.10	0.10	0.93	10.17	3.89	0.97	12.21	11.43	0.99
20	bagasse	aq. ammonia	6.20	0.13	0.92	10.82	3.81	0.97	12.81	12.19	0.99
21	bagasse	aq. ammonia	8.76	3.32	0.94	17.59	10.06	0.98	14.43	37.65	0.99
22	bagasse	aq. ammonia	8.70	3.74	0.96	17.65	10.46	0.97	14.43	37.74	0.99

[a] LT=long-term treatment; ST=short-term treatment; AFEX=ammonia fiber explosion.

Table XXI. Summary of the xylan slopes (*B*) and intercepts (*A*) determined from Equation 5 for the 22 samples used to test the network's predictive ability.

Sample No.	Biomass	Treatment[a]	1-h Xylan			6-h Xylan			72-h Xylan		
			B	*A*	R^2	*B*	*A*	R^2	*B*	*A*	R^2
1	corn stover	LT lime w/Air	6.18	5.82	0.99	17.70	32.14	0.99	14.92	80.34	0.99
2	corn stover	LT lime w/N_2	5.97	2.94	0.96	14.72	21.74	0.97	8.37	59.48	0.99
3	corn stover	ST lime	4.88	5.57	0.93	13.99	36.84	0.98	10.48	80.22	0.98
4	corn stover	ST lime	4.81	6.01	0.97	12.93	39.83	0.98	6.75	78.99	0.99
5	bagasse	ST lime	6.73	1.44	0.94	7.49	18.05	1.00	6.37	37.54	0.99
6	bagasse	ST lime	3.69	7.77	0.77	13.93	39.85	0.99	11.36	83.77	0.98
7	rice straw	ST lime	7.49	1.74	0.93	8.20	23.42	1.00	7.03	47.81	0.99
8	rice straw	ST lime	7.01	5.95	0.92	12.33	44.13	0.99	5.45	80.05	0.94
9	bagasse	dilute acid	2.62	0.00	0.96	4.52	4.27	0.97	7.05	13.32	1.00
10	bagasse	dilute acid	9.52	11.58	0.97	9.34	34.74	0.99	7.00	52.20	0.92
11	rice straw	dilute acid	0.39	0.07	0.86	0.48	0.90	1.00	0.80	2.13	0.99
12	rice straw	dilute acid	8.55	6.64	0.99	13.19	22.19	0.99	10.08	49.53	1.00
13	corn stover	AFEX	4.75	3.61	0.94	8.89	22.57	0.99	6.03	47.81	0.99
14	corn stover	AFEX	4.90	3.19	0.96	8.57	21.75	0.99	6.96	47.77	0.99
15	corn stover	AFEX	4.40	3.62	0.92	9.94	21.59	0.99	5.81	45.71	0.99
16	corn stover	AFEX	5.78	5.13	0.96	9.91	35.24	0.99	5.79	63.73	0.99
17	corn stover	AFEX	5.67	5.26	0.92	11.93	35.54	0.99	4.52	67.52	0.98
18	corn stover	AFEX	5.85	5.35	0.94	11.61	38.41	0.99	5.10	71.24	0.99
19	bagasse	aq. ammonia	6.18	0.94	0.94	8.36	12.48	0.97	9.37	24.69	0.99
20	bagasse	aq. ammonia	6.32	0.87	0.93	8.75	13.13	0.97	10.06	25.74	1.00
21	bagasse	aq. ammonia	5.87	3.89	0.94	13.85	24.28	0.99	7.80	55.03	0.99
22	bagasse	aq. ammonia	6.34	3.83	0.94	14.56	24.82	0.97	8.06	57.28	0.99

[a] LT=long-term treatment; ST=short-term treatment; AFEX=ammonia fiber explosion.

Table XXII. Summary of the total sugar slopes (*B*) and intercepts (*A*) determined from Equation 5 for the 22 samples used to test the network's predictive ability.

Sample No.	Biomass	Treatment[a]	1-h Total Sugar			6-h Total Sugar			72-h Total Sugar		
			B	*A*	R^2	*B*	*A*	R^2	*B*	*A*	R^2
1	corn stover	LT lime w/Air	12.40	4.96	0.97	23.28	24.82	0.99	24.06	75.08	0.99
2	corn stover	LT lime w/N_2	9.84	3.42	0.98	17.38	18.44	0.99	13.28	53.00	0.99
3	corn stover	ST lime	15.14	5.86	0.94	21.56	29.71	0.99	18.60	73.12	0.99
4	corn stover	ST lime	15.75	7.42	0.96	20.03	34.76	0.99	15.98	76.62	0.99
5	bagasse	ST lime	6.30	0.94	0.97	8.33	12.17	1.00	7.51	30.58	0.96
6	bagasse	ST lime	15.20	9.00	0.95	19.48	38.05	0.99	17.36	79.15	0.99
7	rice straw	ST lime	9.69	2.59	0.96	10.64	21.47	0.99	8.02	46.81	1.00
8	rice straw	ST lime	17.96	7.80	0.95	18.09	42.28	0.97	8.25	78.63	0.96
9	bagasse	dilute acid	2.63	1.25	0.99	4.84	5.05	0.99	8.75	10.76	1.00
10	bagasse	dilute acid	4.88	2.55	0.97	11.24	8.11	0.97	9.78	23.84	0.99
11	rice straw	dilute acid	4.60	2.37	0.99	4.66	11.40	0.96	3.48	22.02	0.99
12	rice straw	dilute acid	8.50	3.08	0.99	19.80	14.10	1.00	17.31	46.78	0.96
13	corn stover	AFEX	5.82	3.71	0.98	11.15	16.59	0.99	10.22	42.28	0.99
14	corn stover	AFEX	5.83	4.45	0.98	11.47	16.65	0.99	11.13	44.18	0.99
15	corn stover	AFEX	5.54	3.79	0.94	12.19	17.93	1.00	9.53	43.90	0.99
16	corn stover	AFEX	11.51	9.12	0.98	14.16	31.09	1.00	10.01	60.83	0.99
17	corn stover	AFEX	13.58	10.27	0.96	16.63	35.01	0.99	10.46	68.26	0.99
18	corn stover	AFEX	14.32	10.80	0.98	15.27	39.08	0.99	10.28	72.02	0.99
19	bagasse	aq. ammonia	6.13	0.31	0.93	9.66	6.29	0.97	11.41	15.14	0.99
20	bagasse	aq. ammonia	6.24	0.34	0.92	10.23	6.44	0.97	12.03	16.02	1.00
21	bagasse	aq. ammonia	7.95	3.48	0.94	16.54	14.04	0.98	12.57	42.51	0.99
22	bagasse	aq. ammonia	8.03	3.77	0.96	16.78	14.52	0.97	12.63	43.26	0.99

[a] LT=long-term treatment; ST=short-term treatment; AFEX=ammonia fiber explosion.

Results and Discussion

Correlations for Prediction Samples

The 22 samples used to test the neural networks predictive ability resulted in correlations between structural features and slopes and intercepts similar to the results obtained for the 147 poplar model samples. Figures 41, 42, and 43 illustrate the correlations between biomass digestibility and lignin content and crystallinity index with constant acetyl content.

In Figure 41, the 1-h total sugar slopes and intercepts are significantly increased for low-crystallinity samples compared to high-crystallinity samples. Even at high lignin contents, the samples with low crystallinity exhibited a significant increase in 1-h total sugar slopes and intercepts. Lignin content affected both slopes and intercepts for high-crystallinity samples. However, lignin content had no affect on the low-crystallinity samples suggesting that crystallinity plays a more important role in controlling initial hydrolysis rates. The relatively flat profile for the low-crystallinity samples in Figure 41 illustrates that decreasing crystallinity increased the 1-h total sugar slopes and intercepts regardless of lignin content. This suggests that regardless of pretreatment type, initial biomass digestibility is controlled by its structural features.

Figure 42 illustrates that both 6-h slopes and intercepts increase with decreasing crystallinity. Unlike the 1-h data, lignin content plays a more important role in affecting biomass digestibility. As lignin decreases, 6-h slopes increase for both low- and high-crystallinity samples (see Figure 42a). However, 6-h intercepts for low-crystallinity samples appear independent of lignin content. Low-lignin samples with high crystallinity achieved higher slopes than low-crystallinity and high-lignin samples, suggesting both lignin and crystallinity are important in affecting 6-h digestibility.

3-d biomass digestibility can be independently controlled by its lignin content or crystallinity. Figure 43 illustrates that high slopes and intercepts were achieved with either low crystallinity and high lignin or high crystallinity and low lignin. In other words, at extended reaction times, crystallinity is less important at low lignin contents. Similarly, lignin content is less important to biomass digestibility at low crystallinity.

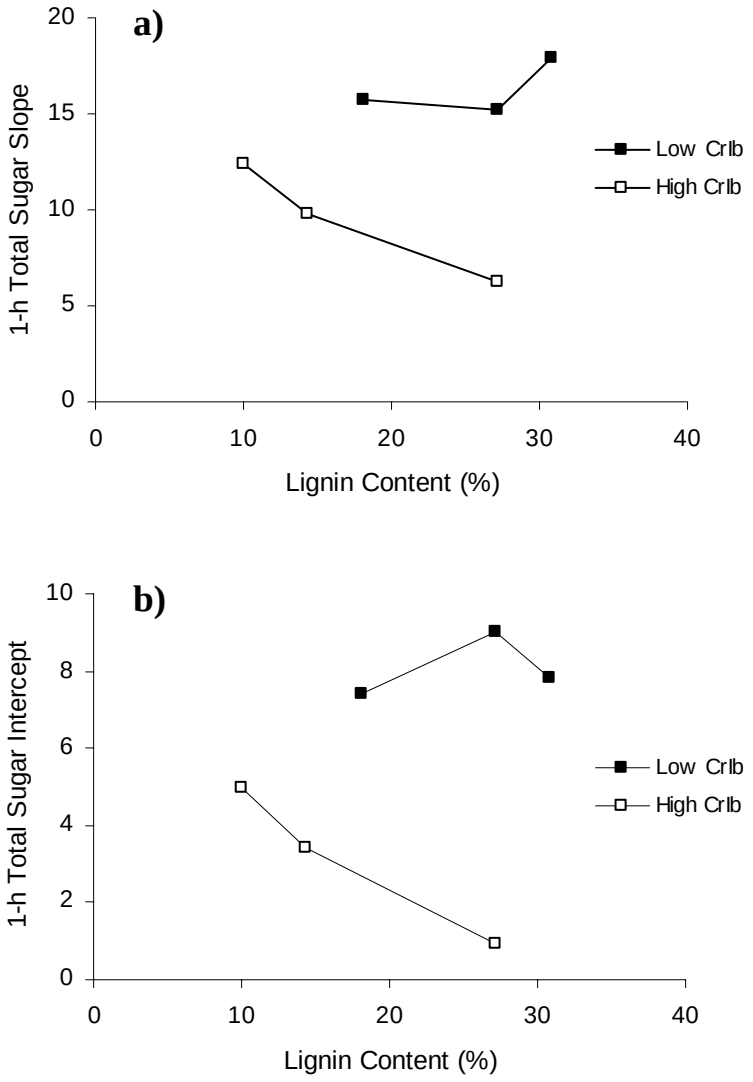

Figure 41. Effects of CrIb and lignin on 1-h total sugar (a) slope and (b) intercept. All samples had a low acetyl content (0.05–0.8%). Low CrIb (11.8–18.5%) and High CrIb (58.8–61.6%). Data from Table XXII.

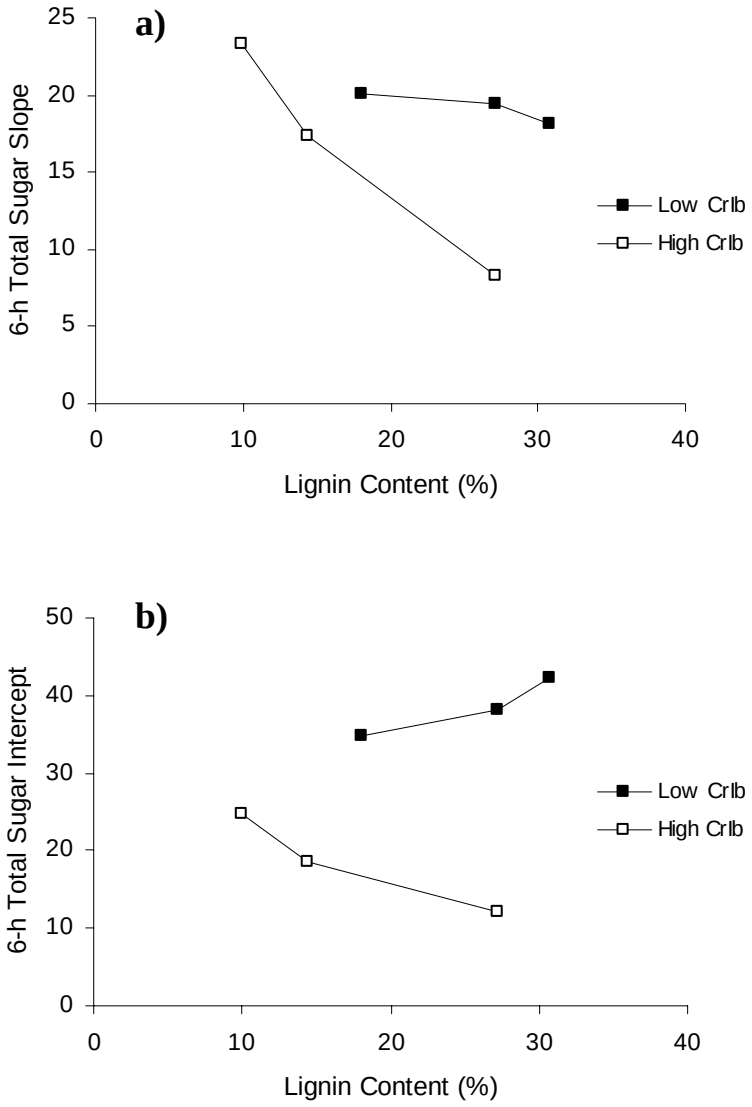

Figure 42. Effects of CrIb and lignin on 6-h total sugar (a) slope and (b) intercept. All samples had a low acetyl content (0.05–0.8%). Low CrIb (11.8–18.5%) and High CrIb (58.8–61.6%). Data from Table XXII.

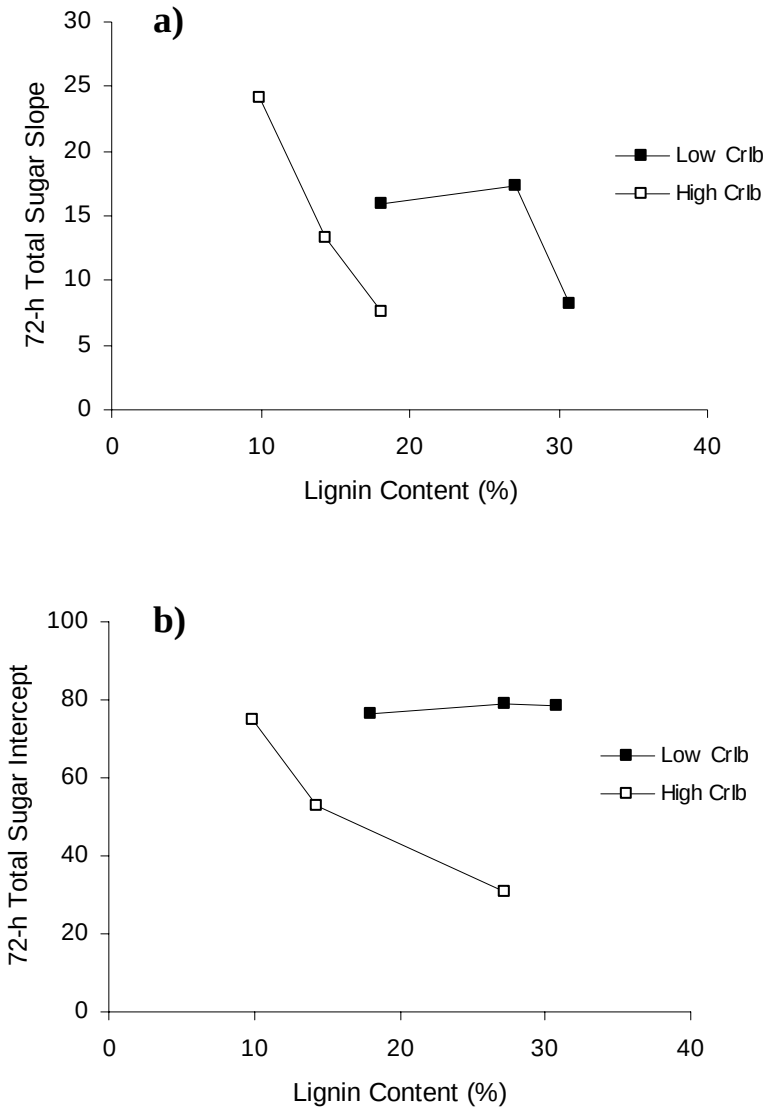

Figure 43. Effects of CrIb and lignin on 72-h total sugar (a) slope and (b) intercept. All samples had a low acetyl content (0.05–0.8%). Low CrIb (11.8–18.5%) and High CrIb (58.8–61.6%). Data from Table XXII.

Predicted 1-h Slopes and Intercepts

After using the previously trained networks to predict 1-h glucan, xylan, and total sugar slopes and intercepts for the 22 samples, the predicted outputs were compared to the experimentally measured outputs as shown in Figures 44 and 45. The predictive abilities of the 1-h networks are summarized in Table XXIII.

The MSEs of the 1-h glucan networks were 17.6 and 16.6 for slopes and intercepts, respectively. This means the average differences between the measured data and the glucan network predicted data were ±4.2% for slopes and ±4.1% for intercepts. Two aqueous ammonia and two lime-pretreated samples fell outside the 95% prediction interval (Figure 45a), but the other aqueous ammonia and lime-treated samples lie within the prediction interval. Thus, the trained glucan networks predicted the slopes and intercepts of the 22 samples fairly satisfactorily. Therefore, the networks can predict 1-h glucan digestibility regardless of biomass type or pretreatment. The 1-h xylan networks resulted in MSE values of 3.5 and 4.6 for slopes and intercepts, respectively. Figure 44b shows the predicted 1-h xylan slope agrees with the measured data within ±2.2%. Figure 45b shows the predicted 1-h xylan intercept agrees with the measured data within ±4%. Similar to the glucan intercept network, the xylan slope network predicted two aqueous ammonia samples outside the 95% prediction interval. Thus, it can be concluded that the trained xylan networks predicted the slopes and intercepts of the 22 samples fairly satisfactorily. Consequently, the networks can predict 1-h xylan digestibility regardless of biomass type or pretreatment technique.

The 1-h total sugar networks resulted in MSE values of 9.5 and 4.3 for slopes and intercepts, respectively. Figure 44c shows the predicted 1-h total sugar slope agrees with the measured data within ±5.8%. Figure 45c shows the predicted 1-h total sugar intercept agrees with the measured data within ±4.2%. It can be concluded that the trained total sugar networks predicted the slopes and intercepts of the 22 samples fairly adequately. Therefore, the networks can predict 1-h total sugar digestibility regardless of biomass type or pretreatment.

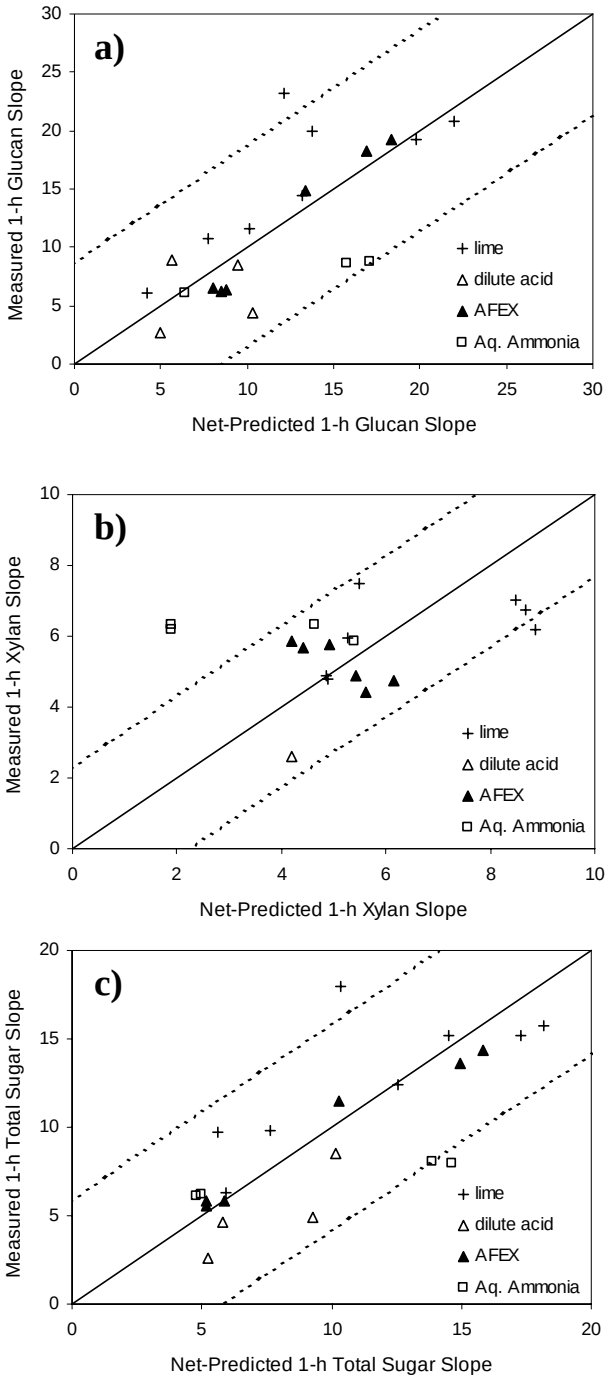

Figure 44. Correlation between experimentally measured and network-predicted slopes for (a) 1-h glucan, (b) 1-h xylan, and (c) 1-h total sugar. Dotted lines describe 95% prediction interval.

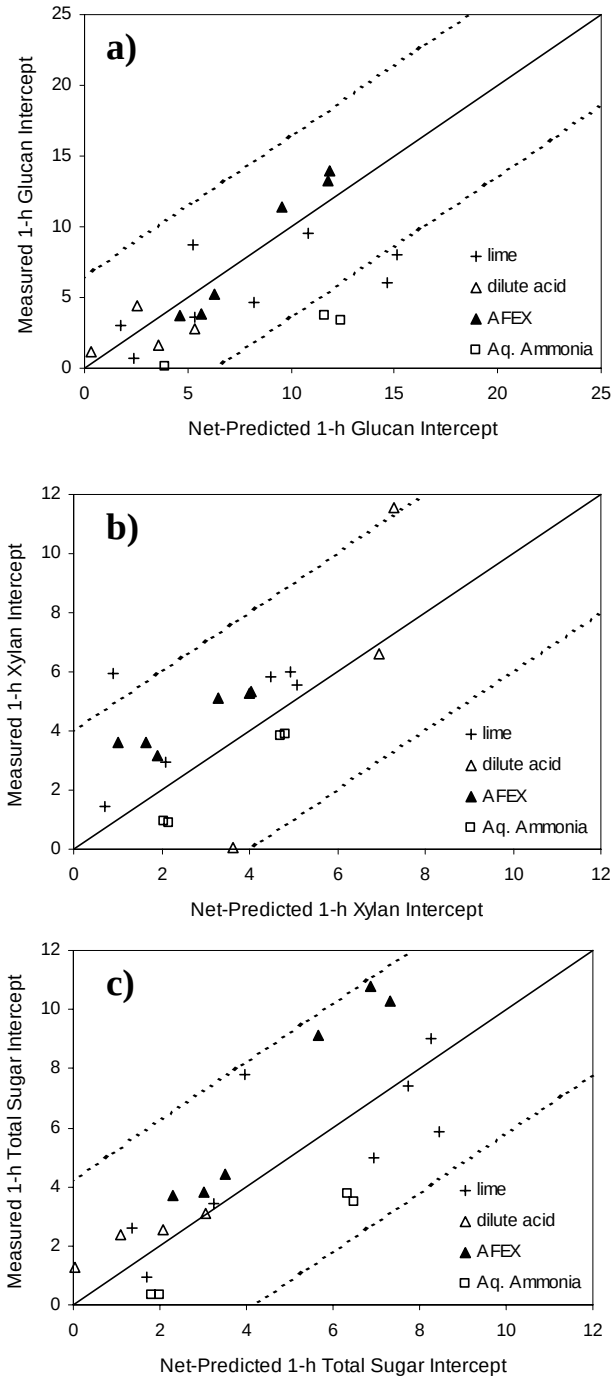

Figure 45. Correlation between experimentally measured and network-predicted intercepts for (a) 1-h glucan, (b) 1-h xylan, and (c) 1-h total sugar. Dotted lines describe 95% prediction interval.

Table XXIII. Summary of the predictive ability of the 1-h slope and intercept neural networks.

		MSE
Glucan	Slope (*B)*	17.6
	Intercept (*A*)	16.6
Xylan	Slope (*B)*	3.5
	Intercept (*A*)	4.6
Total Sugar	Slope (*B)*	9.5
	Intercept (*A*)	4.3

In general, the 1-h networks do a satisfactory job predicting slopes and intercepts for the 22 samples. It should be noted that the aqueous ammonia samples appear to have more scatter than the other pretreated samples.

Predicted 6-h Slopes and Intercepts

After using the previously trained networks to predict 6-h glucan, xylan, and total sugar slopes and intercepts for the 22 samples, the predicted outputs were compared to the experimentally measured outputs as shown in Figures 46 and 47. The predictive abilities of the 6-h networks are summarized in Table XXIV.

The MSEs of the 6-h glucan networks were 22 and 75 for slopes and intercepts, respectively. This means the average differences between the measured data and the glucan network predicted data were ±4.7% for slopes and ±8.7% for intercepts. Thus, the trained glucan networks predicted the slopes and intercepts of the 22 samples fairly satisfactorily. Therefore, the networks predict 6-h glucan digestibility regardless of biomass type or pretreatment.

The 6-h xylan networks gave MSE values of 15 and 138 for slopes and intercepts, respectively. Figure 46b shows the predicted 6-h xylan slope agrees with the measured data within ±4.2%. Figure 47b shows the predicted 6-h xylan intercept agrees with the measured data within ±23.1%. The data in Figure 46b is skewed lower indicating that the predicted slopes are slightly overestimated (i.e., predicted slopes greater than measured slopes). Thus, the 6-h xylan intercept network does a better job than the slope network when predicting outputs. The neural networks predicted 6-h xylan slopes and intercepts equally regardless of biomass type or pretreatment technique.

The 6-h total sugar networks resulted in MSE values of 13 and 51 for slopes and intercepts, respectively. Figures 46c and 47c show predicted 6-h total sugar slopes agree with the measured data within ±6.6% and ±14%, respectively. It can be concluded that the trained total sugar networks predicted the slopes and intercepts of the 22 samples fairly adequately. Therefore, the networks predicted digestibility regardless of biomass type or pretreatment.

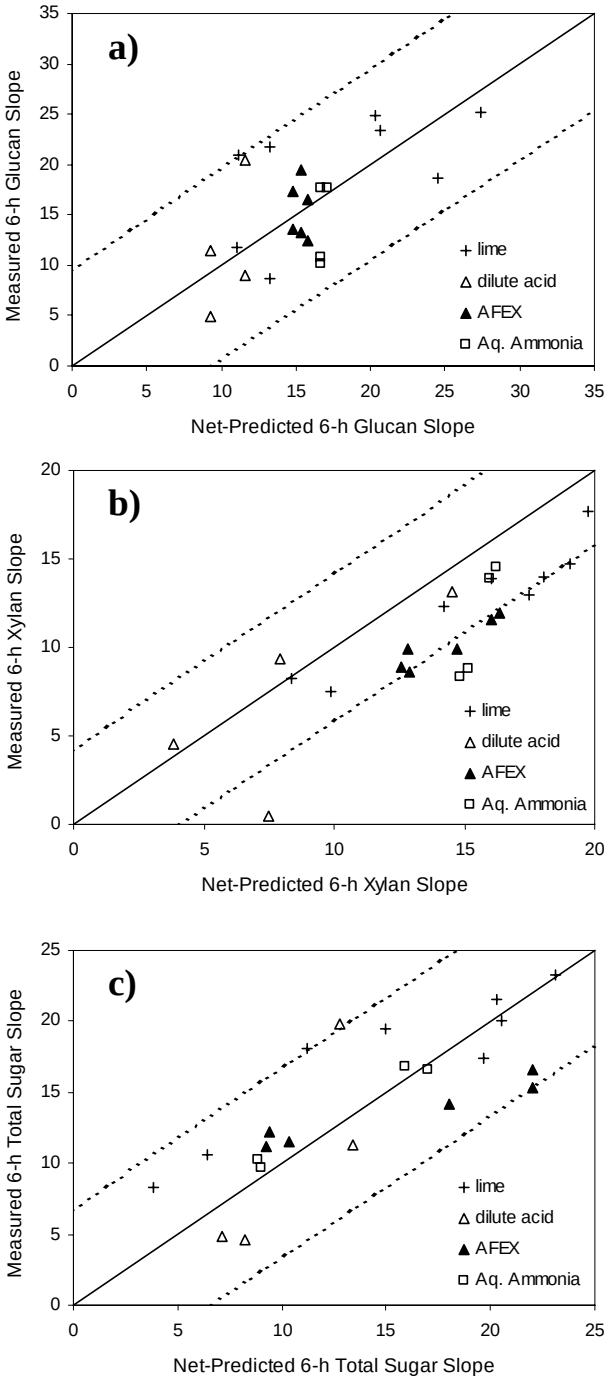

Figure 46. Correlation between experimentally measured and network-predicted slopes for (a) 6-h glucan, (b) 6-h xylan, and (c) 6-h total sugar. Dotted lines describe 95% prediction interval.

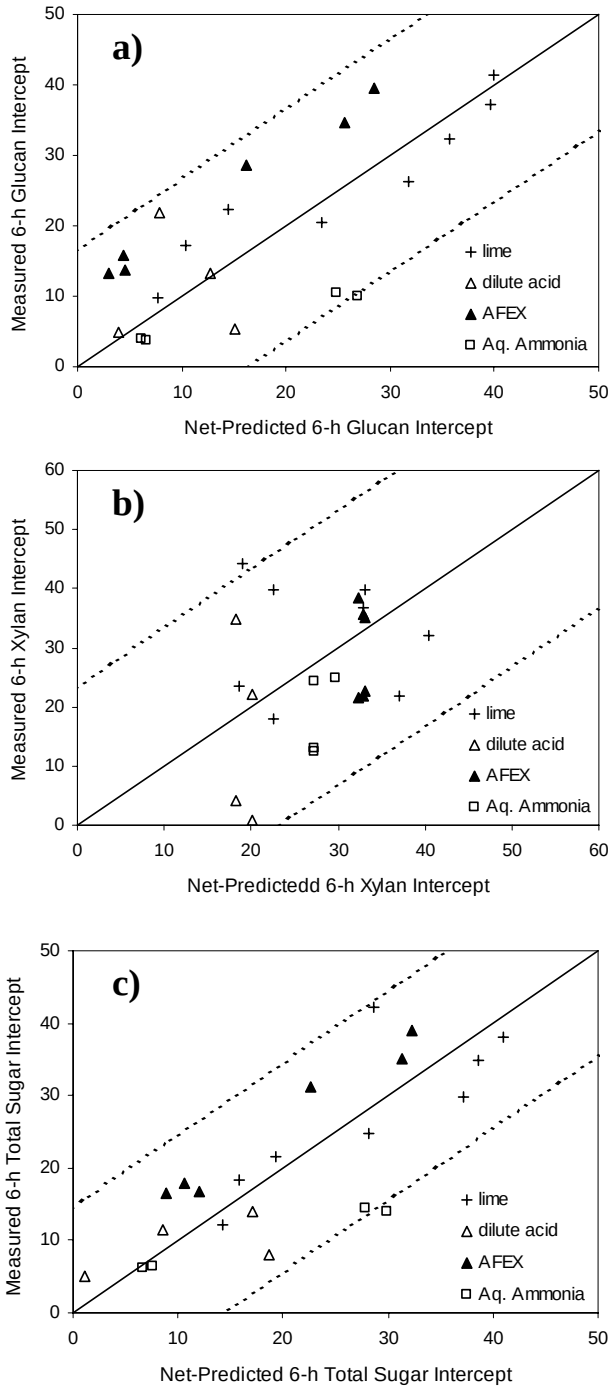

Figure 47. Correlation between experimentally measured and network-predicted intercepts for (a) 6-h glucan, (b) 6-h xylan, and (c) 6-h total sugar. Dotted lines describe 95% prediction interval.

Table XXIV. Summary of the predictive ability of the 6-h slope and intercept neural networks.

		MSE
Glucan	Slope (*B)*	22
	Intercept (*A*)	75
Xylan	Slope (*B)*	15
	Intercept (*A*)	138
Total Sugar	Slope (*B)*	13
	Intercept (*A*)	51

Predicted 72-h Slopes and Intercepts

After using the previously trained networks to predict 72-h glucan, xylan, and total sugar slopes and intercepts for the 22 samples, the predicted outputs were compared to the experimentally measured outputs as shown in Figures 48 and 49. The predictive abilities of the 72-h networks are summarized in Table XXV.

The MSEs of the 72-h glucan networks were 15 and 166 for slopes and intercepts, respectively. This means the average differences between the input data and the glucan network predicted data were ±3.9% for slopes and ±12.9% for intercepts. Thus, the trained 72-h glucan network predicts slopes of the 22 samples fairly satisfactorily; however, the 72-h glucan intercept network has a significant amount of scatter in the data as illustrated in Figure 49a. The networks predict 72-h glucan digestibility equally regardless of biomass type or pretreatment technique.

The 72-h xylan networks gave MSE values of 22 and 199 for slopes and intercepts, respectively. Figure 48b shows the predicted 72-h xylan slope agrees with the measured data within ±4.9%. Figure 49b shows the predicted 6-h xylan intercept agrees with the measured data within ±27.0%. Similar to the 6-h xylan slope network, the 72-h xylan slope network overestimated the experimentally measured slopes as illustrated by the lower skewedness in Figure 48b (i.e., predicted slopes greater than measured slopes). Even though the slope predictions are overestimated, the AFEX-treated material in Figure 48b appears to be consistently higher than the other treatment techniques investigated. Holtzapple et al. (1991) reported that AFEX treatment alters lignin, but with little removal. Previously, we have shown that lignin has a major affect on ultimate digestibility. Therefore, a measure of the total lignin content, as in our case, may lead to difficulties in modeling the digestibility of AFEX-treated biomass. Thus, care should be taken when studying pretreatments that do not remove barriers but instead lead to physical or chemical rearrangement. With the exception of AFEX-treated biomass, the networks equally predicted slopes and intercepts for xyaln digestibility regardless of biomass type or pretreatment technique.

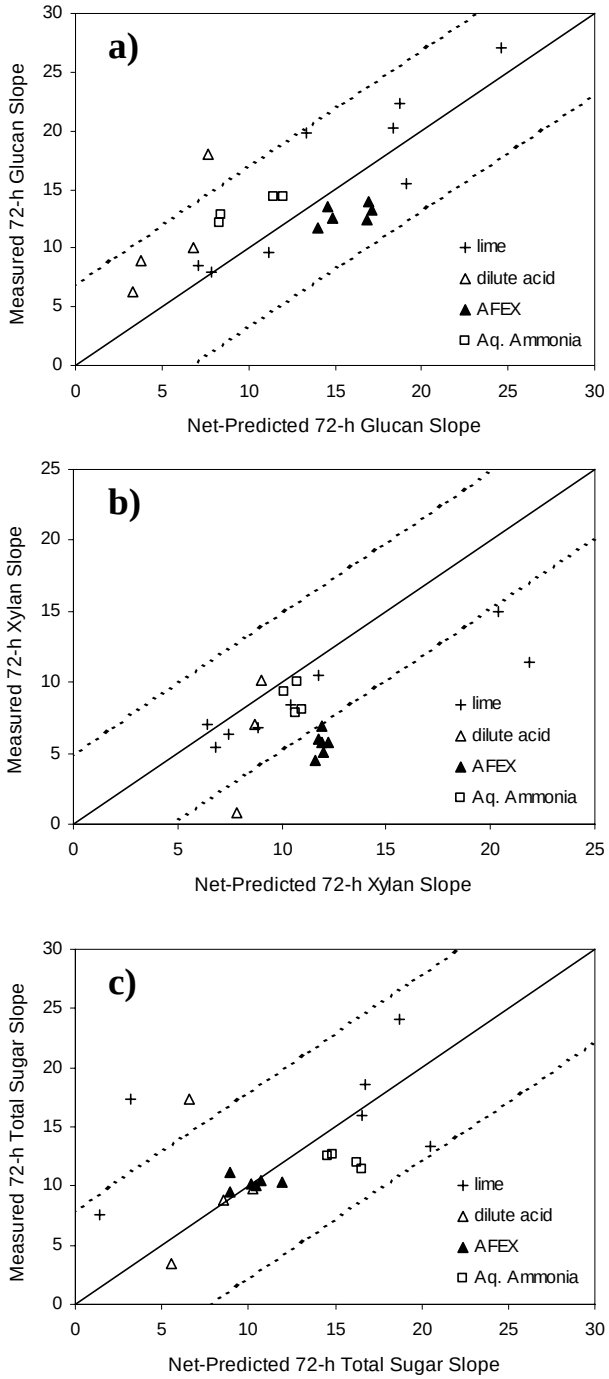

Figure 48. Correlation between experimentally measured and network-predicted slopes for (a) 72-h glucan, (b) 72-h xylan, and (c) 72-h total sugar. Dotted lines describe 95% prediction interval.

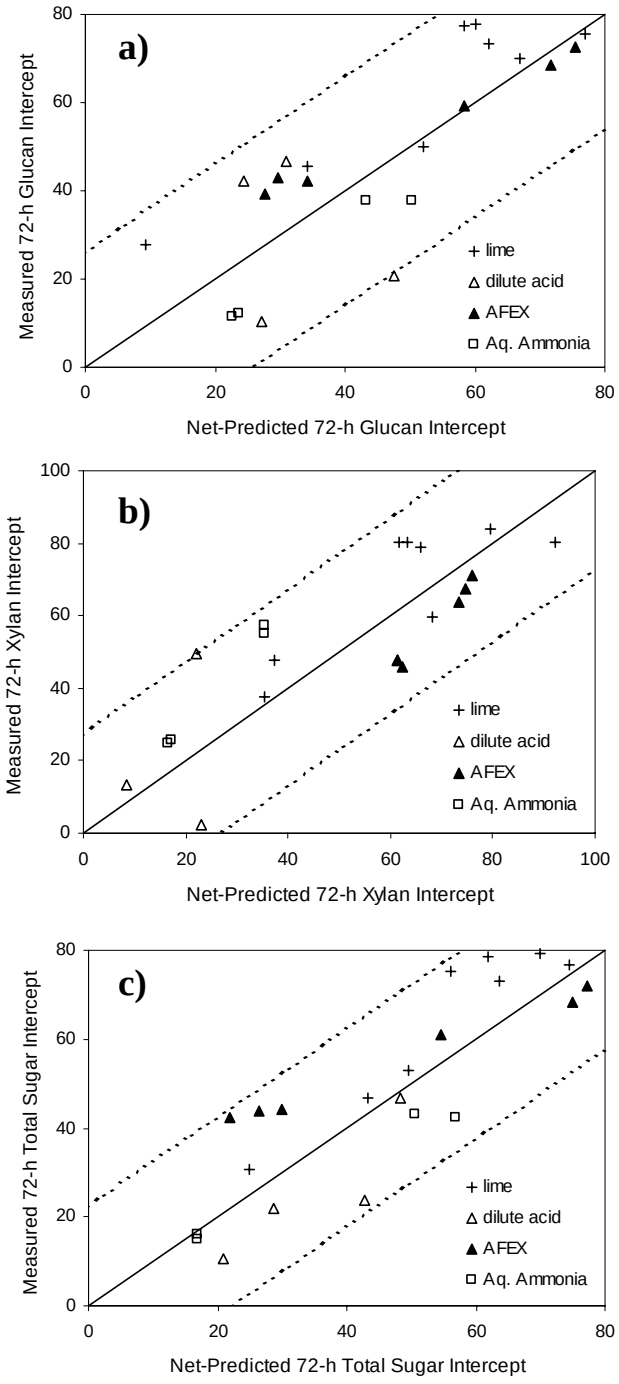

Figure 49. Correlation between experimentally measured and network-predicted intercepts for (a) 72-h glucan, (b) 72-h xylan, and (c) 72-h total sugar. Dotted lines describe 95% prediction interval.

Table XXV. Summary of the predictive ability of the 72-h slope and intercept neural networks.

		MSE
Glucan	Slope (*B)*	15
	Intercept (*A*)	166
Xylan	Slope (*B)*	22
	Intercept (*A*)	199
Total Sugar	Slope (*B)*	36
	Intercept (*A*)	122

The 72-h total sugar networks resulted in MSE values of 36 and 122 for slopes and intercepts, respectively. Figure 48c shows the predicted 72-h total sugar slope agrees with the measured data within ±7.9%. Figure 49c shows the predicted 72-h total sugar intercept agrees with the measured data within ±22.2%. It can be concluded that the trained total sugar slope network is a better predictor of the 22 samples than the intercept network. Figures 48 and 49 illustrate that regardless of biomass type or pretreatment, the networks equally predict digestibility.

In general, lime-treated samples exhibited higher slopes and intercepts at 72 h, thereby attesting to the effectiveness of lime pretreatment in rendering biomass highly digestible.

Predicting Carbohydrate Conversions

The ability to predict sugar conversion regardless of biomass type or pretreatment technique is advantageous. Researchers can use this knowledge to design cost-effective pretreatments.

After predicting slopes and intercepts with the 18 neural networks, Equation 5 was used to back calculate sugar conversions at the enzyme loadings used during hydrolysis experiments. Glucan, xylan, and total sugar conversions calculated from the predicted slopes and intercepts were compared with experimentally measured conversions as shown in Figures 50, 51, and 52, respectively. Figures 53, 54, and 55 are examples of the measured and predicted glucan conversion, xylan conversion, and total sugar conversion, respectively, plotted versus the natural logarithm of enzyme loading. The results show predicted conversions have a high degree of variability between samples as well as at different incubation times. In general, errors for 72-h predicted glucan conversions were larger than for 1 h and 6 h. This was anticipated because larger average absolute errors were observed for 72-h neural-network-predicted slopes and intercepts. The average absolute error for 72-h slopes was 4.1 versus 3.1 and 3.8 for 1-h and 6-h slopes, respectively. Similarly, the average absolute error for 72-h intercepts was 11.2 versus 3.1 and 6.8 for 1-h and 6-h intercepts, respectively.

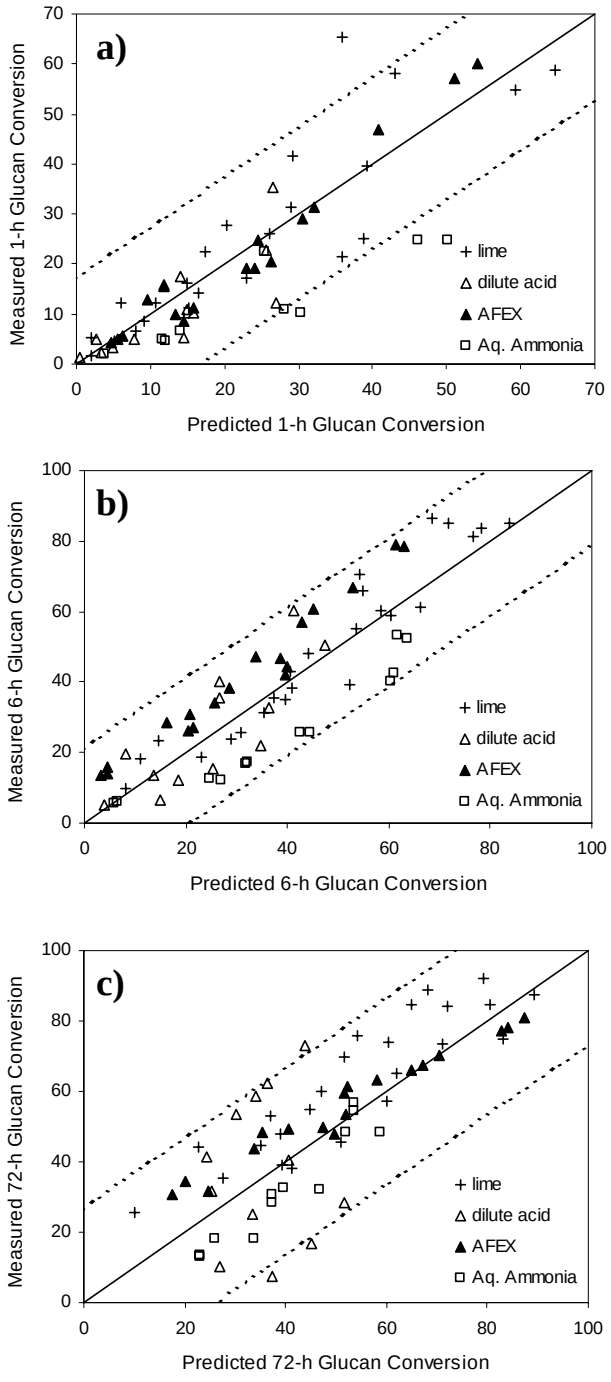

Figure 50. A plot of experimentally measured versus predicted glucan conversions for the 22 prediction samples at (a) 1 h, (b) 6 h, and (c) 72 h.

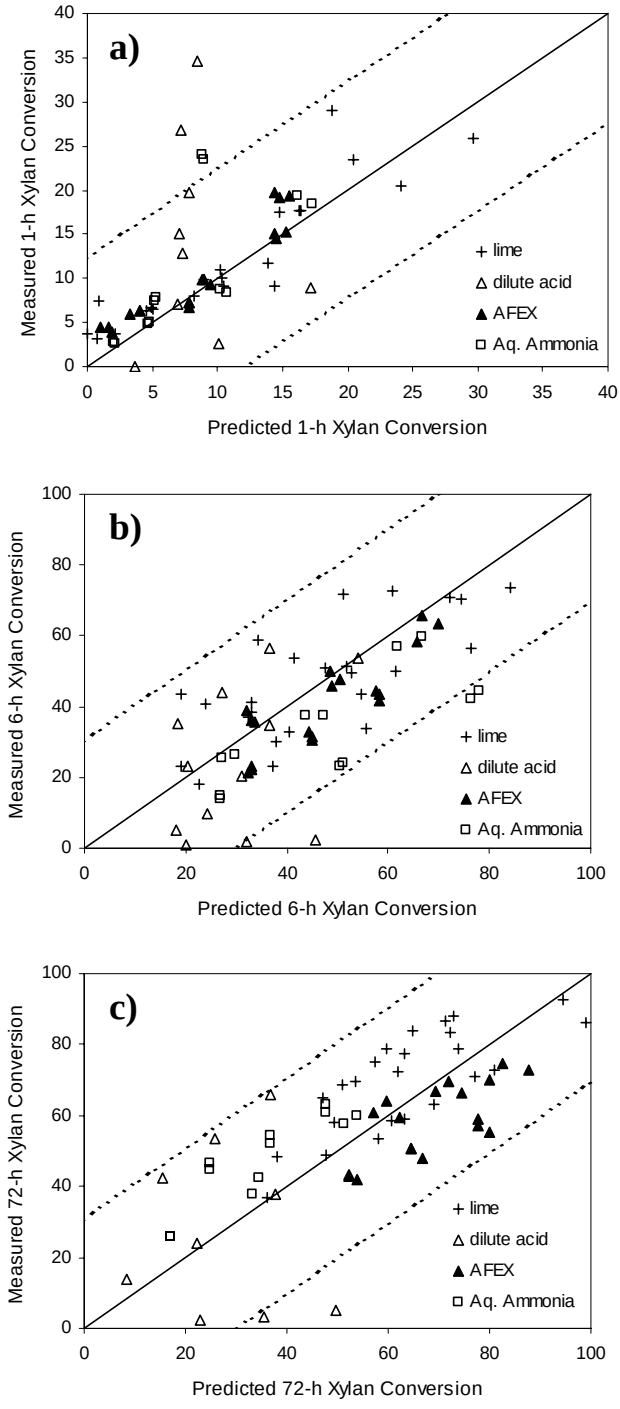

Figure 51. A plot of experimentally measured versus predicted xylan conversions for the 22 prediction samples at (a) 1 h, (b) 6 h, and (c) 72 h.

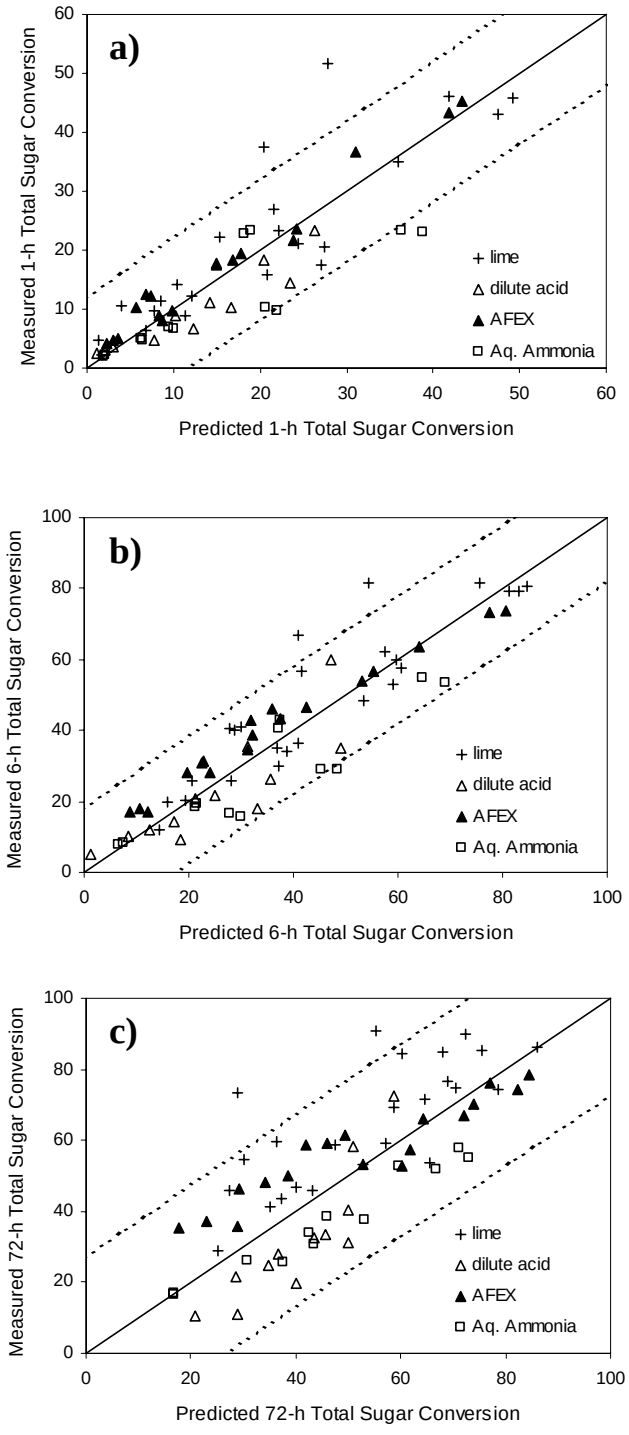

Figure 52. A plot of experimentally measured versus predicted total sugar conversions for the 22 prediction samples at (a) 1 h, (b) 6 h, and (c) 72 h.

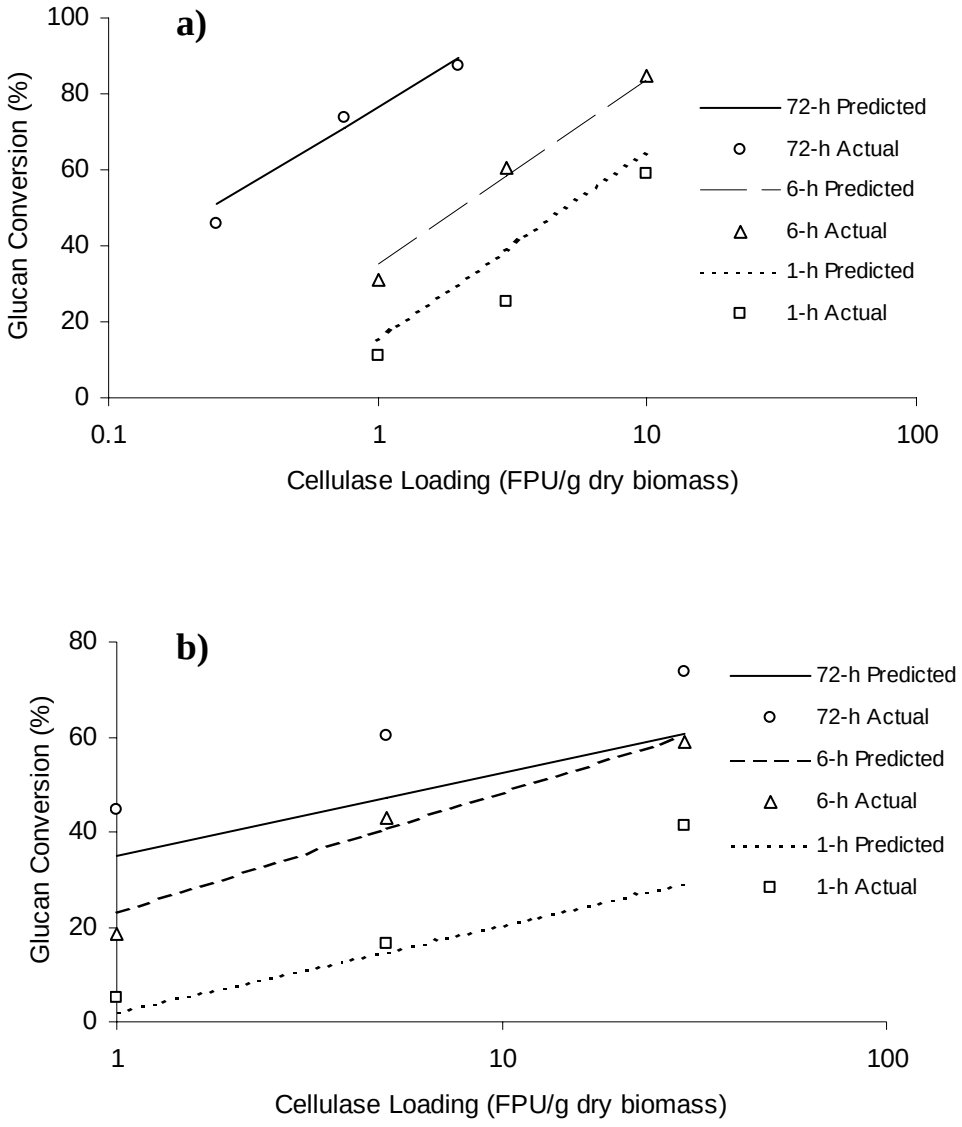

Figure 53. Experimentally measured and predicted glucan conversions plotted versus cellulase loading for 2 of the 22 prediction samples with (a) high reactivity (Sample 4) and (b) low reactivity (Sample 9). Reaction conditions: 10 g biomass/L and 48 CBU/g dry biomass.

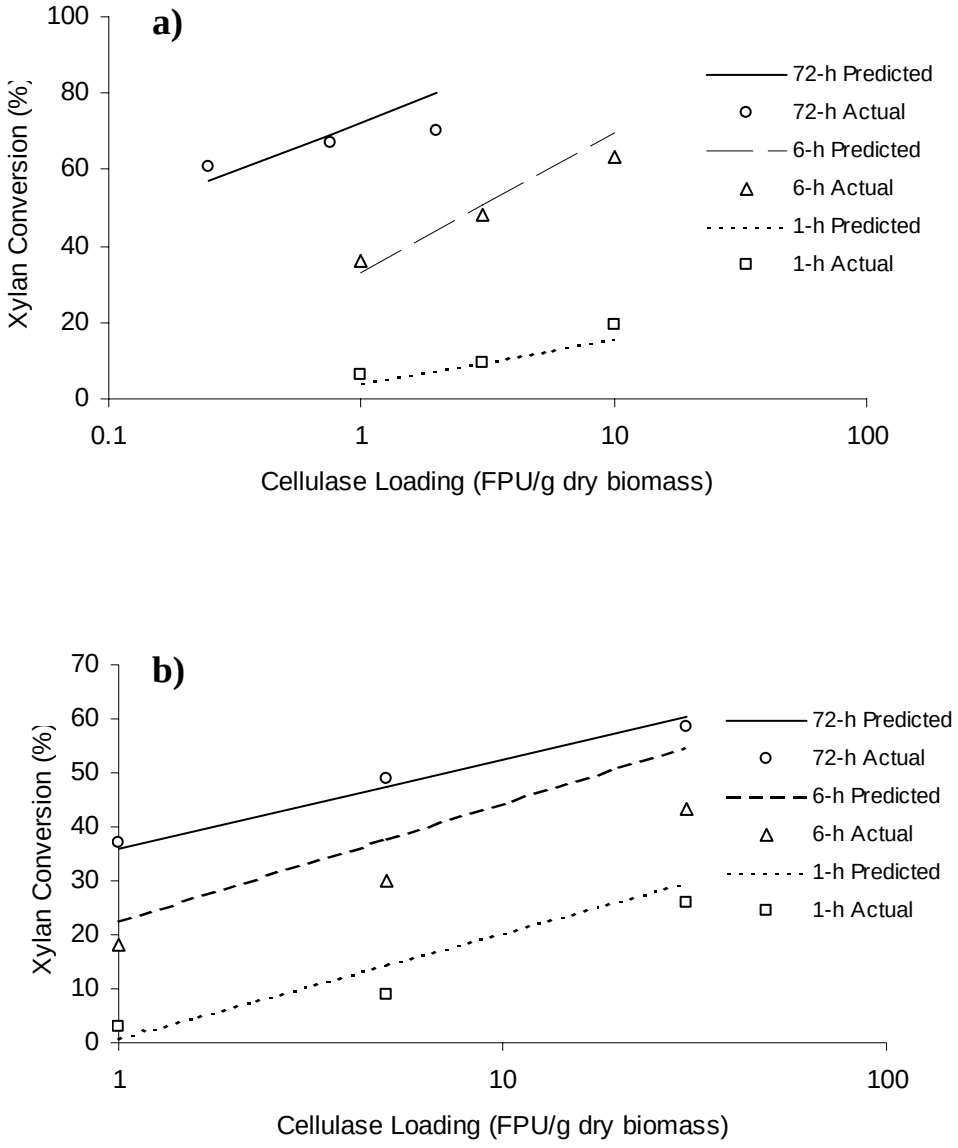

Figure 54. Experimentally measured and predicted xylan conversions plotted versus cellulase loading for 2 of the 22 prediction samples with (a) medium reactivity (Sample 17) and (b) low reactivity (Sample 5). Reaction conditions: 10 g biomass/L and 48 CBU/g dry biomass.

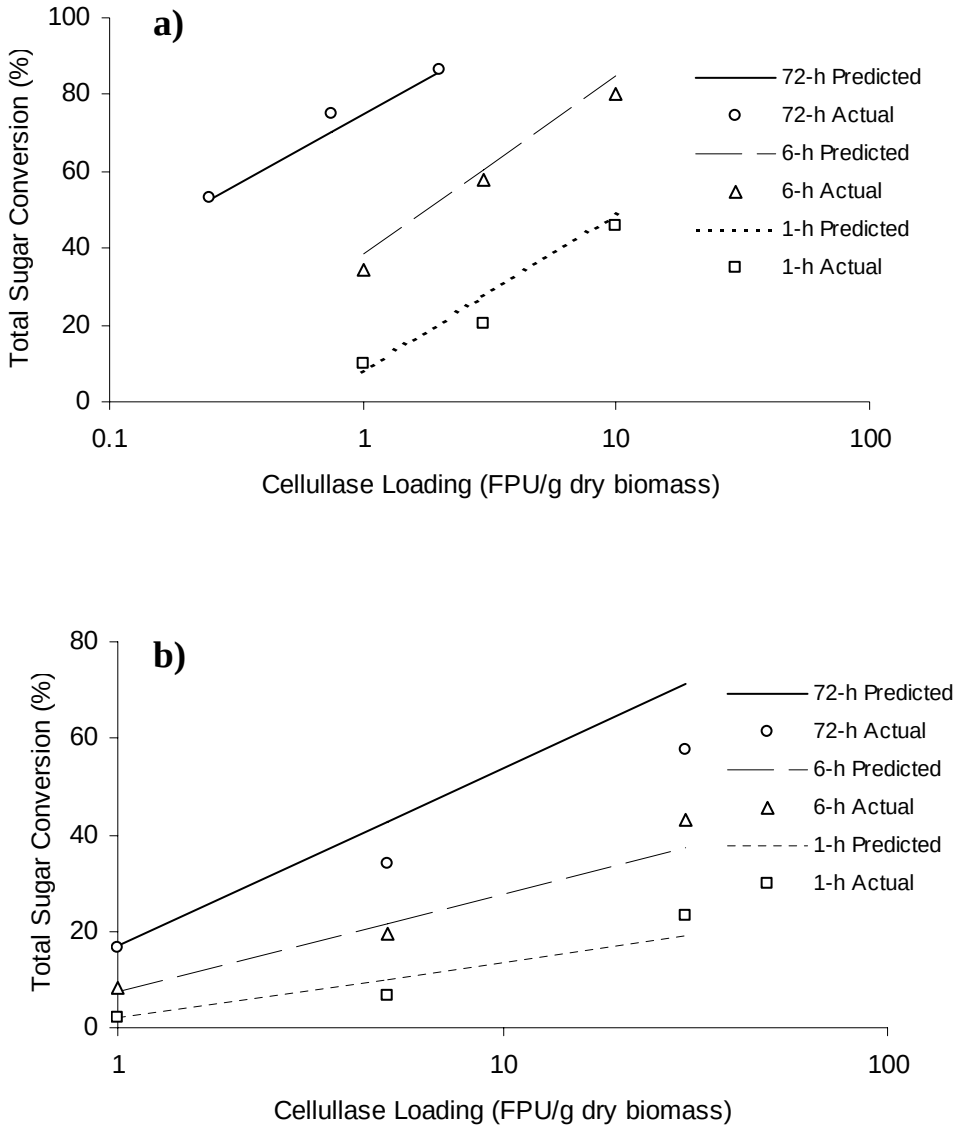

Figure 55. Experimentally measured and predicted total sugar conversions plotted versus cellulase loading for 2 of the 22 prediction samples with (a) high reactivity (Sample 4) and (b) low reactivity (Sample 20). Reaction conditions: 10 g biomass/L and 48 CBU/g dry biomass.

In Equation 5, the slope (*B*) exhibits a more significant effect than intercept (*A*) on predicted conversions because the slope forms a product with the enzyme loading (E_o). Therefore, the larger the MSE for the predicted slope the larger the error in predicting sugar conversions. However, the intercept becomes the more dominant term at low enzyme loadings for highly reactive samples (i.e., when the contribution of the slope and enzyme loading term is smallest).

The 6-h and 72-h xylan predicted conversions were expected to be larger than the measured conversions because the respective networks overestimated the predicted slopes (Figures 46b and 48b). The expectations were not met due to moderately underestimated intercepts for 6-h and 72-h xylan samples in combination with low enzyme loadings at 6 h and 72 h. As a result, the intercept term in Equation 5 was more significant and resulted in predicted xylan conversions less than measured xylan conversions, in most cases.

As illustrated in Figures 35–40 (experimentally measured versus network-simulated) and Figures 44–49 (experimentally measured versus network-predicted), the data do not lie on the diagonal. The data scatter may be a result of glucan, xylan, and total sugar digestibility not being completely determined by acetyl content, lignin content, and crystallinity. This suggests that there are other features that may play a significant role in biomass digestibility. Another reason for the data scatter may be the pretreatment techniques. Even though ball milling was effective in altering crystallinity and not lignin or acetyl, it did affect other biomass structural features. As previously mentioned, ball milling not only reduces biomass crystallinity, but also increases the available surface area and pore volume resulting in additional adsorption sites for the enzymes (Lee and Fan, 1982). Puri (1984) and Nazhad et al. (1995) reported that surface area has a major effect on biomass digestibility; therefore, the reduction in crystallinity due to ball milling is only one of the factors that influences biomass digestibility. Also, lignin removal has been shown to increase biomass swellability resulting in increased available surface area for the enzymes (Wong et al., 1988). As a result, the treatments chosen to alter crystallinity and lignin resulted in changes in

biomass surface area as well. This may explain why acetyl, lignin, and crystallinity could not fully explain biomass digestibility. Lastly, as illustrated in Figure 56, the pretreatments (dilute acid, lime, AFEX, and aqueous ammonia) resulted in at least one structural feature (i.e., acetyl, lignin, glucan, xylan, or total sugar) outside the range of the 147 model samples used to train the networks. As a result, the trained networks had to predict slopes and intercepts with inputs from the 22 samples outside the range in which they were trained (i.e., extrapolation). When predicting outputs, small errors in estimation are magnified by extrapolations, which is called the extrapolation penalty. The extrapolation penalty increases with the degree of extrapolation.

CONCLUSIONS

Neural networks were developed and trained to simulate slopes and intercepts for 147 poplar wood model samples with a variety of lignin contents (0.7–26.3%), acetyl contents (0.1–3.1%), and crystallinity indices (5.4–68.8%). The networks were developed for glucan, xylan, and total sugar slopes and intercepts at 1, 6, and 72 h resulting in a total of 18 neural networks.

The networks performed consistently poorer when simulating slopes and intercepts for xylan compared with glucan and total sugar. This may be due to low biomass xylan content, which makes it difficult to measure small changes in xylan digestibility over such a narrow range. The experiments were conducted for the 147 model samples and 22 prediction samples over an 18-month period. The NREL cellulase activity procedure measures the activity of those enzymes that degrade cellulose (glucanases). Because of the low xylanase activity in the cellulase complex, its activity may have decreased more rapidly than glucanase activity. Therefore, xylan slopes and intercepts showed consistently larger MSE and lower R^2 values compared with glucan and total sugar. Nonetheless, the coefficients of determination (R^2) were 0.81, 0.94, and 0.87 for 1-h, 6-h, and 72-h xylan slopes respectively, whereas the R^2 values were 0.78, 0.95, and 0.99 for 1-h, 6-h, and 72-h xylan intercepts respectively. This suggests the xylan networks simulated slopes and intercepts for the 147 model

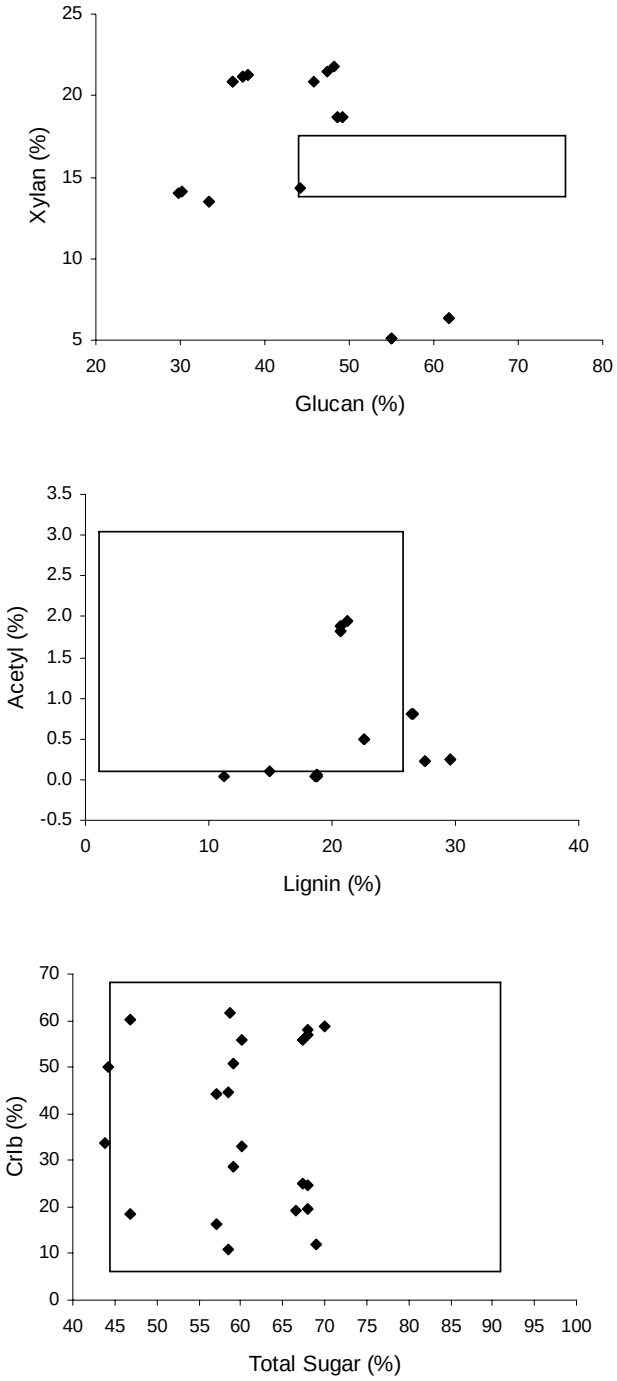

Figure 56. Summary of the 22 samples used to test the network's predictive ability that fall outside of the range of the structural features used to train the networks (boxed regions).

samples fairly satisfactorily.

Biomass samples (corn stover, bagasse, and rice straw) were chemically pretreated with long-term lime, short-term lime, dilute sulfuric acid, AFEX, and aqueous ammonia plus mechanical ball milling to create 22 prediction samples with a broad spectrum of acetyl contents (0.03–1.95%), lignin contents (9.94–31.68%), and biomass crystallinity indices (11.0–61.6%). The various biomass samples were pretreated with different techniques to test the neural networks' ability to predict slopes and intercepts regardless of biomass type or pretreatment. If the networks could accurately predict slopes and intercepts for the 22 prediction samples, then we could say that acetyl, lignin, and crystallinity completely determine the enzymatic digestibility of biomass.

Previously, biomass digestibility was described as a two-step process that involved enzymes passing through barriers such as lignin and acetyl to gain access to the cellulose (Chang, 1999). Once arriving at the cellulose, the effectiveness of the enzymes was determined by biomass crystallinity, i.e., the more crystalline the biomass the less effective the enzymes. This suggests that cellulose crystallinity and not overall biomass crystallinity is a better measure of what impedes enzymatic hydrolysis of cellulose. Because lignin and xylan are mostly amorphous and crystallinity is defined as the weight fraction of crystalline material to total material, biomass crystallinity always underestimates the true cellulose crystallinity. When cellulose crystallinity was used as an input instead of biomass crystallinity, the predictive ability of all 18 networks improved. As an example, MSE values for the 1-h total sugar slope networks with CrIc and CrIb were 9.5 and 13.8, respectively, and MSE values for the 6-h total sugar intercept networks with CrIc and CrIb were 51 and 103, respectively. Therefore, cellulose crystallinity was a better gauge of biomass digestibility at all times.

In addition to investigating the effect of structural features on biomass digestibility, simply increasing the dimensionality of the neural network input matrix permitted investigation of the effect xylan removal has on glucan digestibility and the effect glucan removal has on xylan digestibility. Kong et al. (1992) found that removal of acetyl-free xylan backbone did not facilitate enzymatic hydrolysis. Likewise, our

results indicate there was no correlation between xylan removal and glucan digestibility. However, MSE values of 6-h xylan slope networks with and without 6-h glucan slope as an input were 14.5 and 50, respectively, and MSE values of 72-h xylan intercept networks with and without 72-h glucan intercept as an input were 199 and 465, respectively. Therefore, there was a correlation between glucan removal and xylan digestibility observed at 6 h and 72 h, i.e., the 6 h and 72 h networks predicted xylan slopes and intercepts better when glucan functionality was included as an independent variable. In other words, glucan removal helped destroy the intricate nature of lignocellulosic biomass to permit easier access of enzymes to the xylan backbone.

The neural networks performed equally when predicting slopes and intercepts for the different types of biomass treated with different techniques. In other words, the data were scattered equally for the majority of samples regardless of biomass type or pretreatment. A clear exception was the 72-h xylan slope network where the AFEX-treated corn stover samples had a consistently larger error than the other samples. In general, the AFEX-treated samples had a slightly larger error at 72 h than the other samples. AFEX pretreatment increases biomass digestibility not by reducing the lignin content but through physical and chemical alteration of the lignin. In "Enzymatic Hydrolysis of Model Samples," lignin content played a major role in ultimate biomass digestibility (72 h). As a result, the 72-h slope networks were less effective in correlating lignin content with AFEX-treated corn stover digestibility.

The calculated carbohydrate conversions from predicted slopes and intercepts indicated that acetyl content, lignin content, and crystallinity do not completely explain biomass digestibility. As discussed previously, other structural features such as surface area and pore volume, which were not investigated in this study, may play a significant role as well. Caulfield and Moore (1974) suggested coupling crystallinity measurements with surface area measurements to more effectively study the influence of each aspect of morphology on biomass digestibility. Also, the 147 poplar wood model samples used to train the networks and the 22 samples used to test the networks predictive ability were air-dried after pretreatment. When air-dried from the water-swollen state, biomass

capillaries collapse and the physical features are drastically altered (Fan et al., 1980). Crystallinity was measured on dry biomass samples by X-ray diffraction. When performing enzymatic hydrolysis, the crystallinity may have changed because of its rehydrated state. As a result, the neural networks may have had difficulty discerning a firm correlation between crystallinity and biomass digestibility. Ideally, biomass samples should be solvent dried instead of air-dried to preserve the physical characteristics of water-swollen biomass such as crystallinity and surface area. Lastly, pretreatment of the 22 samples resulted in glucan and xylan contents outside the range of the 147 model samples used to train the networks. As a result, the trained networks predicted slopes and intercepts with inputs from the 22 samples outside the range in which they were trained (i.e., extrapolation). The errors associated with extrapolation may explain the discrepancies between the measured and predicted conversions. Additional studies performed with samples whose structural features fall within the range of the 147 model samples would resolve this issue.

PREDICTING CELLULOSE CRYSTALLINITY

INTRODUCTION

X-ray diffraction is a well-established method for determining the mass fraction of crystalline material in a lignocellulosic biomass sample (Andersson et al., 2004; Balta-Calleja and Vonk, 1989). However, the complex chemical composition of biomass complicates the crystallinity determination because the separation of amorphous background from the diffraction pattern of cellulose crystallites is difficult. It has been shown that solid-state NMR measurements such as ^{13}C CP-MAS (cross polarization magic angle spinning) can determine the intrinsic crystallinity of pure cellulose (Teeaar et al., 1987; Zhbankov et al., 1987). It is characteristic of NMR spectra that chemically equivalent carbons can be distinguished if they are in different magnetic environments. The C-4 peaks of anhydroglucose units in crystalline and noncrystalline domains appear at δ=89 and δ=84, respectively. For pure cellulose samples, the results obtained from ^{13}C CP-MAS correlate well with corresponding crystallinities obtained by X-ray diffraction (Horii et al., 1982; Teeaar et al., 1987). However, ^{13}C CP-MAS NMR cannot determine biomass crystallinity due to overlapping hemicellulose and lignin signals.

^{13}C CP-MAS NMR with spin locking permits the determination of biomass crystallinity by eliminating the signals associated with hemicellulose and lignin carbons (Teeaar et al., 1987). Spin locking is based on differences in proton spin relaxation time constants due to different magnetic environments, i.e., different packing of the cellulose chains (Teeaar et al., 1987; Newman and Hemmingson, 1990). The pulse sequence of spin locking experiments is given in Figure 57 with a preparation pulse t_p, a spin-locking pulse t_{sl}, a contact time t_c in which cross polarization occurs, a data acquisition time t_a, and a recovery delay time t_d (Newman and Hemmingson, 1990). The spin-locking sequence differs from basic cross-polarization by adding t_{sl}. As shown in Figure 58, subspectra of crystalline cellulose and amorphous lignin and hemicellulose can be separated by a linear combination of two spectra measured with and without spin-lock.

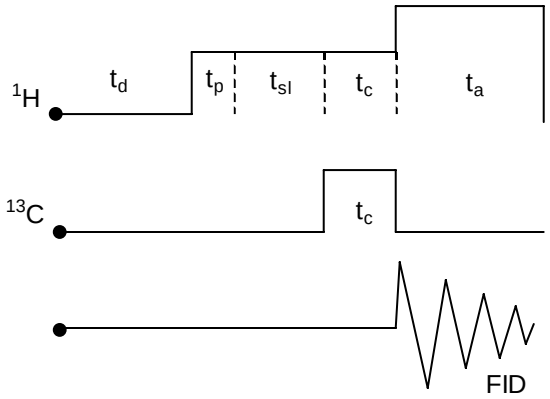

Figure 57. Representation of a spin-locking pulse sequence (Newman and Hemmingson 1990). FID = free induction decays.

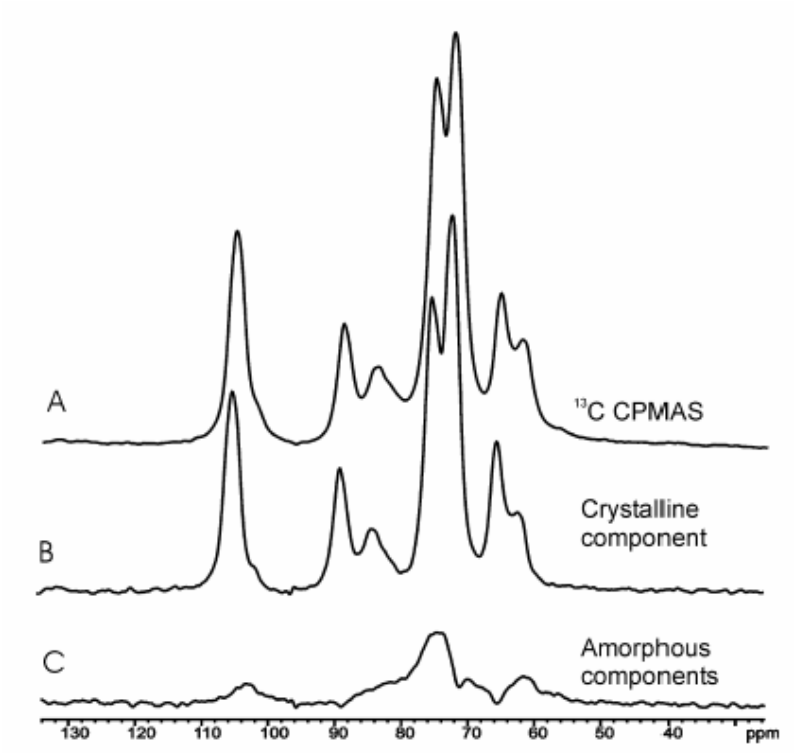

Figure 58. Spectra typical of (A) normal ^{13}C CP-MAS measurement, (B) CP-MAS with spin-locking measurement, and (C) difference between the two spectra (Liitia et al., 2003).

Purpose

The purpose of this study is to develop an empirical SAS model to determine cellulose crystallinity as a function of structural features that can be easily determined by standard NREL procedures (glucan, xylan, and lignin) and X-ray diffraction (biomass crystallinity).

Materials and Methods

Substrate Preparation

Avicel pH 101 (Fluka BioChemika) was ball milled for 1 and 2 days to generate cellulose with different crystallinities. The procedures for ball milling and crystallinity measurements by X-ray diffraction are described in "Materials and Methods – Enzymatic Hydroysis of Model Samples." Raw and ball milled Avicel, hydrolytically isolated lignin (Aldrich), and birchwood xylan (Sigma) were physically mixed in different ratios (Table XXVI) to create 15 samples with a variety of compositions and cellulose crystallinities. The samples were mixed thoroughly to ensure the components were homogeneously distributed. The glucan, xylan, and lignin contents of the 15 samples were determined on a weight percent basis.

NMR Measurement

All ^{13}C CP-MAS NMR measurements were performed with a Bruker Avance-400 Solids NMR spectrometer, based on a Linux workstation, operating at 75.5 MHz. The spinning speed was 6000 Hz, acquisition time 20 μs, contact time 1 μs, and delay between pulses 2 s. In addition to the ordinary cross-polarization experiment, another experiment with a spin-lock pulse time of 16 μs was performed to spectroscopically remove the interfering hemicellulose and lignin signals in the amorphous spectral region. During the spin-lock pulse, some loss of magnetization occurs through relaxation, which is faster for the amorphous hemicellulose and lignin matrices (Liitia et al., 2003).

Table XXVI. Summary of structural features of the fifteen samples used to develop an empirical model in SAS to predict cellulose crystallinity.

Sample	Cellulose (%)	Xylan (%)	Lignin (%)	CrIb (%)
1	33.5[a]	33.0	33.5	49.9
2	50.2[a]	24.9	24.9	64.8
3	85.0[a]	7.5	7.5	79.6
4	14.9[a]	50.0	35.1	33.6
5	60.0[a]	24.9	15.1	70.3
6	33.5[b]	33.0	33.5	22.2
7	50.2[b]	24.9	24.9	35.1
8	85.0[b]	7.5	7.5	41.3
9	14.9[b]	50.0	35.1	17.6
10	60.0[b]	24.9	15.1	36.5
11	33.5[c]	33.0	33.5	20.1
12	50.2[c]	24.9	24.9	25.0
13	85.0[c]	7.5	7.5	37.5
14	14.9[c]	50.0	35.1	18.6
15	60.0[c]	24.9	15.1	35.2

[a] Cellulose was not ball milled, CrIc = 82.1%.

[b] Cellulose was ball milled for 1 day, CrIc = 48.3%.

[c] Cellulose was ball milled for 2 days, CrIc = 38.6%.

The cellulose crystallinity was determined from the areas of the crystalline (86–92 ppm) and amorphous (79–86 ppm) C4 signals as give by Equation 23 (Teeaar et al., 1987)

$$\mathrm{CrIc} = \frac{A_{86-92\,ppm}}{(A_{79-86\,ppm} + A_{86-92\,ppm})} \times 100 \tag{23}$$

where CrIc is the fraction of crystalline cellulose divided by total cellulose.

SAS Modeling

Biomass crystallinity (M1), glucan content (M2), lignin content (M3), xylan content (M4), and were used as independent variables to determine cellulose crystallinity with SAS v9.0. The following code was written in SAS to identify the best model to predict cellulose crystallinity.

```
* CrI.sas
options ls=120 ps=75 nocenter nodate;
title 'Regression of CrIc on CrIb, Mcellulose,
     Mlignin, Mxylosed';
* CrIc = crystallinity of cellulose;
* M1 = crystallinity of biomass measured by XRD;
* M2 = mass fraction of cellulose;
* M3 = mass fraction of lignin;
* M4 = mass fraction of xylan;
data CrI; input CrIc M1 M2 M3 M4 @@; M5=M1*M1;
     M6=M2*M2; M7=M3*M3; M8=M4*M4; M9=M1*M2;
     M10=M1*M3; M11=M1*M4; M12=M2*M3; M13=M2*M4;
     M14=M3*M4; M15=M1*M2*M3; M16=M1*M3*M4;
     M17=M2*M3*M4; M18=M1*M2*M3*M4;
cards;
82.1 49.9 33.5 33.5 33.0
82.1 64.8 50.2 24.9 24.9
```

```
82.1 79.6 85.0  7.6  7.5
82.1 33.6 14.9 35.1 50.0
82.1 70.3 60.0 15.1 24.9
48.3 22.2 33.5 33.5 33.0
48.3 35.1 50.0 25.0 25.0
48.3 41.3 85.0  7.6  7.4
48.3 17.6 14.9 35.0 50.0
48.3 36.5 60.1 15.0 24.9
38.6 20.1 33.5 33.5 33.0
38.6 25.0 50.2 25.0 25.0
38.6 37.5 85.0  7.4  7.5
38.6 18.6 14.9 50.0 35.1
38.6 35.2 60.1 24.9 15.1
proc corr; var CrIc M1 M2 M3 M4;
proc reg; model CrIc=M1 M2 M3 M4 M5 M8/selection =cp
     rsquare adjrsq sse mse best=7;
```

After determining the best combination of independent variables based on the C(p), R^2, SSE, and MSE of the empirical models, the top three models were investigated more closely with the following commands.

```
proc reg; model CrIc=M1 M4/vif r;
proc reg; model CrIc=M1 M2 M5 M8/vif r;
proc reg; model CrIc=M1 M3 M5 M8/vif r;
```

Results and Discussion

A summary of the statistics used to determine the best empirical model for predicting cellulose crystallinity is given in Tables XXVII and XXVIII. Models 1, 2, and 3 were investigated for their goodness of fit by comparing the F statistics and variance inflation factors for the parameters in each model. As seen in Table XXVIII,

Table XXVII. Statistical selection method for best empirical model to predict cellulose crystallinity.

Model	C(p)[a]	R^2	Adjusted R^2	MSE	Variables in Model[b]
1	3.20	0.93	0.92	31.16	M1 M4
2	3.57	0.96	0.95	20.48	M1 M2 M5 M8
3	3.62	0.96	0.94	20.61	M1 M3 M5 M8
4	4.69	0.95	0.93	25.40	M1 M5 M8
5	4.71	0.95	0.93	25.44	M1 M4 M5
6	4.78	0.96	0.94	23.38	M1 M4 M5 M8
7	5.53	0.96	0.94	22.65	M1 M3 M4 M5 M8

[a] C(p) is a statistic used to choose the best multiple regression model.

[b] M1=biomass crystallinity; M2=glucan content; M3=lignin content; M4=xylan content; M5=$M1^2$; M8=$M4^2$.

Table XXVIII. Statistical summary of the top three models used to predict cellulose crystallinity.

Model	Parameter	Variance Inflation	F	Pr > F
1	M1	1.31	77.67	<0.0001
	M4	1.31		
2	M1	34.31	61.16	<0.0001
	M2	5.62		
	M5	31.50		
	M8	4.74		
3	M1	35.58	60.77	<0.0001
	M3	2.59		
	M5	32.16		
	M8	2.05		

Model 1, which included biomass crystallinity and xylan content, proved superior to the other models. Model 1 performs better than the other models because of its lower C(p) statistic, which balances the pros and cons of other selection criteria along with the problem of over- and under-specification. Additionally, lower variance inflation factors were associated with Model 1 coefficients, which is a measure of how much the variance of a coefficient is increased because of collinearity (i.e., no collinearity when VIF = 1). Severe collinearity results in very large standard errors and therefore very inaccurate estimates. As a result, Model 1 was chosen to predict cellulose crystallinity as given by Equation 24

$$\mathrm{CrIc} = 1.097 \times M1 + 0.939 \times M4 - 11.433 \qquad (24)$$

where $M1$ is biomass crystallinity measured by X-ray diffraction (XRD) and $M4$ is xylan content.

^{13}C CP-MAS NMR spectroscopy was used to verify the ability of the empirical model to predict cellulose crystallinity. As a standard, ^{13}C CP-MAS NMR spectroscopy and X-ray diffraction measurements were performed on an α-cellulose sample (CrI = 61%). If the two techniques resulted in similar CrI values, then NMR spectroscopy can measure cellulose crystallinity. Basic CP-MAS and CP-MAS with a spin lock time of 8 μs were performed to determine the purity of the α-cellulose sample (i.e., a pure sample should have identical spectra with and without spin lock). A linear combination of the experiments with and without spin lock is shown in Figure 59. CrI values from NMR with and without spin-lock were 63% and 58%, respectively, whereas the CrI value measured by X-ray diffraction was 61%. The small difference in NMR measurements suggests there may be a small amount of something other than cellulose in the α-cellulose sample. The good agreement between NMR and XRD values suggests that ^{13}C CP-MAS NMR spectroscopy can determine cellulose crystallinity.

Andersson et al. (2004), Hult et al. (2002), and Liitia et al. (2003) have reported the ability of solid-state ^{13}C CP-MAS NMR spectroscopy with spin locking to measure cellulose crystallinity of lignocellulosic biomass. ^{13}C CP-MAS NMR spectroscopy and XRD were performed on Sample 5 (DL00-DA007-DC3) of the 147 poplar wood model

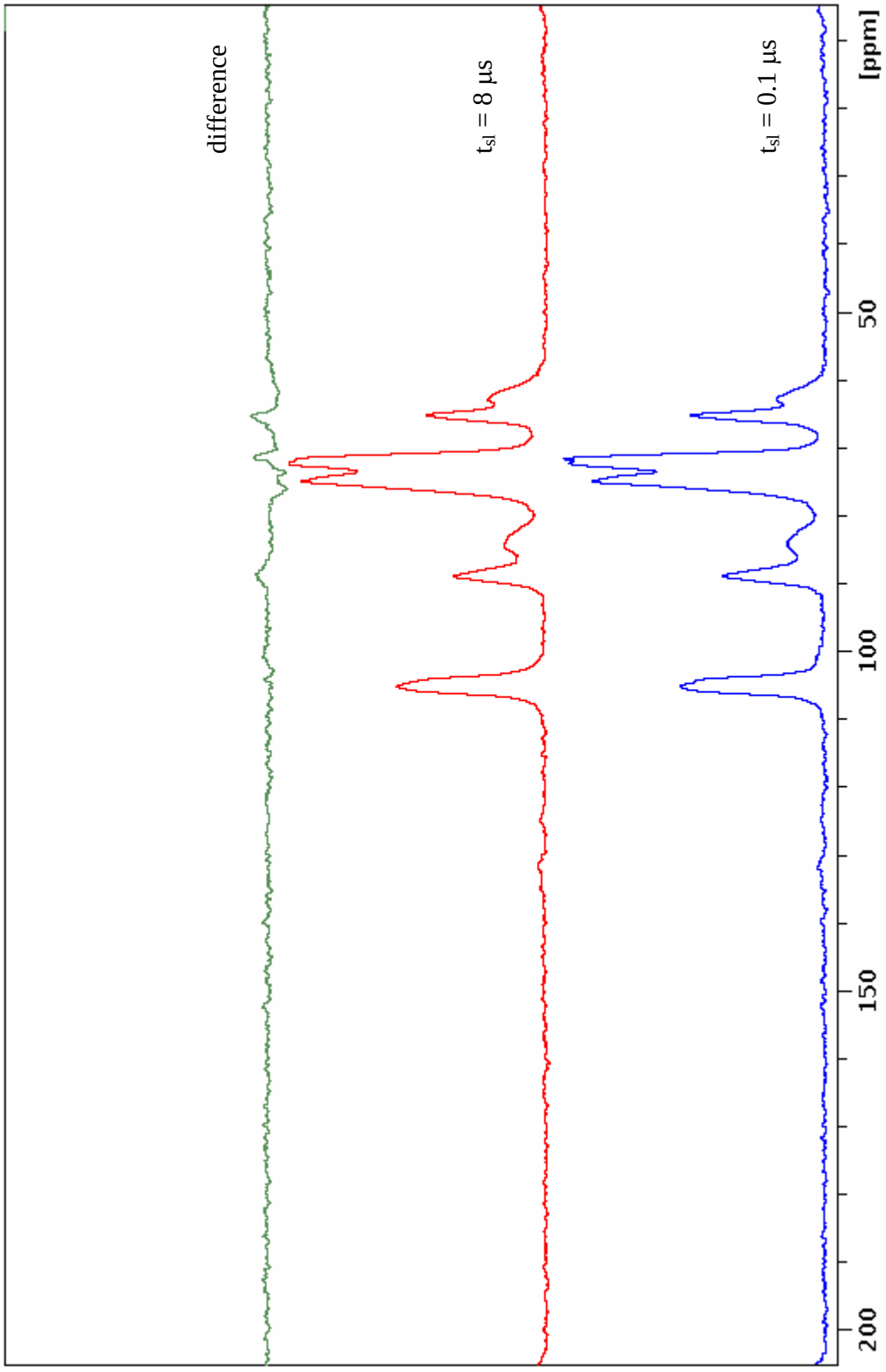

Figure 59. Relative ^{13}C CP-MAS NMR spectra of α-cellulose with and without spin lock.

samples. Basic CP-MAS and CP-MAS with a spin lock time of 16 μs were performed to determine cellulose crystallinity of Sample 5. A linear combination of the experiments with and without spin lock is shown in Figure 60. CrI values from NMR with and without spin-lock were 24.6% and 38.8%, respectively, whereas the CrIb value from XRD was 32.1%. To determine the potential of the SAS developed empirical model to predict cellulose crystallinity, the crystallinity values determined by NMR and the empirical model (Equation 24) were compared. The cellulose crystallinities determined by CP-MAS NMR with spin lock and by the empirical model developed in SAS were 38.8% and 37.4%, respectively. As a result, the empirical model was successful in predicting cellulose crystallinity for Sample 5.

Theoretically, cellulose crystallinity, which is the weight fraction of crystalline cellulose to total cellulose, should always be greater than biomass crystallinity, which is the weight fraction of crystalline material to total material, for a lignocellulosic biomass sample. Equation 24 predicted cellulose crystallinity greater than biomass crystallinity for all the 147 poplar wood model samples. However, Equation 24 failed to predict cellulose crystallinity greater than biomass crystallinity for the four prediction samples that were acid treated, which resulted in extremely low xylan contents (i.e., < 7). As discussed previously, cellulose crystallinity calculated from Equation 24 instead of biomass crystallinity measure by XRD improved the predictive ability of all the 18 neural networks as shown in Table XXIX. The cellulose crystallinity calculated from Equation 24 may not represent the true cellulose crystallinity of the samples used in this study; however, they did provide a better measure of biomass digestibility suggesting Equation 24 did a reasonable job predicting cellulose crystallinity.

CONCLUSIONS

In this study, our data demonstrate that ^{13}C CP-MAS NMR spectroscopy and XRD provide comparable results of cellulose crystallinity for pure cellulose samples. Also, ^{13}C CP-MAS NMR with spin lock could remove the overlapping signals associated with amorphous hemicellulose and lignin matrices from the C-4

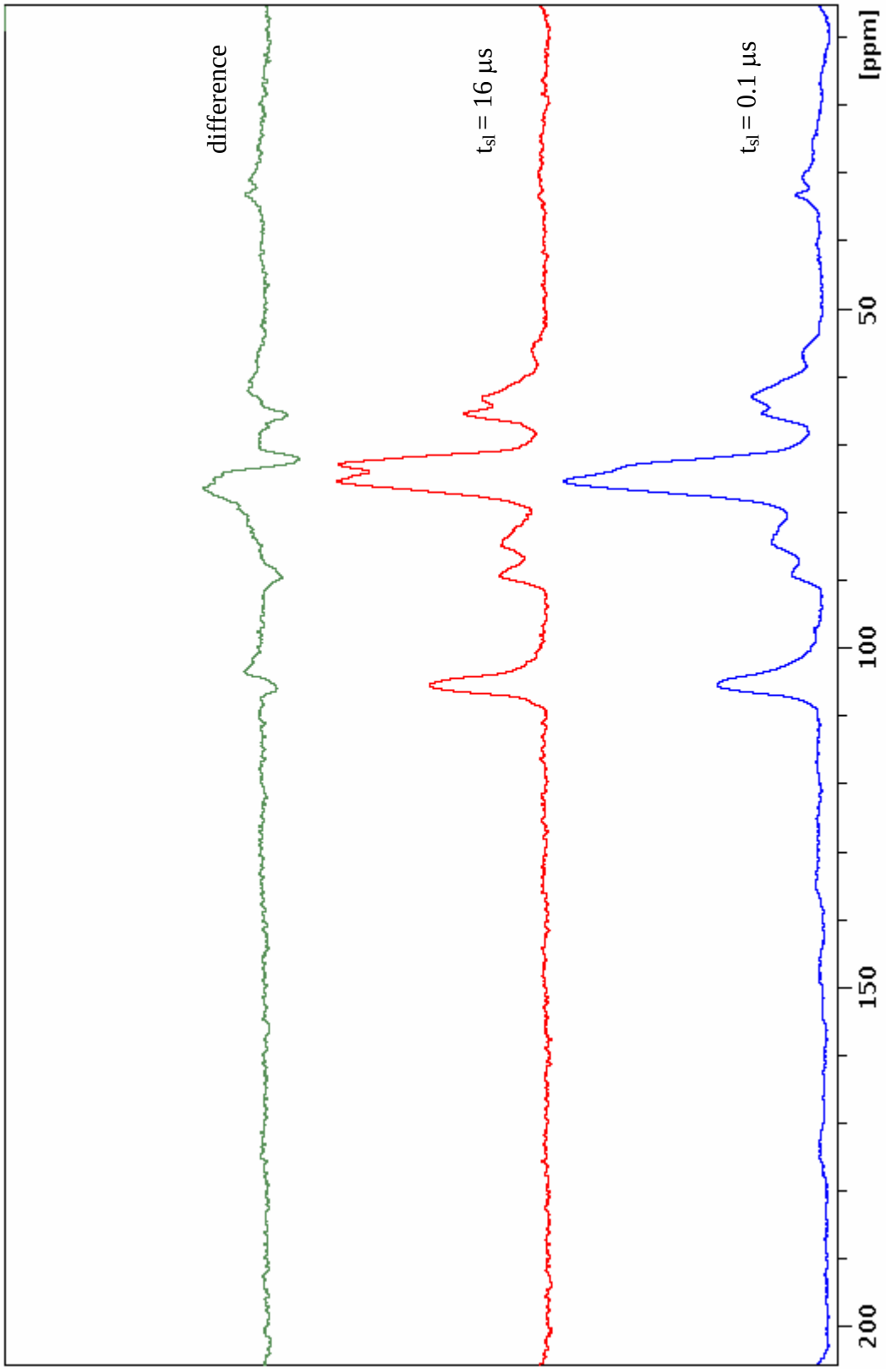

Figure 60. Relative ^{13}C CP-MAS NMR spectra of Sample 5 of the 147 model samples with and without spin lock.

Table XXIX. Comparison of neural networks predictive ability with biomass crystallinity and cellulose crystallinity.

	Time	Network	MSE with CrIb[a]	MSE with CrIc[b]
Glucan	1	Slope	19.5	17.6
	1	Intercept	24.5	16.6
Glucan	6	Slope	44	22
	6	Intercept	88	75
Glucan	72	Slope	74	26
	72	Intercept	260	166
Xylan	1	Slope	13	11
	1	Intercept	5	4.5
Xylan	6	Slope	25	21
	6	Intercept	268	264
Xylan	72	Slope	56	36
	72	Intercept	581	465
Total Sugar	1	Slope	22	9.5
	1	Intercept	4.3	4.2
Total Sugar	6	Slope	29	19
	6	Intercept	103	51
Total Sugar	72	Slope	38	36
	72	Intercept	365	122

[a] Biomass crystallinity measured by X-ray diffraction.

[b] Cellulose crystallinity calculated with Equation 24.

anhydroglucose signals, thereby allowing the determination of cellulose crystallinity according to Teeaar et al. (1987).

The crystallinities calculated with Equation 24 were greater than those measured by XRD for the 147 poplar wood model samples suggesting the calculated crystallinities more closely resembled the inherent cellulose crystallinity. The crystallinity value calculated with Equation 24 improved the predictive ability of the 18 neural network models as shown in Table XXIX. Therefore, cellulose crystallinity provided a better measure of biomass digestibility than overall biomass crystallinity.

IMPLICATIONS

INTRODUCTION

A major hindrance of current biomass processing schemes is the high cost associated with enzymes and pretreatments. Despite the high costs, pretreatment is an essential prerequisite to alter biomass structural features, thereby improving the susceptibility of biomass to enzymatic hydrolysis (Chang, 1999). Most pretreatments can be classified as either chemical (e.g., acid and alkaline) or physical (e.g., milling and irradiation). Economic evaluations of processes that convert biomass to bioethanol indicate that pretreatment is the single most expensive process step, accounting for roughly one-third of the overall processing cost (Lynd et al., 1996). The pretreated biomass is subsequently hydrolyzed through the synergistic action of a complex mixture of enzymes to produce soluble monosaccharides (glucose, xylose, arabinose, and mannose). The sugars are an intermediate in the chemical route before being fermented. Enzyme production alone can account for as much as 30% of the total process cost (Lynd et al., 1996). A thorough understanding of what structural features hinder enzymatic hydrolysis has the potential to aid in the design of more effective and economically feasible conditions of the two major contributors to the high cost of current biomass technologies: pretreatment techniques and enzyme loading.

A mathematical model that accurately predicts biomass digestibility for different types of biomass that have been subjected to different pretreatments has been the main focus of a massive amount of research since the 1970s (Kadam et al., 2004; Chang, 1999; Claeyssens et al., 1990; Lee and Fan, 1982; Holtzapple et al., 1990; Pere et al., 1995; Medve et al., 1998; Davies and Henrissat, 1995; Ghose and Ghosh, 1978). The capability to predict carbohydrate conversion could lead to major breakthroughs in lower costs of current biomass conversion processes. A successful mathematical model has the potential to lead to the design of selective pretreatments that can alter one or more structural features in order to render biomass digestible, which will lead to more efficient

and economical pretreatments. By reducing pretreatment costs, more economically viable biomass conversion processes could serve as an alternative to fossil fuels.

Purpose

The purpose was to predict carbohydrate conversions with neural networks for typical biomass samples. Instead of using the neural networks directly, the figures could be used to predict conversion at different enzyme loadings and reaction times.

Materials and Methods

The neural networks developed to predict total sugar slopes and intercepts at 1, 6, and 72 h were used to predict carbohydrate conversions for a typical biomass sample (i.e., glucan content = 54% and xylan content = 16%) at a variety of lignin contents (5–25%). The figures illustrating these data have a biomass crystallinity range of 15–55% at both high (3%) and low (0.2%) acetyl content.

Results and Discussion

Figures 61 and 62 show the 1-, 6-, and 72-h total sugar conversions predicted by the neural networks at a variety of lignin contents for low- and high-acetyl content biomass samples, respectively. Most chemical pretreatments significantly reduce acetyl content and depending on the duration and severity of the pretreatment could considerably reduce lignin content as well. Therefore, samples with low (0.2%) or high (3%) acetyl content over a wide range of lignin contents (5–25%) were investigated for their reactivity with the neural network models. Most physical pretreatments (e.g., mechanical ball milling) alter biomass crystallinity. Therefore, samples with a high (55%), medium (35%), and low (15%) biomass crystallinity were investigated. General rules or guidelines were established from the data and summarized in Table XXX. Tables XXXI and XXXII can be used to interpolate total sugar conversions at various lignin contents, crystallinities, and enzyme loadings for low (0.2%) and high (3%) acetyl samples, respectively.

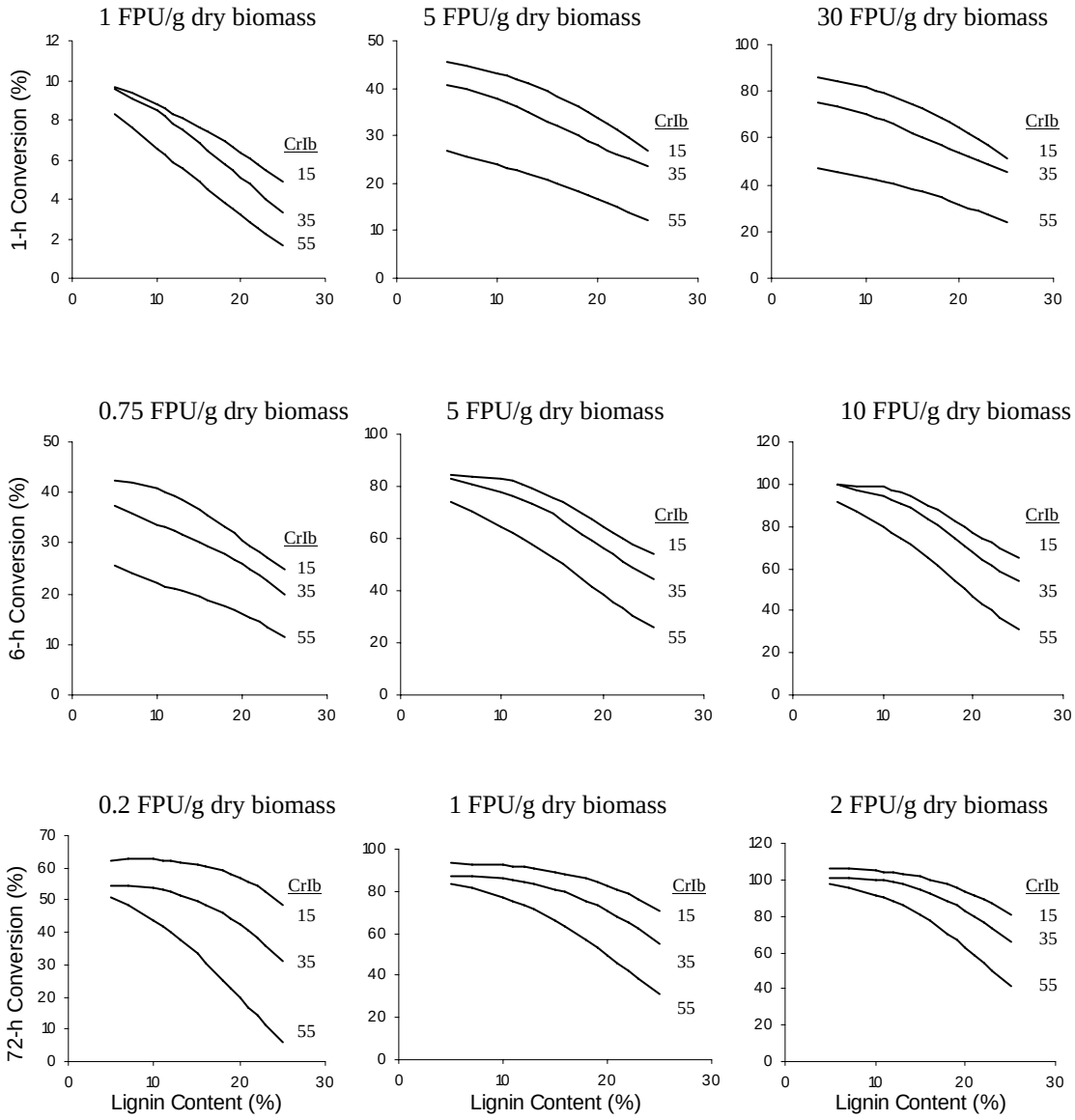

Figure 61. Neural network predicted total sugar conversions as a function of lignin content and biomass crystallinity of deacetylated biomass (acetyl content = 0.2%). Predicted for a 54% glucan and 16% xylan sample, which falls within the range used to train the networks with the 147 model samples (i.e., glucan = 44.4–76.5% and xylan = 13.9–17.5%).

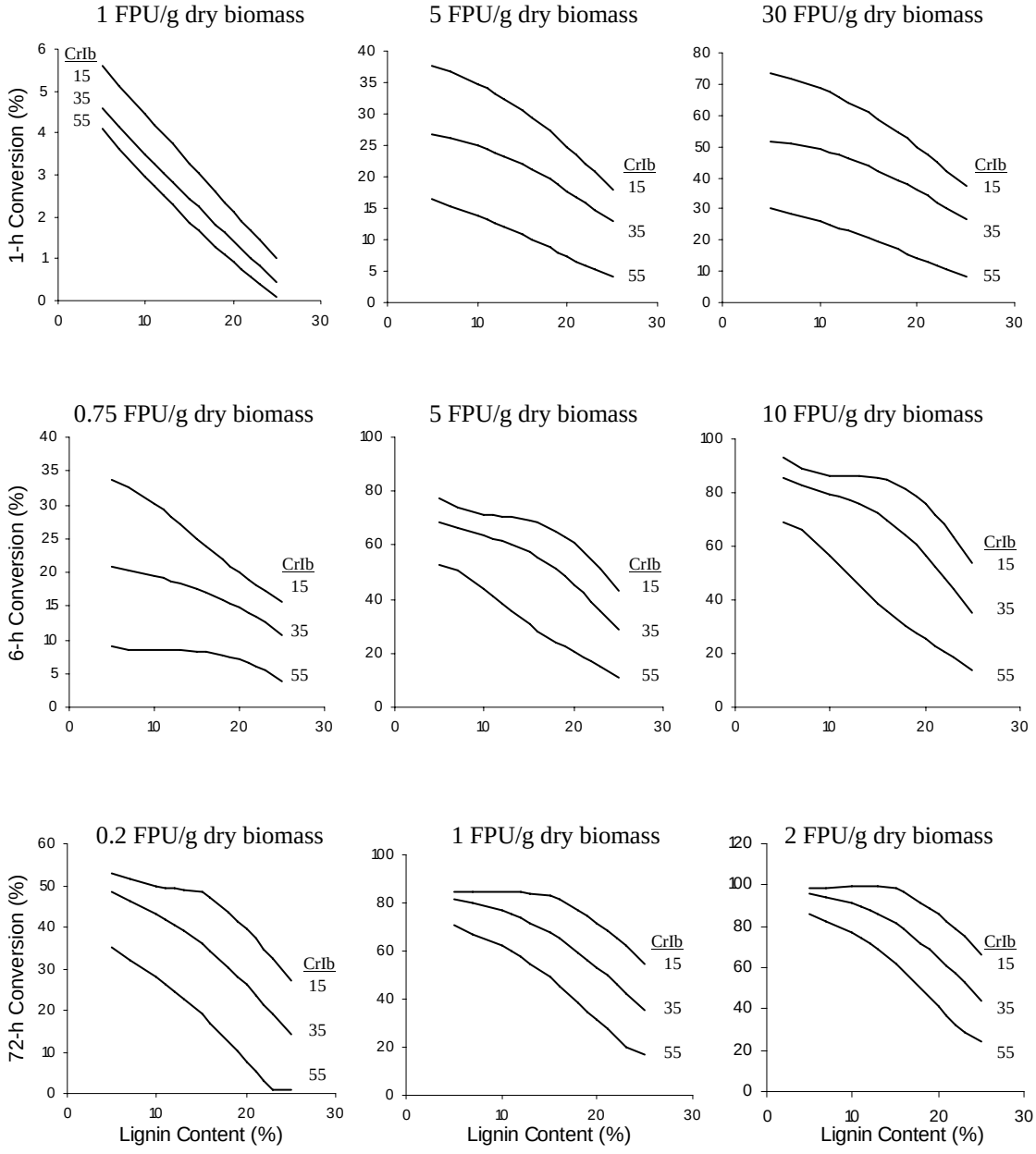

Figure 62. Neural network predicted total sugar conversions as a function of lignin content and biomass crystallinity of acetylated biomass (acetyl content = 3%). Predicted for a 54% glucan and 16% xylan sample, which falls within the range used to train the networks with the 147 model samples (i.e., glucan = 44.4–76.5% and xylan = 13.9–17.5%).

Table XXX. Minimum biomass structural features and enzyme loadings required to achieve a 1-h conversion >40%, 6-h conversion >80%, or 72-h conversion >80%.

Enzyme Loading (FPU/g dry biomass)	Acetyl Content (%)	Lignin Content (%)	CrIb (%)	Incubation Time (h)
5	0.2	5	35	1[a]
5	0.2	13	15	1
30	0.2	13	55	1
30	0.2	25	35	1
30	0.2	25	15	1
30	3	16	35	1
30	3	23	15	1
5	0.2	7	35	6[b]
5	0.2	12	15	6
10	0.2	7	55	6
10	0.2	16	35	6
10	0.2	18	15	6
10	3	7	35	6
10	3	18	15	6
1	0.2	7	55	72[c]
1	0.2	16	35	72
1	0.2	21	15	72
2	0.2	15	55	72
2	0.2	20	35	72
2	0.2	25	15	72
1	3	5	35	72
1	3	16	15	72
2	3	7	55	72
2	3	15	35	72
2	3	21	15	72

[a] Total sugar conversions >40%.

[b] Total sugar conversions >80%.

[c] Total sugar conversions >80%.

Table XXXI. Summary of network predicted total sugar conversions at various lignin contents and crystallinities for a deacetylated (0.2%) biomass sample.

L[a] (%)	A[b] (%)	CrIb[c] (%)	Enzyme Loading (FPU/g dry biomass)															
			1	5	10	20	30	0.75	1	5	10	30	0.2	0.5	1	2	5	10
			1-h Conversion (%)					6-h Conversion (%)					72-h Conversion (%)					
25	0.2	55	2	12	17	22	24	12	14	26	31	39	6	20	31	42	56	67
23	0.2	55	2	14	19	24	27	14	16	31	37	47	11	27	38	50	65	77
22	0.2	55	3	15	20	26	29	14	17	33	40	51	14	30	42	54	70	82
21	0.2	55	3	16	21	27	30	15	18	36	43	55	17	33	46	58	75	87
20	0.2	55	3	17	22	28	31	16	20	39	47	60	20	37	50	63	80	92
19	0.2	55	4	17	23	29	33	17	21	42	51	65	23	40	53	66	84	97
18	0.2	55	4	18	24	31	34	18	22	44	54	70	25	43	57	70	88	-
16	0.2	55	4	20	26	33	37	19	24	50	61	80	31	49	63	77	96	-
15	0.2	55	5	21	27	34	38	19	24	53	65	84	33	52	66	80	99	-
13	0.2	55	6	22	29	36	40	20	26	58	71	93	38	57	71	86	-	-
12	0.2	55	6	23	30	37	41	21	27	60	74	97	40	59	74	88	-	-
11	0.2	55	6	23	31	38	42	22	28	62	77	-	42	61	76	90	-	-
10	0.2	55	7	24	31	39	43	22	28	64	80	-	44	63	77	92	-	-
7	0.2	55	8	26	33	41	46	24	31	70	87	-	49	67	82	96	-	-
5	0.2	55	8	27	35	42	47	25	33	74	92	-	51	70	84	98	-	-
25	0.2	35	3	23	32	41	46	20	24	45	54	68	31	45	55	65	79	89
23	0.2	35	4	25	34	43	49	23	27	49	59	74	36	51	62	73	88	99
22	0.2	35	4	26	35	45	50	24	28	51	62	78	38	54	65	77	92	-
21	0.2	35	5	27	37	46	52	25	29	54	65	81	40	56	68	80	96	-
20	0.2	35	5	28	38	48	53	26	31	56	68	85	42	59	71	83	99	-
19	0.2	35	5	29	39	49	55	27	32	59	71	90	44	61	73	86	-	-
18	0.2	35	6	30	40	51	57	28	33	62	74	94	46	63	76	88	-	-
16	0.2	35	6	32	43	54	61	29	35	67	81	-	49	66	79	93	-	-
15	0.2	35	7	33	44	56	62	30	36	69	84	-	50	68	81	94	-	-
13	0.2	35	8	35	47	59	66	32	38	73	89	-	52	70	84	97	-	-
12	0.2	35	8	36	48	60	67	32	39	75	91	-	53	71	85	98	-	-
11	0.2	35	8	37	49	62	69	33	40	77	93	-	53	72	86	99	-	-
10	0.2	35	8	38	50	63	70	34	40	78	94	-	54	72	86	-	-	-
7	0.2	35	9	40	53	66	74	36	43	81	97	-	54	73	87	-	-	-
5	0.2	35	10	41	54	68	75	38	44	83	-	-	54	73	87	-	-	-
25	0.2	15	5	27	37	46	52	25	29	54	65	82	49	61	71	81	93	-
23	0.2	15	5	30	40	51	57	27	32	58	69	87	53	66	76	87	-	-
22	0.2	15	6	31	42	53	60	28	33	60	72	90	54	68	79	89	-	-
21	0.2	15	6	33	44	55	62	29	34	62	75	94	56	70	81	92	-	-
20	0.2	15	6	34	46	58	64	31	36	65	77	97	57	72	83	94	-	-

Table XXXI. Continued

L[a] (%)	A[b] (%)	CrIb[c] (%)	Enzyme Loading (FPU/g dry biomass)															
			1	5	10	20	30	0.75	1	5	10	30	0.2	0.5	1	2	5	10
			1-h Conversion (%)					6-h Conversion (%)					72-h Conversion (%)					
19	0.2	15	7	35	47	60	67	32	37	67	80	-	58	73	84	96	-	-
18	0.2	15	7	36	49	62	69	33	39	69	83	-	59	74	86	98	-	-
16	0.2	15	7	38	52	65	73	36	41	74	88	-	60	76	88	-	-	-
15	0.2	15	8	39	53	67	75	37	43	76	90	-	61	77	89	-	-	-
13	0.2	15	8	41	55	70	78	39	45	79	94	-	62	78	91	-	-	-
12	0.2	15	8	42	56	71	79	39	46	81	96	-	62	79	91	-	-	-
11	0.2	15	9	43	57	72	81	40	47	82	98	-	62	79	92	-	-	-
10	0.2	15	9	43	58	73	82	41	47	83	99	-	63	79	92	-	-	-
7	0.2	15	9	45	60	75	84	42	48	84	99	-	63	80	93	-	-	-
5	0.2	15	10	46	61	77	86	42	49	84	-	-	62	80	93	-	-	-

[a] L=lignin content

[b] A=acetyl content

[c] CrIb=biomass crystallinity

Table XXXII. Summary of network predicted total sugar conversions at various lignin contents and crystallinities for an acetylated (3%) biomass sample.

L[a] (%)	A[b] (%)	CrIb[c] (%)	Enzyme Loading (FPU/g dry biomass)															
			1	5	10	20	30	0.75	1	5	10	30	0.2	0.5	1	2	5	10
			1-h Conversion (%)					6-h Conversion (%)					72-h Conversion (%)					
25	0.2	55	0	4	6	7	8	4	5	11	14	18	1	10	17	24	33	40
23	0.2	55	0	5	7	9	11	5	7	15	18	24	1	12	20	28	39	47
22	0.2	55	1	6	8	10	12	6	8	17	21	27	3	15	24	33	44	53
21	0.2	55	1	7	9	12	13	7	8	19	23	30	5	18	27	37	49	59
20	0.2	55	1	7	10	13	14	7	9	20	25	33	8	21	31	41	55	65
19	0.2	55	1	8	11	14	16	7	10	22	28	36	10	24	35	46	60	71
18	0.2	55	1	9	12	15	17	8	10	24	30	40	12	27	39	50	65	76
16	0.2	55	2	10	14	17	19	8	11	28	36	47	17	33	46	58	74	87
15	0.2	55	2	11	15	18	21	8	12	31	39	52	19	36	49	62	79	92
13	0.2	55	2	12	16	20	23	8	13	36	45	61	23	41	55	69	87	-
12	0.2	55	3	13	17	21	24	8	13	38	49	66	25	43	57	72	90	-
11	0.2	55	3	13	18	22	25	8	13	41	53	72	26	45	60	74	93	-
10	0.2	55	3	14	18	23	26	8	14	44	57	77	28	47	62	77	96	-
7	0.2	55	4	15	20	26	29	9	15	51	66	90	32	52	67	82	-	-
5	0.2	55	4	16	22	27	30	9	16	53	69	94	35	55	71	86	-	-
25	0.2	35	0	13	18	23	27	11	13	29	35	45	14	26	35	44	56	65
23	0.2	35	1	15	21	27	30	13	16	35	44	57	19	32	43	53	66	76
22	0.2	35	1	16	22	29	32	13	17	39	48	63	21	36	46	57	71	82
21	0.2	35	1	17	23	30	34	14	18	42	53	69	24	39	50	61	76	87
20	0.2	35	1	18	25	32	36	15	19	45	57	74	26	41	53	65	80	92
19	0.2	35	2	19	26	33	38	15	20	48	60	80	28	44	56	69	85	97
18	0.2	35	2	20	27	35	39	16	21	51	64	84	30	47	59	72	89	-
16	0.2	35	2	21	29	38	42	17	23	56	70	92	34	52	65	78	96	-
15	0.2	35	2	22	30	39	44	17	24	58	72	95	36	54	68	81	99	-
13	0.2	35	3	23	32	41	46	18	25	60	76	-	39	58	72	86	-	-
12	0.2	35	3	24	33	42	47	19	25	62	77	-	40	59	74	88	-	-
11	0.2	35	3	24	34	43	48	19	26	62	78	-	42	61	75	90	-	-
10	0.2	35	3	25	34	44	49	19	26	63	79	-	43	62	77	91	-	-
7	0.2	35	4	26	36	45	51	20	27	66	83	-	46	65	80	94	-	-
5	0.2	35	5	27	37	46	52	21	28	68	86	-	48	67	81	96	-	-
25	0.2	15	1	18	25	33	37	15	20	43	53	70	27	43	55	66	82	94
23	0.2	15	1	21	29	37	42	17	22	51	63	83	32	49	62	75	92	-
22	0.2	15	2	22	31	40	45	18	24	55	68	89	35	52	66	79	96	-
21	0.2	15	2	23	33	42	48	19	25	58	72	95	37	55	69	82	-	-
20	0.2	15	2	25	35	44	50	20	26	61	76	99	39	58	72	86	-	-

Table XXXII. Continued

L[a] (%)	A[b] (%)	CrIb[c] (%)	Enzyme Loading (FPU/g dry biomass)															
			1	5	10	20	30	0.75	1	5	10	30	0.2	0.5	1	2	5	10
			1-h Conversion (%)					6-h Conversion (%)					72-h Conversion (%)					
19	0.2	15	2	26	36	46	52	21	27	63	79	-	42	60	75	89	-	-
18	0.2	15	3	27	38	48	55	22	28	65	81	-	43	63	77	92	-	-
16	0.2	15	3	29	41	52	59	24	31	68	85	-	47	67	82	96	-	-
15	0.2	15	3	31	42	54	61	25	32	69	86	-	48	68	83	98	-	-
13	0.2	15	4	32	45	57	64	27	34	70	86	-	49	69	84	99	-	-
12	0.2	15	4	33	46	58	66	28	35	71	86	-	49	69	84	99	-	-
11	0.2	15	4	34	47	60	67	29	36	71	86	-	49	69	84	99	-	-
10	0.2	15	4	35	48	61	69	30	36	71	86	-	50	70	85	99	-	-
7	0.2	15	5	37	50	64	72	33	39	74	89	-	51	70	85	99	-	-
5	0.2	15	6	38	51	65	73	34	40	77	93	-	53	71	85	98	-	-

[a] L=lignin content

[b] A=acetyl content

[c] CrIb=biomass crystallinity

CONCLUSIONS

Numerous combinations of lignin content, acetyl content, biomass crystallinity, and enzyme loading were investigated for a typical biomass sample (glucan content = 54% and xylan content = 16%) with the neural network models. Many chemical pretreatments significantly reduce acetyl content and alter lignin content but have a small effect on crystallinity; therefore, general guidelines to achieve moderate 1-h total sugar conversions and high 6-h and 72-h total sugar conversions were investigated for high-crystallinity samples. After analyzing the results, a lignin content ≤13% is necessary to achieve 1-h total sugar conversions >40% at a 0.2% acetyl content, 55% biomass crystallinity, and 5 FPU/g dry biomass enzyme loading. A lignin content ≤7% is necessary to achieve 6-h total sugar conversions >80% at a 0.2% acetyl content, 55% biomass crystallinity, and 10 FPU/g dry biomass enzyme loading. Lastly, a lignin content ≤7% at a 0.2% acetyl content, 55% biomass crystallinity, and 1 FPU/g dry biomass enzyme loading, or a lignin content ≤15% at a 0.2% acetyl content, 55% biomass crystallinity, and 2 FPU/g dry biomass enzyme loading is necessary to achieve 72-h total sugar conversions >80%.

CONCLUSIONS

Systematic studies on the effect of substrate concentration and enzyme loading indicated the inhibition pattern was noncompetitive, which agrees with the inhibition pattern used to develop the HCH-1 Model. Also, the degree of inhibition was lowest at a substrate concentration of 10 g/L. Higher inhibition was experienced at higher substrate concentrations because of the increased quantity of glucose in the reaction vessel (i.e., the more substrate present resulted in higher sugar conversions up to 5 g/L). The range of enzyme loadings and substrate concentrations over which the simplified HCH-1 Model was valid for lime pretreated corn stover are 0.25–50 FPU/g dry biomass and 10–100 g/L, respectively. To minimize product inhibition and maintain the linearity of Equation 5 for the 147 poplar wood model samples and the 22 prediction samples, the recommended experimental conditions are an enzyme loading of ≤30 FPU/g dry biomass, a substrate concentration of 10 g/L, and a cellobiase loading of ≥48 CBU/g dry biomass.

Under the recommended conditions, the 147 poplar wood model samples were enzymatically hydrolyzed and the slopes (*B*) and intercepts (*A*) were determined at 1, 6, and 72 h. Then, sugar conversions were calculated with Equation 5. The results showed that lignin and crystallinity have a major effect on 1-h and 6-h sugar conversions whereas acetyl exhibits a minor effect. Therefore, a low crystallinity index was sufficient to achieve a moderate increase in conversion regardless of acetyl or lignin content. Also, low lignin in conjunction with low crystallinity was sufficient to achieve higher conversions regardless of acetyl content. Low acetyl content with a moderate lignin content contributed to a moderate increase in 1-h and 6-h conversions. This suggests that even though acetyl alone is not a major player in affecting biomass digestibility, when combined with the reduction of other structural features it does enhance biomass digestibility. The ultimate digestion of biomass appears to be controlled by a slightly different mechanism. Low lignin was sufficient to achieve high conversions regardless of crystallinity or acetyl content. When low crystallinity and low

lignin are considered together, nearly complete conversion of the poplar wood model samples was observed at a 5 FPU/g dry biomass enzyme loading (i.e., >95%). Therefore, a pretreatment designed to alter both lignin content and crystallinity would be sufficient to render biomass highly digestible. This would allow for the design of more effective and less expensive pretreatment techniques.

In the neural network modeling study, a total of 18 neural networks were developed to predict slopes and intercepts for glucan, xylan, and total sugar at 1, 6, and 72 h. It should be noted that the slopes and intercepts were determined by plotting conversion versus the natural logarithm of enzyme loading. The networks performed consistently poorer when simulating and predicting slopes and intercepts for xylan compared with glucan and total sugar. Xylan slopes and intercepts showed consistently larger MSE and lower R^2 values compared with glucan and total sugar. Nonetheless, glucan, xylan, and total sugar networks simulated slopes and intercepts for the 147 model samples fairly satisfactorily.

The 22 prediction samples were created with various types of biomass (corn stover, bagasse, and rice straw) chemically pretreated with long-term lime, short-term lime, dilute sulfuric acid, AFEX, and aqueous ammonia plus mechanical ball milling. The various biomass samples were pretreated with different techniques to test the neural networks' abilities to predict conversion regardless of biomass type or pretreatment. The neural networks performed equally when predicting conversions for the different types of biomass treated with different techniques. In other words, the data were scattered equally for the majority of samples regardless of biomass type or pretreatment. A clear exception was the 72-h xylan slope network where the AFEX-treated corn stover samples had larger MSEs than the other samples. The lime-treated, acid-treated, and aqueous-ammonia-treated samples had MSE values of 3.04, 3.25, and 1.8, respectively, whereas AFEX-treated samples had a larger MSE value of 6.21.

Our results indicate no correlation exists between xylan removal and glucan digestibility. However, there was a correlation between glucan removal and xylan digestibility observed at 6 h and 72 h (i.e., the 6 h and 72 h networks predicted xylan

slopes and xylan intercepts better when glucan slopes and glucan intercepts, respectively, were included as independent variables). In other words, glucan removal helped destroy the intricate nature of lignocellulosic biomass to permit the enzymes easier access to the xylan backbone.

The crystallinities calculated with Equation 24 were greater than those measured by XRD for the 147 poplar wood model samples suggesting the calculated crystallinities more closely resembled the inherent cellulose crystallinity. The neural networks predictive ability improved when cellulose crystallinity calculated with Equation 24 was used as an independent variable instead of biomass crystallinity. Therefore, cellulose crystallinity provided a better measure of biomass digestibility.

REFERENCES

Andersson S, Wikberg H, Pesonen E, Naunu S, Serimaa R. 2004. Studies of crystallinity of Scots pine and Norway spruce cellulose. Trees 18:346-353.

Annema A. 1995. Feed-forward neural networks: vector decomposition analysis, modeling and analog implementation. Boston: Kluwer Academic Publishers.

Balta-Calleja F, Vonk C. 1989. X-ray scattering of synthetic polymers. Amsterdam: Elsevier.

Beltrame P, Carniti P, Focher B, Marzetti A, Sarto V. 1984. Enzymatic hydrolysis of cellulosic materials - kinetic study. Biotechnol Bioeng 26:1233-1238.

Bertran M, Dale B. 1985. Enzymatic hydrolysis and recrystallization behavior of initially amorphous cellulose. Biotechnol Bioeng 27:177-181.

Blasig J, Holtzapple M, Dale B, Engler C, Byers F. 1992. Volatile fatty acid fermentation of AFEX-treated bagasse and newspaper by rumen microorganisms. Resour Conserv Recycling 7:95-114.

Bothast R, Nichols N, Dien B. 1999. Fermentations with new recombinant organisms. Biotechnol Prog 15:867-875.

Browning BL. 1967. Methods of wood chemistry. New York: Interscience Publishers.

Brett C, Waldron K. 1996. Physiology and biochemistry of plant cells walls, 2nd ed. New York: Chapman & Hall Press.

Caulfield D, Moore W. 1974. Effect of varying crystallinity of cellulose on enzymatic hydrolysis. Wood Sci 6:375-379.

Chang S. 1999. Lime pretreatment of lignocellulosic biomass. Ph.D. Dissertation. Texas A&M University, College Station, TX.

Chang S, Holtzapple M. 2000. Fundamental factors affecting biomass enzymatic reactivity. Appl Biochem Biotechnol 84-86:5-37.

Claeyssens M, Tomme P, Brewer C, Hehre E. 1990. Stereochemical course of hydrolysis and hydration reactions catalysed by cellobiohydrolases I and II from *Trichoderma reesei*. FEBS Letters 263:89-92.

Colin C. 2003. The coming oil crisis. New York: Multi-Science Publishing Company.

Converse A, Ooshima H, Burns D. 1990. Kinetics of enzymatic hydrolysis of lignocellulosic materials based on surface area of cellulose accessible to enzyme and enzyme adsorption on lignin and cellulose. Appl Biochem Biotechnol 24/25:67-73.

Coward-Kelly G, Aiello-Mazzari C, Kim S, Granda C, Holtzapple M. 2003. Suggested improvements to the standard filter paper assay used to measure cellulase activity. Biotechnol Bioeng 82:745-749.

Cowling E. 1975. Physical and chemical constraints in the hydrolysis of cellulose and lignocellulosic materials. Biotechnol Bioeng Symp 5:163-181.

Creagh A, Ong E, Jervis E, Kilburn D, Haynes C. 1996. Binding of the cellulose-binding domain of exoglucanase cex from *Cellulomonas fimi* to insoluble microcrystalline cellulose is entropically driven. Proc Natl Acad Sci 93:12229-12234.

Davies G, Henrissat B. 1995. Structures and mechanisms of glycosyl hydrolases. Structure 3:853-859.

Demuth H, Beale M. 2004. Neural network toolbox: user's guide (for use with Matlab®). Version 4.0 The MathWorks.

Desai SG, Converse AO. 1997. Substrate reactivity as a function of the extent of reaction in the enzymatic hydrolysis of lignocellulose. Biotechnol Bioeng 56:650-655.

Divne C, Stahlberg J, Teeri T, Jones A. 1998. High-resolution crystal structures reveal how a cellulose chain is bound in the 50A long tunnel of cellobiohydrolase I from *Trichoderma reesei*. J Mol Biol 275:309-325.

Dwivedi C, Ghose J. 1979. Model on hydrolysis of bagasse cellulose by enzyme from *Trichoderma reesei* QM-9414. J Ferment Technol 57:15-24.

Eriksson T, Karlsson J, Tjerneld F. 2002. A model explaining declining rate in hydrolysis of lignocellulose substrates with cellobiohydrolase I (Cel7A) and

endoglucanase I (Cel7B) of *Trichoderma reesei*. Appl Biochem Biotechnol 101:41-60.

Fan L, Gharpuray M, Lee Y. 1981. Evaluation of pretreatments for enzymatic conversion of agriculture residues. Biotechnol Bioeng Symp 11:29-45.

Fan L, Lee Y, Breadmore D. 1980b. Mechanism of the enzymatic hydrolysis of cellulose: effects of major structural features of cellulose on enzymatic hydrolysis. Biotechnol Bioeng 22:177-199.

Fan L, Lee Y, Breadmore D. 1981a. The influence of major structural features of cellulose on rate of enzymatic hydrolysis. Biotechnol Bioeng 23:419-424.

Foresee R, Hagan M. 1997. Gauss-Newton approximation to Bayesian regularization. Proceedings of the 1997 International Joint Conference on Neural Networks pp 1930-1935.

Gama F, Teixeira J, Mota M. 1994. Cellulose morphology and enzymatic reactivity: a modified solute exclusion technique. Biotechnol Bioeng 43:381-387.

Gharpuray M, Lee Y, Fan L. 1983. Structural modification of lignocellulosics by pretreatments to enhance enzymatic hydrolysis. Biotechnol Bioeng 25:157-172.

Ghose T, Ghosh P. 1978. Bioconversion of cellulosic substances. J Appl Chem Biotechnol 28:309-320.

Giustolisi O. 2004. Sparse solution in training artificial neural networks. Neurocomputing 56:285-304.

Gonzalez G, Caminal G, de Mas C, Lopez-Santin J. 1989. A kinetic model for pretreated wheat straw saccharification by cellulase. J Chem Tech Biotechnol 44:275-288.

Goyal A, Ghosh B, Eveleigh D. 1991. Characteristics of fungal cellulases. Bioresour Technol 36:37-50.

Gregg DJ, Saddler JN. 1996. Factors affecting cellulose hydrolysis and the potential of enzyme recycle to enhance the efficiency of an intergrated wood to ethanol process. Biotechnol Bioeng 51:375-383.

Grethlein H, Allen D, Converse A. 1984. A comparative study of the enzymatic hydrolysis of acid-pretreated white pine and mixed hardwood. Biotechnol Bioeng 26:1498-1505.

Grethlein H. 1985. The effect of pore size distribution on the rate of enzymatic hydrolysis of cellulosic substrates. Biotechnol. 3:155-160.

Grohmann K, Mitchell D, Himmel M, Dale B, Schroeder H. 1989. The role of ester groups in resistance of plant cell wall polysaccharides to enzymatic hydrolysis. Appl Biochem Biotechnol 20/21:45-61.

Hagan M, Demuth, Beale M. 1996. Neural network design. Boston: PWS Publishing.

Hoh Y, Yeoh H, Tan T. 1992. Properties of β-glucosidase purified from *Aspergillus niger* mutants USDB-0827 and USDB-0828. Appl Microbiol Biotechnol 37:590-593.

Holtzapple M, Caram H, Humphrey A. 1984. The HCH-1 model of enzymatic cellulose hydrolysis. Biotechnol Bioeng 26:775-780.

Holtzapple M, Cognata M, Shu Y, Hendrickson C. 1990. Inhibition of *Trichoderma reesei* cellulase by sugars and solvents. Biotechnol Bioeng 36:275-287.

Holtzapple M, Jun J, Ashok G. 1991. The ammonia freeze explosion (AFEX) process: a practical lignocellulose pretreatment. Appl Biochem Biotechnol 28/29:59-74.

Holtzapple M, Ripley E, Nikolaou M. 1994. Saccharification, fermentation, and protein recovery from low-temperature AFEX-treated coastal bermudagrass. Biotechnol Bioengr 44:1122-1131.

Holtzapple M, Ross M, Chang N, Chang V, Adelson S, Brazel C. 1997. Biomass conversion to mixed alcohol fuels using the MixAlco Process. Fuels and Chemicals from Biomass. American Chemical Society, Washington, DC.

Holtzapple M. 1993a. Cellulose. In: Macrae R, Robinson RK, Sadler MJ, editors. Encyclopedia of food science, food technology, and nutrition. London: Academic Press. 2731-2738.

Holtzapple M. 1993b. Hemicellulose. In: Macrae R, Robinson RK, Sadler MJ, editors. Encyclopedia of food science, food technology, and nutrition. London: Academic Press. 2324-2334.

Holtzapple M. 1993c. Lignin. In: Macrae R, Robinson RK, Sadler MJ, editors. Encyclopedia of food science, food technology, and nutrition. London: Academic Press. 2731-2738.

Horii F, Hirai A, Kimaru R. 1982. Solid-state high-resolution 13C-NMR studies of regenerated cellulose samples with different crystallinities. Polym Bull 8:163-170.

Huang A. 1975. Kinetic studies on insoluble cellulose-cellulase system. Biotechnol Bioeng 17:1421-1433.

Huang X, Penner M. 1991. Apparent substrate inhibition of the *Trichoderma reesei* cellulase system. J Agric Food Chem 39:2096-2100.

Hult E, Liitia T, Maunu L, Hortling B, Iversen T. 2002. A CP/MAS 13C-NMR study of cellulose structure on the surface of refined kraft pulp fibers. Carbo Polym 49:231-234.

Ingram L. 1999. Enteric bacterial catalysts for fuel ethanol production. Biotechnol Prog 15:855-866.

Kadam K, Rydholm E, McMillan J. 2004. Development and validation of a kinetic model for enzymatic saccharification of lignocellulosic biomass. Biotechnol Prog 20:698-705.

Kadam KL, Camobreco V, Glazebrook B, Forrest L, Jacobson W, Simerith D, Blackburn W, Nehoda K. 1999. Environmental life cycle implications of fuel oxygenates production from California biomass. NREL/TP-580-25688: Golden, CO.

Kim S. 2004. Lime pretreatment and enzymatic hydrolysis of corn stover. Ph.D. Dissertation. Texas A&M University, College Station, TX.

Kim T, Kim J, Sunwoo C, Lee Y. 2003. Pretreatment of corn stover by aqueous ammonia. Biores Technol 90:39-47.

Klyosov A. 1990. Trends in biochemistry and enzymology of cellulose degradation. Biochemistry 29:10577-10585.

Kong R, Engler C, Soltes E. 1992. Effects of cell wall acetate, xylan backbone, and lignin on enzymatic hydrolysis of aspen wood. Appl Biochem Biotechnol 34:23-35.

Koullas D, Christakopoulos R, Kekos D, Macris B, Koukios E. 1992. Correlating the effect of pretreatment on the enzymatic hydrolysis of straw. Biotechnol Bioeng 39:113-116.

Lee Y, Fan L. 1982. Kinetic studies of enzymatic hydrolysis of insoluble cellulose: analysis of the initial rates. Biotechnol Bioeng 24:2383-2406.

Lenz J, Esterbauer H, Sattler W, Schurz J, Wrentschur E. 1990. Changes of structure and morphology of regenerated cellulose caused by acid and enzymatic hydrolysis. J Appl Polym Sci 41:1315-1326.

Liitia T, Maunu S, Hotling B, Tamminen T, Pekkala O, Varhimo A. 2003. Cellulose crystallinity and ordering of hemicelluloses in pine and birch pulps as revealed by solid-state NMR spectroscopic methods. Cellulose 10:307-316.

Liu W, Madsen N, Braun C, Withers S. 1991. Reassessment of the catalytic mechanism of glycogen debranching enzyme. Biochemistry 30:1419-1424.

Lynd L, Cushman J, Nichols R, Wyman C. 1991. Fuel ethanol from cellulosic biomass. Science 251:1318-1323.

Lynd L, Elander R, Wyman C. 1996. Likely features and costs of mature biomass ethanol technology. Appl Biochem Biotechnol 57/58:741-761.

Lynd L, Weimer P, Van Zyl W, Pretorius I. 2002. Microbial cellulose utilization: fundamentals and biotechnology. Microbiol Mol Biol Rev 66:506-577.

MacKay D. 1992. Bayesian interpolation. Neural Comp 4:415-447.

Mandels M, Medeiros J, Andreotti R, Bissett F. 1981. Enzymatic hydrolysis of cellulose: evaluation of cellulase culture filtrates under use conditions. Biotechnol Bioeng 23:2009-2026.

Mansfield S, Mooney C, Saddler J. 1999. Substrate and enzyme characteristics that limit cellulose hydrolysis. Biotechnol Prog 15:804-816.

Mansfield S, Saake B, Gubitz G, de Jong E, Puls J, Saddler J. 1998a. Identification, purification, and characterization of the predominant endoglucanases from two brown-rot fungal strain of *Gloeophyllum*. In Carbohydrates from *Trichoderma reesei* and other microorganisms: structures, biochemistry, genetics and applications. Cambridge: The Royal Society of Chemistry. pp 227-244.

Mansfield S, Saddler J, Gubitz G. 1998b. Characterization of endoglucanases from the brown-rot fungi *Gloeophyllum sepiarium* and *Gloeophyllum trabeum*. Enzyme Microb Technol 23:133-140.

Medve J, Karlsson J, Lee D, Tjerneld F. 1998. Hydrolysis of microcrystalline cellulose by cellobiohydrolase I and endoglucanase II from *Trichoderma reesei*: adsorption, sugar production pattern, and synergism of the enzymes. Biotechnol Bioeng 59:621-633.

Miller G. 1959. Use of dinitrosalicylic acid reagent for determination of reducing sugar. Anal Chem 31:426-428.

Millet M, Baker A. 1975. Pretreatments to enhance chemical, enzymatic, and microbiological attack of cellulosic materials. Biotechnol Bioeng Symp 5:193-219.

Moore R, Dennis C. 1999. Botany virtual resource library. The McGraw-Hill Company. http://www.mhhe.com/biosci/pae/botany/botany_map/images/cd303.gif.

Mosier N, Wilker J, Ladisch M. 2004. Rapid chromatography for evaluating adsorption characteristics of cellulase binding domain mimetics. Biotech Bioeng 86:756-764.

Movagarnejad K, Sohrabi M, Kaghazchi T, Vahabzadeh F. 2000. A model for the rate of enzymatic hydrolysis of cellulose in heterogeneous solid-liquid systems. Biochem Engr J 4:197-206.

Nazhad M, Ramos L, Paszner L, Saddler J. 1995. Structural constraints affecting the initial enzymatic hydrolysis of recycled paper. Enzyme Micro Technol 17:68-74.

Newman R, Hemmingson J. 1990. Determination of the degree of cellulose crystallinity in wood by carbon-13 nuclear magnetic resonance spectroscopy. Holzforschung 44:351-355.

Nidetzky B, Hayn M, Macarron R, Steiner W. 1993. Synergism of *Trichoderma reesei* cellulases while degrading different celluloses. Biotechnol Lett 15:71-76.

Nieves R, Ellis R, Tood R, Johnson T, Grohmann K, Himmel M. 1991. Visualization of *Trichoderma reesei* cellobiohydrolase I and endoglucanase I on aspen cellulose by using monoclonal antibody-colloidal gold conjugates. Appl Env Microbiol 45:239-244.

NREL. 2004. Technical Report. Biomass analysis technology team laboratory analytical prodedure. National Renewable Energy Laboratory. Golden, CO.

Ohmine K, Ooshima H, Harano Y. 1983. Study on enzymatic hydrolysis of cellulose by cellulase from *Trichoderma viride*. Biotechnol Bioeng 25:2041-2053.

Ong E, Greenwood J, Gilkes N, Kilburn D, Miller R, Warren R. 1989. The cellulase-binding domains of cellulases: tools for biotechnology. Trends Biotechnol 7:239-243.

Pere J, Siika-Aho M, Buchert J, Viikari L. 1995. Effects of purified *Trichoderma* cellulases on the fiber properties of kraft pulp. Tappi J 78:71-78.

Puls J, Wood T. 1991. The degradation pattern of cellulose by extracellular cellulases of aerobic and anaerobic microorganisms. Bioresource Technol 36:15-19.

Puri V. 1984. Effect of crystallinity and degree of polymerization of cellulose on enzymatic saccharification. Biotechnol Bioeng 26:1219-1222.

Ramos L, Breuil C, Saddler J. 1992. Comparison of steam pretreatment of eucalyptus, aspen and spruce wood chips and their enzymatic hydrolysis. Appl Biochem Biotechnol 34/35:37-47.

Rao M, Srinivas J. 2003. Neural networks: algorithms and applications. London: Alpha Science.

Rivers D, Emert G. 1988. Factors effecting the enzymatic hydrolysis of municipal solid waste components. Biotechnol Bioeng 31:278-281.

Rosenblatt F. 1961. Principles of neurodynamics. Washington DC: Spartan Press.

Saddler J, Mooney C, Mansfield S, Touhy M. 1998. The effect of initial pore volume and lignin content on the enzymatic hydrolysis of softwoods. Bioresource Technol. 64: 113-119.

Sangseethong K, Meunier-Goddik L, Tantasucharit U, Liaw E, Penner M. 1998. Rationale for particle size effect on rates of enzymatic saccharification of microcrystalline cellulose. J Food Biochem 22:321-330.

Scheiding W, Thoma M, Ross A, Schugerl K. 1984. Modeling of the enzymatic hydrolysis cellobiose and cellulose by a complex enzyme mixture of *Trichoderma reesei* QM 9414. Appl Microbiol Biotechnol 20:176-182.

Schou C, Rasmussen G, Katoft MB, Henrissat B, Schulein M. 1993. Stereochemistry, specificity, and kinetics of the hydrolysis of reduced cellodextrins by nine cellulases. Eur J Biochem FEBS 217:947-953.

Segal L, Creely J, Martin A, Conrad C. 1959. An empirical method for estimating the degree of crystallinity of native cellulose using the X-ray diffractometer. Textile Res. J. 29:786-794.

Sewalt V, Beauchemin K, Rode L, Acharya S, Baron V. 1997a. Lignin impact on fiber degradation IV: enzymatic saccharification and *in vitro* digestibility of alfalfa and grasses following selective solvent delignification. Bioresource Technol 61:199-206.

Sewalt V, Glasser W, Beauchemin K. 1997b. Lignin impact on fiber degradation III: reversal of inhibition of enzymatic hydrolysis by chemical modification of lignin and by additives. J Agri Food Chem 45:1823-1828.

Sinitsyn A, Gusakov A, Vlasenko E. 1991. Effect of structural and physicochemical features of cellulosic substrates on the efficiency of cellulose hydrolysis. Appl Biochem Biotechnol 30:43-59.

Sinner M, Puls J, Dietrichs H. 1979. Carbohydrate-composition of nut shells and some other agriculture residues. Starke 31:267-269.

Sinnott M. 1990. Catalytic mechanisms of enzymatic glycosyl transfer. Chem Rev 90:1171-1202.

Srishdsuk M, Kleman-Leyer K, Keranen S, Kirk T, Teeri T. 1998. Modes of action on cotton and bacterial cellulose of a homologous endoglucanase-exoglucanase pair from *Trichoderma reesei*. Eur J Biochem 251:885-892.

Stahlberg J, Johansson G, Pettersson G. 1988. A binding-site deficient, catalytically active, core protein of endoglucanase III from the culture filtrate of *Trichoderma reesei*. Eur J Biochem 173:179-183.

Sullivan JT. 1959. A rapid method for the determination of acid-insoluble lignin in forages and its relation to digestibility. J Anim Sci 18:1292-1298.

Sun Y, Cheng J. 2002. Hydrolysis of lignocellulosic materials for ethanol production: a review. Bioresource Technol 83:1-11.

Szczodrak J, Fiedurek J. 1996. Technology for conversion of lignocellulosic biomass to ethanol. Biomass Bioenergy 10:367-375.

Tarantili P, Koullas D, Christakopoulos P, Kekos D, Koukios E, Macris B. 1996. Cross-synergism in enzymatic hydrolysis of lingocellulosics: mathematical correlations according to a hyperbolic model. Biomass Bioenergy 10:213-219.

Teeaar R, Serimaa R, and Paakkari T. 1987. Crystallinity of cellulose, as determined by CP/MAS NMR and XRD methods. Polym Bull 17:231-237.

Teeri T. 1997. Crystalline cellulose degradation: new insight into the function of cellobiohydrolases. Tibtech 15:160-167.

Teymouri F, Laureano-Perez L, Alizadeh H, Dale B. 2004. Ammonia fiber explosion treatment of corn stover. Appl Biochem Biotechnol 113/16:951-963.

Thompson D, Chen H, Grethlein H. 1992. Comparison of pretreatment methods on the basis of available surface area. Biores Technol 39:155-163.

US Department of Energy. 1998. Biofuels, a solution for climate change. DOE/GO-10098-580.

Van Wyk J. 2001. Biotechnology and the utilization of biowaste as a resource for bioproduct development. Trends Biotechnol 19:172-177.

Vinzant T, Ehrman C, Adney W, Thomas S, Himmel M. 1997. Simultaneous saccharification and fermentation of pretreated hardwoods - effect of native lignin content. Appl Biochem Biotechnol 62:99-104.

Vrsanska M, Biely P. 1992. The cellobiohydrolase I from *Trichoderma reesei* QM 9414: action on cello-oligosaccharides. Carbo Res 227:19-27.

Wald S, Wilke C, Blanch H. 1984. Kinetics of the enzymatic hydrolysis of cellulose. Biotechnol Bioeng 26:221-230.

Walseth CS. 1952. The influence of the fine structure of cellulose on the action of cellulases. Tappi 35:233-238.

Wang X, Tang Z, Tamura H, Ishii M, Sun W. 2004. An improved backpropagation algorithm to avoid the local minima problem. Neurocomputing 56:455-460.

Weimer P, Weston W. 1985. Relationship between the fine structure of native cellulose and cellulose degradability by the cellulase complexes of *Trichoderma reesei* and *Clostridum thermocellum*. Biotechnol Bioeng 27:1540-1547.

Withers S, Dombroski D, Berven L, Miller R, Warren T, Kilburn D, Gilkes N. 1986. Direct 1H NMR determination of the stereochemical course of hydrolyses catalysed by glucanase components of the cellulase complex. Biochem Biophys Res Commun 139:487-494.

Withers S, Tull D, Gebler J, Braun C, Aebersold R, Wang Q, Warren T, Kilburn D, Gilkes N. 1993. Mechanistic studies on cellulases. In Proceedings of the Second TRICEL Symposium on *Trichoderma reesei* Cellulases and Other Hydrolases. Helsinki, pp 117-123.

Wong K, Deverell K, Mackie K, Clark T, Donaldson L. 1988. The relationship between fiber porosity and cellulose digestibility in steam exploded *Pinus radiata*. Biotechnol Bioeng 31:447-456.

Wyman C. 1994. Alternative fuels from biomass and their impact on carbon dioxide accumulation. Appl Biochem Biotechnol 45/46:897-915.

Zhang S, Wolfgang D, Wilson D. 1999. Substrate heterogeneity causes the nonlinear kinetics of insoluble cellulose hydrolysis. Biotechnol Bioengr 66:35-41.

Zhbankov R, Ioclovich M, Treimanis A, Lippmaa E, Teejaer R, Kaputskii F, Grinshpan D, Lushkin L. 1987. Determination of the degree of crystallinity of cellulose by high-resolution solid-state carbon-13 NMR. Khim Drev 1:3-6.

Zupan J, Gasteiger J. 1999. Neural networks in chemistry and drug design. Berlin: Wiley Press.

APPENDIX A

ENZYMATIC HYDROLYSIS

Enzymatic Hydrolysis of Lime Pretreated Corn Stover

Distilled water and corn stover were added to appropriately sized screw cap test tubes. Reactions were performed at 10, 20, 50, 100 g/L corn stover concentration. Citrate buffer (1.0 M, pH 4.8) and sodium azide solution (0.01g/mL) were added to the slurry to keep pH constant and prevent the growth of microorganisms, respectively. The test tubes were placed in a 100-rpm air-bath shaker. When the temperature reached 50^{o}C, cellulase and cellobiase were added to the reaction flask. Samples were removed after 1, 6, and 72 h and then glucose, xylose, and reducing sugars were measured. See the following for the complete hydrolysis procedures.

1. Prepare 1 L of 1-*M* citrate buffer (pH 4.5) and 500 mL of 0.01-g/L sodium azide solution. (Citrate buffer is prepared as follows: dissolve 210 g of citric acid monohydrate in 1000 mL of distilled water, then adjust the pH to 4.5 by adding NaOH.)
2. Determine the moisture contents of the biomass (i.e., corn stover) using NREL standard procedure No. 001.
3. Place 0.2 g dry weight of biomass and necessary distilled water, citrate buffer, and sodium azide in a screw-capped test tube according to Table A-1.
4. Place the test tube inside the 100-rpm shaking air bath at 50^{o}C.
5. When the temperature reaches 50^{o}C (ca. 1 h), add diluted cellulase according to Table A-2 (filter paper activity ≅ 65 FPU/mL enzyme solution) and 50 μL cellobiase (activity ≅ 321 CBU/g). This is considered time zero for the reaction mixture.
6. Remove flasks from shaking air bath after 3-d incubation time.

Table A-1. Preparation of biomass slurry for enzymatic hydrolysis

Liquid components (mL)	Substrate concentration			
	10 g/L	20 g/L	50 g/L	100 g/L
Distilled water	18.175	8.975	3.455	1.615
Citrate buffer	1	0.5	0.2	0.1
Sodium azide	0.6	0.3	0.12	0.06

7. Boil flasks for 15 min to denature the enzyme, thereby quenching the reaction. Cool flasks in cold water bath.
8. Transfer contents of flasks to 15-mL centrifuge tubes. Centrifuge at 4500 rpm for 5 min.
9. Using a 0.22-μm nylon membrane filter, filter a 1.5-mL aliquot in micro-centrifuge tube to be frozen until sugar analysis is ready to be performed.
10. Perform DNS assay and/or HPLC analysis to measure the concentrations of glucose, xylose, and cellobiose for each sample.

Enzymatic Hydrolysis Procedure for Fundamental Study of Biomass

1. Prepare 1 L of 1-M citrate buffer (pH 4.5) and 500 mL of 0.01-g/L sodium azide solutions. (Citrate buffer is prepared as follows: dissolve 210 g of citric acid monohydrate in 1000 mL of distilled water, then adjust the pH to 4.5 by adding NaOH.)
2. Determine the moisture contents of the biomass (i.e., model lignocelluloses) using NREL standard procedure No. 001.

Table A-2. Preparation of diluted enzyme for enzymatic hydrolysis

Enzyme loading (FPU/g biomass)	Cellulase enzyme (mL)	Distilled water (mL)	Total volume (mL)
0.1	0.025	16.225	16.250
0.25	0.05	12.95	13.00
0.5	0.1	12.90	13.00
0.75	0.1	8.57	8.67
1	0.1	6.40	6.50
1.5	0.1	4.23	4.33
2	0.1	3.15	3.25
3	0.15	3.10	3.25
5	0.25	3.00	3.25
10	0.5	2.75	3.25
20	1	2.25	3.25
30	1	1.17	2.17
50	1.5	0.45	1.95

3. Place 0.2 g dry weight of biomass and 18 mL of distilled water in a 50-mL screw-capped Erlenmeyer flask.
4. Add 1.0 mL of citrate buffer and 0.6 mL of sodium azide solution into the flask.

5. Place the flask inside the 100-rpm shaking air bath at 50^{o}C.
6. When the temperature reaches 50^{o}C, add diluted cellulase according to Table A-2 (filter paper activity ≅ 65 FPU/mL enzyme solution) and 50 μL cellobiase (activity ≅ 321 CBU/g). This is considered time zero for the reaction mixture.
7. Remove flasks from shaking air bath.
8. Boil flasks for 15 min to denature the enzyme, thereby quenching the reaction. Cool flasks in cold water bath.
9. Transfer contents of flasks to 15-mL centrifuge tubes. Centrifuge at 4500 rpm for 5 min.
10. Using a 0.22-μm nylon membrane filter, filter a 1.5-mL aliquot in micro-centrifuge tube to be frozen until HPLC analysis is ready to be performed.
11. Steps 7 to 10 should be completed after 1, 6, and 72 h.
12. Perform DNS assay and/or HPLC analysis to measure the concentrations of glucose, xylose, and cellobiose for each sample.

APPENDIX B

SUGAR MEASUREMENT

DINITROSALICYLIC ACID (DNS) ASSAY

Reducing sugar was measured using the DNS assay (Miller, 1959). A detailed description of the procedure is as follows:

DNS Reagent Preparation

1. Dissolve 10.6 g of 3,5-dinitrosaliculic acid crystals and 19.8 g of NaOH in 1416 mL of distilled water.
2. Add 306 g of Na-K-tartrate (Rochelle salts).
3. Melt phenol crystals under a fume hood at 50^{o}C using a water bath. Add 7.6 mL of phenol to the above mixture.
4. Add 8.3 g sodium meta-bisulfite ($Na_2S_2O_4$).
5. Add NaOH to adjust the solution pH to 12.6.

DNS Reagent Calibration

1. Prepare a 5 mg/mL glucose standard solution in a 50-mL volumetric flask.
2. Place 0.5 mL of the glucose standard solution into test tubes and diluted according to Table B-1.
3. Dispense 1.5 mL of DNS reagent into each test tube using a 5-mL Eppendorf pipette.
4. Place the caps on the tubes and put samples into a vigorously boiling water bath for exactly 5 min.
5. Cool the test tubes for a few minutes in a cold-water bath.
6. Add 10 mL of distilled water to the test tubes.

7. Zero the spectrophotometer (Milton Roy, Spectronic 1001) at 540 nm with distilled water. (Note: To stabilize the spectrophotometer, it should be turned on for at least 1 h before using.)
8. Measure the absorbance.
9. Prepare a calibration curve.

Reducing Sugar Measurement of Samples

1. Centrifuge samples at 4500 rpm for 5 min.
2. Dilute the centrifuged samples into test tubes according to Table B-1 such that the sugar concentration lies between 0.2 to 5 mg/mL. Vortex the diluted samples.
3. Place 0.5 mL of each diluted sample into test tubes.
4. Repeat steps 3 to 8 described in "DNS Reagent Calibration."
5. Calculate the sugar concentration from the absorbance of the samples using the calibration curve.
6. Calculate the reducing sugar yield by following Formula B-1:

$$Y = S \times D \times V / W \qquad \text{(B-1)}$$

where Y = reducing sugar yield (mg equivalent glucose/ g dry biomass)

S = sugar concentration in diluted sample (mg equivalent glucose/mL)

D = dilution factor (V_2/V_1)

V = working liquid volume (mL)

W = weight of dry biomass (g)

Table B-1. Preparation of Glucose Standard Solutions for DNS Assay

Glucose Concentration (mg/mL)	Glucose Standard (5 mg/mL)	Distilled Water (mL)
0.2	0.2	4.8
0.4	0.4	4.6
0.6	0.6	4.4
0.8	0.8	4.2
1.0	1.0	4.0
2.0	2.0	3.0
3.0	3.0	2.0
4.0	4.0	1.0
5.0	5.0	0.0

HPLC CARBOHYDRATE ANALYSIS

Glucose, xylose, and cellobiose were measured using high performance liquid chromatography (HPLC). A Biorad Aminex HPX-87P column was used in "Enzymatic Hydrolysis of Model Samples" and "Predictive Ability of Neural Networks Study." The instrumental conditions are as follows:

For Biorad Aminex HPX-87P column:

Sample injection volume: 20 μL

Eluant: Degassed and 0.22-μm filtered reverse osmosis deionized (RODI) water

Flow rate: 0.6 mL/min

Column temperature: 85°C

Detector: refractive index

The equipment used in HPLC are as follows:

Pump: LDC Analytical Pump, constaMetric 3200

Autosampler: Spectra-Physics, AS100

Column heater: Jones Chromatography

RI detector: Lab Alliance RI 2000

Software: PeakSimple 3.21, SRI Instruments

RODI water: NANOpure Ultrapure Water System

Carbohydrate Standard Preparation

1. Prepare carbohydrate stock solution: dissolve 45°C-dried glucose (0.5 g), xylose (0.1667 g), and cellobiose (0.25 g) in a 100-mL volumetric flask with RODI water.
2. Prepare standard solutions in test tubes according to Table B-2 and then filter with a 0.22-μm nylon filter into HPLC sample vials.

Equipment Setup

1. Degas the eluant by vacuum filtering 4 L of RODI using a 0.22-μm nylon filter. (Note: Degassed mobile phase not be used for more than 3 consecutive days.)
2. After connecting freshly degassed mobile phase to the system, prime pump by removing a sufficient amount of liquid (ca. 50 mL) with a syringe.
3. Turn on the pump, the autosampler, the RI detector, and the computer. Launch PeakSimple 321 software (see below, “Software Setup”) and select “OK” twice from two popup dialog boxes.

Table B-2. Preparation of HPLC standard solutions

Glucose Concentration (mg/mL)	Stock Solution (mL)	RODI Water (mL)
0.125	0.0375	1.4625
0.5	0.15	1.35
1	0.3	1.2
2	0.6	0.9
3	0.9	0.6
4	1.2	0.3
5	1.5	0

4. Turn on the autosampler's refrigerator by loading a user file (see below, "Autosampler Setup").
5. Flush the system for at least 1 h at 2.0 mL/min. Reduce flowrate to 0.18 mL/min.
6. Remove stainless-steel tubing and connect appropriate column.
7. At a flowrate of 0.18 mL/min, turn on the column heater and adjust the temperature setting to the desired temperature (i.e., 85^{o}C). Approximately 1 h is required to reach the desired temperature.
8. After column temperature is stable, gradually increase (i.e., 0.01 mL/min every 30 s) the flowrate to 0.6 mL/min.
9. Edit and Load the autosampler file as described in "Autosampler Setup."
10. Press the spacebar on the computer to run a baseline. If the baseline is straight and not drifting, start running the samples.

Measurement of Sample Sugars

1. Thaw previously filtered and frozen samples.
2. Dilute the samples so that the sugar concentrations fall between 0.125 to 5 mg/mL, 0.042 to 1.7 mg/mL, and 0.063 to 2.5 mg/mL for glucose, xylose, and cellobiose, respectively.
3. Place 0.5–1.2 mL of dilute sample into HPLC sample vials.

4. Load the sugar standards and samples in the autosampler tray. Edit and load a sample file as described in “Autosampler Setup.”
5. Push the run button on the autosampler to initiate measurements.
6. Chromatograms were collected in PeakSimple 3.21. Prepare a calibration curve according to the standard solutions. Calculate sample sugar concentrations according the calibration curve prepared from the standard solutions.

Autosampler Setup

Editing and Loading Autosampler File

1. Press the menu key to display the main menu. Select FILES, EDIT, and INJECTION consecutively to display the edit menu using the arrow keys and the enter key.
2. Adjust the loop size to 20 mL, the number of injections per sample to 1, the cycle time to 20 minutes, and the tray temperature from 20^{o}C to 5^{o}C in increments of 5^{o}C by pressing the “+” or “-“ key to increase or decrease the values.
3. Load the file by selecting FILES and LOAD from the main menu and then pressing the enter key.

Editing and Loading Sample File

1. Press the sample key to display the main sample menu and specify the sample set number.
2. Adjust the loop size, number of injections per sample, and the cycle time as described in “Editing and Loading Autosampler Files.”
3. Specify the position of the first sample vial and the total number of samples using the “+” or “-“ key.
4. Add the sample set to the queue by pressing the enter key.

Software Setup

1. Load control file by selecting from the FILE drop down menu “Open Control File” and selecting proper control file (i.e., Jonathan87P.con). Select “OK” from the popup dialog box that appears.
2. After loading the proper control file, select from the EDIT drop down menu “Channels.”
3. Then press the “Post Run” radial button. From the pop up box, verify the desired file storage location has been typed into the box as well as the auto increment box has been checked to ensure the chromatograms are saved as successive file numbers (i.e., Jonathan87P.asc).
4. Close the pop up boxes by pressing the “OK” buttons.
5. By pressing the “Run” button on the Autosampler, the software will be initiated and a new chromatogram will start each time the autosampler injects a sample.

APPENDIX C

PRETREATMENT TECHNIQUES

Short-Term Lime Pretreatment of Corn Stover, Rice Straw, and Bagasse

1. Grind biomass to achieve more uniform particle size distribution (-40 mesh).
2. Determine moisture content of biomass according to NREL standard procedure No. 001.
3. Load desired amount of biomass into a deep-metal container.
4. Add 0.1 g $Ca(OH)_2$/g dry biomass and 10 g H_2O/g dry biomass to biomass. Stir thoroughly with a spatula to ensure a uniform mixture.
5. Place metal container oven Bunsen burner and bring slurry to a boil, continue boiling for 2 h. After 2-h pretreatment time, allow the slurry to cool enough to be handled.
6. The slurry pH is high (ca. 12) and needs to be adjusted to a range of 5–6 by adding acetic acid (CH_3COOH) all the while monitoring the pH and stirring with a magnetic stirrer.
    a. Transfer slurry to large high-density polypropylene centrifuge bottles.
    b. Add water to fill bottles completely and then place bottles inside centrifuge. (Note: Before placing bottles inside centrifuge, balance bottles so as not to damage the centrifuge rotor.)
    c. Centrifuge at 4200 rpm for 15 minutes. Pour off supernatant and add clean water.
    d. Mix slurry with a magnetic stirrer and measure pH. Add acetic acid if pH is above 6.
    e. Repeat steps b through d until pH is between 5 and 6 and supernatant is clear (ca. 7 cycles).
7. Dry biomass in a 45^{o}C oven for 3 d.
8. Grind dried biomass to ensure more uniform particle size distribution.

Dilute-Acid Pretreatment of Rice Straw and Bagasse

1. Grind biomass (i.e., rice straw or bagasse) to achieve more uniform particle size distribution (-40 mesh).
2. Determine moisture content of biomass according to NREL standard procedure No. 001.
3. The biomass was prepared for acid pretreatment by presoaking the biomass at room temperature overnight in 500-mL autoclavable Pyrex glassware, 0.05 g/mL solids concentration, and 0.01 g/mL solution of H_2SO_4.
4. The presoaked slurry was pretreated at 121^{o}C in an autoclave reactor for 2 h.
5. After pretreatment, allow the Pyrex bottle to cool before opening.
6. Repeatedly wash the biomass with distilled water until the supernatant pH reached 6.
7. Repeat Steps 7 to 8 in "Lime Pretreatment of Corn Stover."

Aqueous Ammonia Pretreatment of Bagasse

1. Repeat Steps 1 to 2 in "Dilute Acid Pretreatment of Rice Straw and Bagasse."
2. Equal amounts of biomass were loaded into four 500-mL autoclavable Pyrex glassware in a 1:6 (2 bottles) and 1:8 (2 bottles) solid to liquid ratio based on weight with a 15% (w/w) aqueous ammonia concentration. (Note: Handle the aqueous ammonia under a fume hood to avoid exposure.)
3. The pretreatment was conducted in a 60^{o}C oven for 12 h. (Note: Cool Pyrex bottles before opening.)
4. Repeat Steps a to e in "Short-Term Lime Pretreatment."
5. Repeat Steps 7 to 8 in "Short-Term Lime Pretreatment."

Long-Term Lime Pretreatment of Corn Stover

1. Reagent loading of 0.5 g lime/g dry biomass was used with a water loading of 10 mL/g dry biomass.
2. Air- and nitrogen-treated samples were pretreated for 2688 h and 2016 h, respectively.
3. Pretreatment temperature was 45^{o}C.

4. A detailed explanation of long-term lime pretreatment can be found in Kim (2004).

AFEX Pretreatment of Corn Stover

1. Reagent loading of 1 g NH_3/g dry biomass with a hold time of 5 seconds was used for all pretreatments.
2. Three different samples were pretreated as follows:
    a. The first sample was pretreated with 0.4 mL H_2O/g dry biomass with a reaction temperature of 90^oC.
    b. The second sample was pretreated with 0.6 mL H_2O/g dry biomass with a reaction temperature of 90^oC.
    c. The third sample was pretreated with 0.6 mL H_2O/g dry biomass with a reaction temperature of 100^oC.
3. A detailed explanation of AFEX pretreatment can be found in Teymouri et al. (2004).

APPENDIX D

ENZYME ACTIVITY MEASUREMENT

CELLULASE ENZYME ASSAY

The standard cellulase enzyme assay according to NREL laboratory analytical procedure No. 006 was used as a basis for determining the amount of enzyme added to the reaction mixtures. In addition to NREL standard procedures, an improved assay according to Coward-Kelly et al. (2003) was used to determine enzyme activity for comparison purposes only. Coward-Kelly et al. (2003) suggested using a 0.5-mL supplemental cellobiase loading to relieve cellobiose inhibition yielding a true representation of cellulase activity free from product inhibition. In the current study, the optimal supplemental cellobiase loading was investigated by performing experiments with no cellobiase, 0.25-mL cellobiase, 0.5-mL cellobiase, 0.75-mL cellobiase, and 1.0-mL cellobiase. Cellobiase activity was 321 CBU/mL according to Sigma's assay. The results are summarized in Table D-1. It was found that cellobiase loadings greater than 0.75 mL resulted in minimal enzyme activity increases. Therefore, if one wants to evaluate product inhibition free enzyme activity, a supplemental cellobiase loading of 0.75 mL is recommended. However, this value may vary depending on the inherent cellobiase activity of the cellulase and/or the activity of the cellobiase.

Table D-1. Enzyme activity as a function of cellobiase loading.

Cellobiase Loading (mL)	Enzyme Activity (FPU/mL enzyme)
0	65
0.25	92
0.50	98
0.75	101
1.00	102

APPENDIX E

MATLAB CODES FOR TRAINING AND SIMULATION AND THEIR ASSOCIATED WEIGHT AND BIAS MATRICES

Exhibit E-1. Matlab codes for training and simulating 1-h glucan slope network.

```
clc
clear
load L_G.m
load A_X.m
load G.m
load CrIc.m
load slope_G_1.m
[L_Gn,minL_G,maxL_G]=premnmx(L_G);
[A_Xn,minA_X,maxA_X]=premnmx(A_X);
[CrIcn,minCrIc,maxCrIc]=premnmx(CrIc);
[Gn,minG,maxG]=premnmx(G);
for I=1:146,
    network_input_GS (I,1)=A_Xn(I)'
end
for I=1:146,
    network_input_GS (I,2)=CrIcn(I)'
end
for I=1:146,
    network_input_GS (I,3)=L_Gn(I)'
end
for I=1:146,
    network_input_GS (I,4)=Gn(I)'
end
[slope_G_1n,minslope_G_1,maxslope_G_1]=premnmx(slope_G_1);
```

Exhibit E-1. Continued

```
net=newff([min(A_Xn)max(A_Xn);min(CrIcn)
   max(CrIcn);min(L_G) max(L_G);min(Gn) max(Gn)], [15 1],
   {'tansig','purelin'},'trainbr');
net.trainParam.show=10;
net.trainParam.epoch=100;
randn('seed',192836547);
net.trainParam.goal=.01;
net=init(net);
net=train(net,network_input_GS',slope_G_1n');
net=train(net,network_input_GS',slope_G_1n');
net=train(net,network_input_GS',slope_G_1n');
net=train(net,network_input_GS',slope_G_1n');
net=train(net,network_input_GS',slope_G_1n');
net=init(net);
net=train(net,network_input_GS',slope_G_1n');
net=train(net,network_input_GS',slope_G_1n');
net=train(net,network_input_GS',slope_G_1n');
net=train(net,network_input_GS',slope_G_1n');
net=train(net,network_input_GS',slope_G_1n');
yn=sim(net, network_input_GS');
y=postmnmx(yn,minslope_G_1,maxslope_G_1);
E=slope_G_1'-y;
min(E)
max(abs(E))
perf=mse(E)
[m,b,r]=postreg(y,slope_G_1')
Rsqr=r^2
```

Exhibit E-2. Final weights and biases for 1-h glucan slope network.

IW{1,1}: Weights to layer 1 from input (15×4 matrix)

0.9862	0.0452	-0.0097	0.4638
0.0162	0.1013	0.0596	-0.0678
-0.0162	-0.1013	-0.0596	0.0678
-0.0162	-0.1013	-0.0596	0.0678
0.0162	0.1013	0.0596	-0.0678
0.1944	0.7978	0.9967	-0.3334
-0.2883	-0.2963	-0.4692	0.8003
0.0162	0.1013	0.0596	-0.0678
-0.5564	-0.0893	1.1576	0.4013
-0.0534	-1.2929	0.6046	0.9617
0.0162	0.1013	0.0596	-0.0678
0.0162	0.1013	0.0596	-0.0678
0.0162	0.1013	0.0596	-0.0678
-0.0162	-0.1013	-0.0596	0.0678
-0.0162	-0.1013	-0.0596	0.0678

b{1}: Bias to layer 1 (15×1 matrix)

0.4644
-0.0528
0.0528
0.0528
-0.0528
0.1723
-0.4461
-0.0528
-0.3100
0.5933
-0.0528
-0.0528
-0.0528
0.0528
0.0528

LW{2,1}: Weights to layer 2 (1×15 matrix)

[-0.1489 0.7160 -0.1489 0.1489 0.1489 0.1489 0.8299 0.1489 -0.1489 0.6480
-0.1489 0.1489 0.6973 0.8000 0.1489]

b{2}: Bias to layer 2 (1×1 matrix)

[-0.381]

Exhibit E-3. Matlab codes for training and simulating 1-h glucan intercept network.

```
clc
clear
load L.m
load A_X.m
load G.m
load CrIc.m
load intercept_G_1.m
[Ln,minL,maxL]=premnmx(L);
[A_Xn,minA_X,maxA_X]=premnmx(A_X);
[Gn,minG,maxG]=premnmx(G);
[intercept_G_1n,minintercept_G_1,maxintercept_G_1]=premnmx(
     intercept_G_1);
[CrIcn,minCrIc,maxCrIc]=premnmx(CrIc);
for I=1:146,
    network_input_G (I,1)=Gn(I)'
end
for I=1:146,
    network_input_G (I,2)=CrIcn(I)'
end
for I=1:146,
    network_input_G (I,3)=A_Xn(I)'
end
for I=1:146,
    network_input_G (I,4)=Ln(I)'
end
[intercept_G_1n,minintercept_G_1,maxintercept_G_1]=premnmx(
     intercept_G_1);
```

Exhibit E-3. Continued

```
net=newff([min(Gn)max(Gn);min(CrIcn)max(CrIcn);minA_Xn)max(
     A_Xn);min(L)max(L)],[15 1],{'tansig','purelin'},
     'trainbr');
net.trainParam.show=10;
net.trainParam.epoch=100;
randn('seed',192836547);
net.trainParam.goal=.01;
net=init(net);
net=train(net,network_input_G',intercept_G_1n');
net=train(net,network_input_G',intercept_G_1n');
net=train(net,network_input_G',intercept_G_1n');
net=train(net,network_input_G',intercept_G_1n');
net=train(net,network_input_G',intercept_G_1n');
net=init(net);
net=train(net,network_input_G',intercept_G_1n');
net=train(net,network_input_G',intercept_G_1n');
net=train(net,network_input_G',intercept_G_1n');
net=train(net,network_input_G',intercept_G_1n');
net=train(net,network_input_G',intercept_G_1n');
yn=sim(net, network_input_G');
y=postmnmx(yn,minintercept_G_1,maxintercept_G_1);
E=intercept_G_1'-y;
min(E)
max(abs(E))
perf=mse(E)
[m,b,r]=postreg(y,intercept_G_1')
Rsqr=r^2
```

Exhibit E-4. Final weights and biases for 1-h glucan intercept network.

IW{1,1}: Weights to layer 1 from input (15×4 matrix)

-0.0295	-0.0607	-0.0071	-0.0025
0.0305	0.0627	0.0074	0.0027
0.0311	0.0640	0.0075	0.0028
0.4576	-0.4986	-0.9164	-0.5309
-0.2148	-0.3371	-0.2845	-0.1289
0.0306	0.0629	0.0074	0.0027
0.0339	0.0698	0.0085	0.0033
0.0307	0.0632	0.0074	0.0027
0.9279	-1.3589	0.0030	-0.1325
0.2872	-1.2237	0.1590	-0.3395
-0.0305	-0.0628	-0.0074	-0.0027
0.7310	0.3784	-0.1581	-0.2085
-0.0313	-0.0644	-0.0076	-0.0028
-0.1273	0.4512	-0.7890	-0.2210
0.0565	-0.4499	-0.7031	0.1940

b{1}: Bias to layer 1 (15×1 matrix)

0.4644
-0.0528
0.0528
0.0528
-0.0528
0.1723
-0.4461
-0.0528
-0.3100
0.5933
-0.0528
-0.0528
-0.0528
0.0528
0.0528

LW{2,1}: Weights to layer 2 (1×15 matrix)

[-0.5577 0.6565 0.1051 -0.0783 0.9835 -0.8270 0.1065 0.6371 0.0998 -0.0252 0.0794 -0.0796 0.8224 0.1132 -1.1093]

b{2}: Bias to layer 2 (1×1 matrix)

[-0.5553]

Exhibit E-5. Matlab codes for training and simulating 6-h glucan slope network.

```
clc
clear
load L.m
load A_G.m
load G.m
load CrIc_G.m
load slope_G_6.m
[Ln,minL,maxL]=premnmx(L);
[A_Gn,minA_G,maxA_G]=premnmx(A_G);
[CrIc_Gn,minCrIc_G,maxCrIc_G]=premnmx(CrIc_G);
[Gn,minG,maxG]=premnmx(G);
for I=1:147,
    network_input_GS (I,1)=A_Gn(I)'
end
for I=1:147,
    network_input_GS (I,2)=CrIc_Gn(I)'
end
for I=1:147,
    network_input_GS (I,3)=Ln(I)'
end
for I=1:147,
    network_input_GS (I,4)=Gn(I)'
end
[slope_G_6n,minslope_G_6,maxslope_G_6]=premnmx(slope_G_6);
net=newff([min(Ln)max(Ln);min(A_Gn)max(A_Gn);min(CrIc_Gn)
     max(CrIc_Gn);min(Gn)max(Gn)],[15 1],{'tansig',
     'purelin'},'trainbr');
net.trainParam.show=10;
net.trainParam.epoch=100;
```

Exhibit E-5. Continued

```
randn('seed',192836547);
net.trainParam.goal=.01;
net=init(net);
net=train(net,network_input_GS',slope_G_6n');
net=train(net,network_input_GS',slope_G_6n');
net=train(net,network_input_GS',slope_G_6n');
net=train(net,network_input_GS',slope_G_6n');
net=train(net,network_input_GS',slope_G_6n');
net=init(net);
net=train(net,network_input_GS',slope_G_6n');
net=train(net,network_input_GS',slope_G_6n');
net=train(net,network_input_GS',slope_G_6n');
net=train(net,network_input_GS',slope_G_6n');
net=train(net,network_input_GS',slope_G_6n');
yn=sim(net, network_input_GS');
y=postmnmx(yn,minslope_G_6,maxslope_G_6);
E=slope_G_6'-y;
min(E)
max(abs(E))
perf=mse(E)
[m,b,r]=postreg(y,slope_G_6')
Rsqr=r^2
```

Exhibit E-6. Final weights and biases for 6-h glucan slope network.

IW{1,1}: Weights to layer 1 from input (15×4 matrix)

-0.0770	-0.0919	0.0290	0.0675
-0.2286	-0.4055	0.4470	0.0972
0.5904	-0.2395	0.8339	-1.0436
-0.3138	0.8601	1.0248	-0.4768
0.3008	1.6993	-0.5281	-0.2796
0.6438	-0.9413	-0.1663	0.5668
0.0770	0.0919	-0.0290	-0.0675
-0.8142	-0.9440	0.5915	-0.4219
0.0770	0.0919	-0.0290	-0.0675
-1.0637	0.3228	0.4990	-0.7329
-0.0770	-0.0919	0.0290	0.0675
1.1580	0.2411	0.1666	0.5855
0.3493	0.7582	0.9094	-1.0425
-0.0770	-0.0919	0.0290	0.0675
-0.0770	-0.0919	0.0290	0.0675

b{1}: Bias to layer 1 (15×1 matrix)

0.0106
-0.2559
-0.1494
-0.5663
-0.7106
-0.7333
-0.0106
0.1126
-0.0106
0.2891
0.0106
0.3472
0.1398
0.0106
0.0106

LW{2,1}: Weights to layer 2 (1×15 matrix)

[-0.1666 -0.9659 0.1666 -0.1666 -0.1666 -0.1666 1.0572 -0.8194 0.8958 -0.8027
0.7077 -0.1666 0.9915 0.7555 0.1666]

b{2}: Bias to layer 2 (1×1 matrix)

[-0.0482]

Exhibit E-7. Matlab codes for training and simulating 6-h glucan intercept network.

```
clc
clear
load L_G.m
load A_X.m
load G.m
load CrIc_G.m
load intercept_G_6.m
[L_Gn,minL_G,maxL_G]=premnmx(L_G);
[A_Xn,minA_X,maxA_X]=premnmx(A_X);
[CrIc_Gn,minCrIc_G,maxCrIc_G]=premnmx(CrIc_G);
[Gn,minG,maxG]=premnmx(G);
for I=1:147,
    network_input_GI (I,1)=CrIc_Gn(I)'
end
for I=1:147,
    network_input_GI (I,2)=A_Xn(I)'
end
for I=1:147,
    network_input_GI (I,3)=L_Gn(I)'
end
for I=1:147,
    network_input_GI (I,4)=Gn(I)'
end
[intercept_G_6n,minintercept_G_6,maxintercept_G_6]=premnmx
     (intercept_G_6);
net=newff([min(CrIc_Gn)max(CrIc_Gn);min(A_Xn)max(A_Xn);min(
     L_Gn)max(L_Gn);min(Gn)max(Gn)],[15 1],{'tansig',
     'purelin'},'trainbr');
net.trainParam.show=10;
```

Exhibit E-7. Continued

```
net.trainParam.epoch=100;
randn('seed',192836547);
net.trainParam.goal=.01;
net=init(net);
net=train(net,network_input_GI',intercept_G_6n');
net=train(net,network_input_GI',intercept_G_6n');
net=train(net,network_input_GI',intercept_G_6n');
net=train(net,network_input_GI',intercept_G_6n');
net=train(net,network_input_GI',intercept_G_6n');
net=init(net);
net=train(net,network_input_GI',intercept_G_6n');
net=train(net,network_input_GI',intercept_G_6n');
net=train(net,network_input_GI',intercept_G_6n');
net=train(net,network_input_GI',intercept_G_6n');
net=train(net,network_input_GI',intercept_G_6n');
yn=sim(net, network_input_GI');
y=postmnmx(yn,minintercept_G_6,maxintercept_G_6);
E=intercept_G_6'-y;
min(E)
max(abs(E))
perf=mse(E)
[m,b,r]=postreg(y,intercept_G_6')
Rsqr=r^2
```

Exhibit E-8. Final weights and biases for 6-h glucan intercept network.

IW{1,1}: Weights to layer 1 from input (15×4 matrix)

0.0313	0.0352	0.1559	-0.0279
0.0313	0.0352	0.1559	-0.0279
-0.3136	-0.1593	-0.0223	1.4229
-0.1944	-0.3640	1.6741	0.0620
0.5178	-0.8172	-0.0392	-0.2834
-0.7619	-0.1184	1.0236	0.2541
0.0313	0.0352	0.1559	-0.0279
0.0313	0.0352	0.1559	-0.0279
0.0313	0.0352	0.1559	-0.0279
-0.0313	-0.0352	-0.1559	0.0279
-0.0313	-0.0352	-0.1559	0.0279
0.7329	0.0201	0.6887	-0.8305
-1.2934	0.5759	-0.1963	-0.4342
-0.0313	-0.0352	-0.1559	0.0279
-0.0313	-0.0352	-0.1559	0.0279

b{1}: Bias to layer 1 (15×1 matrix)

-0.1080
-0.1080
-0.4571
-0.6971
-0.2753
-0.0877
-0.1080
-0.1080
-0.1080
0.1080
0.1080
0.3938
0.4091
0.1080
0.1080

LW{2,1}: Weights to layer 2 (1×15 matrix)

[-0.7396 -0.2122 -0.2122 -0.9975 -0.2122 -0.2122 -0.2122 -0.2122 -0.2122 0.7857
0.2122 -0.5381 0.8548 -0.8274 -0.2122]

b{2}: Bias to layer 2 (1×1 matrix)

[-0.3754]

Exhibit E-9. Matlab codes for training and simulating 72-h glucan slope network.

```
clc
clear
load L.m
load A_X.m
load CrIc.m
load slope_G_72.m
[Ln,minL,maxL]=premnmx(L);
[A_Xn,minA_X,maxA_X]=premnmx(A_X);
[CrIcn,minCrIc,maxCrIc]=premnmx(CrIc);
for I=1:138,
    network_input_GS (I,1)=A_Xn(I)'
end
for I=1:138,
    network_input_GS (I,2)=Ln(I)'
end
for I=1:138,
    network_input_GS (I,3)=CrIcn(I)'
end
[slope_G_72n,minslope_G_72,maxslope_G_72]=premnmx(slope_G_7
     2);
net=newff([min(A_Xn)max(A_Xn);min(Ln)max(Ln);min(CrIcn)
     max(CrIcn)], [15 1], {'tansig','purelin'},'trainbr');
net.trainParam.show=20;
net.trainParam.epoch=100;
randn('seed',192836547);
net.trainParam.goal=.01;
net=init(net);
net=train(net,network_input_GS',slope_G_72n');
net=train(net,network_input_GS',slope_G_72n');
```

Exhibit E-9. Continued

```
net=train(net,network_input_GS',slope_G_72n');
net=train(net,network_input_GS',slope_G_72n');
net=train(net,network_input_GS',slope_G_72n');
net=init(net);
net=train(net,network_input_GS',slope_G_72n');
net=train(net,network_input_GS',slope_G_72n');
net=train(net,network_input_GS',slope_G_72n');
net=train(net,network_input_GS',slope_G_72n');
net=train(net,network_input_GS',slope_G_72n');
yn=sim(net, network_input_GS');
y=postmnmx(yn,minslope_G_72,maxslope_G_72);
E=slope_G_72'-y;
min(E)
max(abs(E))
perf=mse(E)
[m,b,r]=postreg(y,slope_G_72')
Rsqr=r^2
```

Exhibit E-10. Final weights and biases for 72-h glucan slope network.

IW{1,1}: Weights to layer 1 from input (15×3 matrix)

0.0000	0.0000	0.0000
0.8077	0.0929	0.5348
0.0000	0.0000	0.0000
0.0000	0.0000	0.0000
0.0000	0.0000	0.0000
0.0000	0.0000	0.0000
0.5036	0.5064	-0.6639
0.0000	0.0000	0.0000
0.5697	-0.4446	-0.4330
-0.0626	0.9278	0.1463
0.0000	0.0000	0.0000
0.0000	0.0000	0.0000
0.0000	0.0000	0.0000
-0.4887	-1.2632	-0.1965
0.0000	0.0000	0.0000

Exhibit E-10. Continued

b{1}: Bias to layer 1 (15×1 matrix)

```
 0.0000
 0.3316
 0.0000
 0.0000
 0.0000
 0.0000
 0.3417
 0.0000
-0.3115
-0.3921
 0.0000
 0.0000
 0.0000
-0.5095
 0.0000
```

LW{2,1}: Weights to layer 2 (1×15 matrix)

```
[-0.0000   -0.6337   -0.0000   -0.0000    0.0000   -0.0000   -0.7699  0.0000    0.7599   -0.8944
  0.0000    0.0000   -0.0000   -0.6977  0.0000]
```

b{2}: Bias to layer 2 (1×1 matrix)

```
[0.1525]
```

Exhibit E-11. Matlab codes for training and simulating 72-h glucan intercept network.

```
clc
clear
load L.m
load A_G.m
load CrIc.m
load intercept_G_72.m
[Ln,minL,maxL]=premnmx(L);
[A_Gn,minA_G,maxA_G]=premnmx(A_G);
[CrIcn,minCrIc,maxCrIc]=premnmx(CrIc);
[Gn,minG,maxG]=premnmx(G);
for I=1:138,
```

Exhibit E-11. Continued

```
    network_input_GI (I,1)=A_Gn(I)'
end
for I=1:138,
    network_input_GI (I,2)=CrIcn(I)'
end
for I=1:138,
    network_input_GI (I,3)=Ln(I)'
end
[intercept_G_72n,mininterceptG_72,maxintercept_G_72]=premn
     mx(intercept_G_72);
net=newff([min(A_Gn)max(A_Gn);min(CrIcn)max(CrIcn);min(Ln)
     max(Ln)], [15 1], {'tansig','purelin'},'trainbr');
net.trainParam.show=20;
net.trainParam.epoch=100;
randn('seed',196836549);
net.trainParam.goal=.01;
net=init(net);
net=train(net,network_input_GI',intercept_G_72n');
net=train(net,network_input_GI',intercept_G_72n');
net=train(net,network_input_GI',intercept_G_72n');
net=train(net,network_input_GI',intercept_G_72n');
net=train(net,network_input_GI',intercept_G_72n');
net=init(net);
net=train(net,network_input_GI',intercept_G_72n');
net=train(net,network_input_GI',intercept_G_72n');
net=train(net,network_input_GI',intercept_G_72n');
net=train(net,network_input_GI',intercept_G_72n');
yn=sim(net, network_input_GI');
y=postmnmx(yn,mininterceptG_72,maxintercept_G_72);
```

Exhibit E-11. Continued

```
E=intercept_G_72'-y;
min(E)
max(abs(E))
perf=mse(E)
[m,b,r]=postreg(y,intercept_G_72')
Rsqr=r^2
```

Exhibit E-12. Final weights and biases for 72-h glucan intercept network.

IW{1,1}: Weights to layer 1 from input (15×3 matrix)

0.1849	0.4436	2.0048
0.1022	0.3935	2.1109
-0.0919	-1.2824	0.2028
0.1509	0.3021	0.2353
0.1509	0.3021	0.2353
-0.1509	-0.3021	-0.2353
0.6118	2.3543	0.4073
-1.4948	0.5219	0.6287
1.3461	-0.9300	-0.1261
1.4222	-0.2262	-1.2908
-0.1509	-0.3021	-0.2353
0.5802	0.1442	-1.0038
-0.1060	-0.9585	-0.7127
-0.1509	-0.3021	-0.2353
0.1509	0.3021	0.2353

b{1}: Bias to layer 1 (15×1 matrix)

-1.1784
0.6521
-1.0616
0.0388
0.0388
-0.0388
-0.8610
-0.3598
0.5341
0.3309
-0.0388
-0.2098
0.5804
-0.0388
0.0388

Exhibit E-12. Continued

LW{2,1}: Weights to layer 2 (1×15 matrix)

[-0.4082 -0.5304 0.4083 -0.4082 -0.9960 -0.7987 0.5253 0.4082 0.4082 -0.8670
-0.8576 0.6835 1.5270 1.6656 0.4083]

b{2}: Bias to layer 2 (1×1 matrix)

[-0.2638]

Exhibit E-13. Matlab codes for training and simulating 1-h xylan slope network.

```
clc
clear
load L.m
load A.m
load X.m
load CrIc.m
load slope_X_1.m
[Ln,minL,maxL]=premnmx(L);
[An,minA,maxA]=premnmx(A);
[Xn,minX,maxX]=premnmx(X);
[CrIcn,minCrIc,maxCrIc]=premnmx(CrIc);
for I=1:123,
    network_input_GS (I,1)=CrIcn(I)'
end
for I=1:123,
    network_input_GS (I,2)=Ln(I)'
end
for I=1:123,
    network_input_GS (I,3)=An(I)'
end
for I=1:123,
```

Exhibit E-13. Continued

```
    network_input_GS (I,4)=Xn(I)'
end
[slope_X_1n,minslope_X_1,maxslope_X_1]=premnmx(slope_X_1);
net=newff([min(CrIcn)max(CrIcn);min(Ln)max(Ln);min(An)
     max(An);min(Xn)max(Xn)],[151],{'tansig','purelin'},'tr
     ainbr');
net.trainParam.show=20;
net.trainParam.epoch=100;
randn('seed',192836547);
net.trainParam.goal=.01;
net=init(net);
net=train(net,network_input_GS',slope_X_1n');
net=train(net,network_input_GS',slope_X_1n');
net=train(net,network_input_GS',slope_X_1n');
net=init(net);
net=train(net,network_input_GS',slope_X_1n');
net=train(net,network_input_GS',slope_X_1n');
net=train(net,network_input_GS',slope_X_1n');
yn=sim(net, network_input_GS');
y=postmnmx(yn,minslope_X_1,maxslope_X_1);
E=slope_X_1'-y;
min(E)
max(abs(E))
perf=mse(E)
[m,b,r]=postreg(y,slope_X_1')
Rsqr=r^2
```

Exhibit E-14. Final weights and biases for 1-h xylan slope network.

IW{1,1}: Weights to layer 1 from input (15×4 matrix)

-0.0186	0.0322	0.0100	-0.0061
0.8718	0.0751	0.5075	0.8932
0.3201	-0.7804	-0.1902	0.0469
-0.0162	0.0281	0.0088	-0.0054
0.0176	-0.0305	-0.0095	0.0058
0.9855	0.8280	0.5793	0.5775
0.2159	-0.3659	0.9807	0.2793
-0.0145	0.0252	0.0079	-0.0049
-0.6049	-1.2427	-0.4137	-0.4043
0.0180	-0.0312	-0.0097	0.0059
-0.0189	0.0327	0.0102	-0.0061
-0.2083	-0.2964	0.5158	-0.2713
0.0209	-0.0361	-0.0112	0.0067
0.0200	-0.0347	-0.0108	0.0065
-0.0150	0.0261	0.0082	-0.0050

b{1}: Bias to layer 1 (15×1 matrix)

0.0212
0.3367
0.5152
0.0185
-0.0201
-0.6664
-0.2949
0.0167
-0.1704
-0.0206
0.0216
0.2848
-0.0238
-0.0229
0.0173

LW{2,1}: Weights to layer 2 (1×15 matrix)

[0.0558 0.0416 0.0378 -0.0409 0.0393 0.0387 -0.5403 0.0040 0.9413 -0.7355
1.2362 0.8032 0.0572 1.0568 -0.0393]

b{2}: Bias to layer 2 (1×1 matrix)

[-0.4913]

Exhibit E-15. Matlab codes for training and simulating 1-h xylan intercept network.

```
clc
clear
load L.m
load A.m
load X.m
load CrIc.m
load intercept_X_1.m
[Ln,minL,maxL]=premnmx(L);
[An,minA,maxA]=premnmx(A);
[Xn,minX,maxX]=premnmx(X);
[CrIcn,minCrIc,maxCrIc]=premnmx(CrIc);
for I=1:123,
    network_input_GI (I,1)=Ln(I)'
end
for I=1:123,
    network_input_GI (I,2)=An(I)'
end
for I=1:123,
    network_input_GI (I,3)=CrIcn(I)'
end

for I=1:123,
    network_input_GI (I,4)=Xn(I)'
end
[intercept_X_1n,minintercept_X_1,maxintercept_X_1]=premnmx(
     intercept_X_1);
net=newff([min(Ln)max(Ln);min(An)max(An);min(CrIcn)
     max(CrIcn);min(Xn)max(Xn)],[15 1],{'tansig','purelin'
     },'trainbr');
```

Exhibit E-15. Continued

```
net.trainParam.show=20;
net.trainParam.epoch=100;
randn('seed',192836547);
net.trainParam.goal=.01;
net=init(net);
net=train(net,network_input_GI',intercept_X_1n');
net=train(net,network_input_GI',intercept_X_1n');
net=train(net,network_input_GI',intercept_X_1n');
net=train(net,network_input_GI',intercept_X_1n');
net=init(net);
net=train(net,network_input_GI',intercept_X_1n');
net=train(net,network_input_GI',intercept_X_1n');
net=train(net,network_input_GI',intercept_X_1n');
net=train(net,network_input_GI',intercept_X_1n');
yn=sim(net, network_input_GI');
y=postmnmx(yn,minintercept_X_1,maxintercept_X_1);
E=intercept_X_1'-y;
min(E)
max(abs(E))
perf=mse(E)
[m,b,r]=postreg(y,intercept_X_1')
Rsqr=r^2
```

Exhibit E-16. Final weights and biases for 1-h xylan intercept network.

IW{1,1}: Weights to layer 1 from input (15×4 matrix)

0.0436	0.0024	-0.0728	0.0154
-0.0436	-0.0024	0.0728	-0.0154
-0.5918	-0.1113	-1.1204	0.0379
-0.0436	-0.0024	0.0728	-0.0155
-0.0436	-0.0024	0.0728	-0.0155
-0.0436	-0.0024	0.0728	-0.0155
-0.9048	0.0460	0.1379	0.5963
0.0682	0.4254	0.4198	0.8420
-0.0424	-0.0023	0.0708	-0.0149
0.0429	0.0024	-0.0717	0.0152
-0.0424	-0.0023	0.0707	-0.0149
0.0436	0.0024	-0.0728	0.0155
-0.8265	-0.7954	-0.0596	-0.4606
0.0383	0.0021	-0.0637	0.0132
-0.0389	-0.0022	0.0648	-0.0135

b{1}: Bias to layer 1 (15×1 matrix)

0.0072
-0.0072
0.6972
-0.0072
-0.0072
-0.0072
0.0474
-0.3791
-0.0072
0.0072
-0.0072
0.0072
-0.0214
0.0071
-0.0071

LW{2,1}: Weights to layer 2 (1×15 matrix)

[0.0862 0.0864 0.0850 -0.0846 1.1917 -0.0839 0.0846 1.1393 -0.0847 0.0850
0.0848 -0.6867 -0.9522 0.0844 -0.0844]

b{2}: Bias to layer 2 (1×1 matrix)

[-0.1247]

Exhibit E-17. Matlab codes for training and simulating 6-h xylan slope network.

```
clc
clear
load L.m
load A_X.m
load CrIc.m
load slope_G_6.m
[Ln,minL,maxL]=premnmx(L);
[A_Xn,minA_X,maxA_X]=premnmx(A_X);
[CrIcn,minCrIc,maxCrIc]=premnmx(CrIc);
[slope_G_6n,minslope_G_6,maxslope_G_6]=premnmx(slope_G_6);
for I=1:139,
    network_input_GS (I,1)=Ln(I)'
end
for I=1:139,
    network_input_GS (I,2)=A_Xn(I)'
end
for I=1:139,
    network_input_GS (I,3)=CrIcn(I)'
end
for I=1:139,
    network_input_GS (I,4)=slope_G_6n(I)'
end
[slope_X_6n,minslope_X_6,maxslope_X_6]=premnmx(slope_X_6);
net=newff([min(Ln)max(Ln);min(A_Xn)max(A_Xn);min(CrIc_Xn)
     max(CrIc_Xn);min(slope_G_6n) max(slope_G_6n)], [15 1],
     {'tansig','purelin'},'trainbr');
net.trainParam.show=20;
net.trainParam.epoch=100;
randn('seed',192836547);
```

Exhibit E-17. Continued

```
net.trainParam.goal=.01;
net=init(net);
net=train(net,network_input_GS',slope_X_6n');
net=train(net,network_input_GS',slope_X_6n');
net=train(net,network_input_GS',slope_X_6n');
net=train(net,network_input_GS',slope_X_6n');
net=train(net,network_input_GS',slope_X_6n');
net=init(net);
net=train(net,network_input_GS',slope_X_6n');
net=train(net,network_input_GS',slope_X_6n');
net=train(net,network_input_GS',slope_X_6n');
net=train(net,network_input_GS',slope_X_6n');
net=train(net,network_input_GS',slope_X_6n');
yn=sim(net, network_input_GS');
y=postmnmx(yn,minslope_X_6,maxslope_X_6);
E=slope_X_6'-y;
min(E)
max(abs(E))
perf=mse(E)
[m,b,r]=postreg(y,slope_X_6')
Rsqr=r^2
```

Exhibit E-18. Final weights and biases for 6-h xylan slope network.

IW{1,1}: Weights to layer 1 from input (15×4 matrix)

-0.0459	0.0523	-0.0132	-0.1013
-0.1696	-0.4565	0.7264	0.2691
-0.0459	0.0523	-0.0132	-0.1013
-0.0459	0.0523	-0.0132	-0.1013
-0.0459	0.0523	-0.0132	-0.1013
-0.0459	0.0523	-0.0132	-0.1013
0.0459	-0.0523	0.0132	0.1013
0.4938	0.2635	0.0912	-0.6390
-0.0459	0.0523	-0.0132	-0.1013
0.0459	-0.0522	0.0132	0.1013
0.0459	-0.0523	0.0132	0.1013
-0.0459	0.0523	-0.0132	-0.1013
0.6322	-0.7708	0.3782	0.1083
0.9061	0.0956	-0.3111	-0.3117
0.0459	-0.0523	0.0132	0.1013

b{1}: Bias to layer 1 (15×1 matrix)

0.0047
-0.8230
0.0047
0.0047
0.0047
0.0047
-0.0047
-0.8037
0.0047
-0.0047
-0.0047
0.0047
0.0210
0.1445
-0.0047

LW{2,1}: Weights to layer 2 (1×15 matrix)

[0.1255 0.1255 0.1255 -0.1255 -0.1255 1.4128 0.1255 0.1255 -0.1255 0.1240
0.1255 -0.7701 -0.1254 0.5811 0.9140]

b{2}: Bias to layer 2 (1×1 matrix)

[-0.0353]

Exhibit E-19. Matlab codes for training and simulating 6-h xylan intercept network.

```
clc
clear
load L.m
load A.m
load CrIc_G.m
load intercept_G_6.m
[Ln,minL,maxL]=premnmx(L);
[An,minA,maxA]=premnmx(A);
[CrIc_Gn,minCrIc_G,maxCrIc_G]=premnmx(CrIc_G);
[intercept_G_6n,minintercept_G_6,maxintercept_G_6]=premnmx(
     intercept_G_6);
for I=1:139,
    network_input_GI (I,1)=Ln(I)'
end
for I=1:139,
    network_input_GI (I,2)=An(I)'
end
for I=1:139,
    network_input_GI (I,3)=CrIc_Gn(I)'
end
for I=1:139,
    network_input_GI (I,4)=intercept_G_6n(I)'
end
[intercept_X_6n,minintercept_X_6,maxintercept_X_6]=premnmx(
     intercept_X_6);
net=newff([min(Ln)max(Ln);min(An)max(An);min(CrIc_Gn)
     max(CrIc_Gn);min(intercept_G_6n)  max(intercept_G_6n)],
     [15 1], {'tansig','purelin'},'trainbr');
net.trainParam.show=20;
```

Exhibit E-19. Continued

```
net.trainParam.epoch=100;
randn('seed',192836547);
net.trainParam.goal=.01;
net=init(net);
net=train(net,network_input_GI',intercept_X_6n');
net=train(net,network_input_GI',intercept_X_6n');
net=train(net,network_input_GI',intercept_X_6n');
net=train(net,network_input_GI',intercept_X_6n');
net=init(net);
net=train(net,network_input_GI',intercept_X_6n');
net=train(net,network_input_GI',intercept_X_6n');
net=train(net,network_input_GI',intercept_X_6n');
net=train(net,network_input_GI',intercept_X_6n');
yn=sim(net, network_input_GI');
y=postmnmx(yn,minintercept_X_6,maxintercept_X_6);
E=intercept_X_6'-y;
min(E)
max(abs(E))
perf=mse(E)
[m,b,r]=postreg(y,intercept_X_6')
Rsqr=r^2
```

Exhibit E-20. Final weights and biases for 6-h xylan intercept network.

IW{1,1}: Weights to layer 1 from input (15×4 matrix)

0.0000	0.0000	0.0000	0.0000
0.3525	-0.6052	-0.2994	-0.2302
-0.9090	-0.2653	-0.6298	0.0345
0.9789	0.8875	-0.0536	0.2776
-0.2450	-0.3422	0.6032	0.1695
0.0000	0.0000	0.0000	0.0000
0.0000	0.0000	0.0000	0.0000
0.0000	0.0000	0.0000	0.0000
0.3144	-0.2562	-0.0385	0.3228
0.0000	0.0000	0.0000	0.0000
0.0000	0.0000	0.0000	0.0000
0.0000	0.0000	0.0000	0.0000
0.4987	0.2278	0.3257	-1.0622
0.0000	0.0000	0.0000	0.0000
0.0000	0.0000	0.0000	0.0000

b{1}: Bias to layer 1 (matrix 15×1)

0.0000
0.3865
-0.1991
-0.1274
-0.2354
0.0000
0.0000
0.0000
-0.2235
0.0000
0.0000
0.0000
-0.6924
0.0000
0.0000

LW{2,1}: Weights to layer 2 (1×15 matrix)

[0.0000 -0.6567 -0.6602 -0.8374 -0.5530 -0.0000 -0.0000 -0.0000 0.4282 -0.0000
0.0000 -0.0000 -0.9544 0.0000 0.0000]

b{2}: Bias to layer 2 (1×1 matrix)

[-0.041]

Exhibit E-21. Matlab codes for training and simulating 72-h xylan slope network.

```
clc
clear
load L_X.m
load A_X.m
load CrIc_X.m
load slope_G_72.m
[L_Xn,minL_X,maxL_X]=premnmx(L_X);
[A_Xn,minA_X,maxA_X]=premnmx(A_X);
[CrIc_Xn,minCrIc_X,maxCrIc_X]=premnmx(CrIc_X);
[slope_G_72n,minslope_G_72,maxslope_G_72]=premnmx(slope_G_7
     2);
for I=1:140,
    network_input_GS (I,1)=L_Xn(I)'
end
for I=1:140,
    network_input_GS (I,2)=A_Xn(I)'
end
for I=1:140,
    network_input_GS (I,3)=CrIc_Xn(I)'
end
for I=1:140,
    network_input_GS (I,4)=slope_G_72n(I)'
end
[slope_X_72n,minslope_X_72,maxslope_X_72]=premnmx(slope_X_7
     2);
net=newff([min(L_Xn)max(L_Xn);min(A_Xn)max(A_Xn);min(CrIc_X
     n)max(CrIc_Xn);min(slope_G_72n)max(slope_G_72n)],[15
     1], {'tansig','purelin'},'trainbr');
net.trainParam.show=20;
```

Exhibit E-21. Continued

```
net.trainParam.epoch=100;
randn('seed',192836547);
net.trainParam.goal=.01;
net=init(net);
net=train(net,network_input_GS',slope_X_72n');
net=train(net,network_input_GS',slope_X_72n');
net=train(net,network_input_GS',slope_X_72n');
net=train(net,network_input_GS',slope_X_72n');
net=init(net);
net=train(net,network_input_GS',slope_X_72n');
net=train(net,network_input_GS',slope_X_72n');
net=train(net,network_input_GS',slope_X_72n');
net=train(net,network_input_GS',slope_X_72n');
yn=sim(net, network_input_GS');
y=postmnmx(yn,minslope_X_72,maxslope_X_72);
E=slope_X_72'-y;
min(E)
max(abs(E))
perf=mse(E)
[m,b,r]=postreg(y,slope_X_72')
Rsqr=r^2
```

Exhibit E-22. Final weights and biases for 72-h xylan slope network.

IW{1,1}: Weights to layer 1 from input (15×4 matrix)

0.0600	-0.0870	0.0137	-0.0606
-0.0600	0.0870	-0.0137	0.0606
0.9704	-0.2968	-0.2111	-0.0698
0.0600	-0.0870	0.0137	-0.0606
0.4326	0.5520	0.6865	0.3931
0.0600	-0.0870	0.0137	-0.0606
0.0600	-0.0870	0.0137	-0.0606
-0.7837	0.3041	-0.7967	-1.1349
-0.0600	0.0870	-0.0137	0.0606
0.0600	-0.0870	0.0137	-0.0606
1.1056	0.2392	0.2976	-0.8763
0.0600	-0.0870	0.0137	-0.0606
0.0600	-0.0870	0.0137	-0.0606
-0.6199	0.3813	-0.7095	0.6782
0.0600	-0.0870	0.0137	-0.0606

b{1}: Bias to layer 1 (matrix 15×1)

-0.0343
0.0343
0.3806
-0.0343
0.0467
-0.0343
-0.0343
0.6077
0.0343
-0.0343
0.2789
-0.0343
-0.0343
0.8416
-0.0343

LW{2,1}: Weights to layer 2 (1×15 matrix)

[0.1330 -0.1330 0.7767 -0.1330 -0.7899 0.6386 -1.2048 0.1330 0.1330 0.1330 -0.9055 0.1330 0.1330 -0.1330 0.1330]

b{2}: Bias to layer 2 (1×1 matrix)

[0.2811]

Exhibit E-23. Matlab codes for training and simulating 72-h xylan intercept network.

```
clc
clear
load L_X.m
load A.m
load X.m
load CrIc.m
load intercept_G_72.m
[L_Xn,minL_X,maxL_X]=premnmx(L_X);
[An,minA,maxA]=premnmx(A);
[Xn,minX,maxX]=premnmx(X);
[CrIcn,minCrIc,maxCrIc]=premnmx(CrIc);
[intercept_G_72n,minintercept_G_72,maxintercept_G_72]=premn
     mx(intercept_G_72);
for I=1:140,
    network_input_GI (I,1)=CrIcn(I)'
end
for I=1:140,
    network_input_GI (I,2)=L_Xn(I)'
end
for I=1:140,
    network_input_GI (I,3)=An(I)'
end
for I=1:140,
    network_input_GI (I,4)=Xn(I)'
end
for I=1:140,
    network_input_GI (I,5)=intercept_G_72n(I)'
end
```

Exhibit E-23. Continued

```
[intercept_X_72n,minintercept_X_72,maxintercept_X_72]=premn
     mx(intercept_X_72);
net=newff([min(CrIcn)max(CrIcn);min(L_Xn)max(L_Xn);min(An)m
   ax(An);min(Xn)max(Xn);min(intercept_G_72n)max(intercept_
   G_72n)], [15 1], {'tansig','purelin'},'trainbr');
net.trainParam.show=20;
net.trainParam.epoch=100;
randn('seed',192836547);
net.trainParam.goal=.01;
net=init(net);
net=train(net,network_input_GI',intercept_X_72n');
net=train(net,network_input_GI',intercept_X_72n');
net=train(net,network_input_GI',intercept_X_72n');
net=train(net,network_input_GI',intercept_X_72n');
net=init(net);
net=train(net,network_input_GI',intercept_X_72n');
net=train(net,network_input_GI',intercept_X_72n');
net=train(net,network_input_GI',intercept_X_72n');
net=train(net,network_input_GI',intercept_X_72n');
yn=sim(net, network_input_GI');
y=postmnmx(yn,minintercept_X_72,maxintercept_X_72);
E=intercept_X_72'-y;
min(E)
max(abs(E))
perf=mse(E)
[m,b,r]=postreg(y,intercept_X_72')
Rsqr=r^2
```

Exhibit E-24. Final weights and biases for 72-h xylan intercept network.

IW{1,1}: Weights to layer 1 from input (15×5 matrix)

0.0502	0.0034	-0.0197	0.0095	-0.0034
-0.0471	-0.0031	0.0184	-0.0089	0.0032
-0.0641	-0.0047	0.0255	-0.0116	0.0046
0.1987	0.5397	-0.6408	-0.1225	-0.5739
-0.2296	0.2880	-0.2293	0.3777	0.7244
-0.0752	-0.0058	0.0302	-0.0131	0.0057
-0.0582	-0.6319	0.0478	-0.2003	0.5218
-0.1299	-1.1060	-0.4965	-0.1679	0.4196
-0.4052	-0.0102	0.2484	0.0197	0.1044
0.2469	0.4308	0.9953	0.3058	-0.1262
-0.0511	-0.0035	0.0200	-0.0096	0.0035
0.0039	-0.4263	-0.0675	0.8588	0.3914
-0.1378	-0.3920	-0.4108	-0.6054	0.4999
0.0513	0.0035	-0.0201	0.0096	-0.0035
-0.0613	-0.0044	0.0243	-0.0112	0.0044

b{1}: Bias to layer 1 (15×1 matrix)

-0.0128
0.0119
0.0166
0.2132
0.5271
0.0198
-0.5971
0.5143
0.0898
-0.5758
0.0130
0.3694
0.0068
-0.0131
0.0158

LW{2,1}: Weights to layer 2 (1×15 matrix)

[0.5933 -0.6262 -0.0497 0.0543 -0.4578 0.0429 -0.1093 0.7166 -0.6465 -0.0403
-0.7663 0.0758 -1.1401 0.0586 0.5021]

b{2}: Bias to layer 2 (1×1 matrix)

[-0.2196]

Exhibit E-25. Matlab codes for training and simulating 1-h total sugar slope network.

```
clc
clear
load L_TS.m
load A_TS.m
load TS.m
load CrIc_TS.m
load slope_TS_1.m
[L_TSn,minL_TS,maxL_TS]=premnmx(L_TS);
[A_TSn,minA_TS,maxA_TS]=premnmx(A_TS);
[TSn,minTS,maxTS]=premnmx(TS);
[CrIc_TSn,minCrIc_TS,maxCrIc_TS]=premnmx(CrIc_TS);
for I=1:146,
    network_input_GS (I,1)=L_TSn(I)'
end
for I=1:146,
    network_input_GS (I,2)=A_TSn(I)'
end
for I=1:146,
    network_input_GS (I,3)=CrIc_TSn(I)'
end
for I=1:146,
    network_input_GS (I,4)=TSn(I)'
end
[slope_TS_1n,minslope_TS_1,maxslope_TS_1]=premnmx(slope_TS_
     1);
net=newff([min(L_TSn)max(L_TSn);min(A_TSn)max(A_TSn);min(Cr
     Ic_TSn)max(CrIc_TSn);min(TSn)max(TSn)],[15   1],{'tansi
     g','purelin'},'trainbr');
net.trainParam.show=20;
```

Exhibit E-25. Continued

```
net.trainParam.epoch=100;
randn('seed',192836547);
net.trainParam.goal=.01;
net=init(net);
net=train(net,network_input_GS',slope_TS_1n');
net=train(net,network_input_GS',slope_TS_1n');
net=train(net,network_input_GS',slope_TS_1n');
net=train(net,network_input_GS',slope_TS_1n');
net=train(net,network_input_GS',slope_TS_1n');
net=init(net);
net=train(net,network_input_GS',slope_TS_1n');
net=train(net,network_input_GS',slope_TS_1n');
net=train(net,network_input_GS',slope_TS_1n');
net=train(net,network_input_GS',slope_TS_1n');
net=train(net,network_input_GS',slope_TS_1n');
yn=sim(net, network_input_GS');
y=postmnmx(yn,minslope_TS_1,maxslope_TS_1);
E=slope_TS_1'-y;
min(E)
max(abs(E))
perf=mse(E)
[m,b,r]=postreg(y,slope_TS_1')
Rsqr=r^2
```

Exhibit E-26. Final weights and biases for 1-h total sugar slope network.

IW{1,1}: Weights to layer 1 from input (15×4 matrix)

0.0261	-0.0489	0.1466	-0.2310
0.0261	-0.0489	0.1466	-0.2310
0.0261	-0.0489	0.1466	-0.2310
0.0261	-0.0489	0.1466	-0.2310
0.0261	-0.0489	0.1466	-0.2310
-0.0261	0.0489	-0.1466	0.2310
0.0261	-0.0489	0.1466	-0.2310
-0.0261	0.0489	-0.1466	0.2310
0.5967	0.0493	1.1589	-0.3651
0.0261	-0.0489	0.1466	-0.2310
-1.0515	0.0197	-0.1583	0.0638
0.4685	-0.1937	-1.6905	0.3269
0.0261	-0.0489	0.1466	-0.2310
0.0261	-0.0489	0.1466	-0.2310
-0.0261	0.0489	-0.1466	0.2310

b{1}: Bias to layer 1 (15×1 matrix)

-0.0196
-0.0196
-0.0196
-0.0196
-0.0196
0.0196
-0.0196
0.0196
0.4332
-0.0196
0.5069
0.3648
-0.0196
-0.0196
0.0196

LW{2,1}: Weights to layer 2 (1×15 matrix)

[0.3241 0.3241 0.3241 0.3241 -0.3241 -0.3241 0.7965 -0.3241 0.3241 0.8419 -0.6041 0.3241 0.5053 0.3241 -0.3241]

b{2}: Bias to layer 2 (1×1 matrix)

[-0.2253]

Exhibit E-27. Matlab codes for training and simulating 1-h total sugar intercept network.

```
clc
clear
load L.m
load A_X.m
load TS.m
load CrIc.m
load intercept_TS_1.m
[Ln,minL,maxL]=premnmx(L);
[A_Xn,minA_X,maxA_X]=premnmx(A_X);
[TSn,minTS,maxTS]=premnmx(TS);
[CrIcn,minCrIc,maxCrIc]=premnmx(CrIc);
for I=1:146,
    network_input_GS (I,1)=CrIcn(I)'
end
for I=1:146,
    network_input_GS (I,2)=A_Xn(I)'
end
for I=1:146,
    network_input_GS (I,3)=Ln(I)'
end
for I=1:146,
    network_input_GS (I,4)=TSn(I)'
end
[intercept_TS_1n,minintercept_TS_1,maxintercept_TS_1]=premn
     mx(intercept_TS_1);
net=newff([min(CrIcn)max(CrIcn);min(A_Xn)  max(A_Xn);min(Ln)
     max(Ln);min(TSn)max(TSn)],[15 1],{'tansig','purelin'},
     'trainbr');
```

Exhibit E-27. Continued

```
net.trainParam.show=20;
net.trainParam.epoch=100;
randn('seed',192836547);
net.trainParam.goal=.01;
net=init(net);
net=train(net,network_input_GS',intercept_TS_1n');
net=train(net,network_input_GS',intercept_TS_1n');
net=train(net,network_input_GS',intercept_TS_1n');
net=train(net,network_input_GS',intercept_TS_1n');
net=train(net,network_input_GS',intercept_TS_1n');
net=init(net);
net=train(net,network_input_GS',intercept_TS_1n');
net=train(net,network_input_GS',intercept_TS_1n');
net=train(net,network_input_GS',intercept_TS_1n');
net=train(net,network_input_GS',intercept_TS_1n');
net=train(net,network_input_GS',intercept_TS_1n');
yn=sim(net, network_input_GS');
y=postmnmx(yn,minintercept_TS_1,maxintercept_TS_1);
E=intercept_TS_1'-y;
min(E)
max(abs(E))
perf=mse(E)
[m,b,r]=postreg(y,intercept_TS_1')
Rsqr=r^2
```

Exhibit E-28. Final weights and biases for 1-h total sugar intercept network.

IW{1,1}: Weights to layer 1 from input (15×4 matrix)

0.1400	0.6941	0.3669	-0.4279
-0.4324	0.1885	0.2232	-0.5597
-0.4494	-0.6915	0.2500	-0.0752
-0.0458	-0.0034	-0.0284	0.0088
0.0459	0.0034	0.0284	-0.0088
-0.3918	-0.7677	-0.4788	-0.4738
-1.1135	-0.0137	-0.4477	0.0510
0.0461	0.0034	0.0286	-0.0089
0.0423	0.0031	0.0263	-0.0082
-0.0459	-0.0034	-0.0285	0.0088
-0.0458	-0.0034	-0.0284	0.0088
-0.0457	-0.0034	-0.0283	0.0088
-1.2915	0.0360	0.0184	1.0227
0.0457	0.0034	0.0283	-0.0088
-0.0455	-0.0033	-0.0282	0.0088

b{1}: Bias to layer 1 (15×1 matrix)

0.0170
0.5309
0.0965
-0.0230
0.0230
-0.8075
0.2900
0.0231
0.0212
-0.0230
-0.0230
-0.0229
-0.5036
0.0229
-0.0228

LW{2,1}: Weights to layer 2 (1×15 matrix)

[0.0582 -0.0597 -1.0321 1.0266 0.0595 -0.5516 0.0591 -0.0592 0.0598 -0.6463 -0.7123 -1.1192 -0.0585 -0.0599 0.0581]

b{2}: Bias to layer 2 (1×1 matrix)

[-0.3918]

Exhibit E-29. Matlab codes for training and simulating 6-h total sugar slope network.

```
clc
clear
load L.m
load A.m
load A_X.m
load CrIc.m
load slope_TS_6.m
[Ln,minL,maxL]=premnmx(L);
[An,minA,maxA]=premnmx(A);
[CrIcn,minCrIc,maxCrIc]=premnmx(CrIc);
for I=1:147,
    network_input_GS (I,1)=CrIcn(I)'
end
for I=1:147,
    network_input_GS (I,2)=An(I)'
end
for I=1:147,
    network_input_GS (I,3)=Ln(I)'
end
[slope_TS_6n,minslope_TS_6,maxslope_TS_6]=premnmx(slope_TS_
     6);
net=newff([min(CrIcn)max(CrIcn);min(An)max(An);min(Ln)
     max(Ln)], [15 1], {'tansig','purelin'},'trainbr');
net.trainParam.show=20;
net.trainParam.epoch=100;
randn('seed',192836547);
net.trainParam.goal=.01;
net=init(net);
net=train(net,network_input_GS',slope_TS_6n');
```

Exhibit E-29. Continued

```
net=train(net,network_input_GS',slope_TS_6n');
net=train(net,network_input_GS',slope_TS_6n');
net=train(net,network_input_GS',slope_TS_6n');
net=init(net);
net=train(net,network_input_GS',slope_TS_6n');
net=train(net,network_input_GS',slope_TS_6n');
net=train(net,network_input_GS',slope_TS_6n');
net=train(net,network_input_GS',slope_TS_6n');
yn=sim(net, network_input_GS');
y=postmnmx(yn,minslope_TS_6,maxslope_TS_6);
E=slope_TS_6'-y;
min(E)
max(abs(E))
perf=mse(E)
[m,b,r]=postreg(y,slope_TS_6')
Rsqr=r^2
```

Exhibit E-30. Final weights and biases for 6-h total sugar slope network.

IW{1,1}: Weights to layer 1 from input (15×3 matrix)

0.0880	-0.0739	-0.0494
-0.5174	-1.1221	0.1298
-0.0880	0.0739	0.0494
0.6064	0.1241	1.2518
0.6737	0.5363	-1.7033
-2.0658	0.3780	0.7873
-0.7265	0.5354	-0.4888
-1.0666	0.3937	0.8681
-1.3185	0.1071	-1.2448
-1.0236	-0.2306	1.1095
0.0880	-0.0739	-0.0494
0.0880	-0.0739	-0.0494
-0.0880	0.0739	0.0494
-0.0880	0.0739	0.0494
0.1253	0.4971	-1.2270

Exhibit E-30. Continued

b{1}: Bias to layer 1 (15×1 matrix)

```
 0.1969
-0.1095
-0.1969
 0.4932
-1.5270
-0.0266
 0.2783
 0.3473
 0.1597
 2.1698
 0.1969
 0.1969
-0.1969
-0.1969
 0.6366
```

LW{2,1}: Weights to layer 2 (1×15 matrix)

```
[-0.2449   0.4136   0.2449   1.0718   1.0706   0.8153   -0.8025  -0.9100  0.8433   1.9239
 -0.2449   -0.2449   0.2449   0.2449   0.9704]
```

b{2}: Bias to layer 2 (1×1 matrix)

```
[-0.8848]
```

Exhibit E-31. Matlab codes for training and simulating 6-h total sugar intercept network.

```
clc
clear
load L.m
load A.m
load TS.m
load CrIc.m
load intercept_TS_6.m
[Ln,minL,maxL]=premnmx(L);
[An,minA,maxA]=premnmx(A);
[TSn,minTS,maxTS]=premnmx(TS);
```

Exhibit E-31. Continued

```
[CrIcn,minCrIc,maxCrIc]=premnmx(CrIc);
for I=1:147,
    network_input_GS (I,1)=An(I)'
end
for I=1:147,
    network_input_GS (I,2)=CrIcn(I)'
end
for I=1:147,
    network_input_GS (I,3)=Ln(I)'
end
for I=1:147,
    network_input_GS (I,4)=TSn(I)'
end
[intercept_TS_6n,minintercept_TS_6,maxintercept_TS_6]=premn
     mx(intercept_TS_6);
net=newff([min(An)max(An);min(CrIcn)max(CrIcn);min(Ln)
     max(Ln);min(TSn)max(TSn)],[15 1],{'tansig','purelin'},
     'trainbr');
net.trainParam.show=20;
net.trainParam.epoch=100;
randn('seed',192836547);
net.trainParam.goal=.01;
net=init(net);
net=train(net,network_input_GS',intercept_TS_6n');
net=train(net,network_input_GS',intercept_TS_6n');
net=train(net,network_input_GS',intercept_TS_6n');
net=train(net,network_input_GS',intercept_TS_6n');
net=train(net,network_input_GS',intercept_TS_6n');
net=init(net);
```

Exhibit E-31. Continued

```
net=train(net,network_input_GS',intercept_TS_6n');
net=train(net,network_input_GS',intercept_TS_6n');
net=train(net,network_input_GS',intercept_TS_6n');
net=train(net,network_input_GS',intercept_TS_6n');
net=train(net,network_input_GS',intercept_TS_6n');
yn=sim(net, network_input_GS');
y=postmnmx(yn,minintercept_TS_6,maxintercept_TS_6);
E=intercept_TS_6'-y;
min(E)
max(abs(E))
perf=mse(E)
[m,b,r]=postreg(y,intercept_TS_6')
Rsqr=r^2
```

Exhibit E-32. Final weights and biases for 6-h total sugar intercept network.

IW{1,1}: Weights to layer 1 from input (15×4 matrix)

-0.0716	0.0126	0.0219	-0.0275
0.1269	0.8119	-1.0444	-0.1820
0.0710	-0.0124	-0.0218	0.0273
0.0714	-0.0125	-0.0219	0.0274
0.2935	1.0084	0.0121	-0.6272
1.1317	0.0713	0.1808	0.2700
0.9558	-0.6006	-0.0376	-0.2893
0.0713	-0.0125	-0.0218	0.0274
0.0710	-0.0124	-0.0217	0.0273
0.0714	-0.0125	-0.0219	0.0275
0.1542	0.3110	-0.6824	0.6496
0.5006	0.4087	-0.7677	-1.0859
0.0714	-0.0125	-0.0219	0.0275
0.0712	-0.0124	-0.0218	0.0274
0.0713	-0.0125	-0.0218	0.0274

Exhibit E-32. Continued

b{1}: Bias to layer 1 (15×1 matrix)

```
-0.0575
 0.2669
 0.0570
 0.0573
-0.3817
 0.4847
 0.7264
 0.0572
 0.0570
 0.0573
 0.8338
 0.0002
 0.0573
 0.0572
 0.0572
```

LW{2,1}: Weights to layer 2 (1×15 matrix)

```
[0.0999  -0.8299  -0.0991  -0.0996  -0.7567  -1.0153   0.5072  -0.0994  -0.0990  -0.0996
 1.0085   1.1252  -0.0996  -0.0993  -0.0994]
```

b{2}: Bias to layer 2 (1×1 matrix)

```
[-0.6043]
```

Exhibit E-33. Matlab codes for training and simulating 72-h total sugar slope network.

```
clc
clear
load L.m
load A_X.m
load TS.m
load CrIc.m
load slope_TS_72.m
[Ln,minL,maxL]=premnmx(L);
[A_Xn,minA_X,maxA_X]=premnmx(A_X);
[TSn,minTS,maxTS]=premnmx(TS);
[CrIcn,minCrIc,maxCrIc]=premnmx(CrIc);
```

Exhibit E-33. Continued

```
for I=1:139,
    network_input_GS (I,1)=CrIc_Gn(I)'
end
for I=1:139,
    network_input_GS (I,2)=A_Xn(I)'
end
for I=1:139,
    network_input_GS (I,3)=Ln(I)'
end
for I=1:139,
    network_input_GS (I,4)=TSn(I)'
end
[slope_TS_72n,minslope_TS_72,maxslope_TS_72]=premnmx(slope_
     TS_72);
net=newff([min(CrIc_Gn)max(CrIc_Gn);min(A_Xn)max(A_Xn);min(
     Ln)max(Ln);min(TSn)max(TSn)],[15 1],{'tansig','purelin
     '},'trainbr');
net.trainParam.show=20;
net.trainParam.epoch=100;
randn('seed',192836547);
net.trainParam.goal=.01;
net=init(net);
net=train(net,network_input_GS',slope_TS_72n');
net=train(net,network_input_GS',slope_TS_72n');
net=train(net,network_input_GS',slope_TS_72n');
net=train(net,network_input_GS',slope_TS_72n');
net=train(net,network_input_GS',slope_TS_72n');
net=init(net);
net=train(net,network_input_GS',slope_TS_72n');
```

Exhibit E-33. Continued

```
net=train(net,network_input_GS',slope_TS_72n');
net=train(net,network_input_GS',slope_TS_72n');
net=train(net,network_input_GS',slope_TS_72n');
net=train(net,network_input_GS',slope_TS_72n');
yn=sim(net, network_input_GS');
y=postmnmx(yn,minslope_TS_72,maxslope_TS_72);
E=slope_TS_72'-y;
min(E)
max(abs(E))
perf=mse(E)
[m,b,r]=postreg(y,slope_TS_72')
Rsqr=r^2
```

Exhibit E-34. Final weights and biases for 72-h total sugar slope network.

IW{1,1}: Weights to layer 1 from input (15×4 matrix)

0.0000	0.0000	0.0000	0.0000
0.0000	0.0000	0.0000	0.0000
0.3193	-0.6398	-0.0466	-0.4409
0.6151	0.9804	-0.2133	-0.2346
0.1777	-0.0774	0.8437	-0.2819
0.0000	0.0000	0.0000	0.0000
0.0000	0.0000	0.0000	0.0000
0.0000	0.0000	0.0000	0.0000
0.0000	0.0000	0.0000	0.0000
0.0000	0.0000	0.0000	0.0000
-0.5208	0.5320	0.4474	-0.3099
0.0000	0.0000	0.0000	0.0000
0.0000	0.0000	0.0000	0.0000
-0.3212	-0.5746	-0.8766	0.4227
0.0000	0.0000	0.0000	0.0000

Exhibit E-34. Continued

b{1}: Bias to layer 1 (15×1 matrix)

```
 0.0000
 0.0000
 0.3158
 0.2188
-0.6896
 0.0000
 0.0000
 0.0000
 0.0000
 0.0000
 0.1092
 0.0000
 0.0000
-0.3465
 0.0000
```

LW{2,1}: Weights to layer 2 (1×15 matrix)

```
[0.0000   0.0000  -0.8421  -0.5745  -0.9434  -0.0000   0.0000  0.0000   0.0000   0.0000
-0.7929   0.0000   0.0000  -0.7941  0.0000]
```

b{2}: Bias to layer 2 (1×1 matrix)

```
[-0.0226]
```

Exhibit E-35. Matlab codes for training and simulating 72-h total sugar intercept network.

```
clc
clear
load L.m
load A.m
load TS.m
load CrIc.m
load intercept_TS_72.m
[Ln,minL,maxL]=premnmx(L);
[An,minA,maxA]=premnmx(A);
[TSn,minTS,maxTS]=premnmx(TS);
```

Exhibit E-35. Continued

```
[CrIcn,minCrIc,maxCrIc]=premnmx(CrIc);
for I=1:139,
    network_input_GS (I,1)=CrIcn(I)'
end
for I=1:139,
    network_input_GS (I,2)=An(I)'
end
for I=1:139,
    network_input_GS (I,3)=Ln(I)'
end
for I=1:139,
    network_input_GS (I,4)=TSn(I)'
end
[intercept_TS_72n,minintercept_TS_72,maxintercept_TS_72]=pr
     emnmx(intercept_TS_72);
net=newff([min(CrIcn) max(CrIcn);min(An) max(An);min(Ln)
     max(Ln);min(TSn) max(TSn)], [15 1],
     {'tansig','purelin'},'trainbr');
net.trainParam.show=20;
net.trainParam.epoch=100;
randn('seed',192836547);
net.trainParam.goal=.01;
net=init(net);
net=train(net,network_input_GS',intercept_TS_72n');
net=train(net,network_input_GS',intercept_TS_72n');
net=train(net,network_input_GS',intercept_TS_72n');
net=train(net,network_input_GS',intercept_TS_72n');
net=train(net,network_input_GS',intercept_TS_72n');
net=init(net);
```

Exhibit E-35. Continued

```
net=train(net,network_input_GS',intercept_TS_72n');
net=train(net,network_input_GS',intercept_TS_72n');
net=train(net,network_input_GS',intercept_TS_72n');
net=train(net,network_input_GS',intercept_TS_72n');
net=train(net,network_input_GS',intercept_TS_72n');
yn=sim(net, network_input_GS');
y=postmnmx(yn,minintercept_TS_72,maxintercept_TS_72);
E=intercept_TS_72'-y;
min(E)
max(abs(E))
perf=mse(E)
[m,b,r]=postreg(y,intercept_TS_72')
Rsqr=r^2
```

Exhibit E-36. Final weights and biases for 72-h total sugar intercept network.

IW{1,1}: Weights to layer 1 from input (15×4 matrix)

0.1489	0.1695	0.9000	-0.9989
-0.0079	-0.0573	-0.0719	0.1298
-0.3851	-0.2054	-0.3089	0.2815
0.6674	-0.3497	0.3378	-0.1941
-0.2157	-1.7140	0.0730	-0.1164
0.0079	0.0573	0.0719	-0.1298
-0.6493	1.3668	-0.0378	0.0637
0.0079	0.0573	0.0719	-0.1298
-0.8914	0.3769	0.0767	0.3710
0.6122	0.0658	-1.2505	-0.2043
0.0079	0.0573	0.0719	-0.1298
-0.0079	-0.0573	-0.0719	0.1298
1.8894	0.3735	0.3977	-0.1343
-0.2615	-0.7853	1.0453	0.3670
-0.0079	-0.0573	-0.0719	0.1298

Exhibit E-36. Continued

b{1}: Bias to layer 1 (15×1 matrix)

```
-1.1428
-0.0003
 0.2361
 0.4005
-0.4969
 0.0003
 0.8888
 0.0003
 0.5122
 0.6771
 0.0003
-0.0003
-0.8043
-0.5978
-0.0003
```

LW{2,1}: Weights to layer 2 (1×15 matrix)

```
[-1.0951   -0.1707   -0.5722   -0.6809    0.8878    0.1707    0.7241  0.1707   -1.1857   -0.7744
  0.1707   -0.1707   -0.7296   -0.9122  -0.1707]
```

b{2}: Bias to layer 2 (1×1 matrix)

```
[-0.0223]
```

APPENDIX F

NETWORK-SIMULATED SLOPES AND INTERCEPTS

Table F-1. Net-simulated glucan slopes and intercepts.

Sample No.	1 h		Sample No.	6 h		Sample No.	72 h	
	slope	intercept		slope	intercept		slope	intercept
1	0.60	0.81	1	1.07	1.12	1	1.22	6.66
2	7.78	3.28	2	9.37	13.88	2	6.05	37.67
3	10.33	3.20	3	14.44	16.21	3	9.95	50.89
4	0.84	0.45	4	1.67	1.31	4	1.70	4.89
5	7.96	2.98	5	9.76	14.19	5	5.84	32.41
6	10.53	3.19	6	13.50	16.98	6	8.92	45.90
7	0.46	0.30	7	1.27	0.92	7	1.40	3.68
8	8.83	3.23	8	10.51	15.40	8	6.51	36.19
9	10.50	3.30	9	13.47	16.88	9	8.94	43.49
10	1.40	0.32	10	1.45	3.08	10	2.40	5.67
11	10.26	3.44	11	12.13	17.59	11	7.13	38.35
12	11.19	3.55	12	13.74	18.33	12	8.48	40.97
13	2.37	0.65	13	2.07	4.17	13	3.94	10.10
14	9.39	3.40	14	11.35	17.65	14	6.18	48.84
15	13.38	4.21	15	17.31	20.98	15	11.01	53.11
16	2.48	0.56	16	2.86	2.50	16	6.51	5.85
17	13.11	4.85	17	15.07	22.34	17	9.70	58.44
18	14.95	4.90	18	18.02	23.49	18	12.11	59.91
19	2.52	0.70	19	5.38	0.34	19	11.67	6.40
20	12.61	5.43	20	15.68	20.75	20	11.93	44.98
21	13.64	5.78	21	16.06	22.70	21	12.21	49.18
22	1.07	0.25	22	2.64	1.05	22	3.65	6.03
23	10.56	3.34	23	13.92	17.53	23	9.43	44.72
24	13.78	2.43	24	19.70	21.67	24	14.64	61.35
25	1.35	0.47	25	2.95	1.20	25	4.94	7.25
26	12.96	3.32	26	18.16	20.43	26	13.46	58.49
27	13.42	3.15	27	18.95	21.03	27	14.19	60.72
28	1.57	0.43	28	3.35	2.11	28	5.25	7.57
29	12.00	3.50	29	16.35	19.50	29	11.73	52.38
30	13.83	3.10	30	19.02	21.86	30	14.25	61.11
31	1.79	0.54	31	3.57	2.65	31	5.97	8.27
32	11.24	3.46	32	16.03	18.98	32	11.46	48.97
33	12.56	3.42	33	17.54	20.67	33	12.77	55.19
34	3.04	0.92	34	5.44	5.96	34	7.14	13.68
35	12.79	3.74	35	16.80	20.98	35	12.04	52.83
36	15.20	3.50	36	19.86	23.88	36	14.97	63.17
37	2.91	0.51	37	6.09	4.46	37	8.90	12.54
38	14.99	4.33	38	19.37	23.87	38	14.04	61.49
39	15.93	4.27	39	20.48	24.94	39	15.09	64.44
40	4.59	0.94	40	15.54	5.17	40	18.90	31.38
41	17.95	6.59	41	22.01	30.46	41	19.03	69.58
42	20.25	6.85	42	21.51	36.51	42	19.28	79.65
43	2.17	0.78	43	4.13	3.55	43	7.40	10.12

Table F-1. Continued

Sample No.	1 h		Sample No.	6 h		Sample No.	72 h	
	slope	intercept		slope	intercept		slope	intercept
44	13.79	3.46	44	19.50	22.46	44	14.84	62.15
45	14.48	3.27	45	20.27	23.50	46	8.19	10.47
46	2.46	0.88	46	4.27	4.22	47	14.39	58.22
47	13.13	3.49	47	19.70	21.93	48	17.18	69.56
48	15.67	2.80	48	21.83	26.14	49	8.37	11.28
49	2.43	0.86	49	4.43	4.09	50	13.47	53.43
50	11.86	3.65	50	18.17	19.98	52	10.45	16.39
51	11.86	3.65	51	18.17	19.98	53	15.40	60.47
52	2.82	0.93	52	5.87	4.90	54	16.51	66.03
53	13.06	3.75	53	20.12	21.72	55	10.30	18.78
54	14.51	3.67	54	21.24	23.83	56	15.18	62.78
55	2.67	0.45	55	6.71	4.39	57	15.74	65.13
56	13.97	3.85	56	19.73	22.93	58	13.30	25.76
57	14.68	3.83	57	20.26	23.92	59	15.98	68.16
58	4.28	0.94	58	10.04	6.57	60	20.68	83.95
59	15.11	4.70	59	21.06	24.55	61	21.57	46.03
60	20.56	4.21	60	24.27	32.92	62	21.50	73.95
61	6.51	1.78	61	19.35	7.49	64	11.63	19.21
62	19.35	6.99	62	24.06	32.48	65	17.09	66.73
63	23.14	6.91	63	22.20	46.02	66	20.71	81.11
64	2.80	0.75	64	6.45	4.44	67	13.02	22.58
65	14.64	3.73	65	21.87	23.94	68	16.51	59.68
66	18.41	2.74	66	23.27	31.03	70	14.09	28.18
67	2.87	0.62	67	7.29	4.14	71	18.49	71.51
68	12.64	3.77	68	21.12	20.77	72	21.91	85.28
69	19.06	2.78	69	23.43	32.23	73	15.32	28.32
70	3.51	0.74	70	9.32	5.43	74	19.43	70.98
71	16.23	4.14	71	22.76	25.60	75	21.86	81.23
72	20.05	3.30	72	23.53	32.90	76	15.44	30.54
73	3.40	0.86	73	9.26	4.88	77	19.77	73.91
74	15.92	3.99	74	23.84	24.85	78	22.37	84.70
75	19.30	3.34	75	24.05	31.34	79	17.69	37.63
76	3.46	0.67	76	10.37	4.93	80	20.71	77.08
77	17.12	3.96	77	23.59	27.03	81	21.38	79.92
78	20.22	3.19	78	23.26	33.67	82	23.06	52.28
79	4.24	0.81	79	14.39	5.81	83	23.95	79.49
80	18.36	4.31	80	23.97	28.76	84	23.81	85.44
81	19.43	4.17	81	23.67	30.92	85	18.82	34.11
82	7.57	1.87	82	23.35	8.63	86	22.84	78.27
83	19.53	6.57	83	25.51	31.64	87	24.84	87.59
84	21.70	6.96	84	24.75	37.91	88	19.39	36.09
85	4.65	1.77	85	13.28	6.80	89	21.91	74.07
86	19.20	3.72	86	25.44	29.45	90	22.13	75.17
87	21.74	2.86	87	23.46	36.45	91	19.50	36.61
88	4.31	1.28	88	14.45	5.60	92	22.11	75.65
89	17.56	3.95	89	25.29	26.44	94	20.38	39.41
90	18.05	3.89	90	25.18	27.36	95	22.23	76.02
91	4.17	1.14	91	14.07	5.12	96	24.58	88.14
92	18.06	4.16	92	25.33	26.96	97	21.14	43.64

Table F-1. Continued

Sample No.	1 h		Sample No.	6 h		Sample No.	72 h	
	slope	intercept		slope	intercept		slope	intercept
93	21.70	3.23	93	23.12	35.73	98	22.54	80.25
94	4.59	1.25	94	16.13	5.58	100	22.04	44.69
95	18.01	4.32	95	25.35	26.69	102	23.67	84.30
96	21.92	3.39	96	22.60	36.10	103	23.53	54.82
97	4.56	0.87	97	18.12	4.90	104	25.59	83.02
98	18.93	4.72	98	25.27	28.29	105	25.87	90.39
99	18.93	4.72	99	25.27	28.29	106	25.37	46.16
100	4.36	0.77	100	19.28	4.38	107	24.77	83.17
101	19.60	4.31	101	24.26	30.11	108	25.03	85.58
102	20.44	4.13	102	23.55	32.07	109	26.16	45.42
103	7.54	1.99	103	24.00	9.20	110	24.60	79.08
104	17.95	5.81	104	26.33	26.93	111	25.30	87.58
105	21.31	6.11	105	25.55	35.39	112	25.54	46.67
106	4.95	1.40	106	20.53	4.22	113	24.38	78.39
107	20.43	4.36	107	25.15	30.36	114	25.09	86.12
108	21.27	4.06	108	24.36	32.44	115	25.87	46.62
109	4.50	1.28	109	18.82	4.24	116	24.49	78.42
110	17.63	3.97	110	26.16	25.63	117	25.27	87.80
111	21.11	2.90	111	23.92	33.42	118	25.69	46.39
112	4.68	1.26	112	19.89	4.68	120	24.69	78.20
113	16.81	4.39	113	25.55	24.69	121	24.79	46.68
114	20.84	3.41	114	23.74	32.72	122	25.16	78.19
115	4.59	1.35	115	20.03	4.57	123	25.42	80.62
116	16.62	4.38	116	25.68	24.56	124	25.54	62.72
117	21.13	3.22	117	23.44	33.65	125	29.28	84.93
118	4.42	1.12	118	19.27	4.77	126	29.31	86.92
119	16.86	4.36	119	25.45	25.08	127	26.66	39.93
120	18.16	4.15	120	25.47	27.06	128	25.20	69.05
121	5.30	1.69	121	20.95	6.54	130	27.02	38.45
122	19.12	4.85	122	25.59	28.91	131	25.72	61.65
123	20.11	4.53	123	25.15	30.92	132	24.85	72.08
124	9.41	2.78	124	25.35	11.26	133	26.24	39.25
125	19.70	4.18	125	27.04	28.99	134	25.74	57.71
126	19.78	4.10	126	27.02	29.99	135	25.37	74.58
127	3.73	0.73	127	13.40	4.67	136	26.23	40.42
128	14.82	2.95	128	26.25	18.83	137	25.64	61.65
129	18.22	2.58	129	25.38	27.76	138	25.59	79.37
130	3.67	0.49	130	14.30	4.18	139	25.42	43.13
131	11.63	2.01	131	24.48	13.31	140	25.78	65.19
132	17.04	1.27	132	28.02	20.86	141	26.94	84.40
133	4.57	1.01	133	16.55	5.11	142	25.27	48.35
134	10.38	2.15	134	23.48	11.60	143	26.21	68.20
135	16.90	1.57	135	27.18	21.35	144	27.80	85.39
136	4.99	1.09	136	17.92	5.44	145	26.38	60.52
137	11.44	1.95	137	24.99	12.24	146	28.90	72.46
138	16.69	1.70	138	26.52	22.10	147	30.78	73.98
140	12.02	2.42	139	19.26	4.85			
141	16.34	2.53	140	25.82	12.26			
142	6.49	2.13	141	25.94	23.07			

Table F-1. Continued

Sample No.	1 h		Sample No.	6 h		Sample No.	72 h	
	slope	intercept		slope	intercept		slope	intercept
143	12.98	2.78	142	21.34	6.24			
144	16.33	2.97	143	26.55	13.15			
145	8.89	2.17	144	26.06	23.51			
146	14.37	3.16	145	26.45	9.36			
147	17.53	2.68	146	28.18	14.42			
			147	27.91	21.75			

Table F-2. Net-simulated xylan slopes and intercepts.

Sample No.	1 h		Sample No.	6 h		Sample No.	72 h	
	slope	intercept		slope	intercept		slope	intercept
2	6.19	-0.07	2	6.66	12.26	1	0.47	2.75
3	8.07	0.88	3	11.19	18.81	2	5.88	28.82
5	4.72	0.27	5	7.51	9.57	3	8.76	49.12
6	6.82	1.01	6	10.09	15.11	4	1.27	3.27
8	6.73	0.60	8	7.62	12.56	5	6.83	29.23
9	7.73	1.15	9	12.27	14.93	6	8.48	41.30
11	7.12	1.42	11	7.85	13.68	8	6.30	30.80
12	7.61	1.70	12	10.76	16.48	9	9.83	40.79
14	8.03	1.63	13	2.06	2.44	10	1.35	3.39
15	8.47	3.00	14	10.33	22.76	11	7.78	28.19
16	3.79	-0.25	15	13.69	25.66	12	10.36	35.94
17	9.10	3.07	16	4.33	4.71	13	2.20	5.69
18	8.79	3.58	17	12.55	29.57	14	5.87	50.11
19	8.11	1.10	18	14.33	30.24	15	12.06	54.08
20	10.06	4.72	19	10.12	9.80	16	4.52	8.82
21	9.74	5.05	20	14.20	31.52	17	8.37	59.09
24	8.20	1.66	22	1.46	0.30	18	10.73	61.11
26	8.02	1.50	24	16.93	22.65	19	13.29	21.70
30	7.76	1.81	25	1.98	1.27	20	13.35	65.32
32	6.49	1.32	26	13.14	21.80	22	3.08	5.43
33	7.25	1.53	28	2.15	1.68	23	10.68	44.05
34	2.82	-0.04	29	12.01	18.64	24	12.68	61.02
36	7.96	2.28	30	15.99	23.88	25	4.00	6.43
37	3.59	0.00	31	2.41	2.05	26	11.50	54.08
38	8.29	2.84	32	13.03	19.90	27	12.02	57.33
39	8.31	2.96	33	15.57	27.25	28	4.26	7.01
40	6.52	2.19	34	4.23	3.72	29	10.62	48.24
42	8.79	5.76	35	14.67	25.08	30	12.10	61.18
43	2.51	-0.66	36	16.68	25.84	31	4.65	7.89
44	7.98	1.72	37	6.17	7.07	32	10.88	49.77
45	8.26	1.77	38	15.69	28.69	33	12.80	65.33
46	2.29	-0.12	39	16.88	31.93	34	6.17	9.96
47	6.52	1.93	40	17.52	19.21	35	11.54	57.44
48	7.96	2.04	41	16.82	43.60	36	13.27	66.88
49	2.45	-0.14	42	17.43	43.32	37	7.17	17.70
50	6.13	1.80	43	3.36	3.34	38	12.40	64.84
54	7.48	2.12	44	16.96	25.11	39	12.55	71.78
55	3.21	0.02	45	17.36	26.57	40	16.83	58.54
56	7.30	2.23	46	3.73	4.01	41	13.72	84.86
58	4.19	0.81	47	15.96	22.78	42	12.10	87.72
59	7.80	3.02	48	18.67	28.63	43	6.92	10.39
60	7.95	3.25	50	14.43	23.19	44	12.17	64.65
61	7.31	3.02	51	16.37	21.80	46	8.17	8.31
62	9.01	5.73	52	5.69	4.98	47	12.19	59.69
63	7.76	6.07	53	16.63	24.85	48	12.88	75.69
64	3.34	0.16	54	17.68	24.83	49	8.76	11.89
65	7.25	2.29	55	7.05	7.02	50	11.61	58.62
66	8.45	2.26	56	16.48	26.00	51	11.01	68.94
67	3.61	0.33	57	17.18	28.77	52	9.38	16.48

Table F-2. Continued

Sample No.	1 h		Sample No.	6 h		Sample No.	72 h	
	slope	intercept		slope	intercept		slope	intercept
68	6.18	2.40	58	10.29	11.63	53	12.92	62.82
69	8.23	2.45	59	16.65	34.63	54	13.01	70.88
70	4.08	0.56	60	18.69	33.86	55	10.45	21.44
71	7.54	2.69	61	19.23	26.33	56	12.40	67.82
72	8.22	2.58	62	17.22	43.99	57	12.58	71.25
73	4.22	0.58	63	16.63	43.22	58	11.15	29.71
74	7.34	2.71	64	7.08	6.02	59	12.17	75.64
75	8.13	2.63	65	18.20	33.59	60	11.45	85.35
76	4.34	0.59	66	19.44	34.58	61	18.16	74.05
77	7.70	2.75	67	7.88	7.87	62	11.84	87.10
79	4.91	1.08	68	17.30	25.46	64	13.27	18.14
80	7.63	3.21	69	19.46	34.04	65	13.13	78.43
81	7.78	3.18	70	8.93	9.18	66	11.65	85.30
82	6.62	3.75	71	18.01	30.76	67	12.29	28.65
84	8.02	5.68	72	19.49	32.21	68	13.05	66.68
85	5.00	1.28	73	10.50	10.47	70	13.11	25.51
86	7.90	2.98	74	18.57	30.14	71	12.99	75.49
87	8.28	2.73	75	19.20	34.70	72	10.93	85.31
88	5.10	1.16	76	11.51	10.81	73	13.46	36.29
89	7.48	3.20	77	18.38	33.35	74	12.68	77.79
90	7.58	3.19	78	18.83	35.97	75	11.53	83.29
91	5.18	1.08	79	14.16	15.38	76	14.14	38.72
92	7.77	3.15	80	18.16	35.38	77	12.09	81.44
93	8.22	2.90	81	18.11	35.81	78	10.63	88.64
94	5.43	1.36	82	19.40	26.80	79	16.53	51.03
95	7.65	3.42	83	16.49	43.10	80	11.52	83.18
96	8.10	3.17	84	16.87	43.06	81	11.37	83.08
97	5.63	1.44	85	12.86	13.53	82	16.43	74.19
98	7.94	3.58	86	19.06	32.22	83	11.43	86.79
100	5.78	1.51	87	19.23	35.79	84	11.22	88.67
101	8.00	3.71	88	11.38	14.63	85	16.83	48.26
102	8.06	3.66	89	18.11	33.98	86	13.17	81.88
103	6.18	4.64	90	18.33	33.84	87	11.14	85.78
104	7.12	5.85	91	9.12	17.03	88	15.30	45.56
105	7.40	5.71	92	17.72	32.54	89	11.45	84.00
107	8.06	4.47	93	19.01	35.50	90	11.23	87.08
108	8.08	4.38	94	15.08	16.83	91	18.60	50.99
109	5.87	2.13	95	17.83	35.31	92	11.62	80.28
110	7.73	4.27	96	18.93	35.46	93	11.53	85.43
111	8.07	3.98	97	15.53	19.64	94	16.08	56.32
112	6.07	2.51	98	17.70	35.85	95	11.40	83.99
113	7.85	4.51	99	17.73	36.54	96	9.87	87.91
114	8.11	4.21	100	16.19	20.02	97	17.68	60.92
115	6.13	2.64	101	17.57	37.41	98	11.18	87.31
116	8.07	4.26	102	17.69	38.63	100	18.17	63.25
117	8.28	3.76	103	19.47	27.86	102	10.54	89.85
118	6.15	3.17	104	17.20	40.93	103	15.84	75.11
119	8.00	4.78	105	15.88	42.54	104	14.64	89.90
120	8.07	4.69	106	16.71	24.05	105	11.63	88.12

Table F-2. Continued

Sample No.	1 h		Sample No.	6 h		Sample No.	72 h	
	slope	intercept		slope	intercept		slope	intercept
121	6.39	4.07	107	16.81	40.63	106	16.33	73.71
122	7.90	5.11	108	17.04	39.78	107	11.09	88.04
123	7.94	4.94	109	17.01	23.83	108	10.95	87.96
124	6.09	5.56	110	17.06	37.63	109	15.50	74.38
125	7.70	5.72	111	17.08	39.12	110	11.25	88.11
126	7.78	5.65	112	16.77	26.97	111	10.87	89.14
127	5.81	3.82	113	16.74	40.59	112	17.35	74.68
128	7.72	5.35	114	17.00	40.02	113	11.53	87.94
129	8.42	4.18	115	16.91	26.50	114	10.96	88.44
130	6.66	3.65	116	16.99	40.65	115	16.14	74.60
131	8.07	4.64	117	16.99	40.36	116	11.55	89.75
132	9.23	4.33	118	18.35	27.99	117	11.78	87.36
133	7.23	3.87	119	16.49	42.44	118	16.66	76.60
134	8.14	4.66	120	16.64	42.09	119	14.37	85.79
135	9.48	4.66	121	18.28	28.36	120	11.56	88.93
136	7.89	3.74	122	16.77	43.40	121	15.30	73.75
138	9.59	5.13	123	16.61	43.28	122	11.59	86.90
139	7.82	3.94	124	20.18	28.50	123	11.82	86.82
140	8.81	5.15	125	15.96	39.99	124	20.57	81.69
141	8.83	5.62	126	16.45	40.62	125	13.16	86.63
142	7.60	4.35	127	12.21	31.22	126	13.55	86.55
144	8.65	5.49	128	16.77	41.70	127	14.73	70.37
145	6.64	4.49	129	16.51	41.27	128	12.11	86.95
146	7.57	5.30	130	16.92	28.33	129	12.24	82.25
147	8.27	5.57	131	17.19	38.93	130	17.08	71.68
			132	16.60	41.28	131	16.63	82.80
			133	15.93	29.82	132	12.25	83.52
			134	16.96	39.79	133	16.37	69.12
			135	16.30	41.58	134	12.71	81.35
			136	17.12	30.90	135	12.38	85.39
			137	17.21	37.87	136	18.09	73.53
			138	16.19	43.25	137	13.32	82.96
			139	17.30	29.26	138	12.26	88.08
			140	17.68	37.89	139	15.91	73.24
			141	16.39	43.15	140	13.44	83.43
			142	18.59	29.87	141	12.34	87.82
			143	17.88	37.86	142	16.80	74.17
			144	16.33	42.79	143	14.72	83.68
			145	20.57	27.06	144	12.46	86.70
			146	20.05	30.11	145	20.67	76.74
			147	17.17	35.78	146	15.64	81.41
						147	18.13	80.96

Table F-3. Net-simulated total sugar slopes and intercepts.

Sample No.	1 h		Sample No.	6 h		Sample No.	72 h	
	slope	intercept		slope	intercept		slope	intercept
1	0.91	0.42	1	1.99	0.95	1	0.70	5.77
2	7.46	2.60	2	8.78	12.24	2	5.39	34.73
3	9.61	2.81	3	13.00	17.44	3	9.26	46.91
4	0.66	0.20	4	1.41	1.44	4	2.45	5.29
5	7.13	2.23	5	9.11	12.38	5	6.58	33.37
6	9.43	2.58	6	12.24	16.69	6	9.55	43.51
7	0.70	0.11	7	1.10	1.03	7	1.33	3.03
8	8.34	2.59	8	10.10	14.46	8	6.46	36.35
9	9.65	2.75	9	12.56	17.26	9	8.85	42.36
10	1.30	0.02	10	1.55	2.22	10	2.59	3.68
11	9.73	2.82	11	11.73	16.59	11	7.82	39.23
12	10.39	2.96	12	13.09	17.91	12	9.14	41.77
13	2.41	0.21	13	2.38	4.48	13	3.48	8.82
14	9.56	2.93	14	11.14	17.22	14	6.34	44.42
15	12.23	4.02	15	16.15	23.19	15	10.64	54.58
16	2.51	0.13	16	2.93	2.83	16	6.53	7.75
17	12.22	4.56	17	14.50	23.52	17	10.08	56.56
18	13.08	4.69	18	16.99	25.65	18	11.55	59.44
19	3.22	0.56	19	6.95	3.24	19	10.98	8.69
20	12.44	5.42	20	14.39	25.21	20	11.75	52.30
21	13.12	5.85	21	15.24	27.01	21	11.77	56.10
22	0.94	0.14	22	1.77	1.50	22	4.22	5.52
23	9.36	2.75	23	13.04	17.31	23	9.81	45.16
24	12.20	1.96	24	18.19	21.50	24	14.75	61.74
25	1.42	0.32	25	2.44	1.46	25	4.49	4.63
26	11.61	2.98	26	17.38	21.96	26	12.47	59.09
27	12.02	2.83	27	18.06	22.64	27	13.16	61.67
28	1.38	0.28	28	2.75	2.25	28	5.38	7.51
29	10.67	2.99	29	15.70	20.21	29	11.44	52.88
30	12.24	2.65	30	18.17	22.86	30	13.78	61.69
31	1.53	0.36	31	3.08	2.60	31	6.28	8.49
32	9.94	2.99	32	15.23	18.97	32	11.37	50.22
33	11.13	3.00	33	16.77	21.18	33	12.53	56.05
34	2.41	0.62	34	4.51	5.26	34	7.27	15.38
35	11.48	3.24	35	16.33	21.71	35	11.93	53.96
36	13.36	3.03	36	18.98	24.47	36	14.49	62.38
37	2.90	0.37	37	5.81	4.61	37	8.35	14.55
38	13.67	3.99	38	18.66	26.24	38	13.34	63.57
39	14.34	3.94	39	19.52	27.19	39	14.18	66.55
40	5.52	1.12	40	15.90	6.93	40	18.97	39.16
41	16.43	6.28	41	20.46	33.97	41	18.24	72.09
42	17.96	6.40	42	21.67	37.87	42	17.54	82.23
43	1.99	0.54	43	3.98	3.15	43	7.02	9.47
44	12.34	3.17	44	18.91	23.60	44	13.71	63.02
45	12.93	3.00	45	19.64	24.64	46	8.65	12.01
46	2.07	0.57	46	4.29	3.97	47	14.13	60.13
47	11.72	3.11	47	18.70	22.50	48	16.57	72.68
48	13.89	2.51	48	21.20	26.35	49	8.24	11.48
49	2.20	0.59	49	4.48	3.78	50	12.77	54.70

Table F-3. Continued

Sample No.	1 h		Sample No.	6 h		Sample No.	72 h	
	slope	intercept		slope	intercept		slope	intercept
50	10.60	3.23	50	17.46	20.40	52	10.09	15.99
51	10.60	3.23	51	17.46	20.40	53	14.30	60.66
52	2.77	0.69	52	5.87	4.70	54	15.21	66.76
53	11.76	3.43	53	19.36	22.70	55	9.94	18.49
54	13.04	3.38	54	20.55	25.10	56	14.14	62.69
55	2.74	0.42	55	6.73	4.20	57	14.62	65.26
56	12.42	3.49	56	19.24	24.14	58	12.37	28.11
57	13.01	3.48	57	19.82	25.18	59	14.78	67.32
58	4.23	0.80	58	10.07	6.98	60	17.88	83.83
59	13.60	4.42	59	19.97	27.30	61	20.68	50.04
60	17.53	4.04	60	22.38	33.17	62	19.49	75.05
61	6.92	2.21	61	19.23	12.39	64	11.34	18.86
62	17.25	7.08	62	21.98	36.21	65	15.83	67.50
63	19.88	6.86	63	20.52	44.23	66	18.80	81.87
64	3.03	0.59	64	6.77	4.76	67	12.90	23.47
65	13.15	3.45	65	21.00	25.34	68	15.70	59.77
66	16.02	2.51	66	22.69	30.52	70	13.24	27.55
67	3.29	0.52	67	7.98	5.07	71	16.49	71.83
68	11.31	3.43	68	19.68	21.98	72	19.04	82.99
69	16.43	2.54	69	22.95	31.60	73	14.64	28.55
70	3.78	0.70	70	9.73	5.91	74	17.53	71.90
71	14.28	3.88	71	21.88	27.69	75	19.28	82.46
72	17.02	3.09	72	22.60	32.60	76	14.99	32.16
73	3.94	0.76	73	9.94	6.21	77	17.96	75.81
74	14.19	3.77	74	22.40	27.19	78	19.78	84.09
75	16.71	3.16	75	23.05	32.32	79	17.50	41.94
76	3.91	0.66	76	10.78	6.16	80	19.11	80.15
77	14.96	3.71	77	22.56	28.87	81	19.48	82.81
78	17.13	2.99	78	22.77	33.11	82	21.78	56.98
79	4.33	0.83	79	13.59	7.09	83	21.50	82.74
80	15.59	3.93	80	22.95	29.86	84	21.05	86.81
81	16.38	3.78	81	23.16	31.45	85	17.91	37.06
82	7.17	2.44	82	22.37	13.79	86	20.06	80.67
83	16.98	6.54	83	22.88	33.85	87	21.33	85.80
84	18.82	6.64	84	24.21	38.64	88	19.14	42.20
85	4.84	1.52	85	12.49	9.14	89	20.12	78.13
86	16.78	3.61	86	23.35	32.00	90	20.24	79.50
87	18.37	2.79	87	22.20	36.19	91	18.62	40.63
88	4.54	1.14	88	13.62	8.43	92	19.62	77.45
89	15.24	3.73	89	23.14	28.75	93	20.96	85.38
90	15.62	3.68	90	23.23	29.53	94	19.64	44.97
91	4.71	1.07	91	14.17	8.07	95	19.94	77.99
92	15.69	4.00	92	23.11	29.76	96	21.07	86.15
93	18.21	3.14	93	22.08	35.72	97	20.00	45.97
94	4.78	1.20	94	15.39	8.63	98	19.77	79.55
95	15.43	4.09	95	22.88	29.13	100	21.34	47.03
96	18.20	3.25	96	21.85	35.65	102	20.89	85.28
97	5.04	0.99	97	17.47	8.06	103	21.96	57.51
98	16.07	4.48	98	22.83	30.64	104	22.95	85.29

Table F-3. Continued

Sample No.	1 h		Sample No.	6 h		Sample No.	72 h	
	slope	intercept		slope	intercept		slope	Intercept
99	16.07	4.48	99	22.83	30.64	105	22.88	89.86
100	4.68	0.93	100	18.25	7.76	106	23.11	52.38
101	16.52	4.01	101	22.70	30.87	107	20.41	81.99
102	17.15	3.85	102	22.55	32.32	108	20.40	83.98
103	6.81	2.49	103	23.43	13.08	109	24.47	53.07
104	15.70	5.59	104	23.56	28.73	110	21.69	80.13
105	18.61	5.59	105	24.02	36.18	111	21.35	90.81
106	5.21	1.52	106	19.73	9.80	112	23.62	52.39
107	17.57	4.36	107	23.05	32.86	113	21.30	78.72
108	18.21	4.12	108	22.27	34.49	114	21.02	87.17
109	4.84	1.33	109	19.52	9.66	115	23.59	53.91
110	15.45	4.02	110	25.12	27.96	116	21.04	77.96
111	18.11	3.13	111	22.49	34.58	117	20.69	86.49
112	4.80	1.43	112	19.77	9.64	118	23.32	51.37
113	14.60	4.35	113	23.49	26.95	120	20.98	80.53
114	17.88	3.55	114	22.18	33.74	121	21.84	52.46
115	5.11	1.53	115	19.68	10.11	122	20.67	81.57
116	14.73	4.59	116	23.66	27.66	123	20.71	82.74
117	18.46	3.62	117	21.67	35.50	124	24.06	68.45
118	4.71	1.45	118	18.34	9.51	125	26.26	85.37
119	14.93	4.44	119	23.42	27.86	126	26.31	85.98
120	16.08	4.27	120	23.67	29.71	127	24.54	47.39
121	5.23	2.00	121	19.57	10.89	128	22.87	72.05
122	17.03	4.78	122	23.18	32.18	130	25.17	44.99
123	17.87	4.54	123	23.12	33.89	131	23.89	64.59
124	8.68	3.28	124	25.47	14.84	132	22.89	75.62
125	17.32	4.52	125	24.65	31.57	133	24.32	45.69
126	17.35	4.59	126	24.85	32.93	134	23.84	61.39
127	3.91	1.21	127	12.91	8.53	135	23.41	75.71
128	13.20	3.12	128	24.32	23.16	136	24.26	47.52
129	15.97	2.67	129	23.03	30.32	137	23.76	63.87
130	4.24	1.15	130	14.03	8.35	138	23.45	78.88
131	10.73	2.61	131	22.93	18.40	139	23.67	47.31
132	15.23	2.15	132	26.43	25.18	140	24.05	66.80
133	5.11	1.63	133	16.92	9.04	141	24.96	84.00
134	9.89	2.68	134	22.71	16.44	142	23.77	53.27
135	15.40	2.33	135	25.59	24.91	143	24.67	70.77
136	5.68	1.80	136	18.09	9.83	144	26.01	87.13
137	11.02	2.72	137	23.25	17.75	145	26.01	63.16
138	15.51	2.38	138	24.88	25.75	146	27.20	72.86
140	11.86	2.89	139	19.15	8.81	147	28.21	75.95
141	15.60	2.83	140	24.16	17.49			
142	7.26	2.37	141	24.44	26.56			
143	12.68	2.93	142	21.21	9.95			
144	15.55	3.08	143	24.77	17.77			
145	8.82	2.57	144	24.74	26.97			
146	13.21	3.21	145	24.39	12.00			
147	15.68	3.41	146	28.31	17.18			
			147	25.57	23.29			

APPENDIX G

MATLAB CODES FOR PREDICTION

Exhibit G-1. Matlab codes for 1-h glucan slope network prediction.

```
netSG1=net
load CrIc_pred.m
load A_X_pred.m
load L_G_pred.m
load G_pred.m
load slope_G_1_pred.m
[slope_G_1_predn,minslope_G_1,maxslope_G_1]=premnmx(slope_G
     _1_pred);
CrIc_predn=tramnmx(CrIc_pred,minCrIc,maxCrIc);
A_X_predn=tramnmx(A_X_pred,minA_X,maxA_X);
L_G_predn=tramnmx(L_G_pred,minL_G,maxL_G);
G_predn=tramnmx(G_pred,minG,maxG);
for I=1:21,
    finS(I,1)=A_X_predn(I)';
end
for I=1:21,
    finS(I,2)=CrIc_predn(I)';
end
for I=1:21,
    finS(I,3)=L_G_predn(I)';
end
for I=1:21,
    finS(I,4)=G_predn(I)';
end
ypredn=sim(netSG1,finS');
```

Exhibit G-1. Continued

```
ypred=postmnmx(ypredn,minslope_G_1,maxslope_G_1);
E_pred=slope_G_1_pred'-ypred;
perf_pred=mse(E_pred)
[mpred,bpred,rpred]=postreg(ypred,slope_G_1_pred')
Rsqrpred=rpred^2
```

Exhibit G-2. Matlab codes for 1-h glucan intercept network prediction.

```
netIG1=net
load CrIc_pred.m
load A_X_pred.m
load L_pred.m
load G_pred.m
load intercept_G_1_pred.m
[intercept_G_1_predn,minintercept_G_1,maxintercept_G_1]=pre
     mnmx(intercept_G_1_pred);
CrIc_predn=tramnmx(CrIc_pred,minCrIc,maxCrIc);
A_X_predn=tramnmx(A_X_pred,minA_X,maxA_X);
L_predn=tramnmx(L_pred,minL,maxL);
G_predn=tramnmx(G_pred,minG,maxG);
for I=1:21,
    fin5(I,1)=G_predn(I)';
end
for I=1:21,
    fin5(I,2)=CrIc_predn(I)';
end
for I=1:21,
    fin5(I,3)=A_X_predn(I)';
end
for I=1:21,
```

Exhibit G-2. Continued

```
    fin5(I,4)=L_predn(I)';
end
ypredn=sim(netIG1,fin5');
ypred=postmnmx(ypredn,minintercept_G_1,maxintercept_G_1);
E_pred=intercept_G_1_pred'-ypred;
perf_pred=mse(E_pred)
[mpred,bpred,rpred]=postreg(ypred,intercept_G_1_pred')
Rsqrpred=rpred^2
```

Exhibit G-3. Matlab codes for 6-h glucan slope network prediction.

```
netSG6=net
load CrIc_G_pred.m
load A_G_pred.m
load L_pred.m
load G_pred.m
load slope_G_6_pred.m
[slope_G_6_predn,minslope_G_6_pred,maxslope_G_6_pred]=premn
     mx(slope_G_6_pred);
CrIc_G_predn=tramnmx(CrIc_G_pred,minCrIc_G,maxCrIc_G);
A_G_predn=tramnmx(A_G_pred,minA_G,maxA_G);
L_predn=tramnmx(L_pred,minL,maxL);
G_predn=tramnmx(G_pred,minG,maxG);
for P=1:22,
    finP(P,1)=A_G_predn(P)';
end
for I=1:22,
    finP(P,2)=CrIc_G_predn(P)';
end
```

Exhibit G-3. Continued

```
for P=1:22,
    finP(P,3)=L_predn(P)';
end
for P=1:22,
    finP(P,4)=G_predn(P)';
end
ypredn=sim(netSG6,finP');
ypred=postmnmx(ypredn,minslope_G_6,maxslope_G_6);
E_pred=slope_G_6_pred'-ypred;
perf_pred=mse(E_pred)
[mpred,bpred,rpred]=postreg(ypred,slope_G_6_pred')
Rsqrpred=rpred^2
```

Exhibit G-4. Matlab codes for 6-h glucan intercept network prediction.

```
netIG6=net
load CrIc_G_pred.m
load A_X_pred.m
load L_G_pred.m
load G_pred.m
load intercept_G_6_pred.m
[intercept_G_6_predn,mintercept_G_6_pred,maxintercept_G_6
     _pred]=premnmx(intercept_G_6_pred);
CrIc_G_predn=tramnmx(CrIc_G_pred,minCrIc_G,maxCrIc_G);
A_X_predn=tramnmx(A_X_pred,minA_X,maxA_X);
L_G_predn=tramnmx(L_G_pred,minL_G,maxL_G);
G_predn=tramnmx(G_pred,minG,maxG);
for P=1:22,
    finP(P,1)=CrIc_G_predn(P)';
```

Exhibit G-4. Continued

```
end
for P=1:22,
    finP(P,2)=A_X_predn(P)';
end
for P=1:22,
    finP(P,3)=L_G_predn(P)';
end
for P=1:22,
    finP(P,4)=G_predn(P)';
end
ypredn=sim(netIG6,finP');
ypred=postmnmx(ypredn,minintercept_G_6,maxintercept_G_6);
E_pred=intercept_G_6_pred'-ypred;
perf_pred=mse(E_pred)
[mpred,bpred,rpred]=postreg(ypred,intercept_G_6_pred')
Rsqrpred=rpred^2
```

Exhibit G-5. Matlab codes for 72-h glucan slope network prediction.

```
netSG72=net
load CrIc_pred.m
load A_X_pred.m
load L_pred.m
load slope_G_72_pred.m
[slope_G_72_predn,minslope_G_72_pred,maxslope_G_72_pred]=pr
     emnmx(slope_G_72_pred);
CrIc_predn=tramnmx(CrIc_pred,minCrIc,maxCrIc);
A_X_predn=tramnmx(A_X_pred,minA_X,maxA_X);
L_predn=tramnmx(L_pred,minL,maxL);
for P=1:22,
```

Exhibit G-5. Continued

```
    finS(P,1)=A_X_predn(P)';
end
for P=1:22,
    finS(P,2)=L_predn(P)';
end
for P=1:22,
    finS(P,3)=CrIc_predn(P)';
end
ypredn=sim(netSG72,finS');
ypred=postmnmx(ypredn,minslope_G_72,maxslope_G_72);
E_pred=slope_G_72_pred'-ypred;
perf_pred=mse(E_pred)
[mpred,bpred,rpred]=postreg(ypred,slope_G_72_pred')
Rsqrpred=rpred^2
```

Exhibit G-6. Matlab codes for 72-h glucan intercept network prediction.

```
netIG72=net
load CrIc_pred.m
load A_G_pred.m
load L_pred.m
load intercept_G_72_pred.m
[intercept_G_72_predn,minintercept_G_72_pred,maxintercept_G
     _72_pred]=premnmx(intercept_G_72_pred);
CrIc_predn=tramnmx(CrIc_pred,minCrIc,maxCrIc);
A_G_predn=tramnmx(A_G_pred,minA_G,maxA_G);
L_predn=tramnmx(L_pred,minL,maxL);
for P=1:22,
    finP(P,1)=A_G_predn(P)';
end
```

Exhibit G-6. Continued

```
for P=1:22,
    finP(P,2)=CrIc_predn(P)';
end
for P=1:22,
    finP(P,3)=L_predn(P)';
end
ypredn=sim(netIG72,finP');
ypred=postmnmx(ypredn,minintercept_G_72,maxintercept_G_72);
E_pred=intercept_G_72_pred'-ypred;
perf_pred=mse(E_pred)
[mpred,bpred,rpred]=postreg(ypred,intercept_G_72_pred')
Rsqrpred=rpred^2
```

Exhibit G-7. Matlab codes for 1-h xylan slope network prediction.

```
netSX1=net
load L_pred.m
load A_pred.m
load X_pred.m
load CrIc_pred.m
load slope_X_1_pred.m
[slope_X_1_predn,minslope_X_1_pred,maxslope_X_1_pred]=premn
     mx(slope_X_1_pred);
L_predn=tramnmx(L_pred,minL,maxL);
A_predn=tramnmx(A_pred,minA,maxA);
X_predn=tramnmx(X_pred,minX,maxX);
CrIc_predn=tramnmx(CrIc_pred,minCrIc,maxCrIc);
for P=1:20,
    finS(P,1)=CrIc_predn(P)';
end
```

Exhibit G-7. Continued

```
for P=1:20,
    finS(P,2)=L_predn(P)';
end
for P=1:20,
    finS(P,3)=A_predn(P)';
end
for P=1:20,
    finS(P,4)=X_predn(P)';
end
ypredn=sim(netSX1,finS');
ypred=postmnmx(ypredn,minslope_X_1,maxslope_X_1);
E_pred=slope_X_1_pred'-ypred;
perf_pred=mse(E_pred)
[mpred,bpred,rpred]=postreg(ypred,slope_X_1_pred')
Rsqrpred=rpred^2
```

Exhibit G-8. Matlab codes for 1-h xylan intercept network prediction.

```
netIX1=net
load L_pred.m
load A_pred.m
load X_pred.m
load CrIc_pred.m
load intercept_X_1_pred.m
[intercept_X_1_predn,mininterccpet_X_1_pred,maxintercept_X_1
     _pred]=premnmx(intercept_X_1_pred);
L_predn=tramnmx(L_pred,minL,maxL);
A_predn=tramnmx(A_pred,minA,maxA);
X_predn=tramnmx(X_pred,minX,maxX);
CrIc_predn=tramnmx(CrIc_pred,minCrIc,maxCrIc);
```

Exhibit G-8. Continued

```
for P=1:20,
    finI(P,1)=L_predn(P)';
end
for P=1:20,
    finI(P,2)=A_predn(P)';
end
for P=1:20,
    finI(P,3)=CrIc_predn(P)';
end
for P=1:20,
    finI(P,4)=X_predn(P)';
end
ypredn=sim(netIX1,finI');
ypred=postmnmx(ypredn,minintercept_X_1,maxintercept_X_1);
E_pred=intercept_X_1_pred'-ypred;
perf_pred=mse(E_pred)
[mpred,bpred,rpred]=postreg(ypred,intercept_X_1_pred')
Rsqrpred=rpred^2
```

Exhibit G-9. Matlab codes for 6-h xylan slope network prediction.

```
netSX6=net
load L_pred.m
load A_X_pred.m
load CrIc_pred.m
load slope_X_6_pred.m
load slope_G_6_pred.m
[slope_X_6_predn,minslope_X_6_pred,maxslope_X_6_pred]=premn
     mx(slope_X_6_pred);
L_predn=tramnmx(L_pred,minL,maxL);
```

Exhibit G-9. Continued

```
A_X_predn=tramnmx(A_X_pred,minA_X,maxA_X);
CrIc_predn=tramnmx(CrIc_pred,minCrIc,maxCrIc);
slope_G_6_predn=tramnmx(slope_G_6_pred,minslope_G_6,maxslop
     e_G_6);
for P=1:22,
    finS(P,1)=L_predn(P)';
end
for P=1:22,
    finS(P,2)=A_X_predn(P)';
end
for P=1:22,
    finS(P,3)=CrIc_predn(P)';
end
for P=1:22,
    finS(P,4)=slope_G_6_predn(P)';
end
ypredn=sim(netSX6,finS');
ypred=postmnmx(ypredn,minslope_X_6,maxslope_X_6);
E_pred=slope_X_6_pred'-ypred;
perf_pred=mse(E_pred)
[mpred,bpred,rpred]=postreg(ypred,slope_X_6_pred')
Rsqrpred=rpred^2
```

Exhibit G-10. Matlab codes for 6-h xylan intercept network prediction.

```
netIX6=net
load L_pred.m
load A_pred.m
load CrIc_G_pred.m
load intercept_X_6_pred.m
```

Exhibit G-10. Continued

```
load intercept_G_6_pred.m
[intercept_X_6_predn,mininterceptX_6_pred,maxinterceptX_6
     _pred]=premnmx(intercept_X_6_pred);
L_predn=tramnmx(L_pred,minL,maxL);
A_predn=tramnmx(A_pred,minA,maxA);
CrIc_G_predn=tramnmx(CrIc_G_pred,minCrIc_G,maxCrIc_G);
intercept_G_6_predn=tramnmx(intercept_G_6_pred,mininterceptX
     _G_6,maxinterceptX_G_6);
for P=1:22,
    finI(P,1)=L_predn(P)';
end
for I=1:22,
    finI(P,2)=A_predn(P)';
end
for I=1:22,
    finI(P,3)=CrIc_G_predn(P)';
end
for I=1:22,
    finI(P,4)=intercept_G_6_predn(P)';
end
ypredn=sim(netIX6,finI');
ypred=postmnmx(ypredn,mininterceptX_6,maxinterceptX_6);
E_pred=intercept_X_6_pred'-ypred;
perf_pred=mse(E_pred)
[mpred,bpred,rpred]=postreg(ypred,intercept_X_6_pred')
Rsqrpred=rpred^2
```

Exhibit G-11. Matlab codes for 72-h xylan slope network prediction.

```
netSX72=net
load L_X_pred.m
load A_X_pred.m
load CrIc_X_pred.m
load slope_X_72_pred.m
load slope_G_72_pred.m
[slope_X_72_predn,minslope_X_72_pred,maxslope_X_72_pred]=pr
     emnmx(slope_X_72_pred);
[slope_G_72_predn,minslope_G_72_pred,maxslope_G_72_pred]=pr
     emnmx(slope_G_72_pred);
L_X_predn=tramnmx(L_X_pred,minL_X,maxL_X);
A_X_predn=tramnmx(A_X_pred,minA_X,maxA_X);
CrIc_X_predn=tramnmx(CrIc_X_pred,minCrIc_X,maxCrIc_X);
for P=1:21,
    finS(P,1)=L_X_predn(P)';
end
for P=1:21,
    finS(P,2)=A_X_predn(P)';
end
for P=1:21,
    finS(P,3)=CrIc_X_predn(P)';
end
for P=1:21,
    finS(P,4)=slope_G_72_predn(P)';
end
ypredn=sim(netSX72,finS');
ypred=postmnmx(ypredn,minslope_X_72,maxslope_X_72);
E_pred=slope_X_72_pred'-ypred;
```

Exhibit G-11. Continued

```
perf_pred=mse(E_pred)
[mpred,bpred,rpred]=postreg(ypred,slope_X_72_pred')
Rsqrpred=rpred^2
```

Exhibit G-12. Matlab codes for 72-h xylan intercept network prediction.

```
netIX72=net
load L_X_pred.m
load A_pred.m
load X_pred.m
load CrIc_pred.m
load intercept_X_72_pred.m
load intercept_G_72_pred.m
[intercept_X_72_predn,mininterceptX_72_pred,maxintercept_X
     _72_pred]=premnmx(intercept_X_72_pred);
intercept_G_72_predn=tramnmx(intercept_G_72_pred,mininterce
     pt_G_72,maxintercept_G_72);
L_X_predn=tramnmx(L_X_pred,minL_X,maxL_X);
A_predn=tramnmx(A_pred,minA,maxA);
X_predn=tramnmx(X_pred,minX,maxX);
CrIc_predn=tramnmx(CrIc_pred,minCrIc,maxCrIc);
for P=1:21,
    finI(P,1)=CrIc_predn(P)';
end
for P=1:21,
    finI(P,2)=L_X_predn(P)';
end
for P=1:21,
    finI(P,3)=A_predn(P)';
end
```

Exhibit G-12. Continued

```
for P=1:21,
    finI(P,4)=X_predn(P)';
end
for P=1:21,
    finI(P,5)=intercept_G_72_predn(P)';
end
ypredn=sim(netIX72,finI');
ypred=postmnmx(ypredn,minintercept_X_72,maxintercept_X_72);
E_pred=intercept_X_72_pred'-ypred;
perf_pred=mse(E_pred)
[mpred,bpred,rpred]=postreg(ypred,intercept_X_72_pred')
Rsqrpred=rpred^2
```

Exhibit G-13. Matlab codes for 1-h total sugar slope network prediction.

```
netSTS1=net
load L_TS_pred.m
load A_TS_pred.m
load TS_pred.m
load CrIc_TS_pred.m
load slope_TS_1_pred.m
[slope_TS_1_predn,minslope_TS_1_pred,maxslope_TS_1_pred]=pr
     emnmx(slope_TS_1_pred);
L_TS_predn=tramnmx(L_TS_pred,minL_TS,maxL_TS);
A_TS_predn=tramnmx(A_TS_pred,minA_TS,maxA_TS);
TS_predn=tramnmx(TS_pred,minTS,maxTS);
CrIc_TS_predn=tramnmx(CrIc_TS_pred,minCrIc_TS,maxCrIc_TS);
for P=1:22,
    finS(P,1)=L_TS_predn(P)';
```

Exhibit G-13. Continued

```
end
for P=1:22,
    finS(P,2)=A_TS_predn(P)';
end
for P=1:22,
    finS(P,3)=CrIc_TS_predn(P)';
end
for P=1:22,
    finS(P,4)=TS_predn(P)';
end
ypredn=sim(netSTS1,finS');
ypred=postmnmx(ypredn,minslope_TS_1,maxslope_TS_1);
E_pred=slope_TS_1_pred'-ypred;
perf_pred=mse(E_pred)
[mpred,bpred,rpred]=postreg(ypred,slope_TS_1_pred')
Rsqrpred=rpred^2
```

Exhibit G-14. Matlab codes for 1-h total sugar intercept network prediction.

```
netSTS1=net
load L_pred.m
load A_X_pred.m
load TS_pred.m
load CrIc_pred.m
load intercept_TS_1_pred.m
[intercept_TS_1_predn,minintercept_TS_1_pred,maxintercept_T
     S_1_pred]=premnmx(intercept_TS_1_pred);
L_predn=tramnmx(L_pred,minL,maxL);
A_X_predn=tramnmx(A_X_pred,minA_X,maxA_X);
TS_predn=tramnmx(TS_pred,minTS,maxTS);
```

Exhibit G-14. Continued

```
CrIc_predn=tramnmx(CrIc_pred,minCrIc,maxCrIc);
for P=1:22,
    finS(P,1)=CrIc_predn(P)';
end
for P=1:22,
    finS(P,2)=A_X_predn(P)';
end
for P=1:22,
    finS(P,3)=L_predn(P)';
end
for P=1:22,
    finS(P,4)=TS_predn(P)';
end
ypredn=sim(netSTS1,finS');
ypred=postmnmx(ypredn,minintercept_TS_1,maxintercept_TS_1);
E_pred=intercept_TS_1_pred'-ypred;
perf_pred=mse(E_pred)
[mpred,bpred,rpred]=postreg(ypred,intercept_TS_1_pred')
Rsqrpred=rpred^2
```

Exhibit G-15. Matlab codes for 6-h total sugar slope network prediction.

```
netSTS6=net
load L_pred.m
load A_pred.m
load CrIc_pred.m
load slope_TS_6_pred.m
[slope_TS_6_predn,minslope_TS_6_pred,maxslope_TS_6_pred]=pr
     emnmx(slope_TS_6_pred);
L_predn=tramnmx(L_pred,minL,maxL);
```

Exhibit G-15. Continued

```
A_predn=tramnmx(A_pred,minA,maxA);
CrIc_predn=tramnmx(CrIc_pred,minCrIc,maxCrIc);
for P=1:22,
    finS(P,1)=CrIc_predn(P)';
end
for P=1:22,
    finS(P,2)=A_predn(P)';
end
for P=1:22,
    finS(P,3)=L_predn(P)';
end
ypredn=sim(netSTS6,finS');
ypred=postmnmx(ypredn,minslope_TS_6,maxslope_TS_6);
E_pred=slope_TS_6_pred'-ypred;
perf_pred=mse(E_pred)
[mpred,bpred,rpred]=postreg(ypred,slope_TS_6_pred')
Rsqrpred=rpred^2
```

Exhibit G-16. Matlab codes for 6-h total sugar intercept network prediction.

```
netSTS6=net
load L_pred.m
load A_pred.m
load TS_pred.m
load CrIc_pred.m
load intercept_TS_6_pred.m
[intercept_TS_6_predn,minintercept_TS_6_pred,maxintercept_T
     S_6_pred]=premnmx(intercept_TS_6_pred);
L_predn=tramnmx(L_pred,minL,maxL);
A_predn=tramnmx(A_pred,minA,maxA);
```

Exhibit G-16. Continued

```
TS_predn=tramnmx(TS_pred,minTS,maxTS);
CrIc_predn=tramnmx(CrIc_pred,minCrIc,maxCrIc);
for P=1:22,
    finS(P,1)=A_predn(P)';
end
for P=1:22,
    finS(P,2)=CrIc_predn(P)';
end
for P=1:22,
    finS(P,3)=L_predn(P)';
end
for P=1:22,
    finS(P,4)=TS_predn(P)';
end

ypredn=sim(netSTS6,finS');
ypred=postmnmx(ypredn,minintercept_TS_6,maxintercept_TS_6);
E_pred=intercept_TS_6_pred'-ypred;
perf_pred=mse(E_pred)
[mpred,bpred,rpred]=postreg(ypred,intercept_TS_6_pred')
Rsqrpred=rpred^2
```

Exhibit G-17. Matlab codes for 72-h total sugar slope network prediction.

```
netSTS72=net
load L_pred.m
load A_X_pred.m
load TS_pred.m
load CrIc_G_pred.m
load slope_TS_72_pred.m
```

Exhibit G-17. Continued

```
[slope_TS_72_predn,minslope_TS_72_pred,maxslope_TS_72_pred]
     =premnmx(slope_TS_72_pred);
L_predn=tramnmx(L_pred,minL,maxL);
A_X_predn=tramnmx(A_X_pred,minA_X,maxA_X);
TS_predn=tramnmx(TS_pred,minTS,maxTS);
CrIc_G_predn=tramnmx(CrIc_G_pred,minCrIc_G,maxCrIc_G);
for P=1:22,
    finS(P,1)=CrIc_G_predn(P)';
end
for P=1:22,
    finS(P,2)=A_X_predn(P)';
end
for P=1:22,
    finS(P,3)=L_predn(P)';
end
for P=1:22,
    finS(P,4)=TS_predn(P)';
end
ypredn=sim(netSTS72,finS');
ypred=postmnmx(ypredn,minslope_TS_72,maxslope_TS_72);
E_pred=slope_TS_72_pred'-ypred;
perf_pred=mse(E_pred)
[mpred,bpred,rpred]=postreg(ypred,slope_TS_72_pred')
Rsqrpred=rpred^2
```

Exhibit G-18. Matlab codes for 72-h total sugar intercept network prediction.

```
netSTS72=net
load L_pred.m
load A_pred.m
load TS_pred.m
load CrIc_pred.m
load intercept_TS_72_pred.m
[intercept_TS_72_predn,minintercept_TS_72_pred,maxintercept
     _TS_72_pred]=premnmx(intercept_TS_72_pred);
L_predn=tramnmx(L_pred,minL,maxL);
A_predn=tramnmx(A_pred,minA,maxA);
TS_predn=tramnmx(TS_pred,minTS,maxTS);
CrIc_predn=tramnmx(CrIc_pred,minCrIc,maxCrIc);
for P=1:22,
    finS(P,1)=CrIc_predn(P)';
end
for P=1:22,
    finS(P,2)=A_predn(P)';
end
for P=1:22,
    finS(P,3)=L_predn(P)';
end
for P=1:22,
    finS(P,4)=TS_predn(P)';
end
ypredn=sim(netSTS72,finS');
ypred=postmnmx(ypredn,minintercept_TS_72,maxintercept_TS_72
     );
E_pred=intercept_TS_72_pred'-ypred;
perf_pred=mse(E_pred)
```

Exhibit G-18. Continued

```
[mpred,bpred,rpred]=postreg(ypred,intercept_TS_72_pred')
Rsqrpred=rpred^2
```

APPENDIX H

NETWORK-PREDICTED SLOPES AND INTERCEPTS

Table H-1. Net-predicted glucan slopes and intercepts.

Sample No.	1 h		Sample No.	6 h		Sample No.	72 h	
	slope	intercept		slope	intercept		slope	intercept
1	13.18	8.22	1	27.40	14.43	1	24.62	62.05
2	10.14	5.34	2	24.51	10.40	2	19.14	52.20
3	19.81	14.64	3	20.26	31.79	3	18.72	67.03
4	21.94	15.16	4	20.70	35.70	4	18.33	76.94
5	4.22	2.38	5	13.21	7.76	5	7.88	9.42
6	13.79	10.85	6	13.21	39.62	6	13.36	58.41
7	4.96	0.30	7	9.27	3.98	7	3.77	27.14
8	10.32	3.60	8	9.27	15.06	8	6.82	47.61
9	7.78	1.78	9	11.01	23.36	9	7.07	34.24
10	12.12	5.24	10	11.16	39.98	10	11.19	60.23
11	5.62	2.56	11	11.55	7.89	11	3.34	24.36
12	9.46	5.32	12	11.55	12.71	12	7.67	31.00
13	8.07	4.63	13	15.83	3.05	13	14.89	27.65
14	8.79	6.28	14	15.32	4.54	14	14.60	34.32
15	8.48	5.68	15	14.76	4.40	15	13.98	29.73
16	13.41	9.52	16	15.83	16.13	16	16.81	58.40
17	16.91	11.80	17	15.32	25.60	17	16.97	71.76
18	18.35	11.85	18	14.76	28.41	18	17.12	75.54
19	6.39	3.92	19	16.70	6.14	19	8.33	22.60
21	17.14	12.45	20	16.63	6.57	20	8.43	23.55
22	15.81	11.65	21	16.70	26.90	21	11.50	50.28
			22	17.09	24.80	22	12.00	43.22

Table H-2. Net-predicted xylan slopes and intercepts.

Sample No.	1 h		Sample No.	6 h		Sample No.	72 h	
	slope	intercept		slope	intercept		slope	intercept
1	8.87	4.49	1	19.77	40.53	1	20.41	92.33
2	5.28	2.11	2	19.04	37.06	2	10.44	68.19
3	4.86	5.07	3	18.07	32.99	3	11.72	63.19
4	4.89	4.94	4	17.47	33.07	4	8.84	65.86
5	8.68	0.72	5	9.85	22.63	5	7.41	35.54
7	4.18	3.64	6	16.01	22.63	6	21.85	79.49
8	0.44	7.28	7	3.84	18.23	7	8.70	8.29
9	5.48	-1.03	8	7.94	18.23	9	6.46	37.28
10	8.49	0.90	9	8.38	18.68	10	6.79	61.81
12	0.06	6.94	10	14.19	19.08	11	7.85	23.09
13	6.16	1.01	11	7.48	20.20	12	9.05	21.95
14	5.43	1.92	12	14.53	20.20	13	11.79	61.38
15	5.60	1.64	13	12.60	33.05	14	11.91	61.34
16	4.92	3.30	14	12.92	32.99	15	11.94	62.20
17	4.43	4.00	15	12.86	32.42	16	12.24	73.32
18	4.20	4.03	16	14.74	33.05	17	11.62	74.65
19	1.89	2.07	17	16.36	32.99	18	11.99	75.94
20	1.91	2.15	18	16.03	32.42	19	10.10	16.72
21	5.40	4.84	19	14.87	27.32	20	10.77	17.20
22	4.64	4.70	20	15.16	27.30	21	10.67	35.29
			21	16.00	27.32	22	10.96	35.41
			22	16.25	29.81			

Table H-3. Net-predicted total sugar slopes and intercepts.

Sample No.	1 h		Sample No.	6 h		Sample No.	72 h	
	slope	intercept		slope	intercept		slope	intercept
1	12.56	6.93	1	23.10	28.16	1	18.73	56.22
2	7.62	3.25	2	19.69	15.90	2	20.48	49.68
3	17.30	8.44	3	20.33	37.13	3	16.78	63.61
4	18.18	7.74	4	20.50	38.67	4	16.52	74.40
5	5.95	1.69	5	3.88	14.27	5	1.41	24.83
6	14.51	8.25	6	14.94	40.93	6	3.24	69.82
7	5.23	0.05	7	7.16	1.07	7	8.59	20.95
8	9.26	2.09	8	13.38	18.63	8	10.21	42.82
9	5.60	1.34	9	6.42	19.30	9	-4.03	43.21
10	10.35	3.95	10	11.20	28.56	10	-4.10	61.80
11	5.78	1.08	11	8.22	8.51	11	5.55	28.60
12	10.15	3.04	12	12.74	17.07	12	6.59	48.23
13	5.19	2.32	13	9.28	8.80	13	10.17	21.92
14	5.88	3.52	14	10.38	12.02	14	8.98	29.89
15	5.18	3.01	15	9.41	10.66	15	8.93	26.34
16	10.30	5.67	16	18.05	22.63	16	10.43	54.52
17	14.95	7.31	17	22.01	31.26	17	10.68	74.86
18	15.82	6.86	18	22.06	32.32	18	11.98	77.31
19	4.80	1.82	19	9.04	6.71	19	16.56	16.95
20	4.97	2.00	20	8.83	7.52	20	16.29	16.84
21	14.63	6.51	21	17.02	29.90	21	14.56	56.80
22	13.87	6.32	22	15.90	27.77	22	14.90	50.59

VITA

Name: Jonathan Patrick O'Dwyer

Address: 59555 West Sexton Dr.
Plaquemine, LA 70764

Education: B.S., Chemical Engineering, University of Louisiana-Lafayette, December 2000.
Ph.D., Chemical Engineering, Texas A&M University, August 2005.